Wave impact on grass covered outer slopes

B.C. Mous
C1143360
Faculty of Civil Engineering & Geosciences

MSc-thesis
April 2010

TU Delft Delft University of Technology

ROYAL HASKONING

Wave impact on grass covered outer slopes

B.C. Mous

MSc-thesis

Delft, April 16 2010
Faculty of Civil Engineering & Geosciences

C1143360
bartmous@hotmail.com

Royal Haskoning
Barbarossastraat 35
6522 DK Nijmegen
T: +31 (0)24-3284284

Delft University of Technology
Faculty of Civil Engineering & Geosciences
Section of coastal engineering
Stevinweg 1
2628 CN Delft
T: +31 (0)15-2785440

Graduation committee

Prof. dr. ir. M.J.F. Stive
Faculty of Civil Engineering & Geosciences
Section of Coastal engineering
Ir. H.J. Verhagen
Faculty of Civil Engineering & Geosciences
Section of Coastal Engineering
Drs. W.N.J. Ursem
Faculty of Applied Sciences
Botanical Garden TU Delft
Ir. R.M. Bos
Royal Haskoning
Coastal and Rivers II Nijmegen

Preface

This report is my final thesis for the MSc-study Hydraulic Structures at the faculty of Civil Engineering & Geosciences at Delft University of Technology in the Netherlands. The work is done in cooperation with Royal Haskoning.

The subject of this thesis is the erosion induced by wave impacts on dikes protected by a grass cover. Wave impact occurs when a wave approaches the dike and collides on its slope and can cause severe damage. Working on this report certainly has changed my perspective on grass, in general and as a dike cover. It will be interesting to see how the application of grass on dikes will evolve in the future and I will certainly keep a close eye on the developments on this matter in flood defence.

Finally I would like to thank my graduation committee for their guidance and special thanks go to H.J. Verhagen for his enthusiasm and support during our occasional discussions in his office. Furthermore I would like to thank Royal Haskoning for the use of their facilities and the members of the EroGRASS project, who supplied me with valuable data of the experiments on grass performed in Hannover.
Last but not least, I would like to thank the people who supported me during my study: my father, girlfriend and friends.

Bart Mous
Delft, April 2010

Abstract

Against the background of enhanced hydraulic loads due to climate change there will be a need for improvement of the flood defence system in the Netherlands in the future. These days there is a growing interest in grass as a dike cover because it is a cheap and a sustainable dike protection.
Yet at the moment there is a hiatus in the knowledge on the erosion resistance of grass covers on especially the outer slope.
For this reason large scale tests have been performed in the Große WellenKanal (Large Wave Flume) in Hannover in 2008 for both EroGRASS and FLOODsite. With the help of the EroGRASS data the MSc-study presented here aimed to develop a model that describes the initiation of erosion of a grass cover layer on the outer slope by wave attack.
The erosion process was investigated first to gain some insight in the failure mechanisms on the outer slope. For wave-induced erosion of grass cover layers on the outer slope two failure mechanisms can be distinguished which can occur independently of each other.
Aggregate erosion occurs when the soil is cracked and saturated with water. Uplift pressures can then develop underneath the aggregates shortly after a wave impact and on the surface small aggregates may be lifted and washed away. This eventually results in an erosion hole.
Block erosion may occur when impact pressures can penetrate into the soil due to the presence of a large crack or irregularity. The balloon mechanism may then be triggered; at the location of minimum fracture strength a horizontal crack is formed. This crack gradually extends until it reaches a critical size. From this point a large block can instantly erode from the grass cover.
For these erosion mechanisms the Wave Impact Pressure Erosion model has been developed, which describes the initiation of erosion of grass covers on the outer slope by wave impact pressures.
The basic equation of the WIPE model can be adapted to obtain limit states for aggregate erosion block erosion.
The WIPE model was calibrated and verified with the data of the EroGRASS experiments. For aggregate erosion the model behavior resembled the observed progression of aggregate erosion during the experiments after calibration. The WIPE model is considered suitable for the prediction of aggregate erosion of a good quality grass cover. Yet because the grass cover strength is dominated by the grass reinforcement, which decays with depth, the model will require adaptations to make it suitable for grass covers of lower quality.
For block erosion the model was calibrated using a parameter that determines the moment of block erosion and a crack growth parameter, which determines the size of the eroded block. As the model was calibrated on merely two characteristic block erosion events, universal calibration factors for block erosion could unfortunately not be found. To obtain more reliable and uniform results for block erosion more data is required.

Keywords: *erosion, outer slope, grass cover, breaking wave impact, impact pressure, dike.*

Summary

Against the background of enhanced hydraulic loads due to climate change there will be a need for improvement of the flood defence system in the Netherlands in the future to prevent events such as the storm surge disaster in 1953 and the river flooding in the 90's from happening again.
Improving the existing dikes could be done by raising them and applying traditional heavy revetment types such as placed concrete block revetments (pitched revetments) or asphalt, but alternative solutions are being investigated. These days there is a growing interest in grass as a dike cover because it is a cheap and a sustainable dike protection.
Many river dikes have a grass cover and on traditional dikes with a stone revetment grass is usually applied in the higher part of the wave run-up zone already. If it can be confirmed that even during these new conditions grass is a reliable dike cover material and thus has sufficient strength to withstand the enhanced loads on both inner and outer slope an upgrade of the dike could be less drastic or will even be redundant.
A clear physical understanding of the failure of grass cover layers due to different wave loads is indispensable to achieve this. Yet at the moment there is a hiatus in the knowledge on the erosion resistance of grass covers on especially the outer slope. For this reason large scale tests have been performed in the Große WellenKanal (Large Wave Flume) in Hannover in 2008 for both EroGRASS and FLOODsite.
The obtained data during the EroGRASS experiments could provide valuable information to come to a more accurate description of the erosion process of grass covers on the outer slope. With the help of the EroGRASS data the MSc-study presented here aimed to develop a model that describes the initiation of erosion of a grass cover layer on the outer slope by wave attack.

The erosion process was investigated first to gain some insight in the failure mechanisms on the outer slope. For wave-induced erosion of grass cover layers on the outer slope two failure mechanisms can be distinguished which can occur independently of each other:

1. Aggregate erosion: when the soil is cracked and saturated with water uplift pressures can develop underneath the aggregates shortly after a wave impact. At the surface small aggregates may then be lifted and washed away, which eventually results in an erosion hole.
2. Block erosion: impact pressures penetrate into the soil due to the presence of a large crack or irregularity. The balloon mechanism may then be triggered; at the location of minimum fracture strength a horizontal crack is formed. This crack gradually extends until it reaches a critical size. From this point a large block can instantly erode from the grass cover.

For these erosion mechanisms the Wave Impact Pressure Erosion model has been developed, which describes the initiation of erosion of grass covers on the outer slope by wave impact pressures. The basic equation for the WIPE model reads:

$$y_m = \sum_{1}^{N_{imp}} \frac{\left(p_{up}(z) - p_c(z) \right) \cdot t_{imp}}{E_p(z)}$$

This basic equation can be applied to obtain limit states for the types of erosion, which were already identified above: Aggregate Erosion (AE) and Block Erosion (BE). Erosion is expressed as a depth y_m [m] and occurs only when the uplift pressure p_{up} [N/m^2] generated by a wave impact, exceeds the strength, which is given as a critical uplift pressure p_c [N/m^2]. The uplift pressure due to a wave impact on the slope is assumed to last for a characteristic time t_{imp} [s] and the load during one characteristic impact time is assumed to be constant; waves are modelled as block impacts over time. The rate of erosion is determined by the erosion parameter E_p [kg/m^{2}s], which is inversely proportional to the strength of the grass cover. The strength term p_c and the erosion parameter E_p are based on a wave overtopping erosion model by Hoffmans et al. (2009).

The WIPE model was calibrated and verified with the data of the EroGRASS experiments. The erosion observations during and after the test were used as a basis for calibration. Aggregate erosion started to play a role in the erosion process during the tests with a significant wave height of 0.90 m.
During the tests also several cases of block erosion were observed; two of these were suitable for a calibration run. The depth of the scour holes varied between 0.07-0.10m, whereas the equivalent block diameter varied between 0.08-0.48 m. Both eroded sections were adjacent to a joint and also worms were found at the surface of the erosion holes, which may have weakened the grass cover locally.
For aggregate erosion the model was calibrated using only the factor α_{soil} [-], which is included in the erosion parameter. The model behavior resembled the observed progression of aggregate erosion during the experiments. Therefore the WIPE model is considered suitable for the prediction of aggregate erosion of a good quality grass cover. Yet for low root densities excessive erosion rates are predicted since the critical uplift pressure is dominated by the grass strength. Therefore a critical erosion depth was introduced, which is defined as the depth where root density equals the root density of very poor quality grass cover (RAR =0.0002).
Besides the introduction of the critical depth it is expected that more adaptations will be required to make the model more compatible for the prediction of erosion of grass covers of various qualities; for low root densities flow velocities will start to play role in the erosion process.
For block erosion the model was calibrated using the factor α_{soil}, which can be regarded as a parameter that determines the moment of block erosion and the crack growth parameter α_{crack}, which determines the size of the eroded block. As the model was calibrated on merely two characteristic block erosion events, universal calibration factors for block erosion could unfortunately not be found. To obtain more reliable and uniform results for block erosion more data is required.
It is also noted that due to the diminishing strength of the grass cover with depth the chronological order of wave impacts is an important factor in the erosion process and complicates the prediction of erosion of grass covers.
For the model to be applicable in practice it is first of all essential to improve the relation given by Führböter between wave characteristics, the geometry of the dike and impact pressures. This could also include developing a relation between the number of waves and the number of wave impacts.
Furthermore it is desirable to perform additional studies on the strength characteristics of grass and clay. Of particular interest are the root diameter distribution of the grass, a more accurate soil aggregate diameter distribution and describing the soil structure development process.
Moreover it is important to check if there are significant differences between the grass characteristics of different species on several types of dikes. Ideally grass dikes should be categorized and guideline values should be formulated for grass on each of these types of dikes.
When new full scale experiments on the erosion of grass are carried out the calibration of the WIPE model could be improved with the results. As the erosion process was strongly affected by weak locations and irregularities, the installation method of the grass cover should be improved if possible.
A potential improvement for the installation could be to close off part of the wave flume and to assign this space to a dike model with a grass cover, in such a way that the grass cover is given sufficient time to recover from the installation. This area should preferably be outside to allow the grass to grow as it would on a real dike.
Alternatively a device similar to the wave overtopping simulator could be developed to carry out experiments in the field, which has the great benefit that there will be no need to excavate, transport and install the grass sods.
The results of this research could contribute to the development of new design guidelines and the improvement of the assessment guidelines in the future.

Table of contents

List of figures

List of tables

1 Introduction and objective

1.1 General introduction

1.1.1 VTV and SBW

1.1.2 Grass

1.1.3 EroGRASS

1.2 Problem analysis

1.2.1 Problem definition

1.2.2 Objective

1.2.3 Limitations

1.3 Methodology

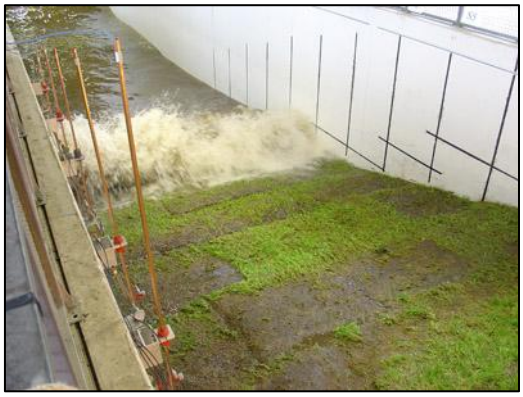

1 Introduction and objective

In this chapter the objectives of this MSc-thesis are given. Section 1.1 gives a general introduction of dikes in the Netherlands and treats the application of grass as a dike cover including the research programs that focus on this matter. Subsequently in section 1.2 the problem is discussed and defined, which eventually leads to the purpose and the objectives of this study. The chapter is concluded with section 1.3 where the methodology to reach these objectives and the structure of the report are explained.

1.1 General introduction

The Netherlands has a long tradition of living with water, from the Middle Ages up until now our country has been in a constant struggle with the sea to keep our feet dry. As the population increased the economical advantage of living in the lower lying areas near water ways and the delta downstream of these rivers became greater and these areas started to be used more intensively. Dikes were constructed and with the development of drainage techniques the creation of polders became possible. Unfortunately the drainage of the polders also caused subsidence of the land resulting in the construction of more dikes. This constant subsidence combined with a rising sea level is the cause that a large part of the Netherlands is lying below sea level nowadays.
Constant monitoring of the sea and the flood defences is required to guarantee high safety levels. Yet no matter how hard one tries flood disasters can never be completely excluded. The storm surge disaster in 1953 painfully illustrated this; dikes are never completely safe and the prevention of flooding during extreme circumstances is not always possible.
After this disaster the delta plan was carried out and five decades later the delta works were completed, providing safety against flooding at a very high standard. Now the hinterland is protected from flooding from the sea, the rivers and the lakes by dunes, dikes and structures; together these form the primary flood defence system.
For the moment this flood defence system protects the Netherlands from flooding, with a sufficiently high safety standard. It is however anticipated that the sea levels will rise and river discharges will increase in the future as a results of climate change. In addition to this the population keeps growing and the risks for flooding therefore gradually increase.
In the future there will thus be a need for improvement of the flood defence system to prevent events such as the storm surge disaster in 1953 and the river flooding in the 90's from happening again.

1.1.1 VTV and SBW

As of 1996 it is required by law that all primary water defences are assessed on safety every five years to verify if they still satisfy the legal requirements. The safety assessments are performed by dike managers using criteria in the Voorschrift Toetsen Veiligheid 2006 (VTV 2006), guidelines which are issued by Rijkswaterstaat (Directorate-General of Transport, Public Works and Water Management) every five years.
To obtain test results that reflect the actual situation in the best possible way it is essential to know what loads have to be absorbed by the dike and whether the dike has sufficient strength to resist these loads. The SBW project (Sterkte & Belastingen Waterkeringen) performs research on these topics and the results of these investigations are used to improve the models and guidelines for strength and loads. In the end these are used once again to draw up the improved safety assessment guidelines for the next VTV.

1.1.2 Grass

Improving the existing dikes could be done by raising them and applying traditional heavy revetment types such as placed concrete block revetments (pitched revetments) or asphalt, but alternative solutions are being investigated. These days there is a growing interest in grass as a dike cover because it is a cheap and a sustainable dike protection; moreover, a green dike is to be preferred from an aesthetic point of view over a solid revetment as it is a more gradual transition between the natural waters and the hinterland.
The application of grass revetments could be a feasible alternative in certain cases as it appeared in

2007, during full scale overtopping tests carried out within the framework of ComCoast [Akkerman, Gerven et al. 2007], that a grass cover is stronger than previously has been expected. This observation has been confirmed during the many overtopping tests that have been carried out within the SBW program since.
Many river dikes have a grass cover and on traditional dikes with a stone revetment, grass is usually applied in the higher part of the wave run-up zone already. When the wave climate becomes more severe and the wave impact zone shifts upwards to the grass cover zone as a result of climate change, the question remains if the grass cover will be able to absorb the wave energy. Also due to the more severe conditions, overtopping discharges will increase; the grassed inner slope is then exposed to greater flow loads and the overtopped water will have to be discharged or stored temporarily.
If it can be proven that, even during these new conditions, grass is a reliable dike cover material and thus has sufficient strength to withstand the loadings on both inner and outer slope, an upgrade of the dike could be less drastic or will even be redundant. Instead of raising and adapting the present (traditional) dikes to cope with climate change and rising sea levels, the dikes will then have to be upgraded only slightly or in the best case; not at all.
Research on the strength of grass against additional wave overtopping loads is carried out within the SBW program. This research is part of the SBW program as well but will, conversely, focus solely on the loads on and the strength of the outer slope of the dike.
Obtaining a good quality grass cover is difficult however. The development of the root system of grass is dependent on the clay quality and simultaneously the clay quality has an influence on the root development of the grass. At the moment there is a hiatus in the knowledge on the strength of grass covers on especially the outer slope. As a consequence the assessments methods in the VTV for sea and river dikes with a grass cover will have to be improved. Therefore a subproject has recently been launched in the SBW program called "Gras golfklap" ("Grass wave impact") with the objective to develop a method for the designing and testing of grass covers in the wave impact zone. There have been some wave impact tests on grass sods in the past, but not enough data was available to draw firm conclusions. Besides SBW there are other projects such as FLOODsite and EroGRASS that aim for innovation of coastal protection and improvement of the knowledge on water defences, including also grass cover layers. These are briefly dealt with in the next sections.

1.1.3 EroGRASS

Recently large scale tests have been performed in the Große WellenKanal (Large Wave Flume) in Hannover for both EroGRASS and FLOODsite. The main objectives of the EroGRASS project were to perform large scale model tests to investigate in detail the failure of grass cover layers due to wave impact, wave run-up and run-down flow and wave overtopping anywhere along the dike profile (seaward slope, dike crest and shoreward slope). [Piontkowitz, Verhagen et al. 2009]
The FLOODsite experiments were aimed at improving the knowledge on erosion by wave overtopping, while the EroGRASS project focussed at the loads and erosion development on the outer slope. Hence the obtained data in the EroGRASS experiments could provide valuable information to come to a more accurate description of the erosion process of grass covers and the underlying clay layers on the outer slope.

1.2 Problem analysis

As explained above the benefits of grass as a dike cover could be great, nevertheless there is still much uncertainty about the strength of and the loading on (completely) green dikes. The grass covers of green river dikes may possibly regularly be wrongfully disapproved, because the current assessment guidelines are rather conservative. To be able to ensure sufficient safety when applying (partly) green dikes in the future and to make the assessment guidelines for the primary water defences less conservative more knowledge has to be acquired.
A clear physical understanding of the failure of grass cover layers due to different wave loads is indispensable today, especially against the background of enhanced hydraulic impact due to climate change. Because grass and clay are non-homogeneous materials, quantifying the strength of green dikes is highly complicated. During the past decades the knowledge of these materials has gradually increased and factors influencing their strength have been identified.
Similarly, describing the loads on the outer slope caused by wave attack has been attempted many

times in the past, but with relatively little success. It is still uncertain whether, for the outer slope, the velocity of flowing water on the slope or the shock pressures generated by breaking wave impacts, are governing for the grass erosion or that erosion is caused by a combination of the two. The impact pressures that can occur are difficult to predict. The pressure of a wave impact greatly differs per wave, even for regular waves, let alone for the natural irregular wave patterns. Consequently, predicting erosion due to wave impact alone is very difficult.

1.2.1 Problem definition

Ample research has been done recently to investigate the resistance of grass against overtopping flow velocities on the inner slope, but theories accurately describing the erosion of grass on the outer slope still lack. There are many phenomena involved with the erosion of a grass cover during wave attack; it is a complicated process that has to be investigated more thoroughly.
The few existing models describing the erosion of grass on the outer slope are mostly empirical and have only a small theoretical basis. Especially including the influence of the presence of weak spots in the covering layer, where erosion is usually initiated, in present models has proven to be difficult.
To be able to make reliable predictions of erosion, which could enable the application of green dikes in the future, more knowledge has to be acquired on the erosion process itself but also on the strength properties of the covering material and the loads on the slope.

1.2.2 Objective

This thesis aims to improve the knowledge of the erosion process of grassed outer slopes. The strength of the grass and the loads on the outer slope should be quantified better to be able to predict erosion of the cover layer. The results could contribute to the development of new design guidelines and the improvement of the assessment guidelines in the VTV in the future. The main goal of this thesis is:

To develop a model that describes the initiation of erosion of a grass cover layer on the outer slope by wave attack.

To accomplish this goal several activities can be distinguished:

- To determine the erosion process of a grass cover layer on an outer slope;
- To identify and quantify influencing factors on the erosion process;
- To determine the strength and the spatial variability of the strength of a grass cover layer;
- To determine the load on, and the distribution of the load, along the slope;
- To develop an erosion model for grass covers on the outer slopes;
- To calibrate and verify the erosion model.

1.2.3 Limitations

- Erosion is associated with the initiation of failure; breach development is not considered here;
- The primary concern of this study is the initiation of erosion of the covering layer by wave impact and run-up and run-down flow. Sliding of the turf by high phreatic levels in the dike and infiltration is not investigated;
- Initiation of erosion is defined as erosion until the critical depth or root density has been reached below which ongoing damage occurs for limited wave action;
- Plunging breakers produce the highest impact pressures, all breaking waves are supposed to be of the plunging type unless stated otherwise.

1.3 Methodology

To reach the objective described in section 1.2.2 a theoretical approach is followed. A desk study will be performed resulting in an overview of existing knowledge and relevant research carried out in the past.
Furthermore an analysis of the experiments carried out for the EroGRASS project in the GWK in Hannover in 2008 will be done. These recently performed large scale experiments are a valuable new source of information and will most probably provide new insights in the erosion process of grass by wave loading. With the help of the desk study and the observations a new erosion model will be

proposed. Subsequently this newly derived model will be verified and calibrated with the help of the EroGRASS data. The structure of the report can be summarized as follows:

- Chapter 2: Characteristics grass on dikes: the types of dikes that are entirely or partly protected by a grass cover are briefly discussed. Furthermore the composition of a grass cover is described including the properties of clay. Furthermore the current qualification guidelines in the VTV for the quality of a grass cover are treated;
- Chapter 3: Wave load: breaking waves exert forces on the outer slope of a dike, these forces are briefly introduced. This is followed by a description of the methods to quantify all relevant parameters during wave loading, including the impact pressures and flow velocities;
- Chapter 4: Erosion process: description and schematisation of the erosion process of grass covers on outer slopes;
- Chapter 5: Grass cover strength: modelling the reinforcing effect of grass in soil poses many problems; these are briefly discussed. Furthermore the strength characteristics of grass and clay are treated;
- Chapter 6: Erosion models: description of current grass cover erosion models including a discussion of the possibilities to combine certain aspects of these theories;
- Chapter 7: Derivation erosion model: the derivation of the model for the prediction of erosion of grass covered outer slopes is explained;
- Chapter 8: Calibration and verification: the WIPE model is calibrated on data of the EroGRASS tests and the model behaviour is analyzed;
- Chapter 9: Conclusions and recommendations.

2 Characteristics grass on dikes

2.1 Green dikes

2.2 Structure of a grass cover layer

2.3 Clay as a dike cover

2.3.1 General

2.3.2 Soil structure

2.3.3 Cracks

2.3.4 Permeability

2.4 VTV guidelines grass qualification

2.4.1 Grass cover management and vegetation type

2.4.2 Root density

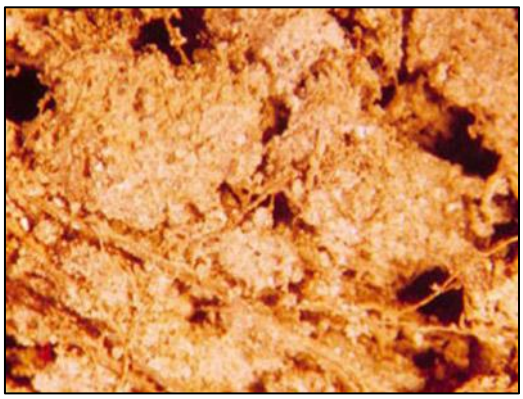

2 Characteristics grass on dikes

Grass on dikes can have several purposes; this chapter focuses on the application of grass as a cover layer to absorb wave induced loads. Which functions the grass cover must fulfil as well as what loads are to be absorbed mainly depends on the type of dike and on its location. Section 2.1 therefore gives an impression of the geometry of several categories of dikes that are fully or partly grass covered. Subsequently the typical composition of a grass cover is discussed in section 2.2. This is followed by a description of the characteristics of clay in dikes in section 2.3, which also includes an introduction on the phenomenon soil structure and the formation of cracks. Finally in section 2.4 the current methods for the qualification of grass covers according to the VTV are briefly dealt with.

2.1 Green dikes

In the Netherlands there are examples of completely green sea dikes (dikes with grass cover and no hard revetment at all) in the provinces of Zeeland and Friesland (Figure 2-1). Yet on many places sea dikes have a revetment, a berm at storm surge level and a grass cover in the wave run-up zone above (the present) storm surge level (Figure 2-2). The slopes of green sea dikes are usually more gentle (1:6–1:8) than the slopes of traditional dikes with a stone revetment.

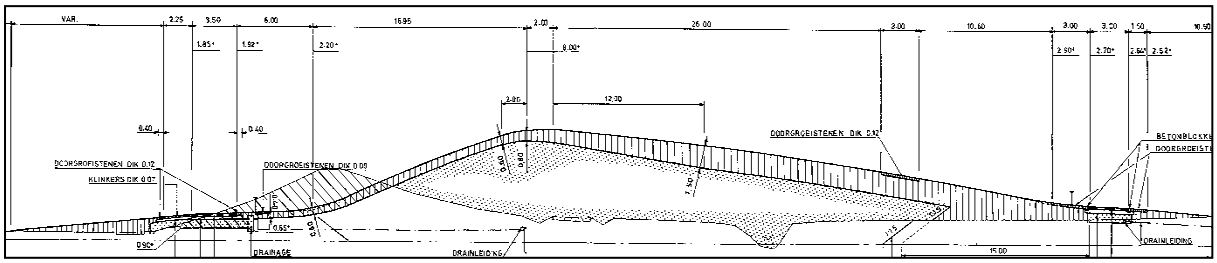

Figure 2-1: Cross section of green Wadden Sea dike at Friesland coast. [WetterskipFryslan 2009]

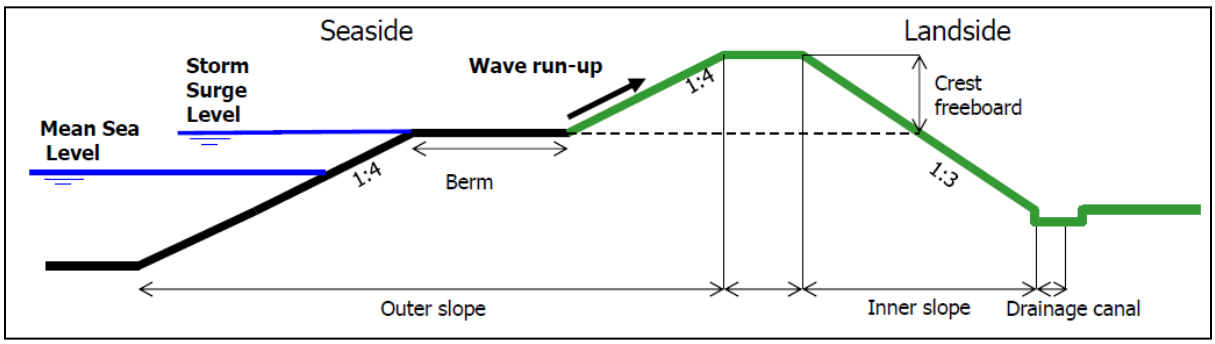

Figure 2-2: Traditional dike with a berm at SSL and a grass cover in the wave run-up zone.

If the wave height is less than 1.6 m, construction of so called green sea dikes or brown sea dikes (with clay cover) is at the moment allowed, according to the former DWW. Also in Denmark and the North of Germany green dikes are frequently applied as a sea defence. Mostly there is an extensive foreland (minimum width of 400 m) present in front of the dikes, which developed over the years due to accretion above the average water level. The transition from the grass dike to the foreland is smooth and the water levels reach the dike only during storms, on average about 20 times per year. During storm surges the wave energy is absorbed by the grass cover but the foreland reduces the wave load on the outer slope.[Muijs and Sprangers 1991]

If a foreland is not present, a rubble layer is placed in the wave loading zone at mean high water. Above this level a maintenance road is located, which also provides protection against overflowing water. Above this road the slope is covered by a grass layer. [Muijs and Sprangers 1991]

Along the rivers completely green dikes occur more frequently than near the sea as the wave load on these dikes is much lower. The grass cover functions as a bank protection and outer slopes of 1:3 can be applied; the inner slopes usually are steep and have a value of 1:3 to 1:2. A schematic overview of such a dike is given in Figure 2-3.

The wave loads induced by shipping are fairly low and a grass cover usually suffices for these waves.

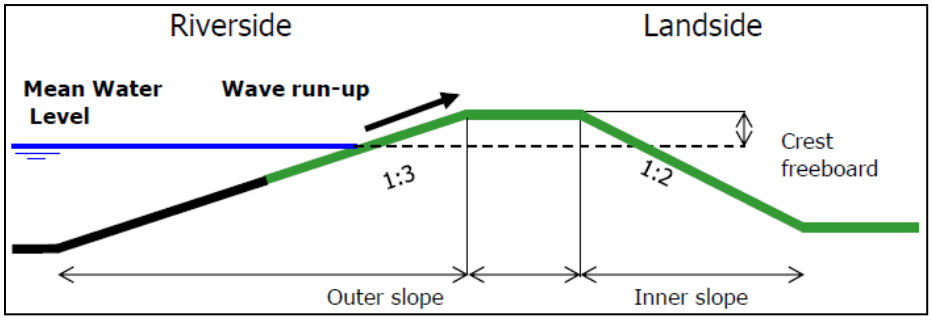

Figure 2-3: Schematic overview of a river dike.

However during high water levels, wind waves can be governing as well and it is expected that this wave load will become more severe in the future. When river discharges increase emergency flood areas will be inundated more frequently and the river will flow in the holms more often as well as a result of projects such as 'Room for the River'. In these temporarily inundated areas and widthways of the river wind induced waves can become more severe as a result of an increased fetch. Ideally the grass covers on the levees around the river should be sufficiently strong to withstand this extra load, but this has to be confirmed.
River dikes can be divided into upper river dikes and tidal river dikes, the upper river dikes are usually sandier than tidal river dikes because of the use of local construction materials. Recent reinforcements of the dikes were carried out with a sand body covered with a clay layer. [de Visser 2007]

2.2 Structure of a grass cover layer

A typical grass cover layer consists of several layers, each with its own characteristics; the various layers are indicated in Figure 2-4. A well developed grass cover is highly erosion resistant; this erosion resistance is partly obtained by the grass sward but mainly caused by the root system.

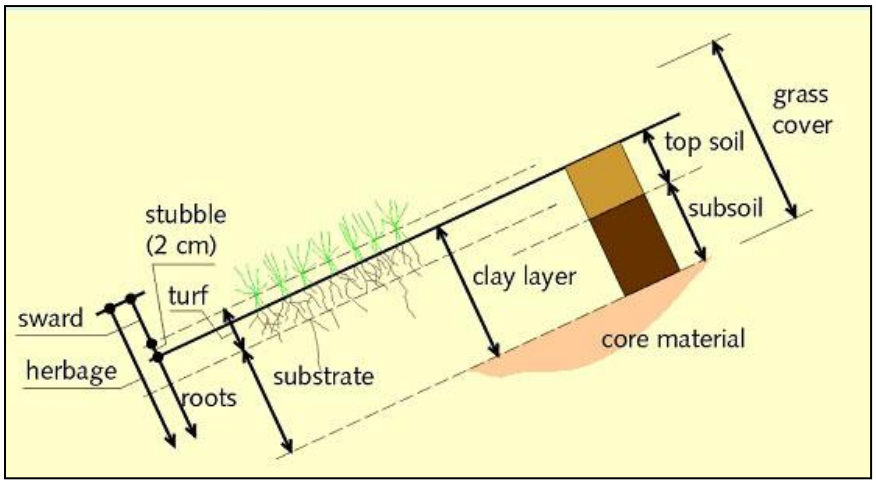

Figure 2-4: Definition sketch of a grass cover layer. [TAW 1997]

The grass leafs add to the resistance against flowing water during wave run-up and run-down as they cover the clay layer providing a sheltered environment for the clay.
The roots penetrate the clay layer causing a soil structure of cracks and aggregates, but at the same time the roots bond the soil together resulting in a tough and flexible layer which has a much higher erosion resistance than bare soil. Apart from the armouring effect of the roots, the roots stimulate chemical processes which develop the cementing substances that are responsible for the bonding forces in the clay. This creates an elastic network which allows a considerable deformation without cracking. Because of this flexibility the grass cover is able to resist wave impacts and the root system prevents soil particles from washing away. The coarser roots penetrate the small and large aggregates of soil; together they form a dense network. Fine root hairs keep the small particles together and anchor the entire grass sod in the substrate. The development of a good quality grass

cover with a well developed root system takes several seasons, on average 4 years. [de Visser 2007]
To develop a root system requires clay with a high sand percentage. In this type of clay roots are developed faster and the root structure has a larger density than in clay with a low sand percentage. To what depth the root system develops is dependent on the type of grass.
However even a rather poor grass cover may be very resistant to surface erosion, but this depends on the clay quality. This was observed during overtopping tests on a poorly developed grass cover at a Groningen sea dike (Delfzijl) [Akkerman et al. 2007]. It was concluded that the poor quality grass was subject to compensating effects; due to the poorly developed root network the quality of the clay was rather good. Vice versa a well developed root system may have a negative influence on the clay quality. The synergy of grass and clay may thus be an important factor for the erosion resistance of the total grass cover; more research should give an explanation of this matter.
Obviously the reinforcing effect of the roots diminishes with depth, thus near the surface the cohesion of the roots is the dominating factor for the strength. As depth increases the root cohesion decreases and at a certain depth the cohesion and friction of the clay become dominating for the strength [Valk 2009].
The three zones of the grass sod that are indicated in Figure 2-4 each have a different erosion resistance and behaviour [TAW 1997]:

- Stubble: consists of loose soil and plant remains. Except for the dead weight of the particles it is assumed to have no strength obtained from clay or root cohesion, it is therefore washed away by run-up and run-down flow relatively quickly.
- Turf: strength is provided by the cohesion of the clay aggregates and the root cohesion. The zone which is directly below the stubble has a high root density which provides additional strength but as depth increases the root cohesion diminishes.
- Substrate: consists of mostly clay and few roots, the strength is thus determined by the clay cohesion and the effect of compaction.

2.3 Clay as a dike cover

2.3.1 General

The term clay can have several definitions, but in civil engineering clay is defined as a cohesive soil that for the major part consists of fine particles with the ability to retain water.
Between the small particles bonding forces are in effect and these forces are large compared to the weight of the particles which causes cohesion. The ability to retain water is caused by the fact that water molecules attach to the surface of the soil particles with relative ease. Also the small pores have a large resistance preventing the transport of water through the clay. Because of this clay usually has a low permeability.
There are many types of clay with various characteristics, the permeability and the shape retention ability can range extensively; clay that has just been excavated differs greatly from clay used for agricultural purposes, even though the particle size distributions of both samples are the same. These differences are mainly caused by external factors such as dehydration and water levels. Because of the properties of clay described above clay is regularly used as a cover layer or as the core of the dike.[TAW 1996] The clay that is used for dikes can be categorized as follows (see also Table 2-1):

- Category 1: Erosion resistant
- Category 2: Moderately erosion resistant clay
- Category 3: Poor erosion resistant clay

To increase erosion resistance, the clay layer is often reinforced by grass revetments; usually vegetation will even spontaneously develop on the clay layer. The interaction between the grass and the clay provides stronger and more durable defence against wave attacks and run-off from overtopping. To have good erosion resistance the clay layer should be divided into two parts during construction. The substrate is the clay layer which is designed to meet civil engineering purposes; well compacted, impermeable, and stiff. The upper layer part should give better aeration and be less compacted in order to allow vegetation to grow, especially in early stages. [TAW 1996]
There seems to be a contradiction in this method since greasy clay is more erosion resistant, while a strong grass sod develops faster on sandier clay with fewer nutrients. For river dikes it is also allowed

to use a single layer of clay of category 2 or higher for both the top layer and the substrate. The stability of the cover layer is increased in this way because the probability that the top layer will slide over the substrate due to poor adhesion is reduced. [Rijkswaterstaat 2008]

Table 2-1: Requirements for the use of clay in dikes. [TAW 1996]

Requirement	*Erosion resistance category*		
	1 Erosion resistant	*2 Moderately erosion resistant*	*3 Poor erosion resistance*
Flow limit w_l Plasticity index I_p Sand content	> 45% and >0.73·(w_l -20) and < 40%	< 45% and > 18 and < 40%	< 0.73·(w_l -20)% and < 18 and > 40%
Water content for working Top layer Core	$I_c \geq 0.75$ $I_c \geq 0.60$	$I_c \geq 0.75$ $I_c \geq 0.60$	$I_c \geq 0.75$ $I_c \geq 0.60$
Organic material content Salt content Chalk content	< 5% < 4g/l < 25%	< 5% < 4g/l < 25%	< 5% < 4g/l < 25%

2.3.2 Soil structure

Because of oscillating water levels and climatic effects clay is frequently exposed to water and has a fluctuating water content which causes shrinkage and swelling. Consequently extensive pores and cracks usually occur in the top part of clay layers. As the boundaries of these cracks are subject to extreme wetting and drying conditions as well more cracks can be formed. As this process continues, the cracks cause the soil to fracture and the soil is broken into small lumps. The formation of cracks and holes in the soil is also induced by biological activities such as the burrowing of animals (worms, insects, moles, mice, etc) and together with the climatic effects these lead to the so called soil structure formation (Figure 2-5).

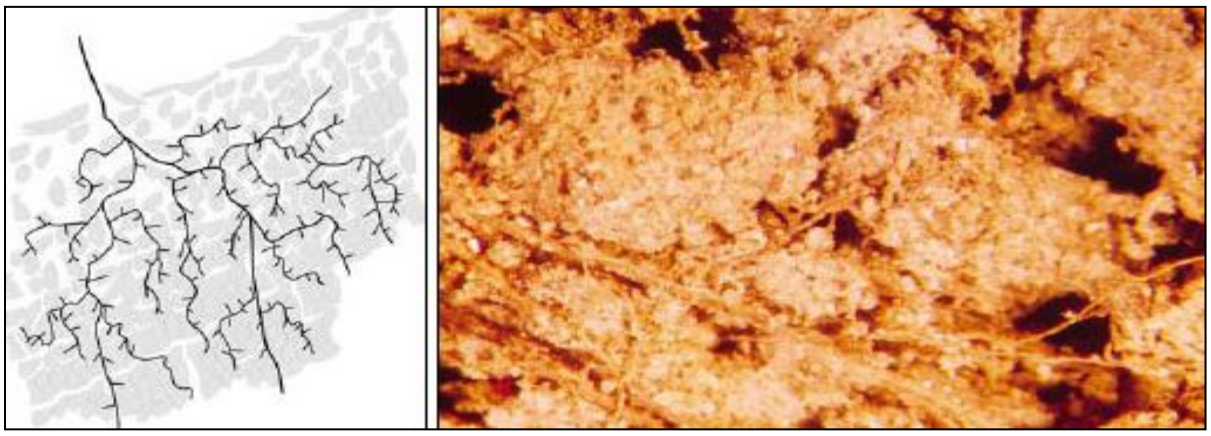

Figure 2-5: Schematic overview soil structure (left) and soil structure in clay (right). [TAW 1996]

The penetrating roots of the grass and other vegetation cause this effect as well but conversely the roots also have a positive influence on the cohesion.
Clay with a soil structure consists of small and large angular lumps of clay or "aggregates", which still have a partly mutual coherence. The aggregates can range from less than 2 mm to as much as 20 cm, the smaller particles are found directly underneath the grass sward. Soil structure limits the resistance of clay against wave loading significantly and decreases with depth. A soil structure develops to a certain depth, depending on:

- Soil-water interactions;
- Atmospheric conditions;

- Time;
- Degree of compaction;
- Way of applying;
- Type of cover layer on top of the clay;
- Thermal stresses;
- Animal behaviour;
- Vegetation;
- Composition of the soil.

[TAW 1996]

2.3.3 Cracks

Cracks are formed constantly in the covering layer, but mostly the formed cracks are small. Quick changes in the water content by for instance rainfall cause small cracks. The formation of these small cracks ultimately results in a fine soil structure in the upper decimetres of the sod [TAW 1996].
In general larger pull cracks are only formed when the soil suddenly shrinks considerably; later when the soil expands again the crack cannot be closed. This is, for instance, the case when clay with high water content is installed above the phreatic level, the water content will diminish until it is in equilibrium with the suction pressure in the vicinity. The result is heavy shrinkage which occurs only once. Due to homogenisation by root penetration and burrowing animals these large pull cracks do not remain long in the upper soil, yet at a few decimetres below the surface the large cracks can remain for years [TAW 1996]. The dense network of roots also prevents larger pull-cracks to occur in the upper regions of the sod.
The above illustrates that the presence of cracks near the surface is greatly affected by moisture content and thus seasonal and weather influences. At the surface many smaller cracks can exist in dry soil by shrinking of the clay during dry periods, but these cracks will eventually close again when the clay expands as a result of increased moisture content in wetter periods. Also clay that is frequently moist by tidal influences cracks less often and develops soil structure only in the upper centimeters to decimeters.
This raises the question whether or not large cracks are present at the surface; in fact there is no satisfying answer to this question. The presence of cracks at the surface varies in time by fluctuating moisture contents during different climatic circumstances. Furthermore large cracks at the surface are usually restructured shortly after they have been formed. The presence of large cracks at the surface of the covering layer is therefore very much dependent on the moment of observation.
In spite of this it is supposed that large cracks are not present at the surface initially, but of course they can reappear during wave loading. At greater depths it is most likely that pull cracks exist though, but the amount of these cracks is rather small.

2.3.4 Permeability

The permeability of compacted clay shortly after application is low; however after a few months soil structure has developed which increases the permeability significantly. This effect is enhanced by the penetration of roots. Holes and cracks as a result of the burrowing of animals can increase the permeability even more [TAW 1999] (Table 2-2).

Table 2-2: Hydraulic permeability of clay. [TAW 1996]

Condition of the clay	*Hydraulic permeability [m/s]*
Directly after construction	10^{-6}
Fine soil structure	10^{-5}
Large cracks and animal tunnels	10^{-4}

Soil structure considerably limits the homogeneity of a clay layer and a network of coarse pores will occur. The properties of a clay layer thus strongly differ from those of individual aggregates.
At greater depths the permeability is generally lower due to compaction, but the occurrence of large cracks and tunnels that deeply penetrate into the dike can increase the permeability of the deeper layers considerably. The permeability of the top layer will almost always lie between 10^{-6} and 10^{-5} m/s for the above reasons. [TAW 1999]

2.4 VTV guidelines grass qualification

The additional strength of the grass cover is obtained by the root system. The VTV 2006 states that there are three methods for the qualification of a grass cover. These methods respectively take into account grass mat management, grass species and root density; they are briefly discussed here.

2.4.1 Grass cover management and vegetation type

The guidelines subscribed by the VTV are specially made for Dutch circumstances as are the qualifications of the management types. The erosion resistance of grass is for a large part determined by the management type. Four types of grass cover management have been defined; these are given in Table 2-3.

Table 2-3: Management specifications for quantification of a grass cover [VTV 2006]:

A	Natural management
B	Adapted agricultural management
C	Intensive agricultural management or regularly and intensively walked upon.
D	Mowing without removal or bad management

It is widely accepted that a good form of management leads to a well-rooted sod because good grassland management ensures a relatively low availability of nutrients. This leads to a great diversity of plant species, both grasses and herbs. Because the plants have difficulty obtaining food, they invest in their root systems. The different plant species each have their own pattern of root growth, which leads to a well-rooted sod. However on the basis of the results of the overtopping test at a Groningen sea dike [Akkerman et al. 2007] the importance of the management form might be questioned. The management form may be less important, but no conclusive evidence has been presented yet.
Management of category A with haying and mowing twice a year or grazing with sheep results in a good quality erosion resistant grass sod. Fertilizers and herbicides are not used in this management type.Management of category B includes grazing with sheep and little fertilizing and results in an average quality grass cover. The density of the grass sod is still high but the thickness and the root penetration in the sod are less than in a good quality grass mat.
Intensive fertilizing and poor maintenance or intensive grazing by horses and cows as in categories C and D yields a poor quality grass mat. Bare spots frequently occur and the root penetration is very limited. Erosion resistance is mainly obtained by the clay in the sod and the substrate. These forms of management are considered not suitable for dikes.
If the management type of the grass mat is unclear or the quality of the grass is doubted then the quality can be assessed by means of the vegetation type. Grass species is an important factor for the characteristics of a root system and by analyzing the different species of vegetation present on the dike, the management type can be determined as they are strongly correlated.[TAW 1999]
In this way the management type is obtained and the quality of the grass can be estimated although for some species the quality also depends on the covering rate.

2.4.2 Root density

Another method to assess the quality of the grass cover is by taking soil samples. Samples for the root density measurement have to be taken with a drill with a diameter of 3 cm on 4 places in a 5 m by 5 m area. Subsequently the sample is divided into pieces of 2.5 cm and the amount of roots in every piece is counted. Roots are defined as clearly visible roots with a length of at least 1 cm. The samples can be categorized according to Table 2-4.

Table 2-4: Root density specifications for quantification of a grass mat. [VTV 2006]

Category	*Root density*
0	Zero roots
1	1 - 5 roots
2	6 - 10 roots
3	11 - 20 roots
4	21 - 40 roots
5	> 40 roots

The measured root density as a function of the depth should be qualified according to Figure 2-6. This optional root investigation has to take place between December and March.

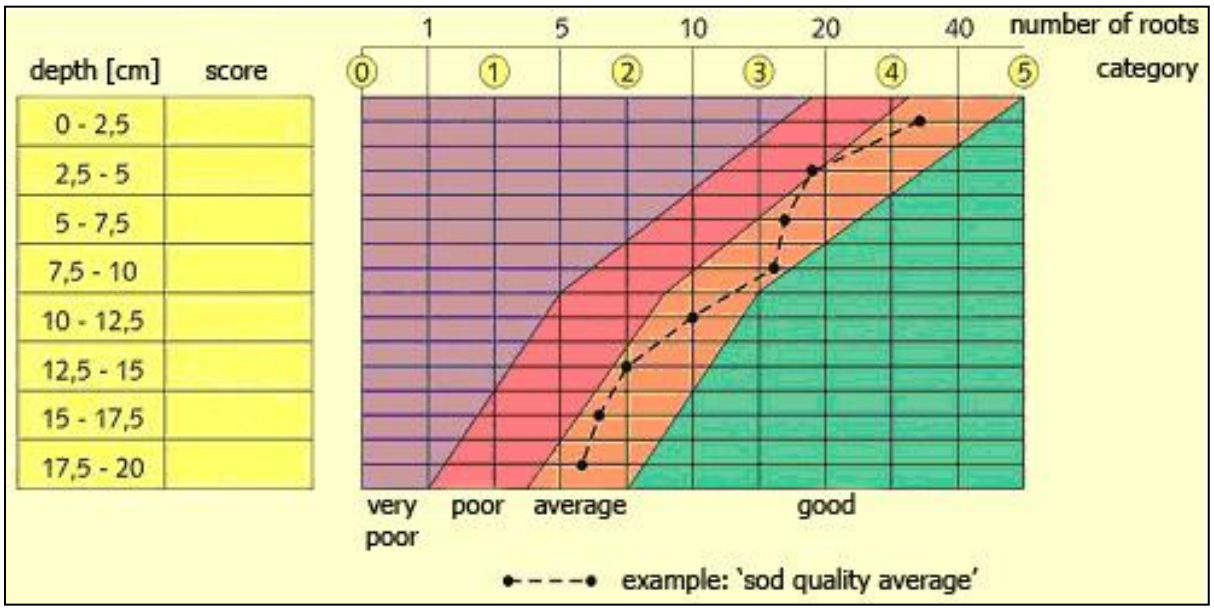

Figure 2-6: Sod quality as function of root density. [modified from: VTV 2006]

3 Wave load

3.1 Breaker type

3.2 Wave loading cycle

3.2.1 Direct impact

3.2.2 Side jetting

3.2.3 Run-up flow

3.2.4 Run-down flow and uplift pressure

3.2.5 Discussion

3.3 Wave impact

3.3.1 Impact pressure

3.3.2 Impact location

3.3.3 Angle of incidence

3.3.4 Spatial pressure distribution

3.4 Wave run-up and run-down

3.4.1 Wave run-up height

3.4.2 Wave run-down height

3.4.3 Wave run-up velocity

3.4.4 Wave run-down velocity

3.4.5 Water layer thickness

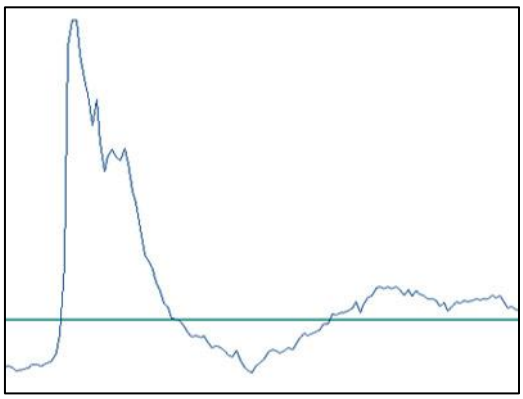

3 Wave load

Wave loading is the subject of this chapter. The type of loading by waves is strongly bound to the breaker type; which will therefore be treated first in section 3.1. Next a qualitative description of the different stages in the wave loading cycle will be given in section 3.2.
Wave impact, run-up and run-down flow are discussed in the subsequent sections 3.3 and 3.4 and the corresponding loads on the slope are quantified. Other loads, such as currents, collisions, floating objects, ice, excavations, etc usually are very exceptional in Dutch circumstances or have less influence and will not be treated.

3.1 Breaker type

The load on the slope is for a large part determined by the way a wave breaks on the slope; the breaker type. The breaker type depends on the surf similarity parameter or Iribarren number which is dependent on the slope and the wave steepness. The Iribarren number ξ_d [-] at the toe of the structure as defined by Battjes (1974) is:

$$\xi_d = \frac{\tan(\alpha)}{\sqrt{H_s / L_0}} \tag{3-1}$$

Where:

ξ_d	= Iribarren number at the toe of the structure	[-]
H_s	= incident significant wave height at the toe of the structure	[m]
L_0	= wave length at deep water	[m]
α	= angle of the seaward slope of the structure	[-]

Surging breakers occur on very steep slopes and are characterized by much reflection. Plunging and collapsing breakers occur on less steep slopes and are characterized by the crest of the wave curling over forward and slamming on the slope. Especially plunging breakers quickly release their energy and consequently this process is very forceful. Plunging waves therefore produce the highest impact pressures.[Führböter and Sparboom 1988] The focus will thus be on plunging breakers in this study.

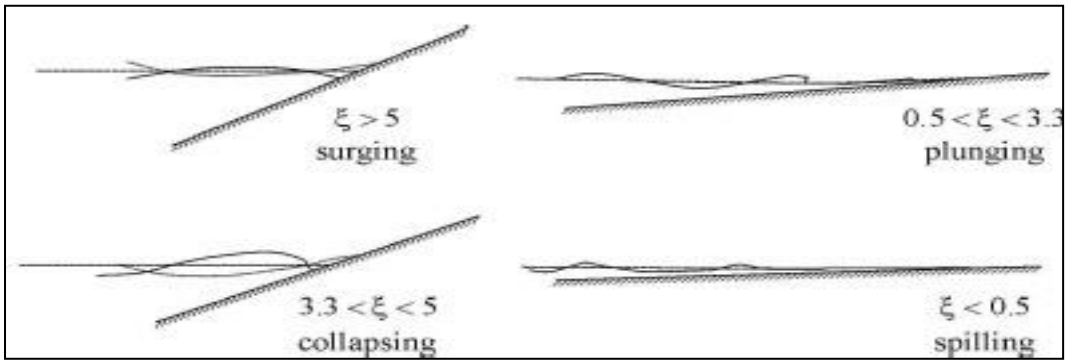

Figure 3-1: Breaker types. [Battjes 1974]

It should be noted that different values of the Iribarren number are used by different authors to describe the breaker type. As depicted in Figure 3-1 plunging breakers are considered to occur for values of ξ_d between 0.5 and 3.3 here.

3.2 Wave loading cycle

The outward slope of a dike is exposed to wave attack; waves that reach the toe of the structure will eventually break and collide on the slope. A large mass of water then impacts on the slope exerting a force on the cover layer. Not all energy will be dissipated in this process however and the water will flow further up the slope until its velocity reaches zero (run-up flow), the wave tongue reverses

direction then and will flow back down the slope (run-down flow). This will cause a shear force on the surface of the slope. The normative load is caused by the wave impacts in the breaker zone and above it by flowing water in the run-up and run-down tongue. This cyclic loading process is described in more detail in the next sections. Currents along the dike are generally not normative for erosion in the Dutch situation, although currents can have an effect on the wave breaking process. Only in exceptional cases the flow velocity can become so high that only a grass cover does not suffice. Because of this currents will not be brought up anymore.

3.2.1 Direct impact

When an incident wave approaches the outer slope of the dike it will break and a large amount of water will collide with the slope. This generates an impact pressure on the grass cover which compresses the covering layer. Also a reaction uplift pressure in the sod is generated shortly after the wave impact, just beneath the point of impact. These pressure variations are very dynamic and are therefore only present for a short period of time, but can be significant in size. At gentle slopes the impact of breaking waves can be attenuated by the layer of water that is present due to wave run-down. For relatively severe wave impacts soil disintegration occurs around the impact area forming cracks in all directions. The permeability of the cover layer is increased by this process.

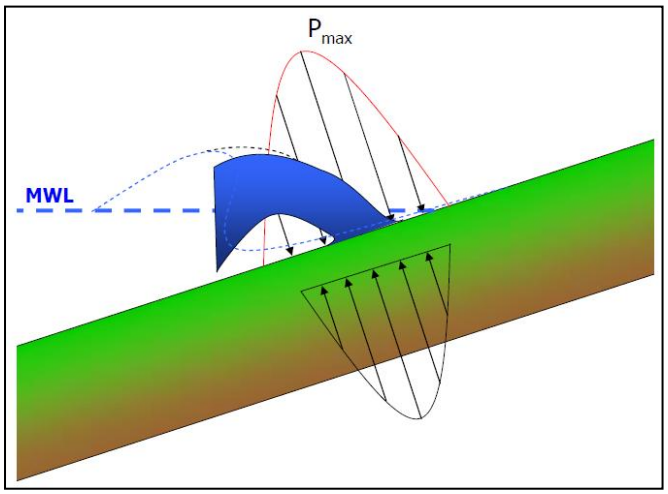

Figure 3-2: Impact pressures and the reaction pressures shortly after the impact.

3.2.2 Side jetting

After the water mass has collided on the slope the water splashes around and will be partly deflected sideways; the water will expand in lateral direction. Splash water and expanding water jets with a velocity that can be several times higher than the impact velocity are present on the slope. [Lesser and Field 1983] High pressures on possible side walls are generated and small particles are eroded easily, speeding up the erosion process.

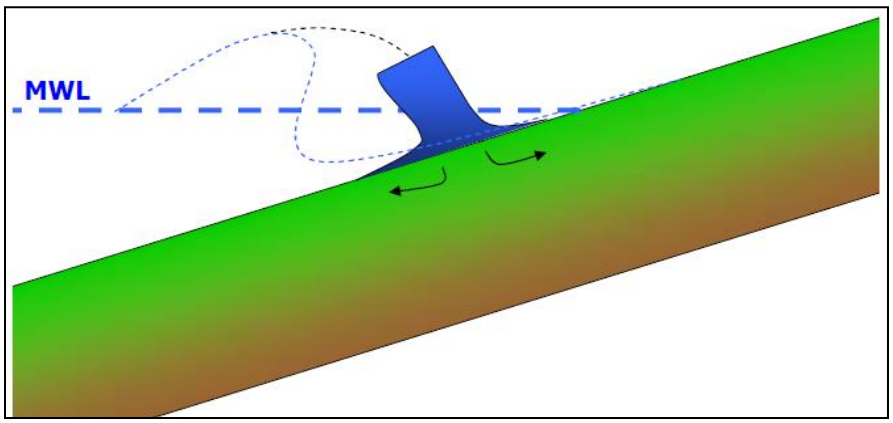

Figure 3-3: Side jetting.

3.2.3 Run-up flow

Part of the deflected water will continue as a water layer rushing up the slope. This run-up water layer still has significant velocity which decays until its run-up height is reached. The flow direction then reverses and the water will flow back down the slope. During both the run-up and run-down phase a shear stress is exerted on the cover layer caused by the flowing water mass. Furthermore pressure fluctuations as a result of turbulence can lift soil aggregates; removal of small pieces occurs when critical shear stresses are exceeded due to drag and lift forces. During wave run-up the wave forces will be directed opposite to gravity forces, whereas wave run-down is driven by the gravity force. However the run-up tongue still has kinetic energy after the wave has broken. Depending on the wave conditions and the slope geometry either the run-up process or the run-down process induces the governing load.

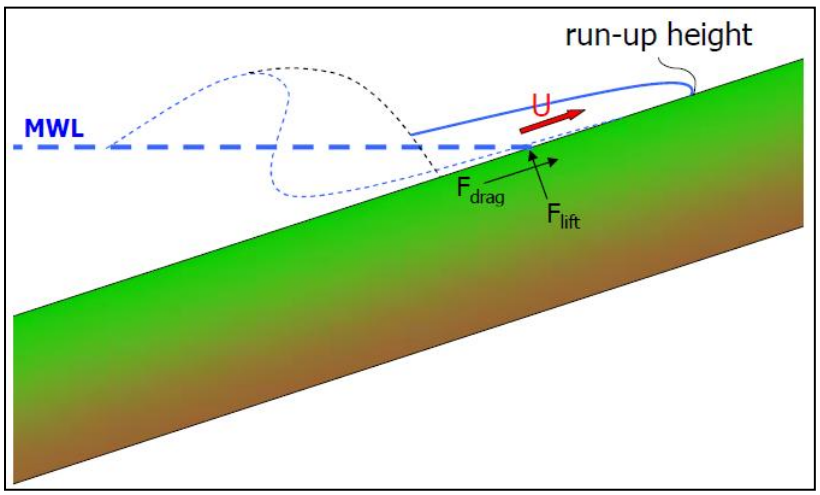

Figure 3-4: Run-up flow causing lift and drag forces.

3.2.4 Run-down flow and uplift pressure

During wave run-down similar forces are present; also here downward flowing water will exert drag and lift forces on the cover layer. In addition to this a decreasing water level coincides with the downward flow gradient which may result in sliding. During maximum wave run-down there will be an incoming wave that a moment later will cause a wave impact. Just before this impact there is a 'wall' of water giving a high pressure under the point of maximum run-down. At the run-down point the grass layer has little water on it and therefore there is a large head difference on this location. This head difference leads to an upward flow in the run-down region which in combination with the run-down flow results in an outward flow and an uplift pressure near the point of maximum wave run-down [Doorn 2007].

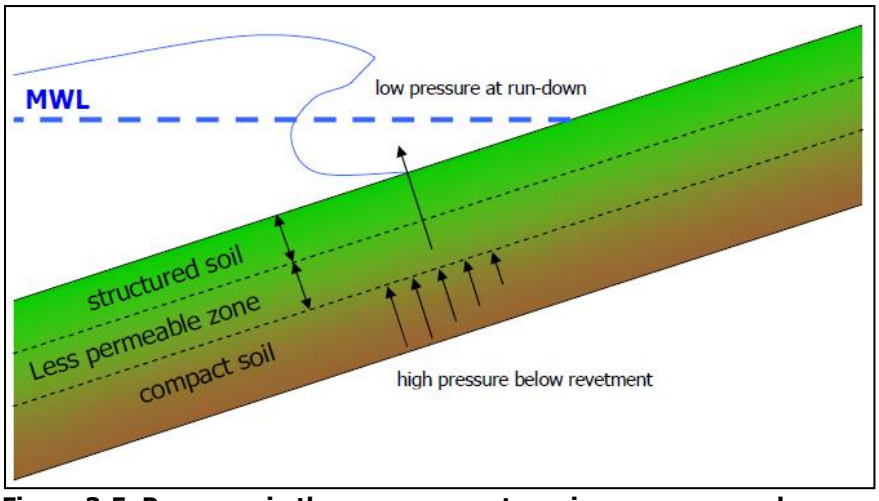

Figure 3-5: Pressures in the grass cover at maximum wave run-down.

This theoretical uplift failure mechanism is mainly important for solid revetments (or pitched block revetments) as the permeability of these cover layers is very low. The permeability of the cover layer is high in the uppermost part of the sod but decreases with depth due to the diminishing effect of soil structure; hence failure by uplift pressures might still occur. Nevertheless this failure mechanism is generally considered irrelevant for grass covers [TAW 1999]; a good quality sod has sufficient strength and flexibility to prevent bursting of the clay.

3.2.5 Discussion

Erosion of a grass cover can be caused by several complicated processes, identifying a governing failure mode and describing the erosion process caused solely by this mechanism is therefore difficult. In the wave impact zone both impact pressures and high flow velocities are present and consequently most erosion occurs here. Further up the slope where the cover layer is subject to only flow velocities erosion is generally less and gradual. Because of this it could be stated that most damage to the grass cover is inflicted by wave impacts and their accompanying impact pressure peaks.
Hence it is assumed that the flowing water in the run-up and run-down tongues merely transports small particles out of the stubble or particles that have been broken loose after fissuring of the clay by an impact. This will be verified in a later stage.
Grass is thus considered not to be significantly damaged by flowing water on the outer slope, unless there is a weak spot in the vicinity. In that particular case grass can be eroded as a result of additional loading or avalanche effects by progressing erosion at the weaker spots. The impact load is considered to be the governing load, however to be able to determine if significant erosion is induced by flow velocities on the outer slope these have to be known as well. Therefore both load types will be discussed in the remaining part of this chapter.

3.3 Wave impact

A desk study on wave impacts on dike slopes is done by van Vledder (1990) who concluded that the forces associated with breaking waves can be divided into two groups. The first group is formed by quasi static pressures that are generated by the wave run-up and run-down on the slope. They are the sum of the hydrostatic water pressure and the pressures caused by the movement on the slope. The second group consists of dynamic forces, which occur only during the impact of the wave within a relative short time in a small area [Witte 1988].
For the dynamic forces three types can be distinguished: quasi static impact pressures, uplift pressures and cyclic shock pressures.

3.3.1 Impact pressure

For plunging and collapsing breakers wave impact pressures can occur when the face of the breaking wave hits the slope or the backwash layer. These pressures can be much higher than the other pressures in the wave breaking process and are of a short duration. The magnitude of the impact pressure is limited by the compressibility of the water and the dissolved air and by the presence of a backwash layer.[van Vledder 1990]
In various studies it is found that the maximum wave impact pressure varies per wave even if the incident waves are regular. A theoretical distribution for maximum impact pressures has therefore been proposed by Führböter in 1966. He suggested a log-normal distribution for the maximum wave impact pressures. This has been confirmed by subsequent studies; for all types of experiments the impact pressures are generally log-normally distributed [Führböter 1986; Witte 1988].
As mentioned above, the air content of the falling water mass greatly affects the magnitude of the impact pressure and Führböter attempted to quantify the air content in an equation for the impact pressure but in the end preferred to use a simpler equation. The most recent and commonly used formula for maximum impact pressure was proposed by Führböter and Sparboom (1988) and is given by equation (3-2):

$$p_{\max,i} = q_i / m \cdot \rho_w g H \qquad (3\text{-}2)$$

Where:

$p_{\max,i}$ = maximum impact pressure not exceeded by i% of the cases. [Pa]

q_i	= impact factor	[-]
m	= front slope 1: m	[-]
ρ_w	= density of water	[kg/m^3]
g	= acceleration of gravity	[m/s^2]
H	= incident wave height	[m]

The decrease of the impact pressure on gentler slopes is the result of the cushioning effect of the water layer that remains after the preceding wave. The thickness of this back-rush water layer increases with gentler slopes so the maximum pressures decrease proportionally.
The maximum value of the impact factor q_i / m for a slope of 1:4 was found to be approximately 6 and for a slope of 1:6 it amounted to 4 [Führböter and Sparboom 1988]. The influence of the wave steepness is however not taken into account in the approach above.
Davidse (2009) performed research on the wave steepness and related the impact factor to the breaker parameter using data from several experiments. This resulted in for example Figure 3-6. On the basis of this figure a maximum value of the impact factor of 8 seems a plausible assumption.

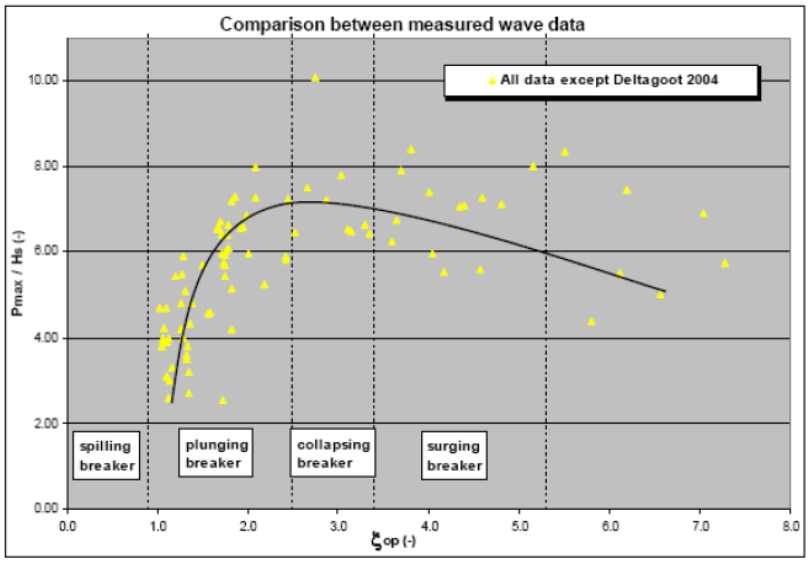

Figure 3-6: Impact factor versus breaker parameter. [Davidse 2009]

The typical time history of a single impact is shown in Figure 3-7; the maximum impact pressure $p_{\max}$ is composed of a quasi static pressure p_1 and a shock pressure p_2 and is defined as the value from the zero level of the pressure cell to the following peak pressure.

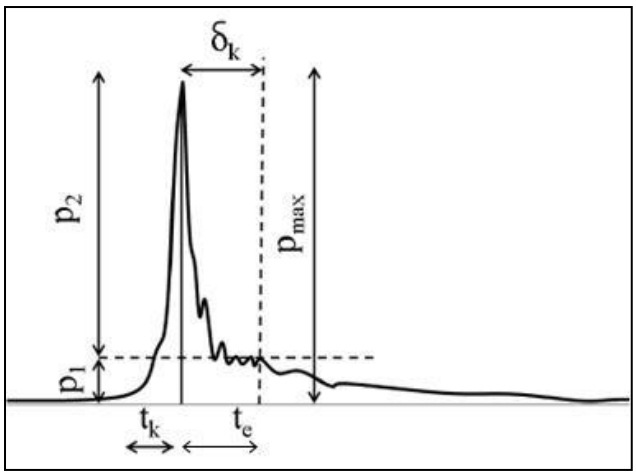

Figure 3-7: Pressure time record during wave impact.

The wave impact can be separated into three time sections. The time needed to reach the maximum pressure is often referred as the compression time or the rise time t_k. Whereas the time needed for the pressure to reduce from the maximum pressure to the quasi-static pressure is often referred to as the expansion time or the fall time t_e. The sum of the compression time and the expansion time is the wave impact duration t_d.

Führböter and Sparboom (1988) found impact durations of 10-200 ms and rising times of 10-60 ms. According to Witte (1988) there seems to be an upper limit to the maximum impact pressure and this limit is inversely proportional to the rising time. In other words: high pressures have very short rise times, while lower pressures are characterized by longer rising times.

After data analysis of wave impact tests on Elastocoast revetments, performed in the GWK in Hannover, a conservative relation was obtained for the rise time t_k.[Oumeraci, Staal et al. 2010] The expression for the normalized rise time for a slope of 1:3 reads:

$$\frac{t_k}{T} = 0.047 \cdot \left(\frac{p_{\max}}{\rho g H_s} \right)^{-0.71} \quad \text{for } 1.6 < \frac{p_{\max}}{\rho g H_s} < 7.5 \tag{3-3}$$

Equation (3-3) gives an upper limit for the rise time for impact on and underneath Elastocoast revetment. Contrary to the rise time, the impact duration t_d has the tendency to increase with increasing impact factor; the following relation was proposed [Oumeraci et al. 2010]:

$$\frac{t_d}{t_k} = 6.2 + 2.7 \tanh\left(\frac{p_{\max}}{\rho g H_s} - 4.5 \right) \quad \text{for } 1.6 < \frac{p_{\max}}{\rho g H_s} < 7.5 \tag{3-4}$$

Where it is suggested that the ratio t_d / t_k must exceed 2.0 (rise time and fall time are identical) and should be not much larger than 12.0 [Oumeraci et al. 2010]

3.3.2 Impact location

Van Vledder (1990) concluded in a desk study that the maximum wave impact pressures occur at about half the wave height below the still water level and that the size of the impact area is approximately half the wave height. Yet an exact definition of the size of the impact zone cannot be given. This is due to the fact that the face of the impinging tongue of the plunging breaker has a high concentration of air pockets, hence it deforms very quickly during the impact process. Even for regular waves these are random processes because the instabilities at the breaking point are influenced by the highly turbulent water-air mixture produced by the preceding breaker. [Führböter 1986]

Later Schüttrumpf (2001) was able to give a better approximation of the impact point. The location of the wave impact on the slope is a function of the surf similarity parameter at the toe of the structure. It can be approximated, for regular as well as irregular waves, with the following formula:

$$\frac{Z_{imp}}{H_s} = 0.8 + 0.6 \tanh\left(\xi_d - 2.1 \right) \tag{3-5}$$

Where:

Z_{imp} = vertical distance below Mean Water Level (MWL) of impact point [m]

For regular waves the location of impact is more or less at a fixed position. For random waves, however, this position varies significantly.

3.3.3 Angle of incidence

To estimate the angle of incidence of a plunging breaker on the outer slope Führboter (1966) [source: Stanczak 2008a] developed a simple equation. The angle of incidence is given in Figure 3-8.

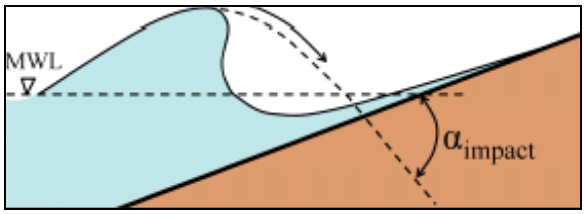

Figure 3-8: angle of incidence of a breaking wave. [Führböter 1966; source: Stanczak 2008a]

$$\alpha_{imp} = \arctan\left(\frac{1+\cot\alpha \cdot f(\alpha)}{\cot\alpha - f(\alpha)}\right) \tag{3-6}$$

And:

$$f(\alpha) = \frac{\sqrt{1+2\cot^2\alpha}-1}{\cot\alpha} \tag{3-7}$$

Where:

α_{imp}	= angle of incidence of a breaking wave on the outer slope	[-]
α	= outer slope angle	[-]

3.3.4 Spatial pressure distribution

The distribution of wave impact pressures was investigated in 1983 by Stive [source: Stanczak 2008a]. The results of large scale model tests were used to derive an equation for the spatial distribution of the pressures on the slope. The parameters involved are depicted in Figure 3-9.

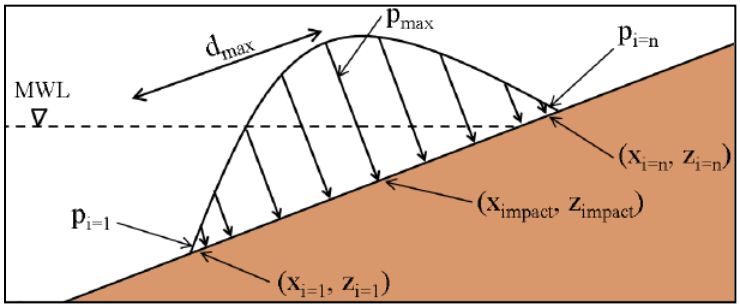

Figure 3-9: Impact pressure distribution on the dike slope. [Stanczak 2008a]

This approach is strongly simplified but gives a deterministic description of the spatial distribution of the impact pressures. The pressure at an arbitrary point p_i on the slope can be determined with equation (3-8).

$$p_i = \left[-\frac{2.75}{H^2}\cdot\left((z_i - z_{imp})^2 + (x_i - x_{imp})^2\right)+1\right]\cdot p_{max} \tag{3-8}$$

Where:

z_i	= z coordinate of the i-th point	[m]
x_i	= x coordinate of the i-th point	[m]
z_{imp}	= $MWL - Z_{imp}$	[m]
x_{imp}	= $z_{impact} / \tan\alpha$	[m]

To avoid negative pressures for a distance from the impact point larger than $d_{\max}$ the following limits were introduced:

$$d_i = d_i \text{ for } |d_i| < d_{\max}$$
$$d_i = 0 \text{ for } |d_i| \geq d_{\max}$$

With: $d_{\max} = \frac{H}{\sqrt{2.75}}$ [m]

In TAW (2003) another method is reported; for wave impacts on asphalt revetments the wave impact pressure can be represented by a triangular shape. The width of the impact load is established to be equal to the significant wave height H_s. The calculation of $p_{\max}$ is done according to the method of Führböter.

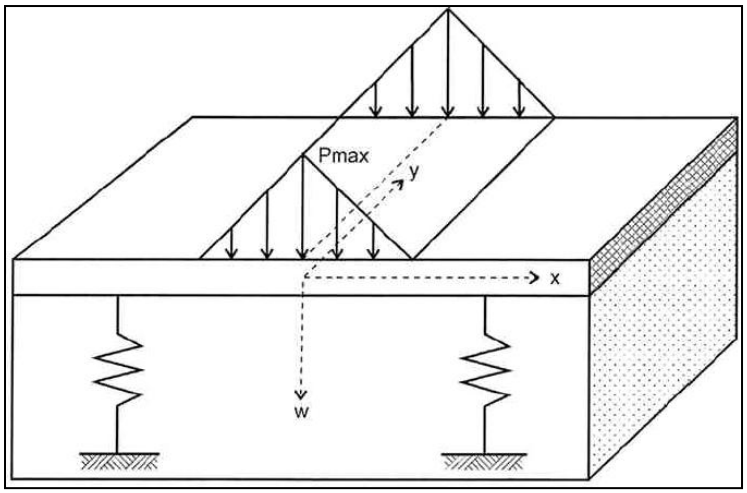

Figure 3-10: Triangular impact pressure distribution. [TAW 2003]

3.4 Wave run-up and run-down

After wave impact the wave tongue will run up the outer slope until it reaches the crest or its velocity reaches zero. To be able to predict erosion it is necessary to quantify the flow velocity. The run-up velocity is related to for instance the wave height and the geometry of the dike. Several methods exist to estimate the velocity of the run-up layer at a certain point; the most recent method was given by Schüttrumpf (2001).

3.4.1 Wave run-up height

After the tongue of the breaking wave has collided on the slope the run-up flow will occur up to a certain height, the run-up height $R_{u,i\%}$. According to Schüttrumpf (2001) the run-up height for both plunging as well as surging breakers can generally be calculated as:

$$\frac{R_{u,i\%}}{H} = c_{1,i} \cdot \tanh\left(c_{1,i}^{*} \cdot \xi_d\right) \quad (3\text{-}9)$$

The coefficients for the maximum run-up height exceeded by i% of the waves are given in Table 3-1.

Table 3-1: Wave run-up coefficients. [Schüttrumpf 2001]

Wave type	*Run-up height* R_i	c_1	c_1^*
Wave spectra	$R_{u,2\%}$	3.0	0.65
Wave spectra	$R_{u,50\%}$	2.25	0.5
Regular waves	R_u	2.25	0.5

3.4.2 Wave run-down height

For plunging breakers the tongue of the breaking wave hits the water layer that remains after the preceding wave. Strong turbulence and thus energy dissipation occurs during this process which reduces the wave run-up height. Wave run-down levels above MWL are observed (Figure 3-11).

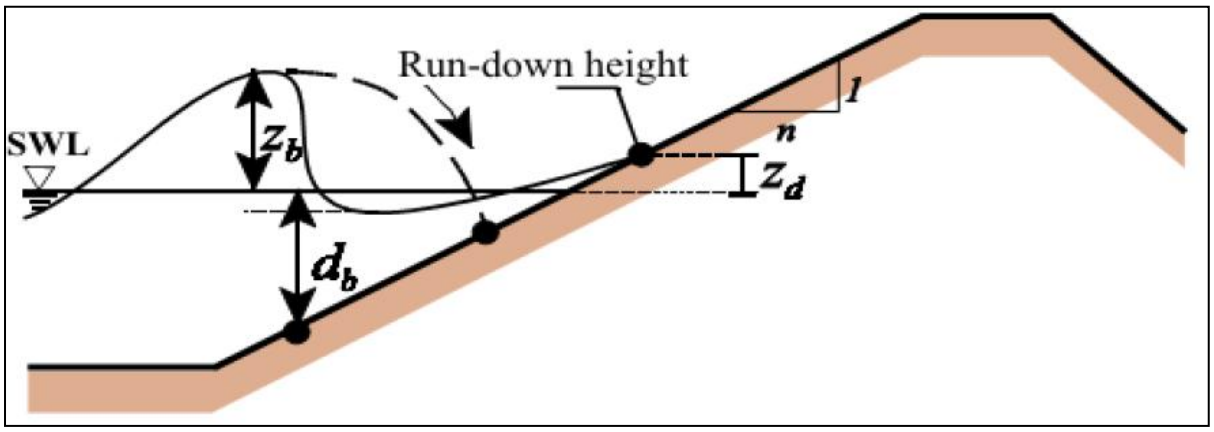

Figure 3-11: Wave run-down height. [Schüttrumpf 2001]

Schüttrumpf (2001) proposed the following equation to predict the run-down height Z_d :

$$\frac{Z_d}{H_s} = 0.7 + 0.7\tanh\left(\xi_d - 2.1\right) \tag{3-10}$$

This gives for the reference level of run-down z_d :

$$z_d = MWL + Z_d \tag{3-11}$$

3.4.3 Wave run-up velocity

According to Schüttrumpf and Oumeraci [Schüttrumpf 2001] the wave run-up velocity u_u [m/s] is defined as the maximum velocity that occurs during wave run-up on any position z_a above MWL on the seaward slope. The wave run-up velocity of regular waves can be derived from a simplified energy equation and is given by equation (3-12), provided that overtopping occurs.

$$u_u = 0.75 \cdot m \cdot \xi_d \sqrt{\frac{\left(R_u - z_a\right)}{H}} \cdot \left(\frac{\pi \cdot H}{T}\right) \tag{3-12}$$

For wave spectra the run-up velocity u_u , the wave height H , the wave period T and the run-up height R_u in equation (3-12) are replaced by respectively $u_{u,50}$, H_s , T_m and $R_{u,2\%}$.

3.4.4 Wave run-down velocity

After model tests on a smooth slope of 1:3 in the Delta flume van der Meer and Klein Breteler (1990) state that the wave run-down velocity is in fact not dependent on the wave height and period, but merely on the run-up level and the location on the slope. The run-down velocity u_d [m/s] is given by [van der Meer and Klein-Breteler 1990]:

$$u_d = 1.1\sqrt{gR_u} \cdot \sqrt{(1 - z_a / R_u)} \tag{3-13}$$

For: $z_a / R_u > -0.4$

And

$$u_d = 0.18 \cdot \sqrt{gH} \cdot (z_a / R_u)^{-2.3} \qquad (3\text{-}14)$$

For: $z_a / R_u < -0.4$

3.4.5 Water layer thickness

Under the assumption that the layer thickness h [m] linearly decreases from MWL with the horizontal run-up length x_z [m] the layer thickness during wave run-up on an arbitrary location x_a on the outer slope for plunging breakers is given by equation (3-15) [Schüttrumpf 2001]:

$$\frac{h(x_a)}{x_z} = c_2\left(1 - \frac{x_a}{x_z}\right) = c_2\left(1 - \frac{x_a}{c_3\sqrt{H \cdot L_0}}\right) \qquad (3\text{-}15)$$

Where:

h	= layer thickness	[m]
x_z	= horizontal run-up length $x_z = c_1\sqrt{H \cdot L_0}$	[m]
x_a	= horizontal coordinate with $x_a = 0$ at MWL	[m]
c_2	= layer thickness coefficient (Table 3-2)	[-]
c_3	= run-up coefficient (1.5 for wave spectra, 1.0 for regular waves)	[-]

The layer thickness coefficients are displayed in Table 3-2. Furthermore equation (3-15) can be simplified by introducing a new parameter; the residual run-up length x_*:

$$h_a(x_*) = c_2(x_z - x_a) = c_2 \cdot x_* \qquad (3\text{-}16)$$

Where:

$c_* = c_2 \cdot n$ =constant

Table 3-2: Layer thickness coefficients for two different slopes. [Schüttrumpf 2001]

Wave type	*Layer thickness*	c_2 *for slope 1:4*	c_2 *for slope 1:6*
Wave spectra	$h_{A,2\%}$	0.054	0.035
Wave spectra	$h_{A,50}$	0.042	0.028
Regular waves	h_A	0.071	0.047

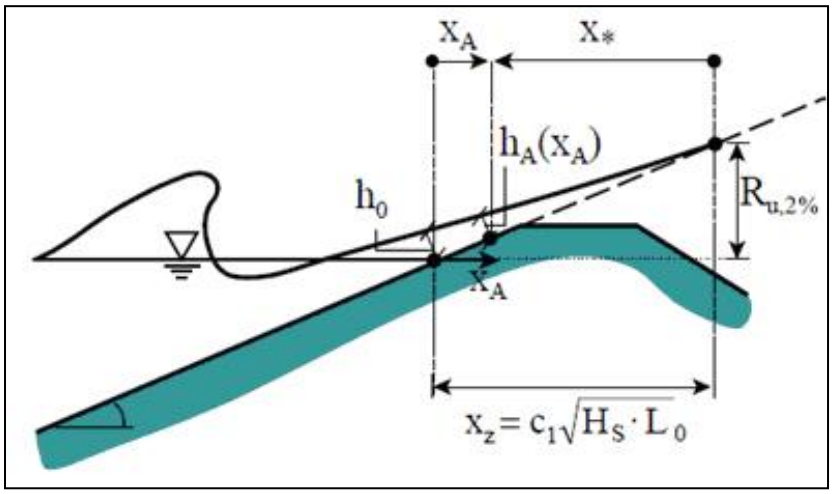

Figure 3-12: Water layer thickness definition sketch. [modified from: Schüttrumpf 2005]

4 Erosion process

4.1 General

4.2 Outer slope erosion

4.2.1 Failure tree

4.2.2 Compression and the apparition of local failures

4.2.3 Increase of permeability and erosion of small pieces

4.2.4 Formation of scour hole and side walls

4.2.5 Block erosion

4.2.6 Initiation of erosion

4.3 Discussion and conclusions

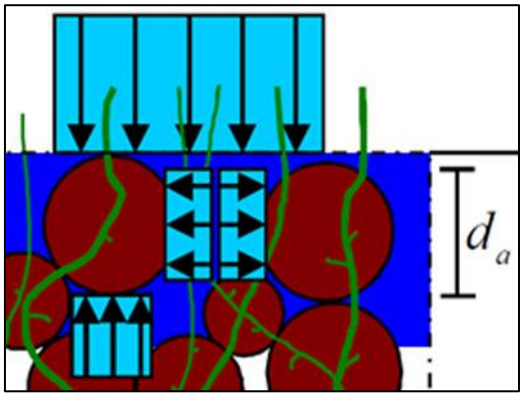

4 Erosion process

A good description of the erosion process is essential before an erosion model for the outer slope can be proposed. The chapter starts with a short introduction on the failure mechanisms of a dike in section 4.1. Subsequently section 4.2 treats the failure mechanism outer slope erosion. The failure mechanisms for outer slope erosion of grass covers are discussed and a thorough description of the erosion process is given. Finally in section 4.3 the chapter ends with discussion and conclusions.

4.1 General

If a structure cannot fulfil one of its functions anymore it is considered to be failing even when most of the geometry has remained the same; it has not collapsed yet. One can speak of collapse of the structure when a large scale change in geometry or an overall loss of coherence has occurred.
A dike can have many different failure mechanisms, the most important ones are displayed in Figure 4-1. The focus of this thesis is the erosion of the outer slope, i.e. the covering layer and the sub layers (indicated with H in Figure 4-1). Obviously this failure mechanism can trigger other mechanisms such as sliding of the outer slope. This can eventually lead to collapse of the structure but this is considered beyond the scope of this research and hence is not reported here.

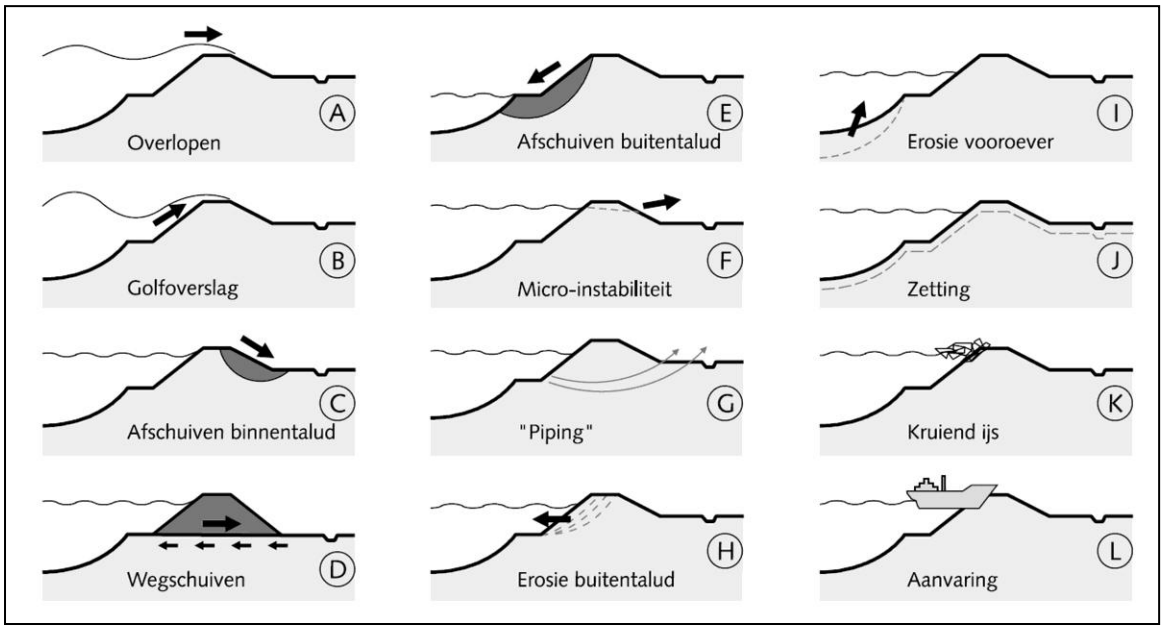

Figure 4-1: Failure mechanisms of a dike. [TAW 1998]

4.2 Outer slope erosion

Clay is a cohesive material and the critical velocity of cohesive materials is higher than of non-cohesive materials. However, contrary to the transport of small individual particles of non-cohesive materials, in clay bigger aggregates can be transported. Furthermore several erosion zones can be identified, each with different erosion behaviour (see also appendix C).
Yet the erosion of grass covers is different from the erosion of bare clay as the grass provides additional strength. The density of the root system and the covering rate influence the erosion rate. Due to the variability of the grass cover layer, bare spots could limit the strength of a grassed slope [van den Bos 2006].
According to results of Delft Cluster in 2002 [source: Valk 2009] the stability of the clay depends on, among others, the following factors:

- Soil structure
- Density
- Percentage clay/sand
- Salinity of the ground and the water

- Humidity of the ground
- Clay mineral structure
- Na+ density
- Organic material
- Other elements (Fe,Al)
- Temperature

For grass covers six failure mechanisms are distinguished in the VTV 2006 which separately or in combination can lead to exposure of the core of the dike:

1. Washing away of small soil particles and small slumps from the roots. If this leads to gradual erosion concerning a large surface, then generally this is not considered as damage. This mechanism can however also lead to such ground displacements that the cover layer becomes uneven or vegetation is disturbed;
2. Sudden washing away of large aggregates as a result of water pressure differences between the cavities and cracks in the substrate and the outside water. Inconsistencies in the covering layer enhance these pressure differences;
3. Breaking up of the sod due to strong local erosion;
4. Breaking up or coiling up of the sod by wave effects or currents when a large hole is present in the vicinity.
5. Erosion of substrate of clay after the grass sod has disappeared (the residual strength);
6. Sliding of the grass sod along a shear plane through the substrate as a result of saturation of the soil and groundwater flow.

The fifth mechanism concerns erosion of the clay substrate, which occurs only when the grass cover has already been damaged severely. It is thus not related to the erosion of the dense root system above the substrate. The sixth concerns shear failure along a slip plane such as shallow slip failures, which are often accompanied by uplift as a result of strong seepage flow. When sliding occurs, it mostly involves failure of the total impermeable clay layer, rather than sliding of the grass cover layer. This category is therefore not considered either in this research and will not be given much attention.
However the first four of these erosion mechanisms concern failure due to wave impact, wave run-up, wave overtopping or flow, which could all be relevant for outer slope erosion. Since mechanism 3 and 4 will occur after an erosion hole has already developed they are not of primary interest though. These are avalanche mechanisms and will thus not trigger the initiation of erosion.
However mechanism 1: washing away of small particles and lumps from the roots and mechanism 2: suddenly washing away of large aggregates can initiate erosion and are of primary concern in this research. The washing away of small particles and lumps from the roots (aggregates) will from now be referred to as aggregate erosion, whereas mechanism 2: sudden failure of large blocks due to pressure differences will be called block erosion in the rest of this research. Both erosion types are displayed in Figure 4-2.

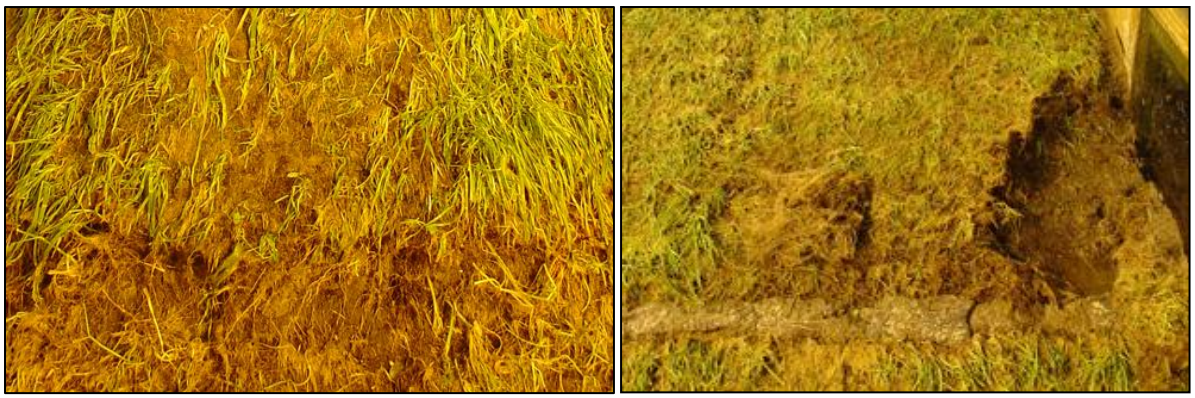

Figure 4-2: Aggregate erosion (left) and block erosion (right) during the EroGRASS experiments.

These mechanisms can be triggered during wave impact or by flowing run-up and run-down water. During the wave impact several processes can be distinguished (Figure 4-3) that can cause erosion:

A Direct hit of shock pressures;
B Splash water around the impact area that can erode the surface with very high velocity;
C Wave run-up and run-down velocities that continuously cause erosion over the surface;
D Uplift forces during wave run-down.

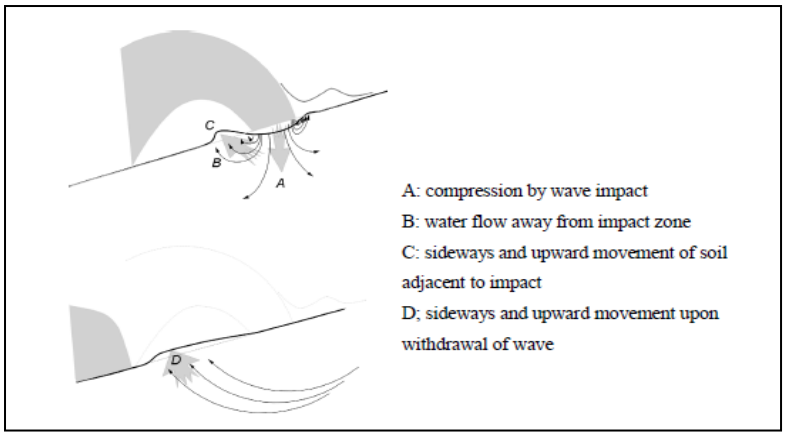

Figure 4-3: Water flow and movement of the soil during wave attack. [TAW 1997]

These processes were already dealt with in chapter 3 and in this research the focus will be on the processes (A, B, and C).

4.2.1 Failure tree

Outer slope erosion can occur in various forms, induced by different loads. The spatial variation of the surface of the grass cover is a leading factor for the occurring erosion phenomena. Erosion develops sooner at weak locations such as dead plants or bare spots than at locations where the sod is densely rooted. At well rooted locations erosion will mostly not occur, however they can be affected by a weak spot in their vicinity.
The load on the weak spot will be partly redistributed to the well rooted sod, which can lead to erosion or weakening of the sod due to the additional load. This can progress until erosion occurs or until the densely rooted sod itself is gradually changed into a weak location. Generally weaker locations are thus vulnerable to different types of loading and will erode faster. The various forms of erosion are summarized in the failure tree depicted in Figure 4-4.

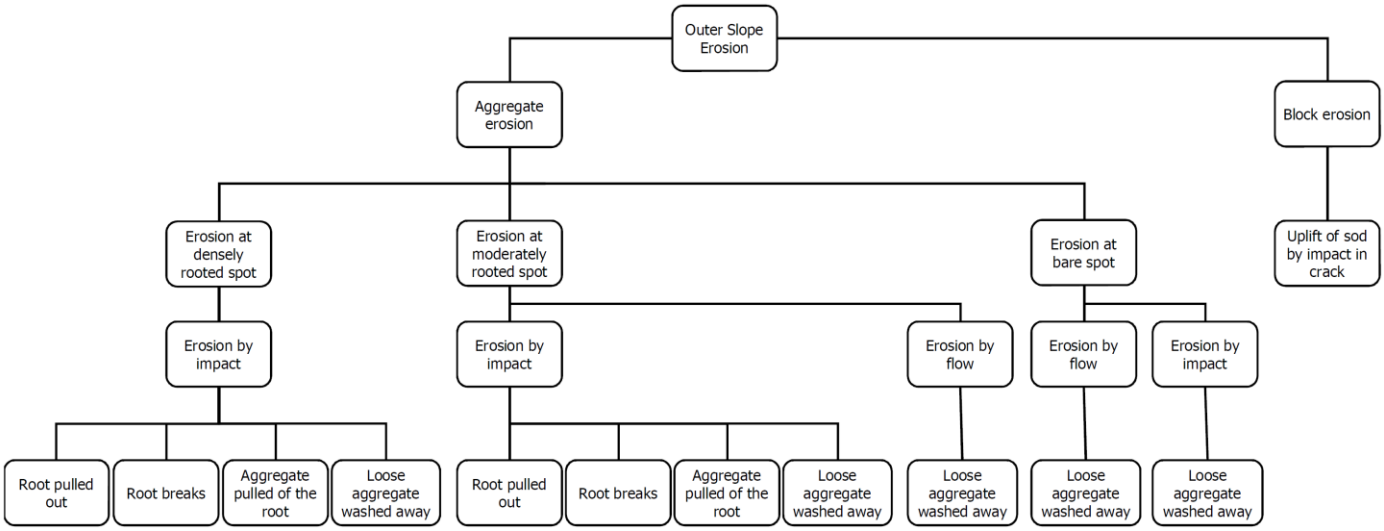

Figure 4-4: Failure tree of erosion of a grassed outer slope.

Several stages can be defined in the erosion process of a grass cover and the also grass cover can be subdivided into a number of zones [TAW 1997; Stanczak 2008a]; each zone has different erosion behaviour. The uppermost layer of the turf, the stubble, generally consists of loose soil and plant

remains; this layer is washed away very quickly by the waves and it is 1 to 3.5 cm thick. Immediately below the stubble is the turf which is loosely packed and usually closely rooted; this part is only slowly eroded away, this highly erosion resistant layer is 1 to 5 cm thick.
In the bottom part of the turf the sod is more closely packed but the number of roots is considerably smaller. The number of roots diminishes with depth up to the subsoil where no roots are present anymore. This soil is more susceptible to erosion.
Especially the erosion of the highly erosion resistant layer of the turf and the lifting of the turf near the subsoil is of interest in this research.

4.2.2 Compression and the apparition of local failures

During wave impact the soil is compressed, which will eventually lead to horizontal deformation of the cover layer. This deformation introduces horizontal stresses caused by lateral compression of the adjacent soil (Figure 4-5). The soil thus undergoes a tensile deformation in the horizontal plane during this process which can cause local failures such as the formation of cracks. It is assumed that roots will reduce cracks but will not nullify this effect.
These cracks are also formed by the impact pressures generated by the falling water mass; the pressures are distributed around the impact point. Soil disintegration occurs around the impact area forming cracks in all directions.

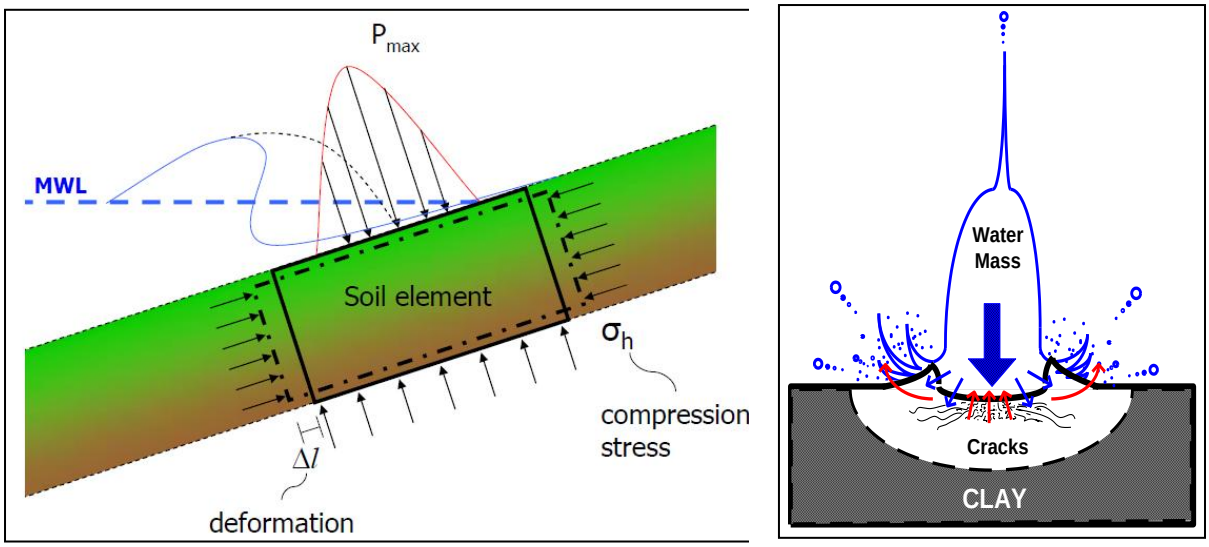

Figure 4-5: Impact causing horizontal deformation (left) and local failure (right [Husrin 2007]).

4.2.3 Increase of permeability and erosion of small pieces

As fissuring of the clay continues the permeability of the sod is increased. Simultaneously the clay pores and the macro pores in between the soil aggregates are gradually filled with water until the soil is saturated. The soil strength is gradually weakened while its water content increases.
When the top layer of the sod is very permeable due to soil structure and small cracks, the breaking wave impacts can even be in direct contact with the pore water (Figure 4-6 left). The impact pressure can then be transmitted to the pore water and because water has universal pressure distribution, pressures in upwards direction can be generated temporarily underneath a soil aggregate (Figure 4-6 right).
The splashing water also exerts a force on these particles which can wash away the uplifted aggregates. Already loose small particles can be lifted up and eroded washed, but also particles supported by a root can erode when they are pulled off their roots or when these roots break or are pulled out.
The erosion of small particles increases permeability even more, and the sod can become spongy, which amplifies all of the processes described above. This was also observed during overtopping test in the field [Bakker, Mom et al. 2008] where a permeability increase eventually led to the balloon mechanism, which occurred in a later stage; a bulge was formed on the inner slope which gradually increased in size.

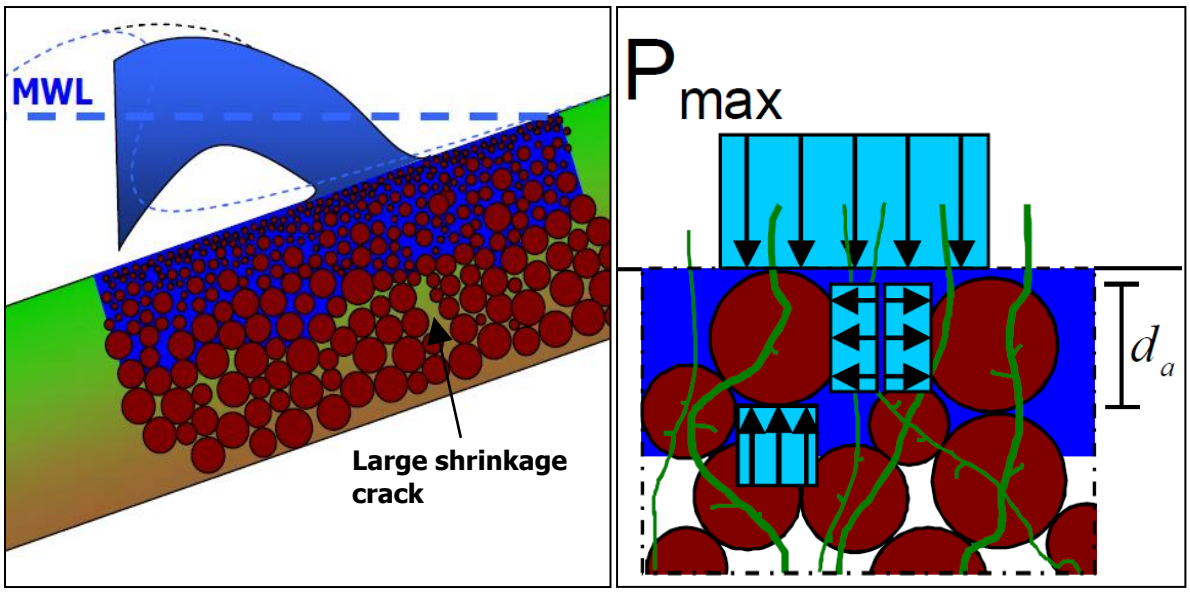

Figure 4-6: Wave impact in direct contact with pore water (left) results in upward pressure (right).

4.2.4 Formation of scour hole and side walls

As small pieces continue to erode and cracks are formed a scour hole develops. The soil adjacent to the scour hole is pushed upwards by the horizontal deformation and the uplift reaction pressures in the soil; side walls are formed. These side walls are subject to side jetting and will eventually break off since the side jet velocity can reach a magnitude of multiple times the impact velocity [Lesser and Field 1983]. As the scour hole becomes deeper it will take the shape of a cliff, because the impact load is not completely symmetrical as a result of the slope of the dike.

4.2.5 Block erosion

Besides the removal of smaller pieces, which forms a scour hole, also block erosion can occur. Before the scour hole has reached the subsoil the total sod is then lifted up after a wave impact. Cracks and cavities in the scour hole are deformed and enlarged due to the persistent wave impacts and the erosion of small pieces. The turf becomes spongier and at a certain moment shrinkage cracks that were already present in the deeper part of the cover layer are opened up or smaller cracks widen due to the deformation of their side walls by subsequent impacts. This allows the water and the impact load to reach deeper parts of the grass cover (Figure 4-7).

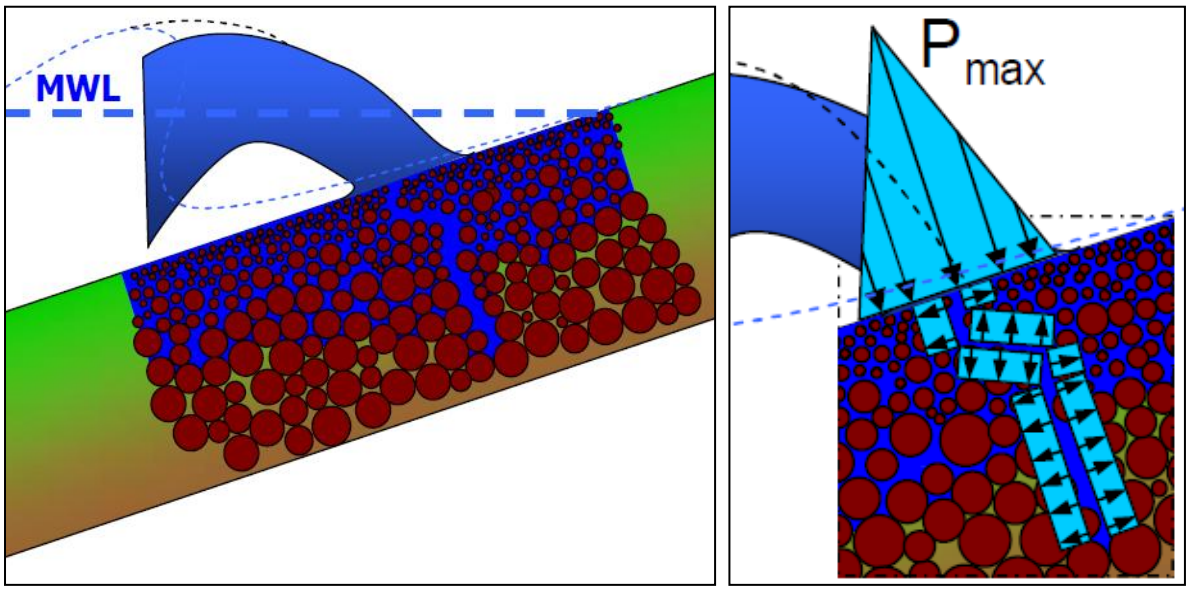

Figure 4-7: Crack opened up after aggregate erosion (left), pressures in the soil (right).

In this stage the explosive effect of impact in water filled cracks can play a major part in the erosion process. Because the substrate is relatively impermeable and the permeability increase caused by the crack is highly localized an uplift pressure can develop underneath large aggregates in the sod. Shortly after the wave impact pressure at the surface has diminished, a high pressure is still present within the crack. Weaker locations can be damaged but also damage to the subsoil at the end of the crack can be inflicted. However the end of deep cracks is mostly in the layer of well compacted clay which, contrary to locations with for instance a low root density just underneath the turf, has a high strength. Weaker locations with less root development can be damaged; small root hairs that anchor the roots in the clay can be broken or pulled out of the saturated clay, allowing the turf to be partially lifted (Figure 4-8 left).
At the weak location in the turf a crack is formed and the created space underneath the turf is filled with water, which will remain there. The result is a bulge, or blister, on the surface of the covering layer. This bulging mechanism shows many similarities with the balloon mechanism and will be named accordingly from now on. As the size of the lifted (loose) section becomes gradually larger the 'balloon' underneath the sod grows as well. Eventually a large block including its root network will be broken loose and it will be washed away instantly (Figure 4-8 right).

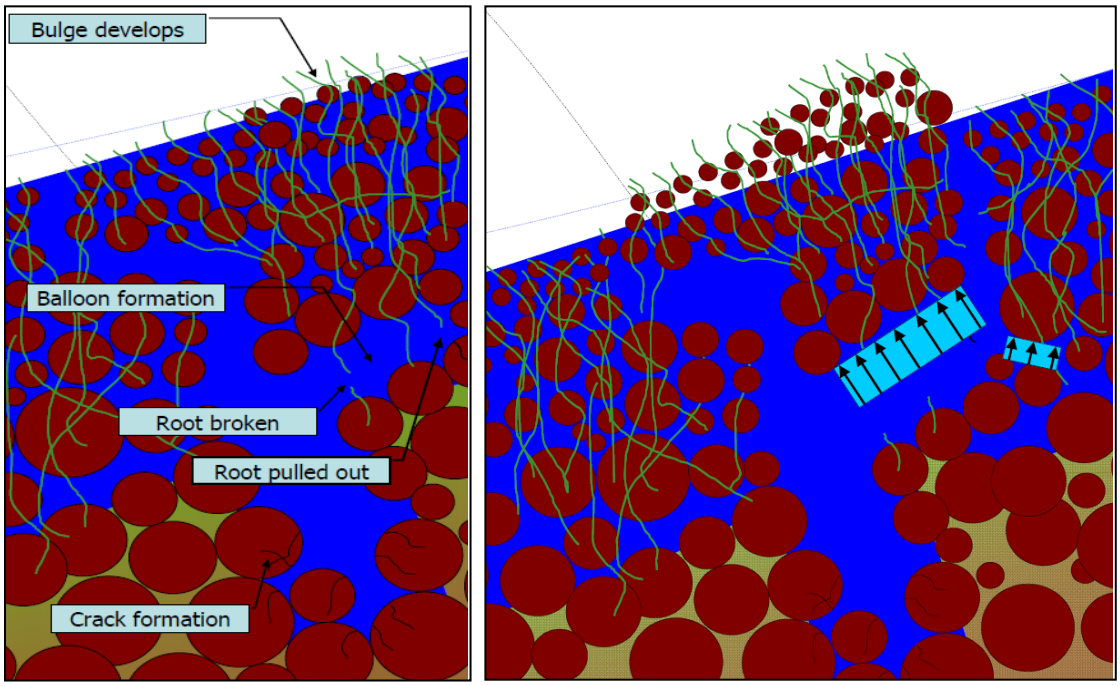

Figure 4-8: Balloon forms under the turf; roots broken or pulled out, cracking at crack end (left), which ultimately leads to the erosion of a large block of the turf (right).

4.2.6 Initiation of erosion

Since the erosion resistance of the stubble is very low, it erodes quickly. The erosion of this layer is therefore not considered as erosion. Below the stubble a highly erosion resistant layer with a dense root network is present. Predicting the erosion of particularly this highly erosion resistant zone is very important as it is the toughest part of the grass cover. When this tough layer has been eroded away the erosion rate will dramatically increase; the damage is ongoing.
Therefore the initiation of erosion is defined as the moment when the point of no return is reached and ongoing damage is triggered. The point of no return could be defined as a critical erosion depth; the strength of the covering layer then has diminished to such an extent that for limited wave action erosion already occurs. This critical depth corresponds to the underside of the highly erosion resistant layer and is estimated to be at a depth of 5-7 cm. With the results of the erosion model an estimate can be given of the critical root density or depth. In this way the critical depth can also be related to a critical root density. The point of no return can be reached after aggregate erosion, but could also be reached instantly by block erosion.

4.3 Discussion and conclusions

Erosion of a grass cover by wave impacts is a complex process and defining separate failure mechanisms is therefore difficult as many erosion phenomena occur simultaneously or quickly succeed one and another.
During wave impacts the permeability of the covering layer is increased. Due to direct wave impacts cracks are formed and crack walls are deformed, furthermore the pores and cavities in the turf are saturated with water. This allows uplift pressures to develop underneath the aggregates shortly after wave impact as water has a universal pressure distribution.
The erosion process of a grass cover can be roughly divided into two main erosion mechanisms: aggregate erosion and block erosion. Small aggregates may be lifted at the surface during wave impact, which eventually leads to aggregate erosion. Simultaneously the turf may be damaged at deeper parts of the grass cover when an irregularity exists in the cover layer that allows impact pressures to penetrate into the soil. Once initial damage has been inflicted the balloon mechanism may be triggered which can lead to block erosion. This is supported by visual observations of horizontal crack formation in the turf during the EroGRASS experiments (Figure 4-9).

Figure 4-9: Horizontal crack formation in the wave impact zone during the EroGRASS experiments.

Failure by the uplift pressures that occur during maximum wave run-down is considered irrelevant for grass covers and erosion due to flowing water is supposed to be negligible; the impact load is governing.
The initiation of erosion is defined as the moment when ongoing damage is triggered. This point of no return could be defined as a critical erosion depth or it can be related to a critical root density. This depth corresponds most likely to the underside of the highly erosion resistant layer which is estimated to be at a depth of 5-7 cm.

5 Grass cover strength

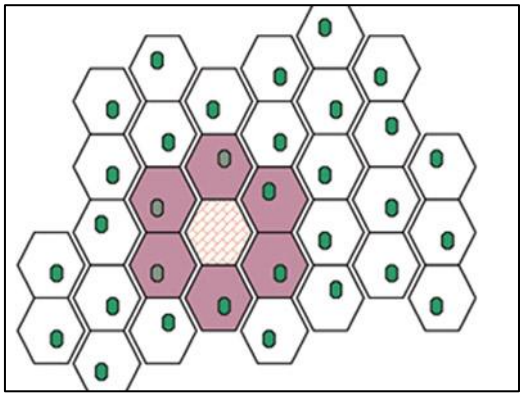

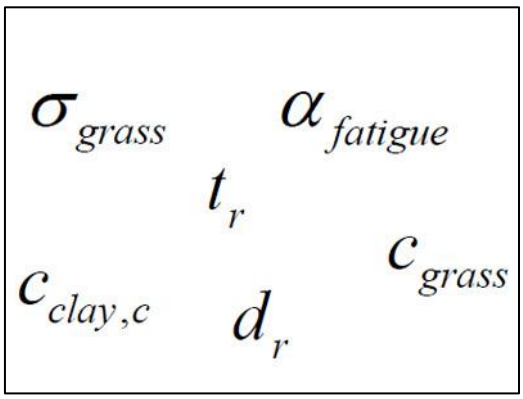

5 Grass cover strength

The strength of a grass cover is not solely dependent on the grass quality or the soil quality. On the contrary; it is the combination and interaction of these two materials which gives the cover layer its strength and flexibility. For modelling purposes it is nevertheless convenient to consider the strength of grass and clay separately. In this chapter the grass strength will be treated first in section 5.1
Several important aspects of the tensile strength of the grass are discussed in section 5.2 including the possibility of using a Fiber Bundle Model for the modelling of the strength. This is followed by section 5.3, which treats the strength characteristics of clay. The chapter is finished with a discussion and conclusions in section 5.4.

5.1 Grass strength

5.1.1 Reinforcing effect of the grass

Several aspects can be distinguished that cause the reinforcing effect of grass. Roots can either interconnect aggregates larger than 0.5 mm by penetration (fiber reinforcement) or keep larger aggregates (3.0-5.0 mm) in place by a dense network influencing internal erosion (filter effect). [Sprangers 1999] Furthermore there is the cementing effect of the biological processes due to the presence of roots. Table 5-1 gives an overview of the processes involved for various particle diameters.

Table 5-1: Mechanism of adherence of soil in turf related to particle diameter. [Sprangers 1999]

Aggregate diameter [mm]	*Mechanism of adherence*
< 0.002	Coagulation
0.002-0.02	Bacterial origin
0.02-0.25	Roots and cementation
0.25-5	Fine network of roots, fungal hyphae, penetration

According to Sprangers (1999) the correlation of the root density with the soil shear strength is often found to be negative; the shear strength often does not reflect soil cohesion as the result of higher root density. Other factors such as soil grain size, moisture content, soil compaction and even the lack of roots seem to be more determining. The importance of moisture content is underlined by Husrin (2007) and Pohl and Richwien (2006) as well.
Sprangers (1999) thus suggests that shear strength is merely determined by soil grain size; larger aggregates have higher shear strength. It is even stated that shear strength cannot be used as a reliable parameter for erosion resistance of grass on clay, because of the above-mentioned reasons. It has to be noted though that Sprangers (1999) found a positive correlation between root weight and shear stress at depths of 5 cm to 15 cm, which is just underneath the highly erosion resistant layer of the grass cover. (see also [Stanczak 2008a])
The root density thus remains an important parameter in the quantification of soil reinforced by roots. In Table 5-2 the guideline values for the root density (RAR) are given for different grass qualities. These values will be applied in this research.

Table 5-2: Guideline values of the root density for different VTV grass qualities.

Grass quality according to VTV	*Number of roots [-]*	*Root density* A_r / A *[-]*
no grass	0	0.0000
very poor	15000	0.0002
poor	30000	0.0004
average	45000	0.0006
good	60000	0.0008

5.1.2 The perpendicular root model

Estimating the root reinforcement of soil is generally done with a modified version of the Mohr Coulomb equation where the reinforcing effect of the roots is represented by an additional cohesion c_{grass}. Mostly this root cohesion is estimated with the help of the simple perpendicular root model

developed by Wu et al. (1979) (see also Figure 5-1). The developed root equation requires the root tensile strength t_r [N/m^2] and the root diameter d_r [m].

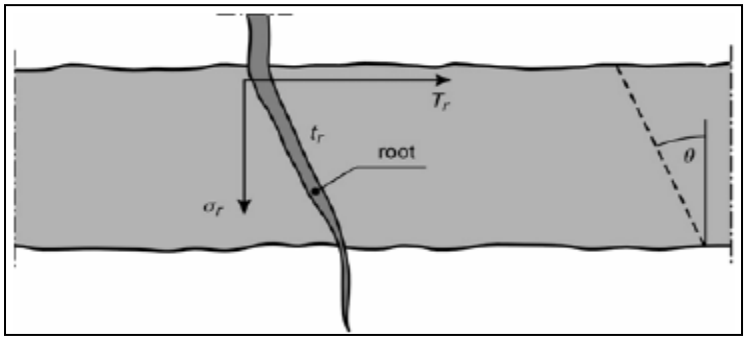

Figure 5-1: Strength schematization of root cohesion. [Hoffmans, Verheij et al. 2009]

Where a root crosses the shear zone the strength can be resolved into components perpendicular ($\sigma_r = t_r \cdot \cos\theta$) and parallel ($T_r = t_r \cdot \sin\theta$) to the shear zone (Figure 5-1). The formulae for the artificial grass cohesion c_{grass} [N/m^2] and the normal grass stress σ_{grass} [N/m^2] read:

$$c_{grass} = t_r \frac{A_r}{A}\left(\cos\theta \tan\varphi + \sin\theta\right) \tag{5-1}$$

$$\sigma_{grass} = t_r \frac{A_r}{A}\cos\theta \tag{5-2}$$

Where:

t_r	= root tensile strength	[N/m^2]
A_r / A	= RAR, Root Area Ratio	[-]
θ	= root angle of rotation	[-]
φ	= angle of internal friction	[-]

The term $\left(\cos\theta \tan\varphi + \sin\theta\right)$ is fairly insensitive to changes in θ and φ, it is close to 1.2 for a large range of θ and φ, hence the root cohesion may be rewritten as:

$$c_{grass} = 1.2 t_r \frac{A_r}{A} \tag{5-3}$$

When the grass cohesion is added to the Mohr Coulomb equation the strength of the grass layer is given by:

$$\tau = c_{clay} + c_{grass} + (\sigma - p_w)\tan\varphi_{eff} \tag{5-4}$$

Where τ [N/m^2] is the soil shear stress, c_{clay} [N/m^2] is the effective clay cohesion, c_{grass} [N/m^2] is the additional cohesion obtained by the roots, σ [N/m^2] is the normal stress, p_w [N/m^2] is the pore water pressure and φ_{eff} [-] is the effective angle of internal friction.

The combination of clay cohesion, the additional grass cohesion and the effective stress contribution represents the shear strength of the grass cover. This shear strength is an average which is valid for the total cover layer, even though there are always inconsistencies present in the grass cover.

Large bare spots or spots with many rampant growing plants (such as common chickweed, creeping thistle, barley, shepherd's purse) and dead plants decrease the quality of the sod. The root

development of a grass sod can be relatively non-homogeneous even though the grass cover might look well covered at first sight. [Sprangers 1996] To include non-homogeneity into a strength model thus involves reckoning with bare spots as well as vegetation with less developed root systems.

5.1.3 Discussion

The static root model of Wu et al. is based on several assumptions; these will be discussed in this section. First of all it can be argued that the orientation of the roots to the shear plane should be taken into account as the angles of the roots in relation to the direction of the force determine the distribution of the stresses. Extended models allowing for inclined roots have been developed, but Gray and Ohashi (1983) [source: Pollen and Simon 2005] have shown from laboratory tests that perpendicular orientations of reinforcing fibers provide comparable reinforcement to randomly orientated fibers. The use of a simple perpendicular root model can thus be justified, assuming that the roots are randomly orientated in the soil.

Yet the second assumption in this model that all roots break and that they all break simultaneously leads to a serious overestimation of the reinforcing effect of the roots. This is mainly due to the assumption that the roots are well anchored and do not pull out and that their full strength is mobilized at the breaking point. [Pollen and Simon 2005]

Root strength is typically mobilized at much larger displacements than soil strength. In soil the peak strength is usually mobilized in the first few millimeters, whereas roots sometimes even straighten to remove their tortuosity before strain is taken up. This suggests that the maximum root strength may not be fully utilized at the time of failure, but the exact overestimation of the strength is unknown as analysis of this phenomenon has been limited to date. [Pollen and Simon 2005]

From laboratory and field tests it appears that root failure occurs by two mechanisms: pull out (slipping caused by bond failure) or rupture (tensile failure). The dominant failure mechanism is a function of the shear strength of the soil, thus frictional bond between roots and soil, and plant species-specific tensile strength. For each type of soil and moisture content a certain threshold in the root surface exists. [Pollen 2006] Above it the frictional bond is greater than the tensile strength and the roots will break. Below this threshold the roots will be pulled out of the soil rather than be broken.

For a root to slip out of the soil the soil-root bond must be broken, the pullout force F_p [kN] can be represented by for instance equation (5-5) [Ennos 1990 ; source: Pollen 2006]:

$$F_{po} = \pi d_r \tau L \qquad (5\text{-}5)$$

Where:

L = root length [m]

Small roots have the tendency to be pulled out while large roots will mostly break [Pollen and Simon 2005]. Root breaking is therefore likely to be the dominant mode of root-failure in dry soils or those with higher shear strengths, whereas soils that are moist or have lower shear strength will show greater root pullout than breaking up to a certain root diameter. [Pollen 2006] Yet it can be doubted if pullout actually occurs; generally the roots in the upper part of the turf are highly interconnected, making pullout unlikely in this part of the turf. At greater depth though, where root density is low, the possibility of pullout of many small roots exists. In that case sudden erosion of large blocks of soil can occur.

Finally the assumption that all roots break simultaneously causes the largest overestimation of the additional root cohesion. Small roots will fail at lower loads than large diameter roots since both the tensile strength and the bond with the soil is less for smaller diameters. The force required to break a root increases linearly with increasing root diameter, but tensile strength is calculated per unit area. Smaller roots are thus stronger per unit area than large roots, resulting in decreasing root tensile strength with increasing root diameter. [Pollen and Simon 2005] Many smaller roots are therefore more efficient than a root network with larger diameters. This also squares with Sprangers (1999) who states that the network as a whole including the many thin roots contributes most to stability.

5.1.4 Conclusions

It is clear that not all assumptions in the static root model of Wu et al. are valid, which leads to errors

in the strength characteristics of many grass erosion models. The model of Wu et al. does not reflect the actual failure process of roots and leads to a large overestimation of the additional strength of root cohesion. Pollen and Simon (2005) therefore suggested using a Fiber Bundle Model (FBM), called RipRoot, instead. This model was primarily developed for riparian vegetation on stream banks, which involves vegetation with large root diameters. Nevertheless the theory behind the model can be valuable for a new grass erosion model. Although this model still does not accurately represent the actual situation, the approximation of the reinforcing effect of roots has significantly improved compared to the model developed by Wu et al. (1979).

5.2 Fiber Bundle Models

In the last decades the development of Fiber Bundle Models has led to a better understanding of composite materials. As a grass cover layer can be regarded as a composite as well an FBM can be useful to model its strength. The basic principle of a FBM is that the maximum load that can be resisted by a bundle of fibers is less than the sum of their individual strength. When a load is applied to a bundle of fibers the load is at first distributed equally between the fibers. Once the load is increased sufficiently for a fiber to break the load of this fiber is redistributed over the remaining intact fibers. The patch with the broken root can now be considered as a very small "bare spot". As this process repeats the load on an individual fiber increases, leading to an avalanche effect until all of the fibers have been broken or the matrix itself fails. In that case the "bare spot" has become too large.

Redistribution of the load of a broken fiber can happen in two ways. The load can be distributed evenly over the intact fibers according to their diameter, which is called global load sharing (GLS), or the load is distributed between the intact fibers in the proximity of the broken fiber; local load sharing (LLS). [Pollen and Simon 2005]

To consider the effect of non-homogeneity Young (2005) suggest to apply the concept of discrete root loading, this concept shows similarities with a FBM with LLS; when a root breaks its load will be distributed over the adjacent roots. The loaded area can be represented as a series of equal sized cells, each associated with an individual root [Young 2005]. The cell size is assumed from the calculated average root spacing.

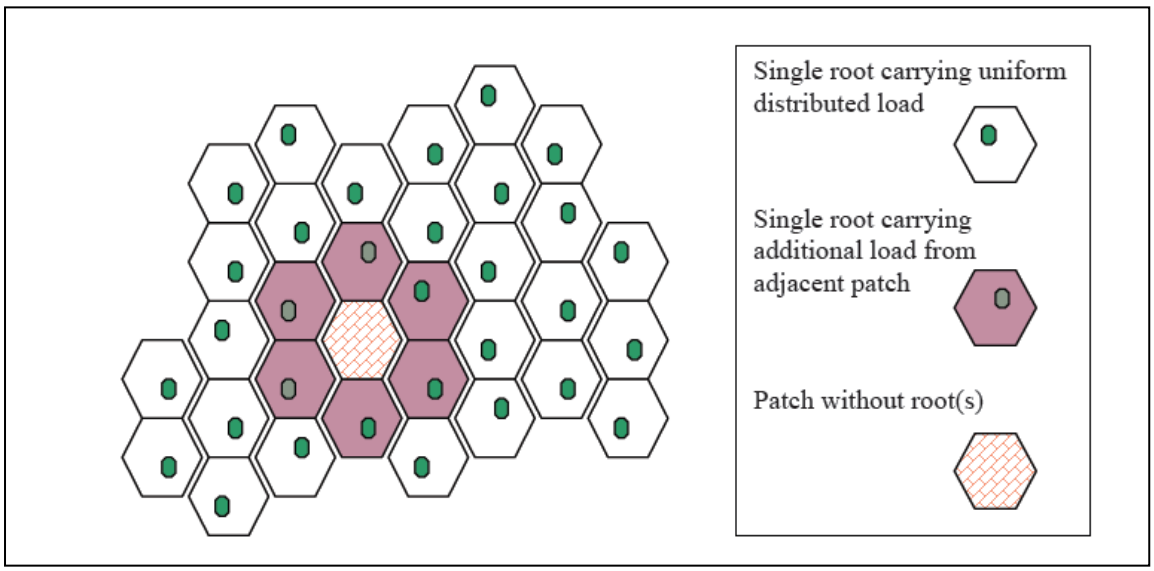

Figure 5-2: Concept of discrete root loading. [Young 2005]

5.2.1 Tensile strength according to diameter

In most grass erosion models the yield stress of grass is considered constant. The additional strength provided by the grass is quantified with the Root Area Ratio, which represents the section of all roots in a certain area. The contribution of two small roots to the additional strength is thus considered equivalent to the reinforcement provided by a single larger root with an equal area. This leads to an inequitable low estimation of the contribution of the smaller roots to the total strength.

An approach that quantifies the strength of a root according to its diameter and its species is

desirable. Unfortunately for most grass species only average root diameters are known and distribution functions lack.
Various authors describe that the tensile strength t_r [N/m^2] of roots of trees and riparian vegetation increases exponentially with diminishing root diameter. (for instance [Genet, Stokes et al. 2005; Pollen and Simon 2005])

$$t_r = ad_r^{-b} \tag{5-6}$$

The negative exponential distribution of tensile strength with root diameter could possibly be explained by higher cellulose concentrations in thinner roots. The cellulose fibers then enhance the tensile strength of the roots. It is however uncertain if this also holds for grassland which has significantly smaller root diameters. At present there is few data on Dutch grassland root diameters available. Based on limited data analysis it is known that Dutch grassland typically has a diameter of 0.13 mm (0.10-0.15 mm) [Paulissen 2009].
To schematize the reinforcing effect of the grass in the manner discussed above a verification of the negative correlation of tensile strength and root diameter for dike grassland is required and the relation between root diameter and tensile strength needs to be defined. Furthermore a root diameter distribution function has to be defined for the implementation of the variable root tensile strength as well as the phenomenon of progressive collapse. The strength of the roots can then be modeled as follows:

$$\sigma_{grass} = \sum n_{r,i} \cdot \sigma_{r,i}$$
$$\sigma_{r,i} = 0.25\pi \cdot d_{r,i}^2 \cdot t_{r,i} \cos\theta$$
$$t_{r,i} = a \cdot d_{r,i}^{-b}$$
$$f(d_{r,i}) = \ldots$$

For modeling purposes it might be useful to define this root diameter distribution function with diameter classes rather than defining a continuous function. In the event that root diameter measurements will be carried out in the future for a proper assessment in the VTV the application of root diameter classes makes sense as well. The model input data will then be equal to the data obtained by field measurements. However because the root diameter distribution of grass and the relationship between diameter and tensile strength is unknown at this moment, this will not be further investigated.

5.2.2 Grass tensile strength suggested by other authors

Various authors investigated the tensile strength of grass; for instance the applied value of the tensile strength by Hoffmans et al. (2009) is $20 \cdot 10^6$ N/m^2.
Choosing an appropriate value for the tensile strength is however difficult. It is still uncertain if grass tensile strength is greater for smaller root diameters due to higher cellulose content. Young (2005) looked into this matter briefly, but in the end applied a safety factor which resulted in the same value as Hoffmans. By taking the average exponential distribution of root diameter and tensile strength of clump grasses Young (2005) gives the following distribution function:

$$t_r = 81 \cdot e^{-1.36 d_r} \tag{5-7}$$

For an average diameter of 0.13 mm this gives an average tensile strength of $t_r = 81 \cdot e^{-1.36 \cdot 0.13}$ which is equal to $67.9 \cdot 10^6$ N/m^2. As Young found this to be rather high he proposed to apply an arbitrary scaling factor of 0.3 which brought the average tensile strength of grass back to approximately $20 \cdot 10^6$ N/m^2.
Valk (2009) suggested that this average value was too low and recommended a value of the tensile strength of $45 \cdot 10^6$ N/m^2. However no theoretical basis was given for this value. Clearly more reliable data on both root diameter distribution and the variation of root tensile strength with their diameter is

needed. Despite the fact that the tensile strength of grass could be higher an average tensile strength of $20 \cdot 10^6$ N/m^2 is adopted from now.

5.2.3 Bare spots and non-homogeneity

Failure of the grass sod usually initiates at the bare spots or at locations with less roots; these are present on every dike. Depending on the size of the bare spot, erosion will occur there. Small bare spots are usually no problem; the spot is still reinforced by the roots that surround it. The load that cannot be absorbed by the bare spots is redistributed equally to the roots at the circumference of the bare spot or, depending on the size of the bare spot, it can erode. However when the size of a bare spot exceeds a certain value, it will erode. The critical size of bare spots is not yet known, as this also depends on the surrounding grass quality.
Besides bare spots certain plant species can cause problems as well. Species rich grass covers are stronger, however if different grass species are present on the cover layer, each species with its own tensile strength, the local strength of the grass layer can be highly variable. Assuming that most dike grass species have only minor differences in tensile strength, weak spots occur only at places where one of the weaker species is growing. Another possibility is that part of the sod consists of dead roots. The erosion of these spots can be predicted by assigning the grass tensile strength for the involved (dead) species to this part of the covering layer while the surrounding (stronger) grass is given its own tensile strength.
Finally the grass quality and thus the tensile strength and the root density are strongly affected by seasonal influences; during winter the sod quality is lowest. Quantifying the seasonal effects on the strength of the sod is beyond the scope of this thesis and will not be discussed in more detail.

5.3 Clay strength

5.3.1 Soil structure and aggregate size

For solid materials the dead weight of the covering layer is one of the resisting forces, this is no different for clay. However due to soil structure, which is the result of continuous shrinking and swelling of the clay layer and biological processes, the substrate is not a solid layer anymore; it consists of small soil aggregates.
The weight of such a soil particle contributes to the erosion resistance; the larger the aggregate the greater the weight and the greater the erosion resistance. The aggregate size depends on the amount of soil structure, which in turn is dependent on, among other biological processes, the root density. Grass that is able to grow on highly erosion resistant clay layers generally has a lower root density than it would have on a clay layer of poor quality; a well developed root network is more difficult to obtain on highly erosion resistant clay than it is on clay with low erosion resistance. As a consequence the soil structure development is less in this clay layer which results in relatively large aggregates. Vice versa the aggregates are smaller in high quality sod, which mainly develops on clay layers with a lower erosion resistance.

5.3.2 Shear strength

The strength of the soil is for a large part determined by the shear strength of the clay caused by its cohesive forces. Obviously the cohesion of clay varies with the quality of the clay, which is dependent on several factors. The composition as well as the density and the degree of compaction have a large influence on the clay quality, but in particular the water content determines the shear strength of clay. When the pore water content exceeds the saturated water content the shear strength of the clay diminishes significantly. The soil can thus lose cohesion due to infiltration.
During laboratory impact tests performed by Stanczak in 2007 three types of clay were used, which correspond to the clay categories as defined in [TAW 1996]. The values in Table 5-3 for the clay cohesion were obtained by averaging the values as given by Stanczak [Stanczak 2008b]. When there is no additional information available on the strength of the clay these values will be used as a guideline in this research.

Table 5-3: Indicative cohesion values of the clay erosion categories.

Clay category according to TAW 1996	*Undrained clay cohesion c_{clay} [kN/m²]*
weak clay / category 3	15.0
moderate clay / category 2	30.0
strong clay / category 1	45.0

Also the dependency of the shear strength on water content was investigated by several authors. In 2003 Kortenhaus [source: Stanczak 2008a] found that depending on the clay quality (clay qualities according to the TAW qualifications) the following relations can be given between the shear strength and the water content:

Weak clay $$\tau_{clay} = 2550 \cdot e^{-33 w_c} \quad (5\text{-}8)$$

Moderate clay $$\tau_{clay} = 2800 \cdot e^{-20 w_c} \quad (5\text{-}9)$$

Strong clay $$\tau_{clay} = 7230 \cdot e^{-12 w_c} \quad (5\text{-}10)$$

Where:

τ_{clay}	= shear strength of clay	[N/m²]
w_c	= water content	[-]

In the erosion model of clay by pressure impacts of Stanczak (2008) this is reflected in the detachability parameter $k_{d,i}$ which for strong clay can be determined with:

$$k_{d,i} = 0.35 \cdot \arctan[110 - (w_c - 0.43)] \cdot 10^{-12} \quad (5\text{-}11)$$

Another approach was given by Pohl and Richwien (2006) (Appendix E) who give a limit value of the pore number to absorb a certain load; the strength of the clay depends on the compression and thus the water content.

5.3.3 Clay rupture strength

Clay is a non homogenous material and its strength is highly variable, which was already highlighted in the previous sections. Among other factors the degree of soil structure, the pore number and the water content have a large influence on the strength of the clay. To be able to guarantee a certain minimum clay strength some assumptions need to be made. Based on the work of Mirtskhoulava [Mirtskhoulava 1991] Hoffmans and Verheij (1997) [source: Hoffmans et al. 2009; Valk 2009] suggested to use the theoretical value of the clay fatigue rupture strength given as:

$$C_f = \alpha_{fatigue} \cdot c_{clay} \quad (5\text{-}12)$$

Where:

C_f	= fatigue rupture strength of clay	[N/m²]
$\alpha_{fatigue}$	= fatigue rupture factor = 0.035	[-]

The fatigue factor is introduced, in the absence of test data, to account for fatigue rupture and is a function of the plasticity index, the porosity, the density of the aggregates and water and mass of the soil particles. Hoffmans et al. (2009) then defined the critical clay strength $c_{clay,c}$ as:

$$c_{clay,c} = (1-n) \cdot 0.6 \cdot C_f \quad (5\text{-}13)$$

With porosity n =0.4 equation (5-13) yields for the critical clay strength $c_{clay,c} = c / 80$.

5.4 Discussion and conclusions

5.4.1 Grass strength

It is expected that the application of a Fiber Bundle Model will represent real situations better than the static root model by Wu et al. However to effectively apply a FBM a root diameter distribution for Dutch grassland is required, which is not available at this moment. Furthermore to successfully implement root pull-out and a variable tensile strength, the root diameter distribution is required as well.
In addition the occurrence of root pull-out in the upper part of the turf can be doubted as the roots are generally highly interconnected there. However at greater depth the possibility of pull-out will exist. Besides the diameter distribution an estimate of the root length distribution is required for the prediction of root pull-out as well. Because of this it is considered unfeasible to implement the effect in an erosion model at this moment.
It is nonetheless clear that the root diameter distribution could have a significant influence on the failure modes of roots as well as on the tensile strength of the roots and thus the strength of the total grass cover, especially if the exponential relation between root diameter and grass tensile strength can be quantified. Undoubtedly more reliable data on both root diameter distribution and the variation of root tensile strength with their diameter is thus needed. Because of this it is unfortunately not possible to model all of the effects discussed above with sufficient accuracy at this moment.
Moreover it is anticipated that the application of a FBM will lead to highly complicated strength modelling. Contrary to this the static root model by Wu et al. provides a simple approach to model the reinforcing effects of the grass on the soil with reasonably good results. Despite its limitations the static root model by Wu et al. will be therefore used to model the reinforcing effect of the grass.
Finally an average tensile strength of $20 \cdot 10^6$ N/m^2 is adopted for the grass tensile strength even though the tensile strength of Dutch grassland might be higher.

5.4.2 Clay strength

The erosion resistance of clay is controlled by a great number of interacting and related factors, because of this giving a clear definition of the erosion process of cohesive materials is difficult. Many authors nevertheless identify moisture content as a leading factor for the strength of clay (for instance: Pohl and Richwien, Stanczak and Kortenhaus).
Also Mirtskhoulava notes that the scour of soils with undisturbed conditions depends greatly on the initial moisture content and that the non-scouring velocities for soil in saturated condition are 2-6 times higher than for the same soils in air-dry conditions. The rupture strength of the clay is thus perhaps underestimated. Consequently the proposed value for the critical clay strength by Hoffmans et al. is a minimum boundary value and should perhaps be increased.
Conversely the condition of the soil can be rapidly disturbed by wave impacts during wave loading; the surface then becomes severely cracked and the soil is saturated with water in short period of time. Because of this the possible underestimation of the clay strength as discussed above is considered to be partly compensated and the clay critical strength $c_{clay,c}$ given by equation (5-13) is adopted. Nevertheless more research on the erosion process of cohesive soil and the appropriate values for the critical clay strength and the clay rupture strength is desirable.

6 Erosion models

6.1 Flow erosion models

6.1.1 EPM

6.1.2 EPM combined with turf element model

6.1.3 Young (2005): shallow slip erosion

6.2 Impact erosion models

6.2.1 De Visser (2007): Semi Quantitative Model

6.2.2 Stanczak (2008): Wave impact in cracks and on a surface

6.2.3 Transition Model and SSEA model

6.3 Discussion

6.4 Conclusions

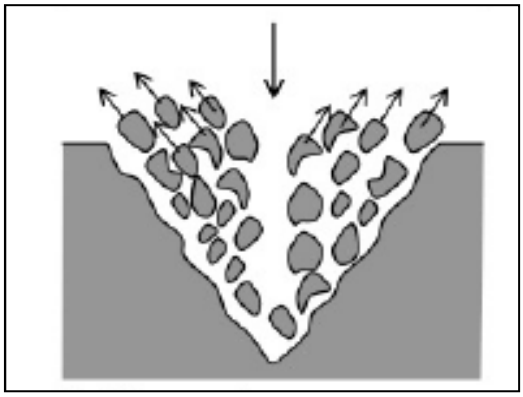

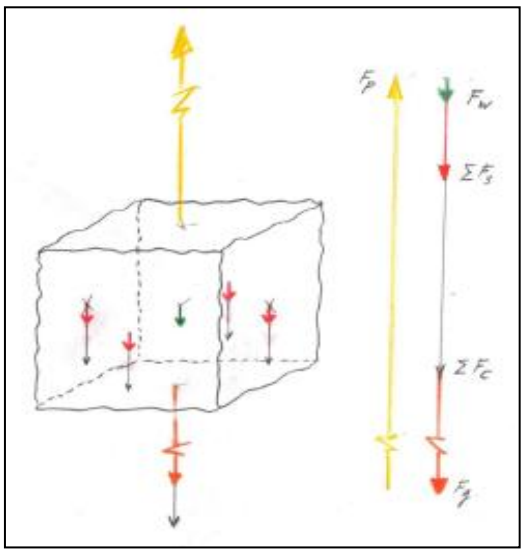

6 Erosion models

When the loads on the dike and the strength of the cover layer are known it is possible to predict the erosion process of the grass cover on the dike. Several grass erosion models have been proposed in the past and also recently more knowledge is acquired about the strength of grass in especially overtopping tests carried out in the field on existing dikes. This chapter is included to provide an overview of the current knowledge and existing theories on the erosion of grass covers and to identify the strong and weak points of these theories.
As the load on the outer slope is a combination of flow and impact, two types of erosion models could be relevant for this research. In section 6.1 an overview is given of some relevant flow erosion models and subsequently in section 6.2 the impact erosion models are described. Finally the general discussion of these theories in section 6.3 will ultimately leads to the conclusions in section 6.4.

Parts in italic are ideas, suggestions and conclusions in the development process and describe the strong and weak points of existing theories.

6.1 Flow erosion models

6.1.1 EPM

To calculate surface erosion on the inner slope the Bare Spots Model (in Dutch: "Erosiegevoelige Plekken Model") was introduced by van den Bos in 2006 [van den Bos 2006] and will be referred to as EPM in the rest of this document.
In the EPM it is assumed that the grass cover layer will fail at the weakest location, i.e. at bare spots of the grass cover that are already bare in the initial situation.
Due to the variability in the quality of the layer, bare spots can always occur somewhere in the sod and the cover layer may fail on these locations. The presence of a bare spot has therefore more influence on the erosion speed than the quality of the grass sod.
Typical bare spots in the order of 10 cm in the flow direction are assumed and the erosion process is compared to scour downstream of a bottom protection. In this case the grass acts as the bottom protection and a scour hole develops in the clay substrate. The following equation for cohesive material has been applied (as derived from scour hole formation theory downstream of bed protections):

$$\frac{y_m}{\lambda} = \left[\frac{(\alpha_{\text{int}} U_0 - U_c)^2}{\psi \Delta^{1.7}} \right] t \qquad (6\text{-}1)$$

Where:

y_m	= erosion depth	[m]
λ	= characteristic length scale (0.2 m)	[m]
α_{int}	= erosion intensity coefficient = 3	[-]
U_0	= depth-averaged flow velocity	[m/s]
U_c	= depth-averaged critical flow velocity	[m/s]
ψ	= $1.3*10^6$	[m^2/s]
Δ	= relative density	[-]
t	= time	[s]

Assuming the formula is limited to an erosion depth y_m [m] smaller than the thickness of the grass sod, the maximum overtopping flow velocity on the slope during an overtopping event can be translated into a characteristic velocity per overtopping event with an equal erosive effect:

$$U_{char} = \frac{1}{\sqrt{2}} U_{\max} \qquad (6\text{-}2)$$

Where:

U_{char}	= characteristic flow velocity	[m/s]
$U_{\max}$	= maximum flow velocity per overtopping event	[m/s]

This translation results in a characteristic velocity for every wave. The summation of every single wave event over a given time period can then give an estimate of the total load during the period. This assumption leads to an adaptation of equation (6-1):

$$\frac{y_m}{\lambda_m} = \left[\frac{\Sigma\left(0.7\alpha U_{\max} - U_c\right)^2}{c\Delta^{1.7}} \right] t \qquad (6\text{-}3)$$

Van den Bos illustrates that the presence of bare spots is very important for the strength of the cover layer. In the EPM the strength of the cover layer is determined by the strength of the bare spots present on the grass cover. This is a plausible assumption as bare clay has a higher erosion rate than grass sod. The influence of the grass quality on the strength of the bare spot could however not be determined. It is expected that erosion develops faster when the bare spot is surrounded by a poor quality grass sod instead of a good quality sod. Also the influence of the distribution of the bare spots is not discussed; it is assumed these are always present to a certain extent. Finally according to the EPM the grass quality is mainly dependent on the covering rate while for instance the VTV qualifies the grass mainly according to the root development. The size of the bare spots has a large influence as well; in practice small bare spots do not erode. This is probably due to the sheltering effect of the surrounding grass and the presence of some roots in the bare spot as well. A critical size of bare spots, especially in relation with the surrounding grass and the quality of this grass, is not yet known. More research should be carried out to solve this problem.

6.1.2 EPM combined with turf element model

This section describes the recently developed erosion model of Hoffmans et al. (2009), which will be referred to as EPM/Hoffmans. Unless stated otherwise the content of this section originates from the publication by Hoffmans et al.

For strength modeling a turf element is introduced describing all the physical forces, for the erosion model the basic erosion relation from the EPM by van den Bos (2006) is adopted. The model is developed to predict the erosion on the inner slope of a dike caused by overtopping flow. With some adaptations it could be used to predict the erosion on the outer slope as well.

The EPM of van den Bos links the initiation of erosion and the presence of bare spots. The model focuses only on the erosion process of existing bare spots by flow; these spots erode faster than parts with a grass cover. Hoffmans et al. (2009) combined several parameters to one erosion formula, which is applicable for the whole (inner) slope instead of solely bare spots. The EPM is the basic erosion relation, but it is suggested to exclude the erosion intensity coefficient α_{int} [-]. Instead a turbulence coefficient ω [-] and an erosion parameter E_{soil} [m/s] are introduced. The load is modelled as an uplift force which is caused by bed pressure fluctuations, whereas the strength is characterized by the weight of the soil, cohesion, shear stresses and root stresses. Furthermore the characteristic length scale of 0.2 m is excluded.

Turbulence

The presence of grass and other vegetation on dike slopes increases the hydraulic roughness of these slopes considerably; this leads to significant turbulence when water flows over the slope.

The bed roughness can be expressed by the Chézy coefficient, which is given by equation (6-4):

$$U_0 = C\sqrt{R_h S_b} \qquad (6\text{-}4)$$

Where:

C	= Chézy coefficient	[$m^{1/2}/s$]
R_h	= hydraulic radius that equals the flow depth	[m]

S_b = energy slope [-]

U_0 = depth averaged flow velocity [m/s]

The depth-averaged relative turbulence intensity r_0 [-] is defined as:

$$r_0 = \frac{\sqrt{k_0}}{U_0} \tag{6-5}$$

Where:

k_0 = depth-averaged turbulent kinetic energy [m^2/s^2]

For uniform flow conditions $k_0 = (c_0 u_*)^2$ in which $c_0 = 1.21$[-] and u_* [m/s] is the bed shear velocity. Using the Chézy equation the depth-averaged relative turbulence intensity r_0 [-] for uniform flow is given by the following equation:

$$r_0 = c_0 \frac{u_*}{U_0} = c_0 \frac{\sqrt{g}}{C} \tag{6-6}$$

Where:

c_0 = coefficient = 1.21 [-]

The depth-averaged turbulence coefficient r_0 depends on the bed characteristics and is estimated in the turf element model at 0.15.

Root model

Because the stability of the clay particles is not only based on gravity but also on the effect of the roots the strength is modelled with the Mohr Coulomb equation. The additional effect of the root system is represented by an artificial cohesion c_{grass}. This root cohesion is estimated according to the root equation by Wu et al. (1979), the equations, which were already mentioned in chapter 5, are repeated below:

$$c_{grass} = t_r \frac{A_r}{A}\left(\cos\theta \tan\varphi + \sin\theta\right) = 1.2 t_r \frac{A_r}{A}$$ Identical to equation (5-3)

$$\tau = c_{clay} + c_{grass} + (\sigma - p_w)\tan\varphi_{eff}$$ Identical to equation (5-4)

Although horizontal roots may have an impact on the condition for motion, the grass normal strength σ_{grass} and the critical grass normal strength $\sigma_{grass,c}$ are here approximated by:

$$\sigma_{grass} = t_r \frac{A_r}{A} + c_{grass} \text{ and } \sigma_{grass,c} = t_{r,c} \frac{A_r}{A} + c_{grass,c} \tag{6-7}$$

Where c_{grass} and $c_{grass,c}$ represent the grass cohesion and the critical grass cohesion.

The static root model assumes that all roots break, and that they all break simultaneously. However, prototype and laboratory experiments have demonstrated that the roots do not all break simultaneously. Therefore the cohesion due to roots and the normal grass stress are probably overestimated. Naturally there are also other forces involved in the erosion process. To investigate all forces acting on clay aggregates the turf element model has been introduced.

Turf element model

Several forces can be distinguished that act on a grass-clay aggregate with the dimensions of a cube (Figure 6-1). The forces on a cube $l_x l_y l_z = l^3$, where l is the characteristic aggregate scale, are:

F_p	= maximum lift force	$F_p = p_{\max} \cdot l_x l_y = p_{\max} \cdot d^2$
F_w	= weight due to gravity	$F_w = (1-n)(\rho_s - \rho_w) g \cdot l_x l_y l_z$
F_s	= shear force	$\Sigma F_s = f(\rho_s - \rho_w) g (l_x + l_y)(l_z)^2$
F_c	= cohesion force	$\Sigma F_c = (c_{grass,c} + c_{clay,c}) \cdot \{2(l_x + l_y) l_z\}$
F_g	= grass reinforcement	$F_g = c_{clay,c} + \sigma_{roots,c}(z = l) \cdot l_x l_y$

Where:

$p_{\max}$	= maximum under pressure at the surface	[kN/m^2]
n	= porosity =0.4	[-]
ρ_s	= Density of the soil	[kN/m^3]
f	= friction factor ($\tan\varphi$)	[-]

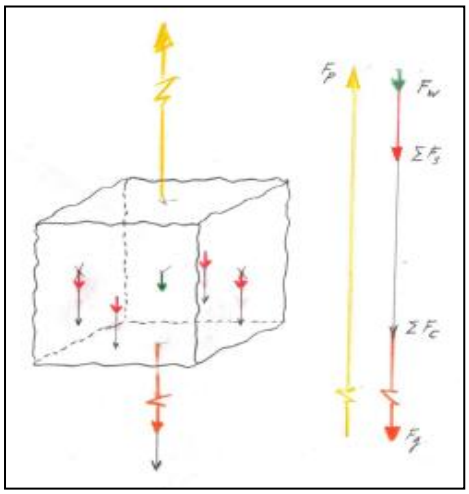

Figure 6-1: Forces on cubic turf. [Hoffmans et al. 2009]

Incipient motion occurs when:

$$F_p \geq F_w + \Sigma F_s + \Sigma F_c + F_g \tag{6-8}$$

Applying $l_x = l_y = l_z = z$ yields:

$$p_{\max} \geq \sigma_s(z) = \left(1 - n + 2f\right)(\rho_s - \rho_w) g z + 4(c_{grass,c}(z) + c_{clay,c}) + \sigma_{grass,c}(z) \tag{6-9}$$

Where:

z	= depth	[m]
$\sigma_s(z)$	= soil strength	[kN/m]

Assuming that cracks are always present in the cover layer due to soil structure, the grass-clay aggregate is only fixed at the underside of the block. The shear and cohesion forces do not act on the side walls; the shear forces reduce to zero and the cohesion forces decrease significantly. Consequently $\sigma_s(z)$ changes into:

$$\sigma_s(z) = (1-n)(\rho_s - \rho_w) g z + c_{clay,c} + \sigma_{grass,c}(z) \tag{6-10}$$

Besides the gradual erosion of a grass cover also the stability of larger areas of the grass cover can influence the failure of the slope. This happens if the maximum under pressure due to flow exceeds the soil strength.
According to research by Emmerling (1973) during turbulent flow conditions the instantaneous pressure $\sigma_{p,b}$ has a standard deviation of three times the mean bed shear stress τ_0 and both the maximum under pressure and the maximum over pressure can reach up to $6\,\sigma_{p,b}$. This means that the maximum pressure peaks by flowing water on the slope can reach up to:

$$p_{\max} = \alpha_\tau \tau_0 \tag{6-11}$$

Where:

α_τ	= pressure fluctuation coefficient = 18	[-]

A particle with a diameter d_a [m] will break loose and move along the slope if the critical condition for movement is reached. This happens when the mean bed shear stress τ_0 equals the critical mean bed shear stress τ_c:

$$\tau_c = \alpha_t^{-1}(1-n)\left((\rho_s - \rho_w) g d_a + \frac{c_{clay,c} + \sigma_{0,grass,c}}{1-n} \right) \tag{6-12}$$

Where:

$c_{clay;c}$	$= c_{clay} / 80$	[N/m^2]

The velocity of flowing water exerts a certain shear stress on the surface, which can initiate the motion of soil particles. The minimum velocity required for the initiation of motion is called the critical velocity. The shear stress is proportional to the velocity squared. The mean bed shear stress defined as $\tau_0 = \rho_w (u_*)^2$ becomes:

$$\tau_0 = \frac{1}{c_0^2} \rho_w (r_0 U_0)^2 = 0.7 \rho_w (r_0 U_0)^2 \tag{6-13}$$

The critical depth averaged flow velocity U_c then is:

$$U_c = \frac{c_0}{r_0} \sqrt{\alpha_\tau^{-1}} \sqrt{\Delta g d_a + \frac{c_{clay,c} + \sigma_{0,grass,c}}{(1-n)\rho_w}} \tag{6-14}$$

Erosion model

According to Partheniades (1965) the erosion rate of cohesive soils is given by:

$$E = \frac{M}{\tau_c}(\tau_0 - \tau_c) \tag{6-15}$$

Where:

E	= erosion rate (mass) per unit area of the bed	[kg/s m^2]
M	= sediment coefficient = 0.00001-0.0005	[kg/s m^2]
τ_0	= bed shear stress	[N/m^2]
τ_c	= critical bed shear stress	[N/m^2]

The factor M / τ_c could also be represented by an overall strength parameter C_E [m^{-1}s^{-1}] which is

inversely proportional to τ_c :

$$\frac{M}{\tau_c} = C_E \quad \text{with: } C_E = \alpha_E \frac{g^2 d_a}{\nu \cdot U_c^{\,2}} \tag{6-16}$$

Where:

α_E	= 1*10^{-10}	[-]
d_a	= aggregate diameter = 0.004 m	[m]
ν	= kinematic viscosity of water = 1*10^{-6}	[m^2/s]

To simulate the erosion of grass during overtopping van den Bos (2006) developed the EPM which reads:

$$y_m = \frac{\left(\omega U_0 - U_c\right)^2 t}{E_{soil}} \text{ And } E_{soil} = \alpha_{soil} \frac{U_c^2}{\sqrt{g d_a}} \tag{6-17}$$

Where:

E_{soil}	= erosion parameter depending on the qualities of both clay and grass.	[m/s]
ω	= turbulence coefficient	[-]

The erosion parameter and the turbulence coefficient are given by equations (6-18) and (6-19):

$$\omega = \left(1.5 + 5 r_0\right) \tag{6-18}$$

$$E_{soil} = \alpha_{soil}\left(C_E^{\,-1}\right) \quad \text{with: } \alpha_{soil} = 1 \tag{6-19}$$

Where:

E_{soil}	= soil parameter	[m/s]

Similar to the EPM, the model is limited by the characteristic length scale of the root system.
Here also the depth-averaged flow velocity U_0 can be replaced by $U_{\max}$ and adding a factor 0.7 to predict the erosion for an overtopping event. The total erosion depth is the sum of the erosion of all individual events. To calculate the erosion depth during a storm, where the overtopping rates and the flow velocities vary in time, the following equation can be used:

$$y_m = \sum_{i=1}^{i=N} \left(E_{soil}\right)^{-1} \left(0.7\omega U_m - U_c\right)^2 t_w \tag{6-20}$$

Where:

U_m	= representative flow velocity during overtopping	[m/s]
N	= number of waves	[-]
t_w	= characteristic time for which the maximum flow velocity occurs	[s]

The EPM/Hoffmans does not link initiation of erosion to a particular place but predicts erosion over the total slope. The basis of this model is the EPM, which contrary to this defines bare spots as the weakest link where erosion will be initiated.
The load model, based on the existence of bare spots, has been adopted from the EPM because a grass layer is irregular and uneven. The EPM/Hoffmans model is therefore based on the initiation of erosion due to irregularities and humps on the surface of the grass layer. The strength modelling is depth variable, mostly physical and has a strong theoretical basis, which is a great advantage.

6.1.3 Young (2005): shallow slip erosion

According to Young [Young 2005] surface erosion, which is a gradual process, cannot be the sole failure mechanism and therefore Young defined another failure mechanism called shallow slip erosion. This mechanism occurs on the inner slope due to infiltrating water. Groundwater outflow and a high phreatic level in the dike could cause instability on parts of the slope.The dominant effect of soil structure, present in the top part of the cover layer, makes it feasible for superficial sliding to occur just underneath the turf. The depth considered is of the order of 30 cm below the surface, which is significantly shallower than normally contemplated for geotechnical sliding failure. [Young 2005]

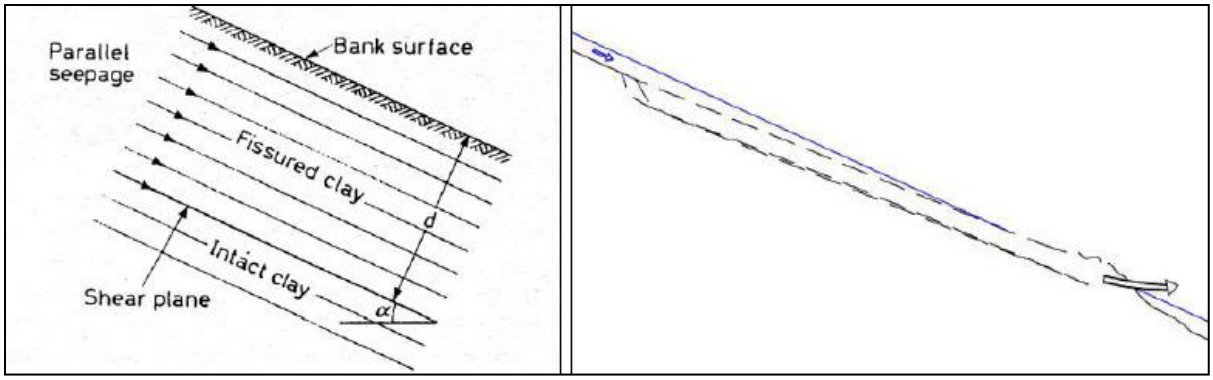

Figure 6-2: Superficial sliding under the turf (left) leads to shallow slip erosion (right). [Valk 2009]

Young developed a sliding prediction model of the turf layer at the inner slope. The initiation of erosion is defined at the location where the stabilizing forces R are smaller than the acting forces S, leading to instability and sliding of the sod. Both the saturated weight of the soil (first part in (6-21) and the shear stress due to overtopping flow (second part in equation (6-21)) are defined as the acting forces:

$$S = \tau_0 = \left(\gamma_s z \sin\alpha\right) + \left(\gamma_w U_0^{\,2} / C^2\right) \tag{6-21}$$

Where:

γ_s	= saturated soil unit weight	[N/m^3]
γ_w	= unit weight water	[N/m^3]
z	= depth to failure surface	[m]

The resisting forces are given by equation (6-22) which is with the modified equation of Mohr Coulomb as described by Hoffmans etal. (2009).

$$R = \tau_c = \left(\sin\theta \cdot t_r \frac{A_r}{A} + \left(\cos\theta \cdot t_r \frac{A_r}{A} + \gamma_{eff} z \cos\alpha \right) \tan\varphi_{eff} \right) \tag{6-22}$$

The sliding model developed assumes full saturation, and parallel seepage flow within the turf layer. As such, no soil cohesion is considered and the structured soil gains its strength from composite action with the grass roots.

According to the stability analysis of Young characteristic depths for shallow slip erosion of the turf layer are 0.2-0.3 m. Recent research [Akkerman et al. 2007] showed however that even during the highest wave overtopping discharge stability would be ensured. Shallow slip failure of the grass cover is unlikely to occur and will therefore not be included in the new model. However, after follow-up field overtopping tests within the SBW framework, the balloon mechanism was observed at some occasions. The precise cause of this balloon mechanism has not yet been retrieved. In the previously mentioned extended EPM model of Hoffmans et al. the balloon mechanism has been taken into account. All of the above was investigated for overtopping flow and thus has a connection with the inner slope; nevertheless it may be important for the outer slope as well.

6.2 Impact erosion models

6.2.1 De Visser (2007): Semi Quantitative Model

In 2007 the behaviour of clay under wave loading was investigated by de Visser by analyzing previous large scale tests on clay. After analysis of the experiments it was concluded that the clay type, expressed as the percentage of sand, was not the governing factor for the erosion of clay by wave loading. The condition of the clay appeared to be more significant. The clay condition is the degree of soil structure, which develops in time and depends on several depth related factors such as seasonal and weather condition, the sand percentage, vegetation, burrowing of animals and compaction.
A soil structure will develop over time and therefore the upper part of the clay layer will always be structured in a few years. An older clay layer will for a larger part be structured. The clay condition can be divided into three conditions: structured clay, moderately structured clay and unstructured clay. Unstructured clay has a significantly lower erosion rate than structured clay; moderately structured clay forms the transition between these two. (Figure 6-3)

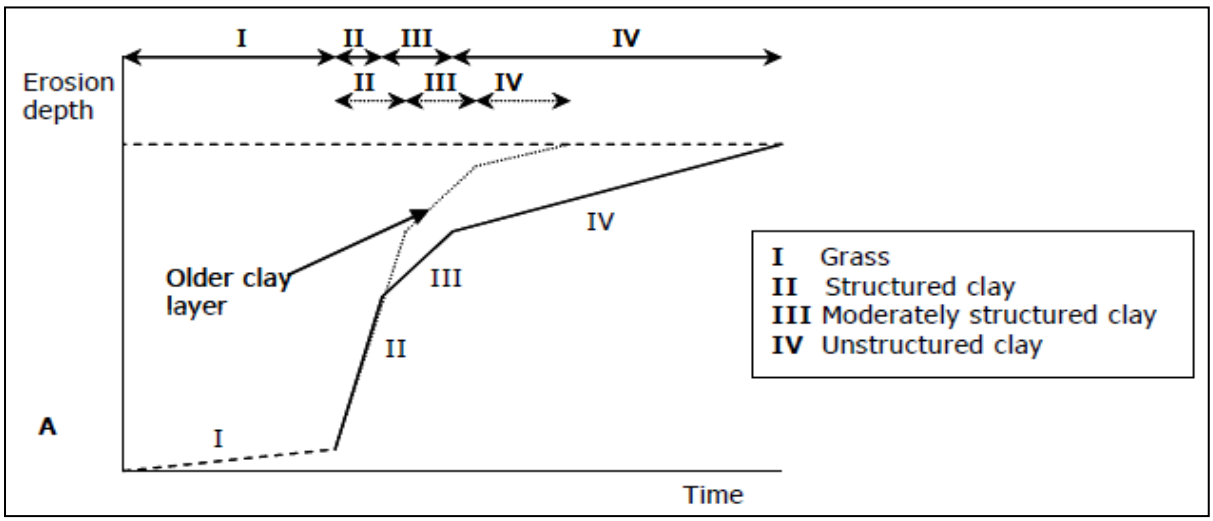

Figure 6-3: The erosion rate is mainly dependent on the clay condition. [de Visser 2007]

Within this subdivision of clay conditions, clay type and the wave conditions are of influence. A higher sand percentage and a higher wave height result roughly in a higher erosion rate. The clay type is however more of influence than the wave characteristics. Unstructured clay with low sand percentage has a very high erosion resistance.
A Semi Quantitative Model to determine the erosion depth over time was developed by de Visser (Figure 6-4).

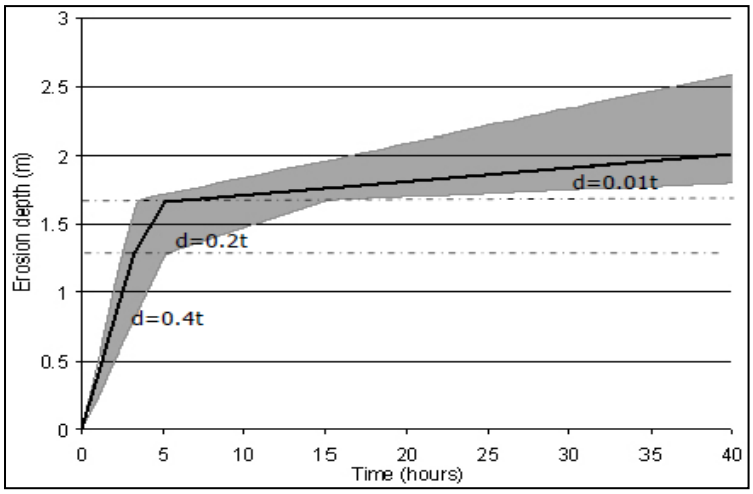

Figure 6-4: Semi Quantative Model. [de Visser 2007]

This model is valid for wave heights between 1.0 m and 1.5 m and consists of a combination of the linear development over time for each clay condition, with the gradient based on the results from the experiments on clay. The transitions between the clay conditions are dependent on the soil structure present in the clay layer. This can be determined with a formula for the soil structure development over time and in depth (Figure 6-5).

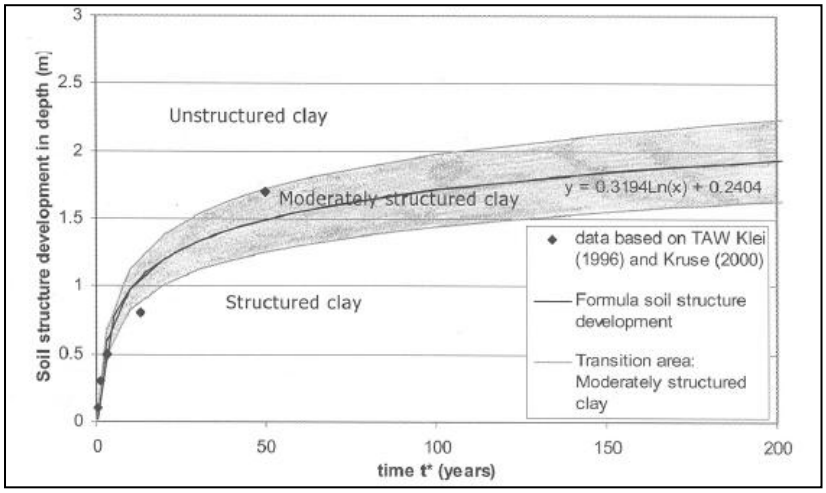

Figure 6-5: Soil structure development in time. [de Visser 2007]

The erosion of clay starts below the water level by the development of a hole, approximately between $0.3\,H_s$ and $1.2\,H_s$ below mean water level. The hole can extend and develop till above mean water level, if the erosion process has sufficient time to continue. After an initial erosion hole has developed in the clay, the erosion profile of clay has a steep slope in the shape of a cliff. [de Visser 2007]

Influencing parameters

On the basis of the present available data of the large scale experiments in the Delta flume, it was not possible to quantify the influence of the clay type and wave characteristics. Based on data of limited experiments on grass under wave loading it could be concluded that a grass cover has a higher erosion resistance against wave loading than clay. For inner slopes this has been indisputably proved by observations at the overtopping tests at Delftzijl [Akkerman et al. 2007]. According to de Visser the erosion rate of unstructured clay with a low sand percentage is approximately similar to the erosion rate of grass.
The breaker type and thus also the slope angle, probably influence the erosion process as well. A different breaker type results in a different load on the slope and therefore in a different erosion mechanism. The available data was however not sufficient to quantify the influence of the breaker type.[de Visser 2007] Besides the clay condition de Visser defined several other factors influencing the erosion process of clay:

- Weak locations will be present in a dike and will be normative for the start of erosion.
- Sand and debris will be present in the water during storm surges, which could initiate or increase erosion by scouring the slope. It also could function as bulkhead after deposition in front of the dike.
- The salt in the seawater could have a certain influence on the erosion development of clay.

By analyzing the large scale tests on clay the influencing parameters on the erosion rate of clay have been identified and these have been ranked to a certain degree. Especially the importance of soil structure on the erosion rate of clay is clearly illustrated by de Visser.
The formula given for soil structure development has however no physical basis and is based on very few data, which is also pointed out by de Visser. In particular the degree of soil structure development in the short term is uncertain, after 10-20 years it seems plausible that the soil structure has developed in a large part of the clay layer (0.5-1.0 m). It is nevertheless still difficult to predict the soil structure development and to quantify the effect of soil structure on the strength of the soil.

The Semi Quantative Model based on this soil structure development gives an indication of the erosion depth in time for a clay cover. The beneficial effect of grass on the strength of the clay layer is confirmed but not included in this model. Furthermore the influence of relevant parameters such as wave height and slope angle on the erosion of clay could regrettably not be quantified.
Less attention is paid to the various erosion mechanisms and the way they are triggered. When and where erosion starts is critical information to predict the subsequent erosion.
The qualitative conclusions of this research such as the importance of soil structure will be considered but the SQM will not be a basis for the new model because it describes the gradual erosion in time and the effect of grass is not included.
It is stated that the erosion rate of unstructured clay with a low sand percentage is approximately similar to the erosion rate of grass, in practice however unstructured clay with a low sand percentage will not easily be present near the surface of the slope. The effect of soil structure in particularly the uppermost part of the cover layer could be neutralized by the grass, this has to be investigated. Also more attention should be paid to the initiation of erosion in the new model and the relevant erosion mechanisms along the slope.

6.2.2 Stanczak (2008): Wave impact in cracks and on a surface

Stanczak performed research in the framework of the FLOODsite project on wave impact on both clay layers and clay layers reinforced with grass. Stanczak suggest that clay layers with and without cracks can fail due to shear stress failure. [Stanczak 2008a]

Impact in cracks

Failure by impact pressures in water-filled cracks caused by breaking waves was theoretically investigated by Führböter in 1966. The result was a conceptual model of the explosive effect in cracks (Figure 6-6). If a water-filled crack with a depth a [m] and a length L_c [m] is subject to an impact pressure p_{max} [kN/m^2], then the pressure is instantly (the speed of pressure propagation (sound in water) is equal to 1485 m/s) transferred to the two side walls of the crack. The forces are absorbed by the compression and the shear strength of the soil behind the walls of the crack. The width of the crack is not involved in the calculation. The weight of the soil body was considered by Führböter (1966) to be negligible compared to the possible impact forces, the shear strength is provided by the cohesion only. Solving the equation S=W leads to $p_{max} = 2c$, meaning failure occurs for impact pressures higher or equal to twice the cohesion.

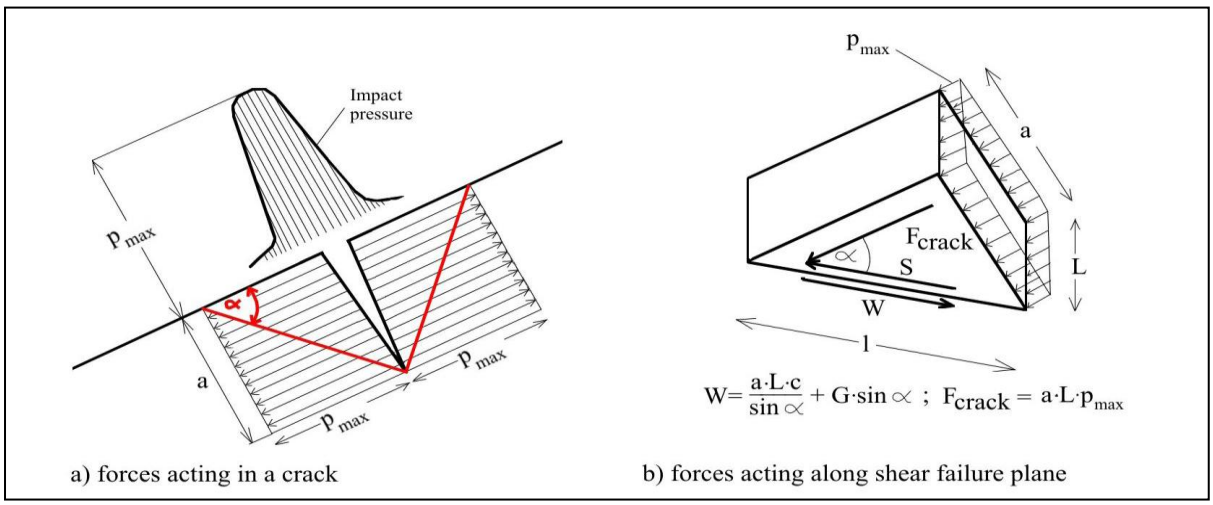

Figure 6-6: Shear failure model. [after Führböter 1966; source: Stanczak 2008a]

The forces involved in the explosive effect in cracks according to Führböter are given as:

$$S = a \cdot L_c \cdot p_{max} \cdot \cos\alpha \qquad \text{Impact force}$$

$$W = \frac{a \cdot L_c \cdot c}{\sin \alpha}$$ Shear strength sliding plane

To verify if shear failure may occur in reality as well Stanczak performed experiments on both clay layers and grass covered clay layers with an artificially induced crack. With a wave impact simulator impact pressures were generated and the erosion was measured. Also the damping effect of a water layer was investigated. The idealized situation assumes soil failure takes place along one shear failure plane in one triangular block. But in reality erosion occurred in the form of small pieces and aggregates (Figure 6-7).
The clay was not homogeneous; it consisted mostly of hard clumps connected by a softer and relatively cohesionless fraction of the soil. During the tests these clumps were pushed out but the failure plane always ran through the weaker parts. For bare clay the impact pressures that could be resisted were lower than the theoretical value of twice the cohesion.

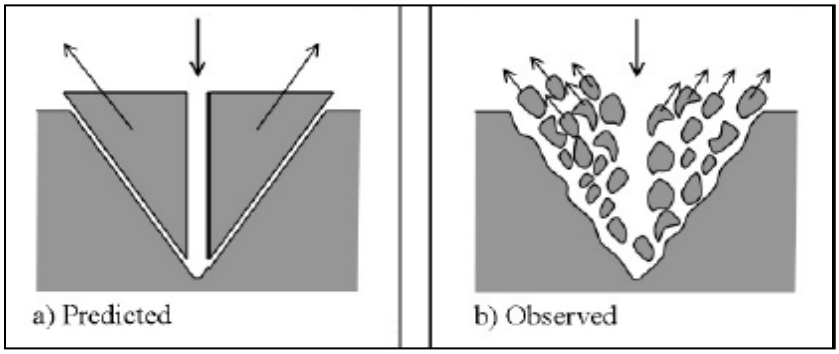

Figure 6-7: Predicted and observed erosion of clay by impact pressure in a crack. [Stanczak 2008b]

The same tests were performed with a grass layer as well. Over a depth of 10 cm the average cohesion by clay and roots combined was assumed to be 48 kPa. In theory failure should have occurred at 96kPa, but the impact simulator was only able to generate a maximum pressure $p_{\max}$ of 24.74 kPa. No failure was thus to be expected which was experimentally confirmed. It should be also mentioned, that pull-cracks in grass cover are very rare, as the dense network of roots prevents from their occurrence.[Stanczak 2007] Nevertheless the conceptual model was partly verified and improved by Stanczak (2007) by including the dead weight of the soil and the shear strength at both sides of the block:

$$G = \left(0.5 \cdot a^2 \cdot L_c \cdot \rho g\right) \Big/ \tan \alpha$$ Dead weight

$$W_s = A \cdot c = \frac{a^2 \cdot c}{\tan \alpha}$$ Shear strength sides

This eventually leads to the following limit state equation:

$$\frac{a \cdot L_c \cdot c}{\sin \alpha} + \frac{0.5 \cdot a^2 \cdot L_c}{\tan \alpha} \rho \cdot g \cdot \sin \alpha + \frac{a^2 \cdot c}{\tan \alpha} = a \cdot L_c \cdot p_{\max} \cdot \cos \alpha \qquad (6\text{-}23)$$

The conceptual model above considers all relevant resisting and mobilizing forces but yet it is impossible to apply for the prediction of shear failure in a crack subject to impact pressures. This is mainly caused by the fact that all resisting forces are dependent on the shape of the mobilized soil block, which depends on the angle of shear failure.
The extended approach by Richwien (2003) [source: Stanczak 2008a] considers also the reaction of the soil and the pore water pressure, but it provides only rough information on the possibility of failure as it is based on a simplified, graphical analysis of forces. When all forces act simultaneously the force that can be absorbed by the soil is significantly larger than the mobilizing force. However in reality there is a small time shift between the pressure force and the reaction forces, the force that

can be absorbed is in this case much smaller.
Yet the time shift between the forces is an important parameter for the erosion behaviour. This problem was already solved in the approach of Führböter (1966) by assuming that the time shift between forces occurs for every impact. The shear failure then occurs within the short time period when the impact pressure is no more present on the surface, but is still present within the crack.
Because this time period is so short the inertia of the soil block starts to play a role, which complicates the modelling of this process [Stanczak 2008a].

Wave impact on surface

For cover layers without cracks Stanczak proposed a formula for the eroded volume after a single wave impact:

$$R_d = p_{\max} \cdot k_{d,p} \cdot e^{-wh} \tag{6-24}$$

Where:

R_d	= volume of the eroded soil	[m^3]
$k_{d,p}$	= empirical detachability coefficient	[m^3/kPa]
w	= water layer damping coefficient	[-]
h	= water layer thickness	[m]

The values of the coefficients in equation (6-24) depend on the strength of the clay. It was also observed that for each soil type a critical impact pressure exists. If the acting pressure is smaller than the critical value no erosion occurs. [Stanczak 2007]
For grass the detachability coefficient $k_{d,g,p}$ [m^3/kPa] is dependent on the Root Volume Ratio, it is given by equation (6-25):

$$k_{d,g,p} = \frac{k_{d,p}}{b \cdot RVR^2} \tag{6-25}$$

Where:

$k_{d,g,p}$	= grass cover detachability coefficient	[m^3/kPa]
RVR	= root volume ratio = $V_r / V_{soil} \cdot 100$	[-]
b	= parameter describing the influence of the roots on the erodibility = 5	[-]

At a certain depth the RVR becomes less than 0.5% and the influence of the roots becomes negligibly small; the value of the detachability coefficient of grass $k_{d,g,p}$ takes the value of the detachability coefficient of the soil $k_{d,p}$. This depth is called the critical depth. [Stanczak 2008a]

The shear failure model is partially confirmed by Stanczak. Shear failure occurred indeed but instead of the predicted erosion in one block erosion it occurred in small lumps and aggregates.
Erosion of small aggregates rather than large blocks seems likelier since clay layers in reality, contrary to compacted clay in laboratory experiments, develop a soil structure.
As cracks frequently occur in clay layers shear failure in cracks is a failure mechanism to be reckoned with. However large cracks in the upper part of a grass layer do occur but are unlikely to remain for a long time; the upper part of the grass cover is quickly restructured due to climatic effects.
The effect of the damping layer appears to be significant for both grass and clay erosion and has to be taken into account. For grass the erosion parameter is adjusted with the RVR*. Below the critical depth, where the influence of the roots is negligible and the detachability parameter is equal to the strength of the substrate soil, an increase in clay cohesion with respect to depth is not taken into account.*
The proposed formula for erosion by a single wave impact could be useful in the new model, but it will be difficult to quantify the thickness of the backwash layer on a real dike. Furthermore no critical impact pressure for grass is given and the presence of bare spots is only partly included by the RVR*.*

6.2.3 Transition Model and SSEA model

Valk (2009) investigated the erosion process on the inner slope of the dike as well with a focus on the transitions of the slope and discussed new failure mechanisms. Profile changes such as the toe of the inner slope, which is normally used as a road, form weak spots. At a transition erosion might be initiated, stimulating the creation of scour holes and finally causing serious damage on the inner slope. The water stream is strongly disrupted when the water hits the horizontal part and impinging forces on the bed and increased turbulence cause enhanced shear stresses on the bed. The water tongue resembles a jet impinging on the bed and in the course of time a scour hole develops due to the jet impact.
When this scour hole reaches a certain depth the upstream soil can become unstable and the erosion hole will develop in upstream direction. This type of erosion is called headcut or retrogressive erosion. Typical heights during the development of headcut erosion are in the order of 0.5 - 1.0 m. Headcut erosion develops faster than surface erosion and will dominate the erosion process from a certain point; this point is called the transition point. An overview of the total erosion process is given in Figure 6-8 [Valk 2009].

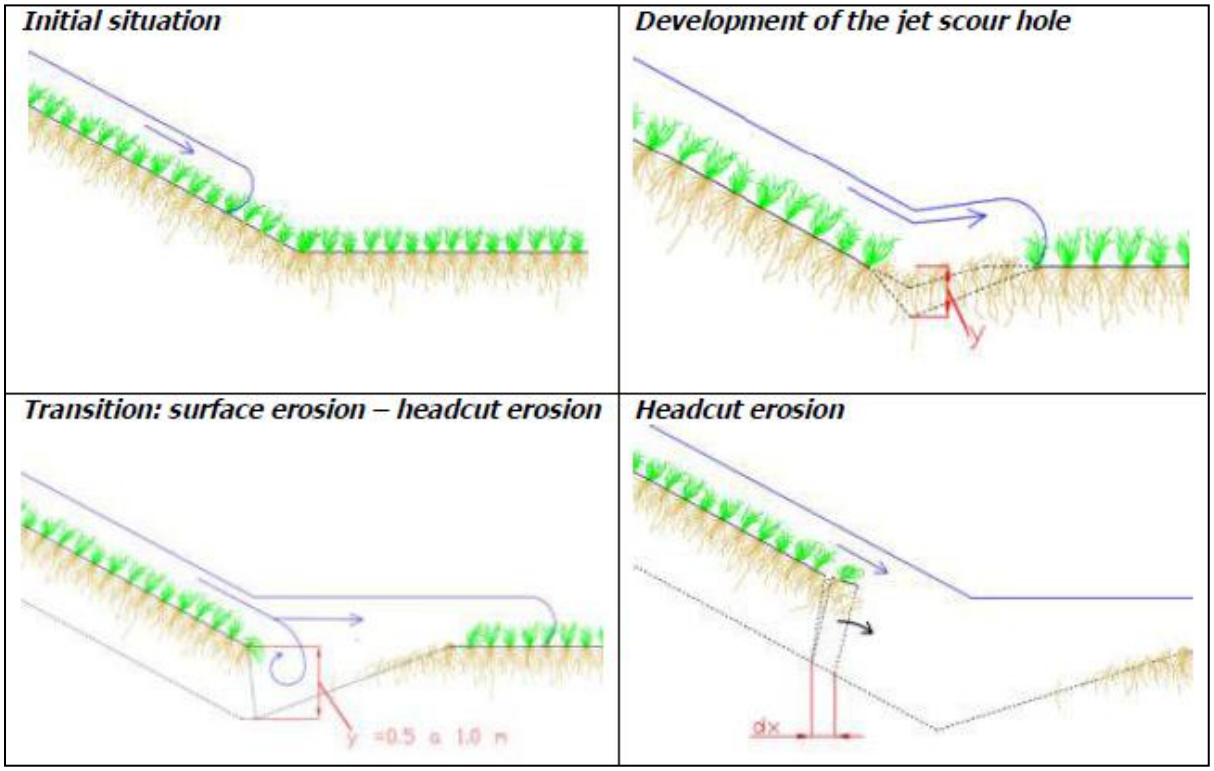

Figure 6-8: Erosion process at inner slope transitions. [Valk 2009]

To predict the erosion at grassed inner slope transitions Valk developed the Transition Model (TM). The model describes the development of the scour hole due to surface erosion and is partly based on the EPM/Hoffmans equations but with the introduction of depth dependency. Although many parameters are the same as in the EPM/Hoffmans some are repeated for the sake of convenience. The final equation for the TM reads [Valk 2009]:

$$\frac{dy}{d\hat{t}} = \frac{\left(\omega^2 \tau_0(d) - \tau_c(d)\right)}{E_{soil}(d)} \qquad (6\text{-}26)$$

In this equation the load terms are given by:

$$\omega = (1.5 + 5r_0)$$ Identical to equation (6-18)

$$\tau_0(d) = \tau_0 e^{-wd} \qquad (6\text{-}27)$$

$$\tau_0 = 0.016 \cdot \frac{1}{2} \rho_w \cdot \left(\frac{1}{(1+\chi)} U \right)^2 \quad (6\text{-}28)$$

Where:

w	= tail water damping coefficient = 0.25	[-]
z	= depth	[m]
χ	= air-water ratio defined as U_a / U	[-]
U	= air-water mixture velocity	[m/s]

The strength terms are given by:

$$\tau_c(z) = \alpha_\tau \left((\rho_s - \rho_w) g d_a + \tau_{total}(z) \right) \quad (6\text{-}29)$$

$$\tau_{total}(z) = 0.021(\tau_{clay}(z)) + \sigma_{grass}(z) \quad (6\text{-}30)$$

$$= 0.021(\tau_{clay,0}(1+\alpha_{cs} \cdot z)) + \sigma_{grass,0} \cdot e^{-\beta z}$$

$$E_{soil} = \frac{\alpha_{soil}}{C_E}, C_E = \alpha_E \frac{g^2 d_a}{\upsilon \cdot U_c^{\,2}}, \alpha_{soil} = 1 \quad \text{(Identical to equations (6-16) and (6-19))}$$

$$U_c = \frac{\alpha_0}{r_0} \sqrt{\Delta g d_a + \frac{\tau_{total}(z)}{\rho_w}} \quad (6\text{-}31)$$

Where:

d_a	= aggregate diameter = 0.004 m	[m]
τ_{total}	= total shear stress obtained by cohesion	[kN/m^2]
α_{cs}	= coefficient of clay cohesion increase over depth	[m^{-1}]
β	= coefficient of root decrease over depth	[m]

For the development of headcut erosion the Site Spillway Erosion Analysis (SSEA) model was adopted, this model is developed at the Stillwater Laboratories of USDA. [source: Valk 2009]
Headcut erosion occurs when the soil becomes unstable due to the shear stresses exerted by the flowing water and the dead weight of the soil. Headcut erosion will however not be the initial failure mechanism.

$$\frac{dx}{dt} = C_{headcut} \left(B - B_c \right) \quad (6\text{-}32)$$

$$B = \left(q H_h \right)^{\frac{1}{3}} \quad (6\text{-}33)$$

Where:

$\frac{dx}{dt}$	= headcut velocity	[ft/hr]
$C_{headcut}$	= material headcut coefficient	[s^2]
B	= hydraulic load	[ft^3/s]
B_c	= critical hydraulic load	[ft^3/s]
H_h	= headcut height = 0.5-1.0 m	[ft]
q	= specific discharge	[ft^3/s ft]

B_c and $C_{headcut}$ both depend on material characteristics. Both parameters are calculated using a headcut erodibility index k_h [-]:

$$C_{headcut} = -0.79\ln(k_h) + 3.04 \quad (6\text{-}34)$$

$$B_c = \left[189 k_h^{0.5} \exp\left(\frac{-3.23}{\ln(101 k_h)}\right)\right]^{0.33} \quad (6\text{-}35)$$

Where:

k_h = headcut erodibility index = 0.03 [-]

Although it has not been verified yet by actual experiments the Transition Model gives a clear insight in the erosion of grass by jet impact. Erosion by jet impact is not entirely equivalent to erosion by wave impact but both loads certainly show similarities. The model can at first sight easily be adapted to a situation where the wave load acts on the transition of the outer slope berm and the upper slope. For wave impact on an outer slope without a berm the model will need more adaptations, but could still be valuable. The jet impact load is represented by a shear stress and a turbulence coefficient. The run-up velocity can be translated to a shear stress as well, but translating the impact pressure to a shear stress could give problems.
Furthermore Valk provides a variable strength profile of the grass cover layer over depth. As the strength of grass on the inner slope most probably will not differ much from the strength of the grass on the outer slope this can be very useful for the new model. Finally headcut erosion is likely to occur on the outer slope as well, but will not be the initiator of erosion and is therefore of less interest for this research.

6.3 Discussion

In this chapter several models describing different erosion processes of grass have been highlighted. These models are based on different assumptions and have been validated with varying methods; a brief summary is given in Table 6-1.

Table 6-1: Summary grass erosion models.

Name	*Model*	*Notes*
de Visser	Semi Quantative Model on the erosion of clay.	Surface erosion, clay strength mainly based on soil structure development.
Stanczak	$R_d = p_{\max} \cdot k_{d,p} \cdot e^{-wh}$	Surface erosion per wave by pressure impact, shear erosion in blocks, critical impact pressure.
Young	$Z = \left(\sin\theta \cdot t_r \frac{A_r}{A} + \left(\cos\theta \cdot t_r \frac{A_r}{A} + \gamma_{eff} z \cos\alpha\right)\tan\varphi_{eff}\right) - \left(\gamma_d z \sin\alpha\right) + \left(\gamma_w U^2 / C^2\right)$	Shallow slip erosion
EPM	$\frac{y_m}{\lambda}\left[\frac{\left(0.7\alpha_{\text{int}} U_{\max} - U_c\right)^2}{\psi\Delta^{1.7}}\right]t$	Surface erosion of bare spots, sum of individual wave overtopping events, characteristic length scale.
EPM Hoffmans	$y_m = \sum_{i=1}^{n} \frac{\left(0.7\omega U_0 - U_c\right)^2}{E_{soil}} t$	Surface erosion on total slope, sum of individual wave overtopping events, no characteristic length scale
Transition Model	$\frac{dy}{d\hat{t}} = \frac{\left(\omega^2 \tau_0(d) - \tau_c(d)\right)}{E_{soil}(d)}$	Surface erosion, jet impact, strength profile varies over the depth.
SSEA	$\frac{dx}{dt} = C_{headcut}\left(B - B_c\right)$	Headcut erosion, occurs at a certain erosion depth.

Shallow slip erosion as defined by Young is considered unlikely to occur on gentle outer slopes and

headcut erosion (SSEA) starts after a certain depth has been reached by surface erosion. The Semi Quantative Model of de Visser provides some insight in the erosion of clay and emphasises especially the significant effect of soil structure on the strength of clay, but cannot be the basis for a model with a reliability approach. The following discussion will not include these models anymore.

Most of the discussed models, such as the EPM and the EPM/Hoffmans, describe the erosion by parallel flow on the slope. Obviously these models have similarities. Their approach can be reduced to the stress based detachment equation for the erosion of cohesive materials developed by Partheniades when it is assumed that $\tau \sim U^2$:

$$E = \frac{M}{\tau_c}\left(\tau_0 - \tau_c\right) = C_E\left(\tau_0 - \tau_c\right) \tag{6-36}$$

The EPM suggests that failure occurs at bare spots and the strength of these bare spots is dependent on the density and the cohesion of the clay; the influence of the grass quality is not quantified.
The EPM/Hoffmans describes the erosion of the total slope using also density and cohesion of the clay for the strength on the assumption that irregularities and humps always occur on the slope. The effect of the grass is included here by implementing an additional cohesion obtained from the tensile strength of the roots, which is dependent on the RAR:

$$C_E \sim \frac{1}{E_{soil}} \sim \frac{1}{U_c^{\,2}} \sim \frac{1}{\sigma_{grass}} \sim \frac{1}{t_r} \sim \frac{1}{RAR}$$

The erosion model of Stanczak uses an approach by Woolhiser (1990) [source: Husrin 2007] similar to equation (6-36):

$$\varepsilon = k_d\left(\tau - \tau_c\right)^a$$

Instead of a shear stress the hydraulic load is represented by an impact pressure and the critical shear stress τ_c assumed to be zero. Stanczak assumes there is always erosion (in the form of transported particles, crack formation or shape deformation) after a hydraulic impact but also states that erosion occurs only when a critical impact pressure is exceeded. The erosion coefficient of the grass is however different from the EPM/Hoffmans, the detachability coefficient depends on the RVR:

$$k_{d,g,p} \sim \frac{1}{RVR^2}$$

In this way the strength profile of the grass is depth variable up to the critical depth, where the cover layer assumes the constant value of the strength of the clay. Furthermore Stanczak calculates the eroded volume by splash erosion due to perpendicular impact [m^3] while the EPM/Hoffmans model predicts the scour depth [m] due to parallel flow on the slope.
The Transition Model is based on the equation developed by Partheniades as well but introduces a depth variable strength profile. The diminishing effect of soil structure and the compaction of the clay at greater depth are taken into account in the strength profile of the clay. The root cohesion is also made depth variable by using actual measured values of the RAR, if this information is not available the RAR and RVR can be approximated by functions based on data of Sprangers. These can be related as: $RVR = 50 \cdot RAR$ [Valk 2009].
It is also noted that the right choice for the characteristic value of the strength of the clay has a significant impact. In the EPM/Hoffmans the minimum boundary value is chosen, which is determined with several safety coefficients for the non-homogeneity of the soil and the degree of saturation. Consequently the clay gives no significant contribution to the residual strength. Valk suggests that the strength of the clay is underestimated by a factor 10 at least.
The effect of the damping water layer appears to be significant for both grass and clay erosion and

the Transition Model as well as the model developed by Stanczak take this effect into account. Although both methods apply the same values to model the damping effect there are differences. The damping layer at transitions mainly consists of the water in the pool that is formed in the scour hole, but the damping layer on the outer slope will consist of a combination of the backwash layer during wave run-down and the pool formed in the erosion hole.
The conceptual model of Stanczak illustrates the significant influence of the presence of cracks on the strength of clay and the failure modes caused by wave impact. This is also stated by Pohl and Richwien (2006) who relate the pore number and the water content of clay to the strength of the cover layer (Appendix E).
The laboratory tests carried out by Husrin and Stanczak indicate that in homogeneous clay block erosion indeed occurs, but also erosion in the form of small pieces was observed [Husrin 2007]. Furthermore some clay samples contained hard lumps; these non homogeneous samples did not erode in the form of a block but disintegrated and eroded in the form of small aggregates.
Although wave impact in cracks in clay can cause significant damage it remains questionable if erosion occurs in blocks in grass covers as well. Large vertical cracks in grass layers are not often present; however due to soil structure many smaller cracks occur; in all directions.
An approach where the wave impact pressure is transferred to the pore water seems more convincing than shear failure by impact in cracks. As more waves collide on the cover layer even more cracks are formed and the turf is compressed. The geometry of the soil is gradually changed; the degree of compaction and the pore number are affected by deformations. As the pore water content increases the strength of the clay gradually diminishes. Furthermore the pore water pressures caused by compressive stresses, which are the result of the breaking of waves, are induced more easily. In fact permeability can increase to such an extent that the impact load is eventually in direct contact with the groundwater in the cavities between the aggregates. Due to the universal pressure distribution of water the wave impacts can be partly transferred through the cracks, this ultimately causes instationary uplift pressures. Furthermore large shrinkage cracks can be opened up when a certain amount of aggregates has eroded, which enables the impacts to reach parts of the substrate, underneath the turf.

6.4 Conclusions

The erosion of grass cover layers by wave impact is a highly dynamic and complicated process. It involves various phenomena which can occur individually, in combination, or subsequently. An overview of the relevant processes of erosion and their mutual relations and influences is given in Figure 6-9.
Theoretically failure of good grass cannot occur unless it is affected by weak spots. Erosion is then initiated at weaker locations such as dead plants or bare spots. Although these are reinforced by the surrounding grass, they can still erode if the size of the weak location is sufficiently large, or when the grass quality of the adjacent area is too low to absorb the additional load. The surrounding grass itself can even collapse as a consequence of undermining effects or tearing of the sod. Despite the fact that the critical size of the bare spots and the influence area of the surrounding grass are important parameters, it has not yet been possible to determine them.
Larger cracks are assumed to occur sporadically; they are mostly quickly restructured due to root penetration and burrowing animals at the surface, but cracks may exist at greater depth.
Nevertheless the explosive effect in cracks is an important phenomenon for the erosion of grass covers by wave impact. Theoretically shear failure of large blocks can occur, however it seems likelier that erosion in lumps and aggregates will occur instead. Due to impact pressures in the network of cracks within the soil small particles can be eroded. This squares with the observed balls of clay (Appendix A) and the failure process described in chapter 4. Nonetheless larger blocks can still erode when irregularities allow impact pressures to penetrate deeper in the soil.
Shallow slip failure by wave overtopping appears to be an irrelevant failure mechanism in practice, even on steep inner slopes. However the balloon mechanism, which shows similarities with shallow slip failure, is a relevant failure mechanism. Erosion of large blocks can be initiated when the grass cover is ripped at a certain dept and water can accumulate underneath the cover layer. Since this phenomenon has occurred several times during grass erosion field tests the balloon mechanism should be taken into account.

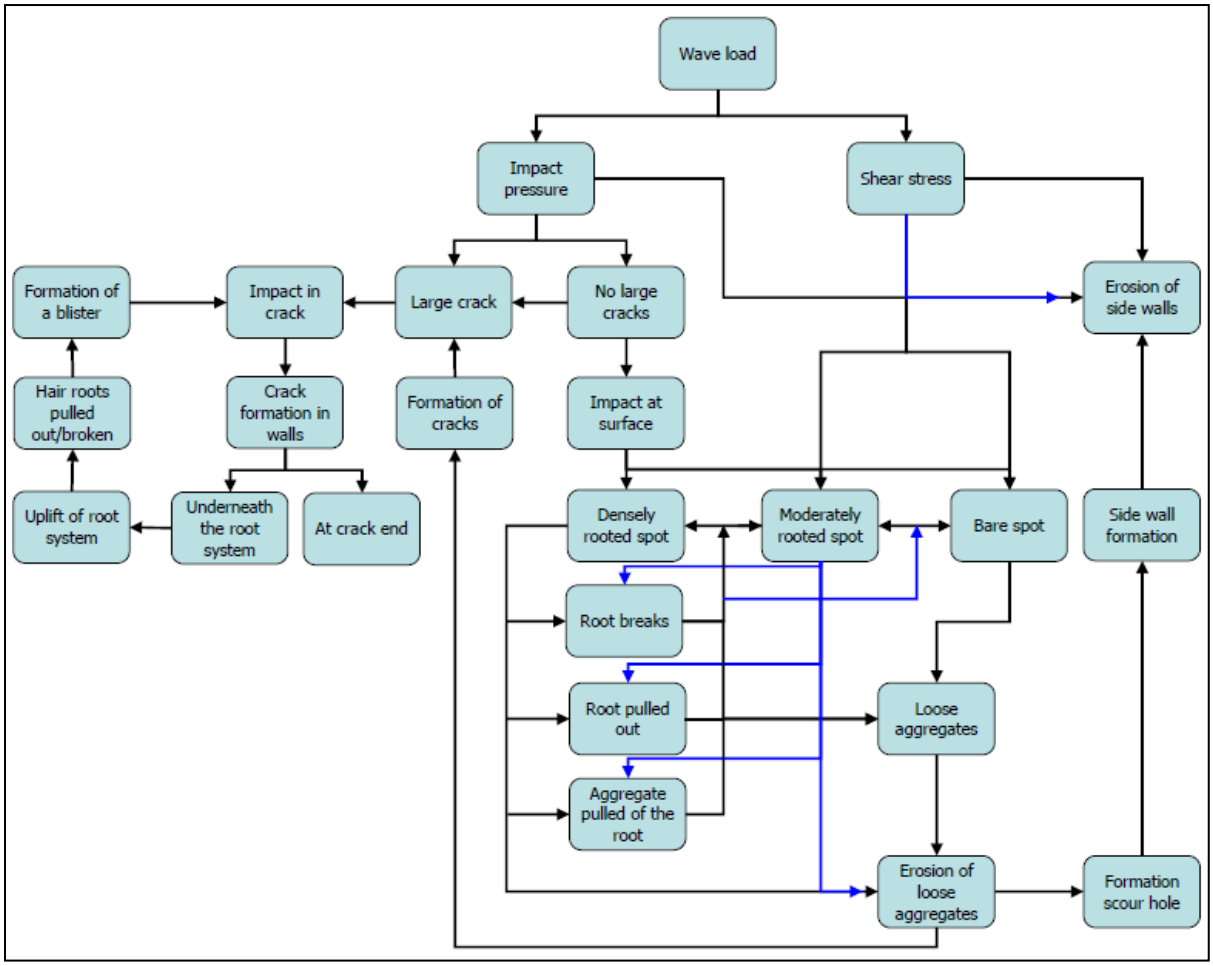

Figure 6-9: Process tree of the erosion of grass covered outer slopes.

Especially the condition of the clay has a significant influence on the failure mode and the erosion rate. The amount of soil structure determines for a large part the erosion resistance of clay and in general a soil structure develops in the upper part of a grass cover. Shortly after installation the grass cover is very compact and mostly unstructured, resulting in a tough cover layer. However after a short period of time a soil structure develops, which weakens the grass cover significantly.
As a soil structure develops, the grass cover will consist of smaller loose aggregates after a certain time. From that moment on the strength of the grass cover will depend on the strength of the individual aggregates and their mutual coherence. The turf element model by Hoffmans et al. gives a physical description of the different strength terms. Erosion resistance is determined by the strength of individual aggregates while their mutual influence is accounted for by shear and cohesion forces at the sides of the aggregates. It will therefore be applied and adapted in the new model.
Besides soil structure the clay strength is affected by several other factors such as moisture content. As moisture content and the other influencing factors fluctuate the shear strength of the clay should too, however there exists controversy how the clay strength is affected by these factors.
The grass strength in static root models could be overestimated because pull-out it is not considered. Furthermore it is uncertain if the grass strength is totally mobilized at the moment of failure because grass strength is typically mobilized at greater displacements than the shear strength of the soil. On the other hand it could be stated that the grass strength is underestimated because of the negative correlation between the tensile strength and the root diameter. This relation is however not verified yet, therefore the value of the tensile strength is chosen at the safe side: $20 \cdot 10^6$ N/m^2.
At present the strength of the grass cover is mainly attributed to the reinforcing effect of the roots and thus the quality of the grass, while the influence of the clay quality is considered of less importance. Yet it might be that clay quality has a greater influence on the strength of the turf, and that the strength is in fact dependent on the synergy of grass and clay.

7 Derivation erosion model

7.1 Basic erosion relation

7.2 Load term

7.2.1 Wave impact pressure

7.2.2 Damping by backwash layer

7.2.3 Influence of crack dimensions

7.2.4 Air water ratio

7.2.5 Conclusion

7.3 Strength terms

7.3.1 Grass strength and depth dependency

7.3.2 Characteristic aggregate diameter and turf area per root

7.3.3 Soil structure and depth dependency

7.3.4 Aggregate

7.3.5 Block erosion

7.3.6 Weak spots

7.4 Erosion parameter

7.4.1 General

7.4.2 Derivation erosion parameter for impact pressure erosion

7.5 Impact time and sequential effect

7.5.1 Characteristic impact time

7.5.2 Chronological order of wave impacts

7.6 Summary of all relevant equations

7 Derivation erosion model

In the previous chapters the uplift pressures caused by breaking wave impacts on the outer slope have been identified as the governing load on the outer slope of dikes with a grass cover. It was concluded that these uplift pressures can lead to erosion of the outer slope and two failure mechanism have been distinguished which can separately initiate failure of the grass cover layer. Moreover relevant effects in the erosion process as well as important parameters for the strength of grass and clay have been recognized.
With the help of these findings a model that predicts the initiation of erosion of a grass cover on the outer slope due to wave impact pressures has been developed. This chapter will explain the derivation of this erosion model.
The basic equation for the Wave Impact Pressure Erosion model (WIPE model) reads:

$$y_m = \sum_{1}^{N_{imp}} \frac{\left(p_{up}(z) - p_c(z) \right) \cdot t_{imp}}{E_p(z)} \tag{7-1}$$

Erosion occurs when the load term, which consist of the uplift pressure p_{up} [N/m^2] generated by a wave impact, exceeds the strength, which is given as a critical uplift pressure p_c [N/m^2]. Both the strength term and the load term are depth dependent. In equation (7-1) t_{imp} [s] is the characteristic time of an uplift pressure due to a wave impact on the slope. The load during one characteristic impact time is assumed to be constant, meaning that uplift pressures are constant during the characteristic impact time and waves are modelled as block impacts over time. Besides the terms described above the model contains an erosion parameter E_p, which is also depth dependent.

First the basic erosion relation is explained in section 7.1. This is followed by a discussion of the load terms in section 7.2. Subsequently in section 7.3 the basic erosion equation is applied to obtain limit states for two types of erosion, which were already identified in chapter 4: Aggregate Erosion (AE) and Block Erosion (BE). After this the erosion parameter is determined in section 7.4. The characteristic impact time is defined in section 7.5 including a brief discussion of other time related problems. Finally in section 7.6 an overview of the relevant equations of the erosion model is given.

7.1 Basic erosion relation

It was already highlighted in the previous chapter that many flow erosion models can be reduced to a shear stress based detachment equation for the erosion of cohesive materials. This basic erosion relation is widely known and can be expressed as follows [Hanson and Cook 2004]:

$$\varepsilon_{flow} = k_d \left(\tau_e - \tau_c \right) \tag{7-2}$$

Where:

ε_{flow}	= erosion rate due to flow	[m/s]
k_d	= detachability coefficient	[m^3/N s]

Erosion occurs when the shear stress τ_0, as a result of the flow velocities, turbulence and the surface roughness, exceeds the critical shear stress τ_c. The strength of the soil is thus represented by the critical shear stress of the material. The rate of erosion is determined by the erosion parameter k_d, which generally is inversely proportional to the strength of the soil.
However this erosion relation is applicable for situations where flow loads or jet loads exert a shear stress on the material, whereas a relation is required that is based on impact erosion. The erosion relation given by equation (7-2) is thus based on a different failure mechanism than the governing failure mechanism during wave impact that has been described in chapter 4.
In the case of wave impacts on slopes, the slope is exposed to impact and uplift pressures in the

impact area instead of shear stresses. As a consequence the shear stress based relation can in fact not be applied to model erosion by impact pressures. However it is not unlikely that these erosion mechanisms, which are depicted in Figure 7-1, have analogous erosion relations.
If the impact pressure p [N/m^2] is considered to be equivalent to a normal stress σ [N/m^2], then according to this relation erosion by impact pressures occurs when the critical uplift pressure p_c [N/m^2] is exceeded by the impact pressure p .

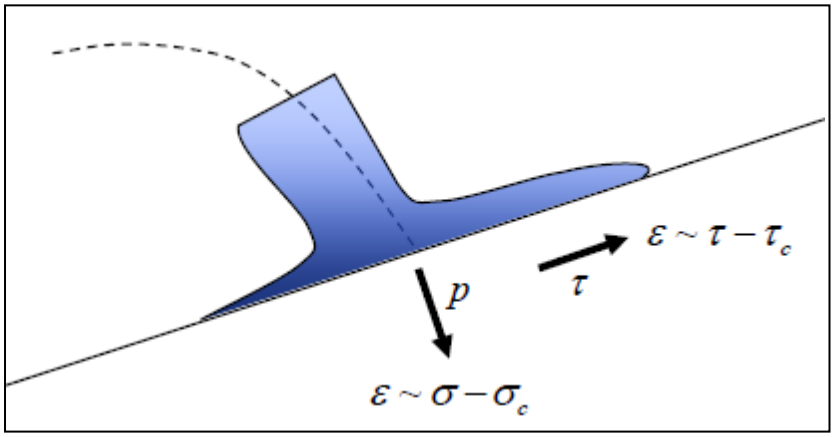

Figure 7-1: Erosion relations during wave loading.

With some modifications this leads to the erosion relation for impact pressures, which is given by equation (7-3):

$$\varepsilon_{imp} = k_p \cdot \left(p - p_c \right) \text{ with } p \sim \sigma \text{ and } \varepsilon_{imp} \sim \sigma - \sigma_c \qquad (7\text{-}3)$$

Where:

ε_{imp}	= erosion rate due to wave impact pressures	[m/s]
k_p	= erosion parameter for wave impacts pressures	

A similar approach was followed by Stanczak (2008) for the development of his impact erosion model. It has to be noted though that the erosion parameter k_p in equation (7-3) differs from the erosion parameter for flow erosion k_d in equation (7-2) and needs to be determined. With equation (7-3) an equation has been found that relates erosion to impact pressures. This relation will serve as a basis for the development of the WIPE model. As the erosion parameter should be dependent on the strength of the grass cover, it needs to be defined to determine the erosion parameter. In the next sections the modelling of the load and the strength is therefore treated first. The erosion parameter for impact erosion is determined after this in section 7.4.

7.2 Load term

7.2.1 Wave impact pressure

To predict erosion depths with the erosion relation given in equation (7-1) impact pressures are required. The model will be verified with the help of the pressure data obtained during the EroGRASS experiments in the GWK. Consequently the loads on the slope are already known and the erosion model can be calibrated by determining the maximum impact pressure for each wave.
However for the model to be applicable in the absence of pressure data, the impact pressures need to be predicted. A conversion from wave characteristics to loads is thus required before the model can be utilized. For the prediction of impact pressures, provided that the wave characteristics are known, it is suggested to use the approach of Führböter (1986; 1988).
This approach was later incorporated into a numerical model called "Golfklap" for the prediction of wave impact pressures on asphaltic revetments [TAW 2003]. The most important equations in Golfklap are briefly described below. The maximum impact pressure is determined by the wave height

and the impact factor and is defined as:

$$p_{\max} = \rho_w g q_i H$$ Identical to equation (3-2)

The distribution of the wave heights is characterized by a Rayleigh distribution. Hence the chance of occurrence $p(H)$ of a wave height H can be predicted using the following equation:

$$p(H) = 4\frac{H}{H_s} e^{\left[-2\left(\frac{H}{H_s}\right)^2\right]}$$ (7-4)

Since the number of waves that actually cause an impact and the intensity of the impact factor have the same probability density function they can be combined according to Führböter [source: TAW 2003] as:

$$p(q) = \frac{1}{\sigma_q \sqrt{2\pi}} e^{-\left[\frac{(q-q_{avg})^2}{2\sigma_q^2}\right]}$$ (7-5)

Where:

$p(q)$	= chance of occurrence of impact factor q	[-]
σ_q	= parameter probability density function impact factor	[-]
q_{avg}	= average impact factor	[-]

Equation (7-5) is obtained for a slope of 1:4 and for other slopes interpolation is required. For steeper slopes little information is unfortunately available. Nevertheless a high reliability can be achieved for slopes varying between 1:3 and 1:8 according to Führböter (1988).
Finally it must be noted that these equations are valid for the unfavorable case of smooth slopes. As grass covers can have a rough surface (for instance local irregularities due to erosion) the impact pressures might be lower. In the above an approach has been suggested to predict impact pressures similar to the method used in Golfklap. This is considered to suffice and the prediction of impact pressures will not be further investigated in this thesis.

7.2.2 Damping by backwash layer

It has been mentioned several times in the previous chapters that the backwash layer has a damping effect on the impact pressure. Since an erosion relation similar to Stanczak (2008) is adopted in the erosion model, theoretically the damping by the backwash layer should be taken into account separately.
It makes little sense though to incorporate this effect in an erosion model for outer slopes; the damping of breaking wave impact pressures by the backwash layer has already been accounted for in the impact factor [Führböter and Sparboom 1988]. The effect of the backwash layer would then be taken into account twice. Nonetheless the damping by the backwash layer is investigated in more detail below to get an indication of the possible qonsequences if this assumption is incorrect.
Because there is no wave breaking involved in the impact load on inner slope transitions caused by overtopped water the damping effect was also implemented in the transition model by Valk (2009). The resulting pressure of an impact after damping by a water layer is given by equation (7-6) [Stanczak 2008a].

$$p = p_{\max} \cdot e^{-wh}$$ (7-6)

Where:

w	= water layer damping coefficient = 0.25	[-]
h	= water layer thickness	[m]

To be able to use this formula the thickness of the backwash layer has to be determined. In chapter 3 a method was presented to calculate the maximum layer thickness on any position on the slope

during wave run-up. Although the maximum water layer thickness is an important parameter to estimate the infiltration in the dike it is not of primary interest for the determination of the damping effect by the backwash layer.
Instead the thickness of the backwash layer should be known at the moment of and at the location of the impact; hence the water layer thickness during wave run-down has to be determined. It is supposed that impact occurs approximately during the moment of maximum wave run-down and that the water layer thickness at the location of maximum wave run-down is equal to zero. From this point the layer thickness decreases linearly with the horizontal run-up length. Equation (3-16) can then be adapted with $x_z = x_d$ to estimate the thickness of the backwash layer during maximum wave run-down at the point of impact, which yields:

$$h_a(x_*) = c_2(x_d - x_a) = c_2 \cdot x_* \tag{7-7}$$

With this adapted equation the layer thicknesses in the impact zone during maximum run-down were determined for the wave conditions of the tests in the GWK (see also Appendix A). The results of this simulation are depicted in Figure 7-2.

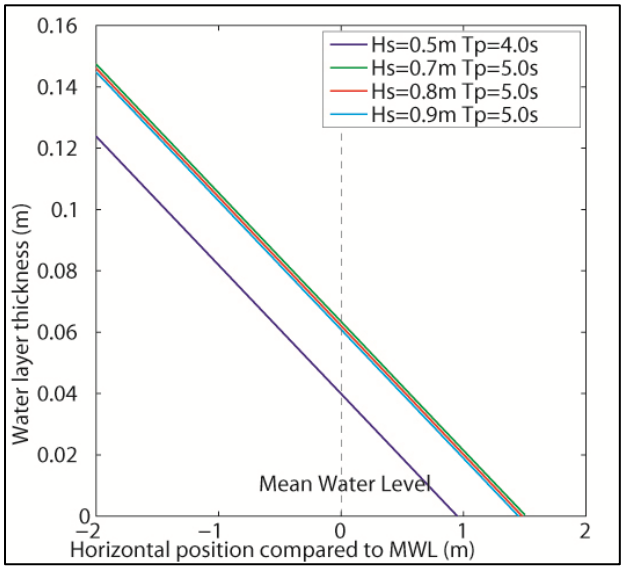

Figure 7-2: Water layer thickness during maximum run-down according to equation (7-7).

It can be concluded that the layer thickness at the impact point is less than 0.15 m for the wave conditions during the tests. With these results an estimate can be given for the damping effect with the help of equation (7-6), which has been plotted in Figure 7-3.

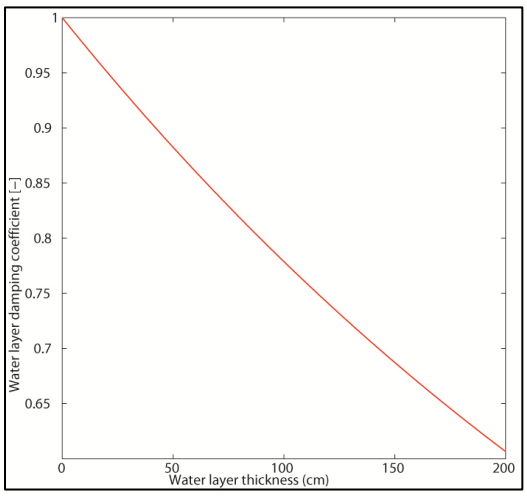

Figure 7-3: Pressure damping as a function of water layer thickness.

Equation (7-6) gives the damping effect as a function of water layer thickness and it was obtained by water impact experiments on clay with a water layer on the surface. However the impacts were not generated by waves but by dropping a mass of water on the covering layer from a certain fall height by opening a valve. The impact pressures could be predicted with high accuracy because there was no influence by wave breaking processes; hence the damping effect could be determined reasonably accurate as well.
Fortunately the damping effect is rather marginal for small water depths as can be concluded from Figure 7-3: for layer thicknesses of approximately 15 cm, the pressure reduction is in the order of 3.5 percent. The damping by the backwash layer can therefore safely be excluded from the model, as this does not cause a significant loss of accuracy.

7.2.3 Influence of crack dimensions

Usually cracks are filled with water only, but during a wave impact they actually are filled with an air-water mixture. This mixture can have a significantly larger compressibility than pure water due to the presence of air bubbles. The result is a higher rate of energy dissipation (pressure damping) and a lower velocity of pressure propagation (50-300 m/s) [Husrin 2007], The additional pressure damping that is caused by an air-water mixture is discussed in the next section.
The crack width is usually left out of consideration but according to Müller (2003) the crack width has influence on the pressure magnitude as well. The air content, and thus the damping effect of the water-air mixture, depends on the crack width.
During experiments it was observed that the propagation speed of the pressure pulse inside the crack increased from 50–60 m/s for 0.5 mm cracks to 250–300 m/s for 10–18.25 mm wide cracks. Thus it can be concluded that the pressure propagation is higher for increasing crack widths; smaller cracks have a greater damping effect on the pressure in the crack [Müller, Wolters et al. 2003]. This was mainly attributed to the aeration of the water, which is probably greater in small cracks as small air bubbles seem to adhere to the walls of small cracks due to capillary forces.
Furthermore the experiments indicated that the pressure magnitude was not affected by changes in crack cross section; even sudden changes in geometry such as sudden curves and angles did not affect the pressure propagation at all [Müller et al. 2003]. It is expected that this also applies for pressure propagation into fissured soil.
For especially cracks with small widths (0.5-3.0 mm), there is thus a tendency for the pressure to reduce in magnitude as the distance from the crack entrance increases (see also Appendix F). To estimate the reduction of the pressure with increasing distance in the crack the following formula [Wolters and Müller 2004] was proposed:

$$P_{end} = \frac{1}{10L_c}\rho_w g H \qquad (7\text{-}8)$$

Where:
L_c = crack length [m]

Equation (7-8) should however be considered merely as a guideline value since deriving a physically based relationship has not yet been possible. As the cracks in a grass cover generally have an irregular shape and are of small width an impact pressure can be transmitted into the soil but these are reduced with increasing distance from the crack entrance. The relation between pressure in the crack and crack depth can thus be characterized as follows:

$$P_{crack} \sim \frac{P_{\max}}{d_c} \qquad (7\text{-}9)$$

Where:
d_c = distance in the crack [m]

To quantify this relation the results of the laboratory experiments by Müller (2003) (see Appendix F) were approximated with an equation according to relation (7-9). For 0.5 mm, 1.0 mm and 3.0 mm cracks this yields Figure 7-4.

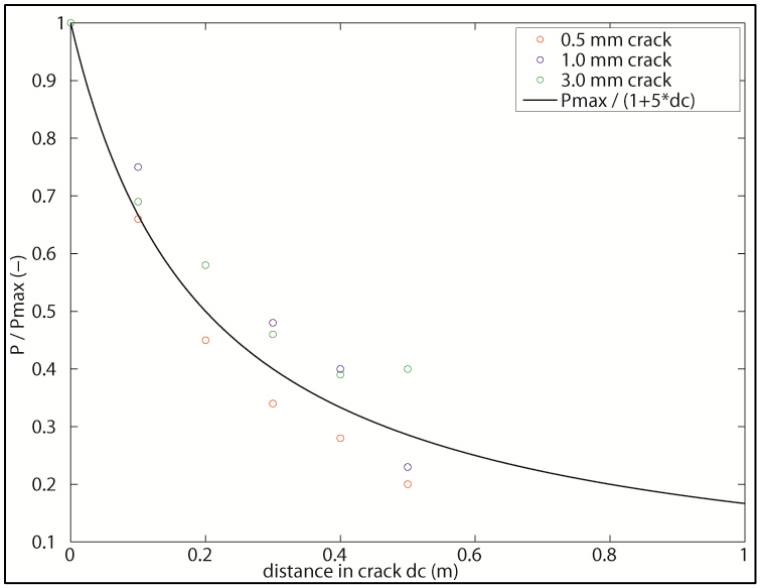

Figure 7-4: Approximation of impact pressure reduction in small cracks.

The pressure damping by the cracks in the cover layer can thus be represented by equation (7-10):

$$p_{crack}(d_c) = \frac{p_{\max}}{1+\mu \cdot d_c} \qquad (7\text{-}10)$$

Where:

μ = pressure reduction coefficient = 5 [m^{-1}]

Another phenomenon to take into consideration is the fact that the impact pressures are transmitted not only into the crack walls, but also, to some extent, inside the dike, through the crack[Berkenbrink 2007 source: Husrin 2007]. This transmission has however not been quantified yet.

7.2.4 Air water ratio

It was already highlighted in chapter 3 that the presence of air bubbles in a breaking wave has a cushioning effect; the wave impact pressure on the cover layer is reduced when air is entrained. Yet there is no exigency to model the damping of the impact pressures on the surface as a result of aeration; it is already accounted for implicitly in the impact factor of Führböter. Nonetheless the air content remains an important parameter for the pressure propagation within water-filled cracks. This effect was already modelled in the previous section (7.2.3) where it was suggested that the impact pressures within small water-filled cracks are damped due to the presence of air bubbles in these cracks. Hence the air content in cracks is not included separately in the WIPE model.
The influence of the air content on the magnitude of the impact pressure of a breaking wave was investigated by Bullock and Crawford et al. (2001). Furthermore the difference between the aeration of salt and fresh water might be important for the pressure damping in river and sea dikes (see also Appendix G). However during the small scale tests it was concluded that the impact pressures generated by fresh water were only slightly higher than the impact pressures generated by salt water. The effect of the higher aeration in salt water might be significantly greater though in full scale waves.[Bullock, Crawford et al. 2001]

7.2.5 Conclusion

Although the impact pressures generated by waves are damped by the backwash layer, there is no need to model this effect separately. Additional pressure damping occurs when the impact pressure enters a small crack and propagates into the crack; its magnitude diminishes with crack distance. This effect is taken into account and therefore the uplift pressure at a distance d_c [m] in the crack is approximated with equation (7-11):

$$p_{up} = \frac{p_{\max}}{(1+\mu d_c)} \tag{7-11}$$

Where:

p_{up}	= uplift pressure underneath an aggregate after wave impact	[N/m^2]
d_c	= distance in the crack from the surface	[m]
μ	= pressure reduction coefficient = 5	[m^{-1}]

7.3 Strength terms

For the erosion process two erosion mechanisms are important: surface erosion and block erosion. Therefore two different critical strengths should be defined; one for the erosion of small aggregates (AE) and one for block erosion (BE). Aggregate erosion is a process where each individual soil aggregate erodes separately, while block erosion involves the instantaneous erosion of large pieces of soil (many aggregates at once).
The turf element model by Hoffmans et al., which was discussed in section 6.1.2, is used as a basis to model the strength of the grass cover as it provides a clear physical description of the strength. The strength of the grass cover is thus based on the root model by Wu et al. The most important parts of the modeling of the strength according to Hoffmans et al. (2009) are repeated in adapted form below. Because the grass strength is depth dependent an index 0 is introduced for the strength at the surface. The forces on a cube $l_x l_y l_z = d_a^{\,3}$, where d_a is the aggregate diameter, are:

F_p	= maximum lift force	$F_p = p_{up} \cdot l_x l_y$
F_w	= weight due to gravity	$F_w = (1-n)(\rho_s - \rho_w) g \cdot l_x l_y l_z$
F_s	= shear force	$\Sigma F_s = f(\rho_s - \rho_w) g (l_x + l_y)(l_z)^2$
F_c	= cohesion force	$\Sigma F_c = (c_{grass,c} + c_{clay,c}) \cdot \{2(l_x + l_y) l_z + l_x l_y\}$
F_g	= grass reinforcement	$F_g = \sigma_{grass,c} \cdot l_x l_y$

Where:

p_{up}	= maximum uplift pressure under the aggregate	[N/m^2]
f	= friction factor ($\tan\varphi$)	[-]

Incipient motion occurs when:

$$F_p \geq F_w + \Sigma F_s + \Sigma F_c + F_g$$

Subsequently applying $l_x = l_y = l_z = z$ yields the basic equation for the initiation of motion:

$$p_{up} \geq \sigma_s(z) = (1 - n + 2f)(\rho_s - \rho_w) g z + 4(c_{grass,c}(z) + c_{clay,c}) + c_{clay,c} + \sigma_{grass,c}(z) \tag{7-12}$$

Where:

$\sigma_{grass,c}(z) = t_{r,c} \frac{A_r}{A} + c_{grass,c}(z)$ and $c_{grass,c}(z) << \sigma_{grass,c}$		[N/m^2]
z	= depth	[m]
$c_{clay;c}$	= $c_{clay} / 80$	[N/m^2]

Equation (7-12) will be adapted for the two specific erosion mechanisms. This yields a limit state equation for surface erosion of fixed aggregates and a limit state equation for the erosion of blocks. In both limit states the strength of the grass cover is for a major part determined by the reinforcement due to roots. As the root density is depth dependent, the decline of the root density with respect to depth is treated before the two limit state equations are discussed.

7.3.1 Grass strength and depth dependency

As depth increases the grass strength diminishes because the root density is less at greater depth. The grass strength is thus variable with depth and several authors have tried to derive an equation that gives the variation of the root density with depth. Sprangers carried out field measurements in 1999 and derived an exponentially decreasing function for RVR depth profiles of 24 Dutch grasslands. Stanczak (2007) carried out laboratory tests and derived a similar function for the RVR. Good agreement was observed and Stanczak stated that the function represents an average quality grass cover.

The calculation of the grass strength is however based on the RAR. Fortunately Valk (2009) was able to relate the RVR and RAR by comparing the function of Stanczak with data of Sprangers, as was already mentioned in chapter 6: $RVR = 50 \cdot RAR$. Furthermore Valk gave an expression for the RAR with respect to depth:

$$\frac{A_r}{A} = \frac{0.0746}{100} \cdot e^{-\beta z} \tag{7-13}$$

Where:

β	= 22.32	[-]
z	= depth	[m]

Based on the same data another exponential function was proposed by Hoffmans et al. (2009):

$$\frac{A_r}{A} = RAR_0 \cdot e^{-\left(\frac{z}{z_{ref}}\right)} \tag{7-14}$$

Where:

RAR_0	= Root Area Ratio at the surface	[-]
z_{ref}	= 0.10	[m]

Equation (7-13) is based on mean values and corresponds according to Stanczak to an average quality grass mat. Equation (7-14) on the other hand requires the root density at the surface, consequently the quality of the grass mat is accounted for. To make both functions more equivalent and compare them equation (7-13) is changed into:

$$RAR(z) = RAR_0 \cdot e^{-22.32z} \tag{7-15}$$

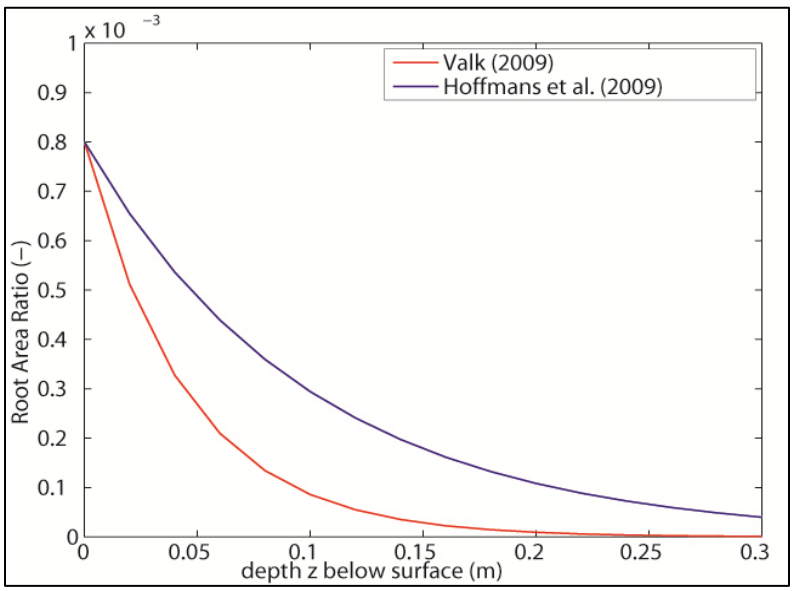

Figure 7-5: Predicted RAR depth profiles for good quality grass (RAR_0 = 0.0008).

It can be observed that the equation of Hoffmans et al. predicts higher root densities than the equation of Valk and also the roots penetrate further into the soil. Yet it is questionable if low root densities at a depth of 0.20 m and greater are still effectively reinforcing the soil. The reinforcement of the root system can mainly be attributed to the root system holding together the clay aggregates. At low root densities (i.e. greater depth) not all clay aggregates are reinforced by the root system.
It is not unlikely that at a certain threshold of the root density the reinforcing effect of the roots is nullified. Stanczak and Valk therefore chose zero root density at z =0.20 m and greater assuming that the reinforcing effect of the roots is negligible in this region, even though roots might still be present there. It is expected that the equation by Valk is more realistic than the one provided by Hoffmans and therefore it is adopted in this research. Equation (7-15) is thus used to introduce depth dependency for the root density which results in the following equations for the grass strength:

$$\sigma_{grass,c}(z) = t_{r,c} \cdot RAR_0 \cdot e^{-22.32z} \tag{7-16}$$

$$c_{grass,c}(z) = 1.2 \cdot t_{r,c} \cdot RAR_0 \cdot e^{-22.32z} \tag{7-17}$$

7.3.2 Characteristic aggregate diameter and turf area per root

It is assumed there are no loose aggregates at the surface; consequently each root supports a small block of soil with a certain dimension, depending on the number of roots in the area. The turf area per root A_t [mm^2] can be calculated by simply dividing the cover layer area by the number of roots:

$$A_t = \frac{A}{n_r} \tag{7-18}$$

Where:

n_r = number of roots [-]

The root spacing s [m], the average distance between two roots, is equal to the square root of the turf area per root:

$$s = \sqrt{A/n_r} \tag{7-19}$$

The characteristic aggregate diameter d_a due to soil structure applied in recent models is 4 mm. For good grass quality the root spacing at the surface is 4 mm as well, thus it can safely be assumed that each aggregate in a uniformly rooted high quality sod is supported by a root.
Assuming a root diameter d_r =0.13 mm and a root tensile strength t_r =20·10^6 N/m^2 the root properties of Dutch grassland can be determined (Table 7-1).

Table 7-1: Root properties of Dutch dike grassland.

Quality grass according to VTV	*Number of Roots No./m^2*	RAR_0 *[-]*	*Turf area per root* A_t *[mm^2]*	*Root spacing s [mm]*	$c_{0,grass,c}$ *[kN/m^2]*	$\sigma_{0,grass,c}$ *[kN/m^2]*
very poor	15.000	0.0002	67	8	4.8	4.0
poor	30.000	0.0004	33	6	9.6	8.0
average	45.000	0.0006	22	5	14.4	11.9
good	60.000	0.0008	17	4	19.2	15.9

Where:

d_r =0.13 mm

$c_{0grass,c} = 1.2 \cdot t_{r,c} RAR_0$ using θ =45°, φ =35° and $t_{r,c}$ =20·10^6 N/m^2

$\sigma_{0,grass,c} = t_{r,c} RAR_0$

For very poor quality sod the root spacing increases to 8 mm which is just twice the characteristic aggregate diameter. Therefore it is not unlikely that at the surface a root in a poor quality sod is still

able to support all the aggregates around it. In fact as this difference is not very large, perhaps the characteristic aggregate diameter could even be related to the turf area per root instead of using an equal characteristic aggregate area for all cases.
This assumption also squares with the fact that the degree of soil structure is generally lower when the clay layer is penetrated by a less developed root system (for instance less macrobiotic pores and less root penetration). As a consequence each root supports a single aggregate when no weaker spots occur in the considered area of the grass cover. The characteristic aggregate diameter d_a [m] is then equal to the root spacing s :

$$d_a = \sqrt{A/n_r} = s \tag{7-20}$$

7.3.3 Soil structure and depth dependency

The fact that the root density has an influence on the aggregate size was emphasized several times already. According to van Essen (1994) [source: Sprangers 1999] a structure of fine aggregates can be found in densely rooted zones whereas larger aggregates are found in zones with a lower root density. Perhaps the aggregate diameter should therefore be related to the root density, according to the following relation:

$$d_a = \sqrt{\frac{A}{n_r}} = \sqrt{\frac{1}{RAR(z)/0.25 \cdot \pi \cdot d_r^2}} \tag{7-21}$$

The aggregate size is then inversely proportional to the number of roots per square meter. However root growth is not the sole process that affects the degree of soil structure, hence it is preferred to use a simpler approach where the aggregate size increases linearly with depth.
According to Sprangers (1999) the aggregate diameter at a depth of 0.20 m varies between 2 mm and 200 mm. Therefore at a depth of 0.20 m a characteristic aggregate diameter of 20 mm is adopted. The relationship between aggregate diameter and depth for good quality grass is then given by equation (7-22).

$$d_a = \sqrt{A/n_r} + 0.08 \cdot z \tag{7-22}$$

Both relations are plotted in Figure 7-6; it can be observed that the distributions according to root density (blue graph) and the linear distribution (red graph) give corresponding results up to a depth of 0.10m. The linear distribution in equation (7-22) is therefore adopted for the decreasing effect of soil structure.

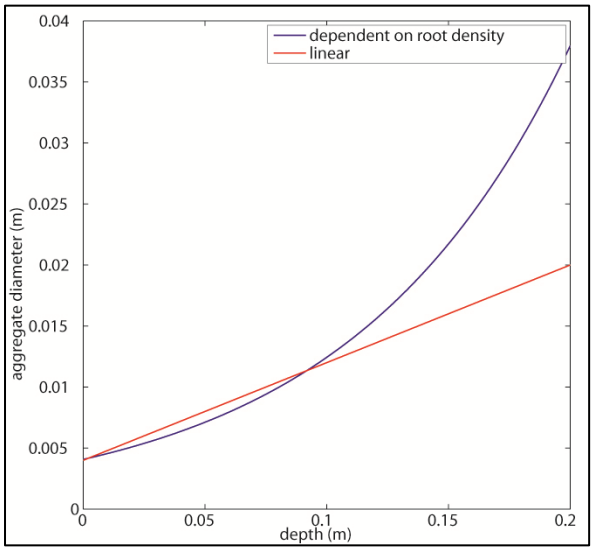

Figure 7-6: Relations between aggregate diameter and depth for good quality grass.

7.3.4 Aggregate erosion

At a certain moment the uppermost part of the turf is cracked and saturated with water, which enables the wave impact pressures to cause uplift pressures underneath small aggregates.
It is assumed that cracks are present everywhere at the surface of the cover layer due to soil structure and impact pressures. Furthermore it is supposed that an aggregate can only be exposed to uplift pressures, when the grass-clay aggregate is fixed at three sides at most and not at the underside. When the aggregate is fixed at 4 sides or more the uplift pressure cannot easily develop directly underneath this aggregate, since the area around the aggregate is not cracked then.
The strength of an aggregate then depends on the number of sides of the block n_s [-] that have physical contact with the surrounding soil, therefore equation (7-12) with $z = d_a$ is changed into:

$$p_{up} \geq \left(1 - n + 0.5 n_s \cdot f\right)(\rho_s - \rho_w) g d_a + n_{s\cdot}(c_{clay,c} + c_{grass,c}(d_a)) + \sigma_{grass,c}(d_a) \tag{7-23}$$

In this way the amount of small cracks and pores in the soil partly determines the erosion resistance of an aggregate. When the number of cracks in the grass cover increases the friction and cohesion forces of the clay become smaller, which is in line with the expectations. The condition of the soil can then be divided into 4 classes as n_s ranges from 0 to 3. At the surface a particle will break loose if the critical condition for movement is reached. Incipient motion at the surface occurs when the uplift pressure p_{up} induced by the wave impact, exceeds the critical uplift pressure p_c [N/m^2].With $c_{grass,c}(d_a) = c_{0,grass,c}$ and $\sigma_{0,grass,c}(d_a) = \sigma_{0,grass,c}$ this condition becomes:

$$p_c = (1 - n + 0.5 n_s f)\left((\rho_s - \rho_w) g d_a + \frac{n_s \cdot (c_{clay,c} + c_{0,grass,c}) + \sigma_{0,grass,c}}{1 - n + 0.5 n_s f} \right) \tag{7-24}$$

Yet if at the surface the cover layer is severely cracked cohesion forces will not act on the sidewalls of the block. Soil aggregates can still be in contact with the surrounding soil though and wall friction can still play a role. In that case the soil aggregate is fixed at the underside of the block by only a root and equation (7-24) can be simplified. The equation for the soil strength $\sigma_s(z)$ for aggregates at the surface then reads:

$$\sigma_s(z) = \left(1 - n + 0.5 n_s f\right) \cdot (\rho_s - \rho_w) g d_a + \sigma_{grass,c}(z) \tag{7-25}$$

When the highly erosion resistant layer of the turf has been eroded, the erosion process will accelerate significantly and there will be ongoing damage; this is considered to be at a depth of 5 cm.

7.3.5 Block erosion

There is a possibility that the turf does not only erode gradually at the surface but that it fails instantly at greater depths as well; erosion of large blocks may occur. Block erosion occurs on the condition that a large crack is present or that another hole or local irregularity reaches deeper parts of the turf, allowing impact pressures to penetrate into the soil.
The crack walls are deformed horizontally due to the impact pressures in the cracks and consequently soil aggregates may move and are compressed against the surrounding soil. Macro pores can become clogged and eventually this will allow uplift pressures to develop at larger surfaces than only the aggregate areas. This is also enhanced by the increase in size of the aggregates due to the diminishing effect of soil structure in deeper parts of the cover layer.
However before uplift pressures can develop underneath a larger soil block area A_{block} [m^2] (equal to $d_{block}{}^2$) a horizontal crack has to be formed. For cracks to develop the soil has to be fractured first and fracturing of the soil is most likely to occur at the location of minimum fracture resistance σ_f [N/m^2], which is defined as follows:

$$\sigma_f \geq (1-n)(\rho_s - \rho_w)gz + \frac{0.5 n_s f(\rho_s - \rho_w) g \cdot z^2}{d_{block}} + \sigma_{grass,c}(z) \quad (7\text{-}26)$$

Where:

n_s	= side wall coefficient	[-]
d_{block}	= block diameter	[m]

The block area A_{block} at the moment of initial crack formation is assumed to be proportional to the characteristic aggregate size ($A_{block,0} = d_a^2$). As can be observed from equation (7-26) the fracture resistance consists of the weight of the column of soil, the friction of this column of soil due to the surrounding soil and the grass normal strength. This is contrary to equation (7-25) for surface erosion of small aggregates, where the friction of only a small aggregate is considered.
As a result of the packing of aggregates and possible overlapping of aggregates the friction of the whole column of soil contributes to the fracture resistance, whereas clay and grass cohesion are still assumed to be negligible due to soil structure and the fact that these forces are not immediately mobilized during the crack formation process. However the walls of the crack are compressed during wave impacts in the crack. Consequently the blocks of soil in the crack wall are pushed against the surrounding soil, which enables friction to develop at one or more sides of the blocks. The factor n_s determines the influence of friction due to surrounding soil and can be considered as a parameter that represents to what extent the soil is structured or has inconsistencies.
Differentiation of equation (7-26) to z gives the location $z_{\min}$ [m] where the fracture resistance σ_f is at a minimum. As obtaining the derivative of the fracture resistance is rather complicated, an equation for the depth of minimum fracture strength is not given; $z_{\min}$ is approximated with the software package Matlab instead.
When a crack has been formed it will grow according to the balloon mechanism (chapter 4) and once the crack reaches a critical length part of the turf may be ripped out of the subsoil, leading to block erosion. To model the block erosion process, the eroded blocks are assumed to be box-shaped with base A_{block} [m^2] and height $z_{\min}$ [m].
Although the deeper parts of the grass cover could have more coherence due to vertical and horizontal compression by wave impacts and the weight of the grass cover, small cracks are expected to be present in the side walls of the crack or to be easily opened up again. The length of these cracks is supposed to be equal to the aggregate diameter.
Hence the initial block area $A_{block,0}$ will be equal to the base of an aggregate (d_a^2) but as the horizontal crack extends, the block area and thus the uplift force increase as well. Once a critical value of the block area has been reached the block can be washed away. Failure can thus occur by a single extreme impact pressure but also by milder, more frequently occurring impact pressures. By applying $l_x = l_y = d_{block}$ and $l_z = z_{\min}$ the limit state equation for block erosion can be determined:

F_p	= maximum lift force	$F_p = p_{up} \cdot A_{block}$
F_w	= weight due to gravity	$F_w = (1-n)(\rho_s - \rho_w) g \cdot A_{block} z_{\min}$
F_s	= shear force	$\Sigma F_s = 0.5 n_s \cdot f(\rho_s - \rho_w) g \cdot d_{block}) \cdot z_{\min}^2$
F_c	= cohesion force	$\Sigma F_c = (n_s \cdot d_{block}) \left(\int_0^{z_{\min}} c_{grass,c}(z) + c_{clay,c} \cdot z_{\min} \right)$
F_g	= grass reinforcement	$F_g = \sigma_{grass,c}(z_{\min}) \cdot A_{block}$

Incipient motion occurs when:
$F_p \geq F_w + \Sigma F_s + \Sigma F_c + F_g$

$$p_{up} \cdot A_{block} \geq (1-n)(\rho_s - \rho_w) g \cdot A_{block} z_{\min} + 0.5 n_s \cdot f(\rho_s - \rho_w) g \cdot d_{block} z_{\min}^2$$
$$+ \left(\int_0^{z_{\min}} c_{grass,c}(z) + c_{clay,c} \cdot z_{\min} \right) \cdot n_s \cdot d_{block} + \sigma_{grass,c}(z_{\min})$$

Dividing by A_{block} yields the critical uplift pressure for block erosion:

$$p_{up} \geq (1-n)(\rho_s - \rho_w) g z_{\min} + \frac{0.5 \cdot n_s f(\rho_s - \rho_w) g \cdot z_{\min}^2}{d_{block}} + \frac{n_s \left(\int_0^{z_{\min}} c_{grass,c}(z) + c_{clay,c} \cdot z_{\min} \right)}{d_{block}} + \sigma_{grass,c}(z_{\min}) \quad (7\text{-}27)$$

Unlike the erosion resistance of small aggregates, which is not influenced by cohesion due to cracks, the erosion resistance of large blocks is probably increased by cohesion forces. Horizontal roots can provide support between the block and the soil in its vicinity. Furthermore it is not unlikely that the side walls of the block are partly packed together again due to the compression caused by the impacts. In combination with the diminishing soil structure some sections of the block sides may thus have cohesion.
Unlike the critical clay cohesion, which is constant, the grass cohesion in equation (7-27) is variable with respect to depth and needs to be integrated. The equation for the critical uplift pressure for block erosion is reduced again to equation (7-24) for $d_{block} = d_a$ and $z_{\min} = d_a$, since the grass cohesion for small aggregates can be assumed constant. Moreover it can be reduced to equation (7-25) if in addition the grass cohesion $c_{grass,c}$ and the clay cohesion $c_{clay,c}$ are neglected.

Crack growth and failure criterion

Once an initial crack has been formed the crack can grow or block erosion can occur, this is dependent on the magnitude of the impact pressure. An overview of the possible events is given in Figure 7-7. Erosion can occur when the uplift pressure exceeds the total strength of the grass cover p_c and the crack length is increased when the load exceeds only the fracture strength σ_f.

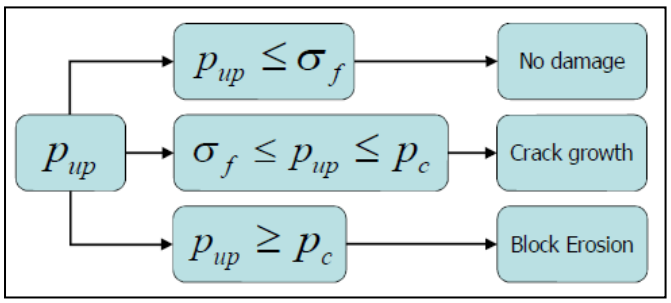

Figure 7-7: Crack growth or block erosion depending on the magnitude of the load.

When the fracture strength is exceeded the block of soil is slightly lifted which causes crack extension at the fixed ends of the block. As the increase of the crack length should also depend on the clay quality the increase of the block area ΔA_{block} is assumed to be equal to the residual uplift pressure divided by the fracture strength and the clay critical strength:

$$\Delta A_{block} = \frac{\left(p_{up} - \sigma_f \right) A_{block}}{\alpha_{crack} (\sigma_f + c_{clay,c})} \quad (7\text{-}28)$$

Where:

α_{crack} = crack growth parameter =1.0 [-]

When the uplift pressure does not exceed the fracture strength no damage occurs and the crack does

not grow. For a given grass cover strength a critical block size exists for which block erosion can occur. As the critical clay strength is rather low, equation (7-28) for $c_{clay,c} \to 0$ can be rewritten as:

$$\frac{\Delta A_{block}}{A_{block}} = \frac{\left(p_{up}\right)}{\sigma_f} - 1 \tag{7-29}$$

In Figure 7-7 it is displayed that block erosion can be triggered when the critical strength p_c is exceeded by the uplift pressure p_{up}. Yet in this case the total block has to be lifted during an impact, hence inertia plays a role. Since the WIPE model is static it is suggested that erosion occurs only when the following criterion, as a compensation for inertia and other dynamic effects, is satisfied:

$$\frac{(p_{up} - p_c) \cdot t_{imp}}{E_p} > z_{\min} \tag{7-30}$$

7.3.6 Weak spots

Weak spots at the surface have not been taken into account yet in the WIPE model, yet failure due to the presence of cracks and other inconsistencies in the grass cover layer has been treated extensively.
It is anticipated that weak spots at the surface do not notably influence the block erosion process, whereas the presence or the formation of local irregularities and cracks is essential to induce block erosion. Wave impact induced block erosion will most probably not occur if the impact pressures cannot penetrate deeper into the soil.
Contrary to this weak spots at the surface will influence the aggregate erosion process. It was already explained that a location which has less root development, both depth and surface related, is more susceptible to erosion. In theory erosion is thus initiated at weaker locations such as dead plants or bare spots. However the surrounding grass has a reinforcing effect on the weak location because horizontal roots can penetrate the weak location below the surface and vertical roots can absorb additional loads from adjacent locations.
At a weak spot there is either a lower root density or there are no roots at all. The dimensions of such a weak spot determine if the grass cover will fail at this location; weak locations with a small area generally do not cause problems, but for each grass quality there will exist a critical size for damage.
As the WIPE model considers uniformly rooted grass covers the presence of bare spots and other weak locations such as dead plants is not included in the model.
It has to be noted though that for lower root densities and bare spots impact pressures might not be the only relevant load in the erosion process. It is expected that flow velocities will start to affect the aggregate erosion process for low root densities or when the critical bare spot size is exceeded. Taking into account bare spots in the model by merely adjusting the strength characteristics of the grass cover will not be sufficient. In that case the model will require more adaptations; an additional load due to flowing water needs to be defined and possibly the strength modeling will change as well. These adaptations will however not be further investigated.
Nonetheless an approach will be given to include weak spots in the model. The concept of local load sharing (LLS) can be applied to model the effect of surrounding grass on weak locations at the surface. A possible approach to account for weak spots at the surface is presented below.

Weak spots at the surface

For rectangular weak spots the following holds (Figure 7-8) for the area of the weak spot A_{ws} [m^2], the circumference of the weak location C_{ws} [m] and the area of the strip of surrounding grass that supports the weak location A_{sg} [m^2]:

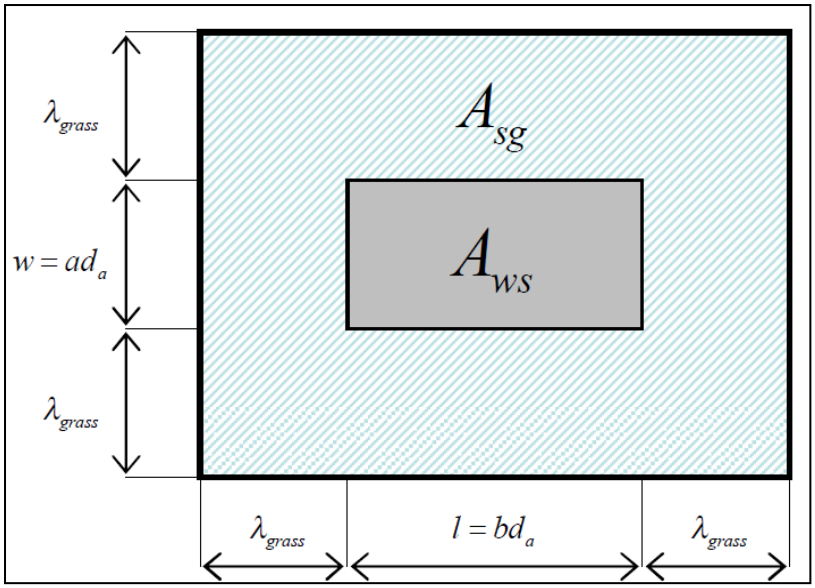

Figure 7-8: Weak spot and the surrounding grass in the influence area.

In the event of circular weak spots the dimensions can be rewritten as:

$$A_{ws} = 0.25\pi\left(ad_a\right)^2$$

$$C_{ws} = 2\pi ad_a$$

$$A_{sg} = 0.25\pi\left(ad_a + 2\cdot\lambda_{grass}\right)^2 - 0.25\pi\left(ad_a\right)^2 = \pi\left(\lambda_{grass}ad_a + \lambda_{grass}^2\right)$$

The influence length is an important parameter to quantify the reinforcing effect of the grass that surrounds a weak spot. For now the influence length estimated at 20 cm, which corresponds to the depth where root density on average becomes negligible small. As the weak spot is supported by the surrounding grass, the root density should be modified for this area. For this purpose the area of the weak spot A_{ws} and the area of surrounding grass A_{sg} are added together, which will be referred to as the influence area A_i [m^2]. For the influence area the modified Root Area Ratio RAR' [-] can be calculated with equation (7-31).

$$RAR' = \frac{A_{r,ws} + A_{r,sg}}{A_i} \tag{7-31}$$

7.4 Erosion parameter

7.4.1 General

There are several methods available to determine the erosion parameter for soil or clay. In 2004 Hanson and Cook developed a simple method to determine soil erodibility in situ with a submerged jet testing apparatus and an analysis tool was presented based on data of soil erodibility tests carried out at a large amount of locations in the Powder River basin of Northeastern Wyoming (Appendix H). Later in 2008 the same data was analyzed by Thoman and Niezgoda; a model was developed that relates the critical shear stress of soil to its five most significant parameters (Appendix H).
Both the studies of Thoman and Niezgoda and Hanson and Cook are useful contributions to a more uniform classification of soil erodibility in the future. Yet the erodibility parameter for erosion of cohesive soils without roots by shear stress was determined during these investigations. These studies are therefore less relevant for this research, but it can be concluded from these studies that it is widely accepted that the erosion parameter should be inversely proportional to the strength characteristics of the material. Ideally the erosion parameter should be determined experimentally and subsequently defined by a function with a physical basis.

Particularly incorporating the effect of the grass in the erosion parameter is troublesome. It can for instance be accomplished by adjusting the erosion parameter of clay with grass properties similar to the method of Stanczak (2008) or by defining the erosion parameter as a function of the combined strength of grass and clay in the grass cover as done in the turf element model by Hoffmans et al. (2009) The latter method is preferred as it takes into account the combined strength of the cover layer and the parameter is inversely proportional to the strength. Yet this erosion parameter is applicable to erosion by shear stress and should be converted to be applicable in the model for impact erosion; this is elaborated in the next section.

7.4.2 Derivation erosion parameter for impact pressure erosion

The EPM/Hoffmans model was already discussed in chapter 6. In this model the erosion parameter C_E [$m^{-1}s^{-1}$], which is inversely proportional to τ_c, was obtained after the Delta flume tests in 1992 [Hoffmans et al. 2009] and is rewritten as:

$$C_E = \alpha_E \frac{g^2 d_a}{\nu \cdot U_c^{\ 2}} \quad \text{with } \alpha_E = 1.0 * 10^{-10} \qquad \text{Identical to equation (6-16)}$$

This erosion parameter was eventually transformed into:

$$E_{soil} = \alpha_{soil} \frac{U_c^2}{\sqrt{g d_a}} \qquad \text{Identical to equation (6-17)}$$

Where:

E_{soil} = erosion parameter depending on the qualities of both clay and grass [m/s]

$E_{soil} \equiv \alpha_{soil} \left(C_E^{\ -1} \right)$ with: $\alpha_{soil} = 20 \cdot 10^3$ [-]

The erosion parameter takes into account both grass and clay strength; these are incorporated in the parameter U_c. The critical flow velocity U_c at the surface (z =0) according to Hoffmans (2009) is equal to:

$$U_c^2 = \left(\frac{c_0^2}{r_0^2} \right) \cdot \left(\frac{1-n}{\alpha_\tau} \right) \cdot \left(\Delta g d_a + \frac{c_{clay,c} + \sigma_{0,grass,c}}{(1-n)\rho_w} \right) \qquad (7\text{-}32)$$

When the soil strength at the surface $\sigma_s(0)$ is inserted in equation (7-32) this yields:

$$U_c^2 = \left(\frac{c_0^2}{r_0^2} \right) \cdot \left(\frac{1}{\alpha_\tau} \right) \cdot \frac{\left((1-n) \cdot (\rho_s - \rho_w) \cdot g d_a + c_{clay,c} + \sigma_{0,grass,c} \right)}{\rho_w}$$

$$U_c^2 = \left(\frac{c_0^2}{r_0^2} \right) \cdot \left(\frac{1}{\alpha_\tau} \right) \cdot \frac{\left(\sigma_s(0) \right)}{\rho_w}$$

If the critical uplift pressure is taken equal to the soil strength $\sigma_s(0)$ at the surface, this gives:

$$p_c = \sigma_s(0)$$

$$U_c^2 = \left(\frac{c_0^2}{r_0^2} \right) \cdot \left(\frac{1}{\alpha_\tau \rho_w} \right) = \frac{1.21^2}{0.15^2} \cdot \frac{1}{18\rho_w} = \frac{3.615 \cdot p_c}{\rho_w}$$

Thus theoretically the relation between the critical impact pressure p_c and the critical flow velocity can be expressed roughly as:

$$\rho_w \cdot U_c^2 = 3.615 p_c \tag{7-33}$$

The erosion parameter E_p can then be expressed as follows:

$$E_p = \alpha_{soil} \frac{p_c}{\rho_w \sqrt{g d_a}} \tag{7-34}$$

Where:

E_p	= impact erosion parameter depending on strength of grass and clay	[m/s]
α_{soil}	= $5.5 \cdot 10^3$	[-]

Subsequently a dimensional analysis of the basic erosion relation of the WIPE model with the erosion parameter E_p [m/s] yields the following unit for the erosion rate:

$$\varepsilon_{imp} \sim \frac{p - p_c}{E_p} = \frac{[N/m^2]}{[m/s]} = \left[\frac{kg}{m^2 s}\right]$$

It is however preferred to express the erosion rate in [m/s] rather than in [kg/m^{2}s]. To accomplish this, the erosion rate is divided by the density of the soil ρ_s [kg/m^3]. This leads to the following basic impact erosion relation:

$$\frac{dy_m}{dt} = \frac{p_{up} - p_c}{E_p} \tag{7-35}$$

Where:

E_p	= impact erosion parameter given by equation (7-36)	[kg/m2 s]

$$E_p = \alpha_{soil} \cdot \frac{\rho_s}{\rho_w} \cdot \frac{p_c}{\sqrt{g d_a}} \tag{7-36}$$

Where:

α_{soil}	= $5.5 \cdot 10^3$	[-]

7.5 Impact time and sequential effect

7.5.1 Characteristic impact time

The WIPE model now predicts the erosion depth over time, which enables it to predict the erosion for a given storm duration. It would have needed no further modifications if the load on the grass cover was constant and continuous. Yet the uplift pressures generated by wave impacts are peak pressures and discontinuous. The slope is exposed to high impact pressures for only a small portion of the storm duration; the total impact time during a storm is therefore defined as:

$$T_{imp} = \sum_{1}^{N_{imp}} t_{imp,w} \tag{7-37}$$

Where:

T_{imp}	= total impact time during the storm	[s]
N_{imp}	= number of wave impacts	[-]
$t_{imp,w}$	= impact duration of an individual wave	[s]

This gives for the relative impact time R_{imp} [-]:

$$R_{imp} = \frac{T_{imp}}{T_{storm}} \tag{7-38}$$

Where:

T_{storm} = storm duration [s]

The averaged impact time t_{imp} [s] can then be determined with this relative impact time R_{imp} :

$$t_{imp} = R_{imp} \cdot T_m \tag{7-39}$$

Where:

T_m = characteristic wave period given by T_{storm} / N_w [s]

N_w = number of waves during a storm [-]

To obtain the average impact time, ideally equations (7-37), (7-38) and (7-39) should be used. However determining the impact time for each individual wave is labour intensive. Furthermore for the prediction of erosion this data is mostly not available. The average impact time was therefore determined for the tests conditions of the EroGRASS experiments in the GWK. For the minimum and maximum wave characteristics during the EroGRASS experiments and the impact pressure exceeded by 50% of the waves according to Führböter, the rise times and impact durations were computed. Equations (3-3) and (3-4) were evaluated to obtain the results in Table 7-2.

Table 7-2: Predicted average rise times and impact durations for the EroGRASS experiments.

Significant wave height H_{m0} [m]	*0.50*	*0.90*
Wave period [s]	4.0	5.0
$p_{\max,50}$ [kPa]	14.7	26.5
Rise time t_k [ms]	86	108
Ratio t_d / t_k [-]	3.75	3.75
Impact duration t_d [ms]	323	405

The rise times and the impact durations in Table 7-2 are approximately a factor 2.0 larger than previously found by Führböter and Sparboom (1988). This can be explained by the fact that the computed values in Table 7-2 represent the upper bound of the rise and impact durations, these values are on the conservative side. Nonetheless a value of 0.350 s is applied for the average impact duration t_{imp} on the surface and the uplift pressure within cracks.

Because of the aspects discussed above it is preferred to use a more practical form of the WIPE model for the prediction of erosion during a storm: one that predicts erosion with respect to the number of waves in a storm. The erosion depth for the number of waves causing an impact N_{imp} [-] can then be predicted according to the following relation:

$$y_m = \sum_{1}^{N_{imp}} \frac{\left(p_{up}(z) - p_c(z) \right) \cdot t_{imp}}{E_p(z)} \tag{7-40}$$

The number of waves causing an impact can be related to the number of waves in a storm, this relation could have the following form:

$$N_{imp} = \alpha N_w \tag{7-41}$$

Where:

α = wave impact coefficient between 0.0 and 1.0 [-]

It is suggested to determine the wave impact coefficient from the EroGRASS experiments by determining the number of wave impacts from either pressure data using a threshold pressure or from visual observations. Also the number of waves must be known which can be accomplished with a reflection analysis.

7.5.2 Chronological order of wave impacts

Besides the problem of predicting impact pressures on the basis of wave characteristics, for which a solution was already presented in section 7.2.1, another time related problem arises. Due to the diminishing strength of the grass cover with depth, the chronological order of the wave impact pressures is an important factor as well.

Because the strength of the grass cover is high at the surface, surface erosion is only initiated by high impact pressures, yet once minor erosion has developed the erosion resistance decreases. After a single high wave has hit the slope and has generated a high impact pressure, all subsequent impact pressures could thus be relevant.

Hence damage can develop gradually once an impact pressure has exceeded a certain threshold value. A few high impact pressures in an early stage of the loading period can severely weaken the grass cover. Subsequent mediocre impact pressures can then cause damage, whereas there would have been no damage if these mediocre impact pressures had occurred early in the loading period, before these high impact pressures have occured. This is contrary to cases where it is supposed that damage occurs due to a single extreme value of the impact pressure. Now the influence of the chronological order of wave impacts complicates the prediction of erosion of grass covers.

Once the probability of occurrence of the impact pressures is known an additional probabilistic analysis should therefore be performed to incorporate the chronological effect. In this analysis the probability of occurrence of high impact pressures in an early stage of the loading period should be investigated. Alternatively numerous loading programs could be generated using simulation techniques. Each loading sequence can then be used as the input load for the WIPE model, will yield numerous predictions for the erosion depth and the moment of failure.

7.6 Summary of all relevant equations

The basic equation for the Wave Impact Pressure Erosion (WIPE) model reads:

$$y_m = \sum_{1}^{N_{imp}} \frac{\left(p_{up}(z) - p_c(z)\right) \cdot t_{imp}}{E_p(z)}$$ Identical to equation (7-1)

Load terms

$$p_{up}(z) = \frac{p_{\max}}{(1+\mu d_c)}$$

$$N_{imp} = \alpha N_w ;\ N_w = T_{storm} / T_m$$

Grass strength terms

$$\sigma_{grass,c}(z) = t_{r,c} \cdot RAR_0 \cdot e^{-\beta z}$$

$$c_{grass,c}(z) = 1.2 \cdot t_{r,c} \cdot RAR_0 \cdot e^{-\beta z}$$

Strength terms Aggregate Erosion

$$p_c(z) = \left(1 - n + 0.5 n_s f\right) \cdot (\rho_s - \rho_w) \cdot g d_a(z) + \sigma_{grass,c}(z)$$

$$E_p(z) = \alpha_{soil} \cdot \left(\frac{\rho_s}{\rho_w}\right) \cdot \frac{p_c(z)}{\sqrt{g d_a}(z)}$$

With recommended values:
$y_{m,crit}$ =0.05 [m]; n_s =2.0 [-]; α_{soil} =5.5·10^3 [-].

Strength terms Block Erosion

For $\frac{(p_{up}(d_{block}) - p_c(d_{block}) \cdot t_{imp}}{E_p(d_{block})} > z_{\min}$ $\quad y_m = z_{\min}$ [m]

Where $z_{\min}$ [m] is the depth of the minimum fracture strength $\sigma_{f,\min}$ [N/m^2].

$$p_c = (1-n)(\rho_s - \rho_w) g z_{\min} + \frac{0.5 \cdot n_s f (\rho_s - \rho_w) g \cdot z_{\min}^2}{d_{block}} + \frac{n_s \left(\int_0^{z_{\min}} c_{grass,c}(z) + c_{clay,c} \cdot z_{\min} \right)}{d_{block}} + \sigma_{grass,c}(z_{\min})$$

$$E_p(d_{block}) = \alpha_{soil} \cdot \frac{\rho_s}{\rho_w} \cdot \frac{p_c(d_{block})}{\sqrt{g d_{block}}}$$

$$\sigma_f = (1-n)(\rho_s - \rho_w) g z + \frac{0.5 n_s f (\rho_s - \rho_w) g \cdot z^2}{d_{block}} + \sigma_{grass,c}(z)$$

$$\Delta A_{block} = \frac{\left(p_{up}(d_{block}) - \sigma_f(d_{block})\right) A_{block}}{\alpha_{crack}\left(\sigma_f(d_{block}) + c_{clay,c}\right)}$$ Where: $A_{block} = {d_{block}}^2$ [m^2]

With recommended values:
n_s =1.0-3.0 [m]; $d_{block,0} = d_a$ [m]; $c_{clay,c} = c_{clay}$ /80 [N/m^2]; α_{soil} 1.0 [-]; α_{crack} =1.0 [-].

Recommended values of parameters for both erosion types

z	= depth	[m]	
α	= 0.0-1.0	[-]	
t_{imp}	= 0.350	[s]	Based on experiments by Oumeraci and Staal et al. (2010)
μ	= 5.0	[m^{-1}]	Based on experiments by Müller et al (2003)
$t_{r,c}$	= $20 \cdot 10^6$	[N/m^2]	
RAR_0	= Root Area Ratio at the surface	[-]	
β	= 22.32	[m^{-1}]	Based on research by Valk (2009)
n	=0.4	[-]	
f	= $\tan\varphi$	[-]	
φ	=35	[°]	
ρ_s	=2000	[kg/m^3]	
ρ_w	= 1000	[kg/m^3]	
g	= 9.81	[m/s^2]	
d_a	= $\sqrt{A/n_r} + 0.08 \cdot z$	[m]	
n_r	= number of roots	[-]	

8 Calibration and verification

8.1 Analysis of EroGRASS data

8.1.1 Wave analysis

8.1.2 Pressure data analysis

8.2 Calibration

8.2.1 Input parameters for calibration of both erosion types

8.2.2 Calibration aggregate erosion (AE)

8.2.3 General results aggregate erosion

8.2.4 Calibration block erosion (BE)

8.2.5 General results block erosion

8.3 Erosion by flow velocities

8.3.1 Surface erosion of loose aggregates

8.3.2 Run-up and run-down velocities

8.3.3 Erosion by flow

8.4 Discussion

8.4.1 Data analysis

8.4.2 Aggregate erosion

8.4.3 Block erosion

8.4.4 Erosion by flow velocities

8.5 Conclusions

8.5.1 Data analysis

8.5.2 Aggregate erosion

8.5.3 Block erosion

8.5.4 Flow velocities

8.6 Calculation example

8.6.1 Prediction of wave impact pressures

8.6.2 Aggregate erosion

8.6.3 Block erosion

8 Calibration and verification

In this chapter the WIPE model will be verified and calibrated. The chapter starts with an analysis of the test data that will be used for the calibration in section 8.1. Subsequently the model is calibrated with this data in section 8.2. In section 8.3 the erosion induced by flow velocities is discussed as it was neglected in the WIPE model. After this the results of the calibration are discussed in more detail in section 8.4 followed by conclusions in section 8.5. The chapter ends with a calculation example in section 8.6.

8.1 Analysis of EroGRASS data

8.1.1 Wave analysis

To verify that the intended wave characteristics during each test were actually observed a wave analysis for each test has been carried out. As merely the characteristics of the incoming wave are important for this study a reflection analysis was performed. The results are displayed in Table 8-1.

Table 8-1: Wave characteristics of incident and reflected waves after reflection analysis.

Test		H_m	$H_{1/3}$	H_{m0}	T_{Hm}	$T_{H1/3}$	T_p	T_{m-10}
		[m]	[m]	[m]	[s]	[s]	[s]	[s]
8 April test 2 0.8 m / 5.0 s	incident	0.531	**0.763**	**0.75**	4.187	4.407	4.712	4.1
	reflected	0.149	**0.21**	**0.199**	4.273	4.603	3.462	4.349
10 April test 1 0.8 m / 5.0 s	incident	0.551	**0.785**	**0.78**	4.213	4.319	4.728	4.065
	reflected	0.135	**0.188**	**0.183**	4.758	5.214	5.006	4.742
11 April test 1 0.9 m / 5.0 s	incident	0.621	**0.857**	**0.866**	4.315	4.391	4.794	4.146
	reflected	0.157	**0.217**	**0.211**	4.221	4.812	1.615	4.369
16 April test 1 0.5 m / 4.0 s	incident	0.339	**0.484**	**0.459**	3.452	3.486	4.075	3.33
	reflected	0.086	**0.121**	**0.113**	3.757	4.059	3.794	3.658
16 April test 2 0.5 m / 4.0 s	incident	0.337	**0.484**	**0.484**	3.411	3.492	4.063	3.33
	reflected	0.088	**0.123**	**0.119**	3.833	4.05	3.795	3.673
16 April test 3 0.5 m / 4.0 s	incident	0.338	**0.485**	**0.485**	3.422	3.503	3.937	3.333
	reflected	0.088	**0.123**	**0.119**	3.837	3.979	3.869	3.671
22 April test 1 0.7 m / 5.0 s	incident	0.481	**0.676**	**0.672**	4.236	4.324	4.899	4.076
	reflected	0.143	**0.204**	**0.199**	4.14	4.949	1.614	4.412
22 April test 2 0.9 m / 5.0 s	incident	0.585	**0.837**	**0.837**	4.174	4.441	5.263	4.139
	reflected	0.143	**0.203**	**0.199**	3.981	4.696	1.614	4.361
22 April test 5 0.9 m / 5.0 s	incident	0.581	**0.849**	**0.815**	4.225	4.309	4.689	4.056
	reflected	0.137	**0.194**	**0.18**	4.768	5.357	5.207	4.758

Most tests have a reasonably good agreement with the desired wave heights; the difference is within 0.05 m. Only the tests on April 22 have a slightly larger difference between the intended wave height and the observed wave height.

8.1.2 Pressure data analysis

Before the erosion model can be calibrated it is vital to check if the input loads are reliable. To accomplish this, a statistical analysis was performed on the pressure records of all available tests.
First the pressure records were examined in L~DAVIS (see also appendix A and B) and per wave period one maximum pressure was identified. By using this method not all input pressures are automatically impact pressures, but the troublesome task of identifying every single wave impact pressure peak for each test was avoided. Especially identifying mediocre wave impact pressure peaks is sometimes arbitrary. The disadvantage is that the quasi static water pressures caused are included in the input, but as these are rather low these will most probably not initiate or cause significant erosion. Subsequently the maximum pressures that occurred when there was no wave loading were

excluded from the analysis if possible.
Analogous to work by Führböter the impact pressures that were generated should theoretically follow a log-normal distribution, but because also non-impact loads are included in the input loads it is expected that the distribution of the input loads will not completely follow a log-normal distribution. Nevertheless the statistical results of the tests with similar wave conditions were compared and plotted on a log-normal scale. Below the results of this analysis are discussed for each wave condition. During the tests the maximum pressures either occurred at pressure transducer DMD 2 or at pressure transducer DMD 3, hence the analysis is restricted to the pressure transducers that measured the highest pressures for each wave condition. The pressure records of all tests and all transducers can be found in Appendix B.

Tests with Hs=0.80 m and Tp=5.0 s

The statistics of the pressure records of pressure transducer DMD 2 during the tests on April 08 and April 10 were compared since highest pressures were measured by this transducer during these tests. Both tests were carried out with H_s =0.80 m and T_p =5.0 s and the results of the statistical analysis are displayed in Table 8-2 and Figure 8-2.

Table 8-2: Statistical analysis of the pressure data of tests with Hs=0.8 m and Tp=5.0 s.

Test	*Pressure transducer*	*No. of maxima [-]*	*Mean value [kPa]*	*Higher 50% [kPa]*	*Higher 66% [kPa]*	*Higher 90% [kPa]*	*Higher 98% [kPa]*	*Higher 99.6% [kPa]*	*Maximum value [kPa]*
08040802	DMD 2	394	3.49	2.93	3.97	6.73	9.75	12.33	16.01
10040801	DMD 2	836	3.34	2.96	3.90	5.93	7.78	12.77	18.76

As can be observed from Figure 8-1 both tests correspond well and it can be concluded that the conditions during both tests were equal. The small difference between both graphs could be explained by the difference in the number of maxima. Both tests are therefore considered suitable for the evaluation of the erosion model.

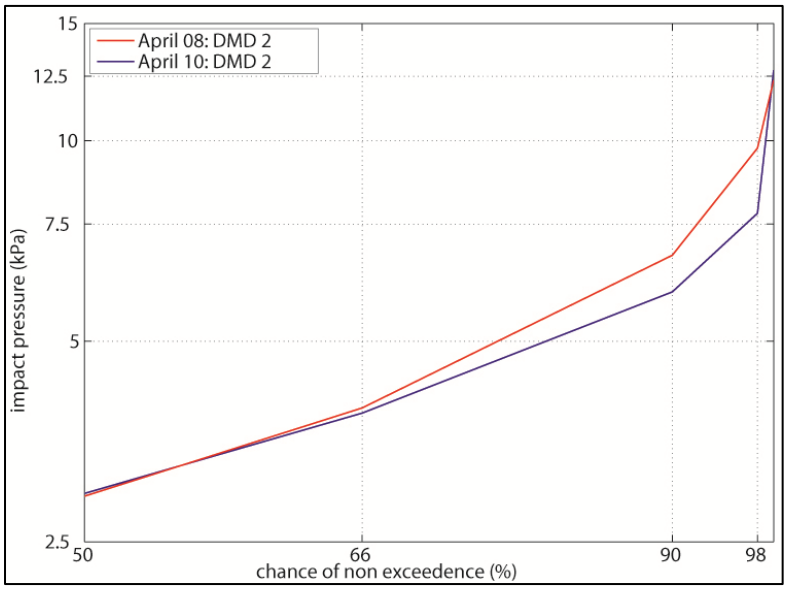

Figure 8-1: Comparison of pressure data of tests with Hs=0.8 m and Tp=5.0 s.

Tests with Hs=0.90 m and Tp=5.0 s

The statistical results of the pressure records of pressure transducer DMD 3 on April 11 and April 22 were compared since the highest pressures occurred near this transducer. All tests were carried out with H_s =0.90 m and T_p =5.0 s and the results of are displayed in Table 8-3 and Figure 8-2. It was expected that the highest pressures during all of these tests would occur at the same location (DMD 3); however from the pressure records of the test at April 11 it appeared that highest pressures occurred at DMD 2. Therefore pressure transducer DMD 2 is also included in the analysis.

Table 8-3: Statistical analysis of the pressure data of tests with Hs=0.9m and Tp=5.0 s.

Test	*Pressure transducer*	*No. of maxima [-]*	*Mean value [kPa]*	*Higher 50% [kPa]*	*Higher 66% [kPa]*	*Higher 90% [kPa]*	*Higher 98% [kPa]*	*Higher 99.6% [kPa]*	*Maximum value [kPa]*
11040801	DMD 2	483	4.41	4.01	4.91	7.04	10.43	15.35	20.32
11040801	DMD 3	517	3.70	3.70	3.85	4.29	5.98	9.89	12.95
22040802	DMD 3	843	4.53	3.78	4.61	7.38	13.74	25.25	33.79
22040805	DMD 3	147	4.47	4.02	4.70	7.29	12.00	15.69	18.89

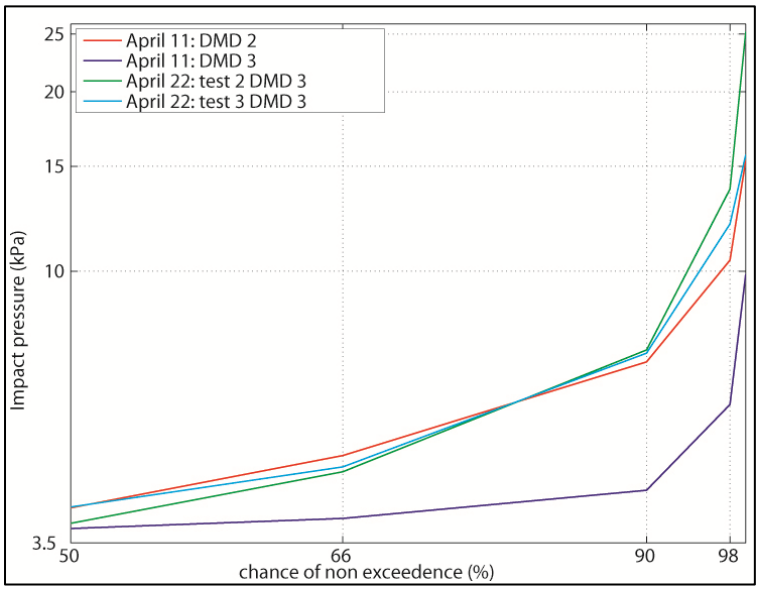

Figure 8-2: Comparison of pressure data of tests with Hs=0.9m and Tp=5.0 s.

During both tests on April 22 maximum pressures occurred at DMD 3, but test 3 was unfortunately of very short duration. Nevertheless the tests on April 22 show a relatively good agreement considering that the sampling time of test 3 on April 22 was rather short, which resulted in only 147 maxima for the analysis.
Furthermore it is clear that the values of the maximum pressures at the expected location of maximum impact pressure on April 11 (DMD 3) vary significantly from the pressures at DMD 3 during the tests on April 22. Yet surprisingly the data of DMD 2 on April 11 correspond reasonably well with the pressure data of April 22. This may indicate a calibration error or that a mistake was made during the post processing of the data. Considering that the maximum pressures occurred at a different location on the slope on April 11 it remains uncertain if the data of the test of April 11 are correct.

Tests with Hs 0.50 m and Tp 4.0 s

The results of the statistical analysis of the pressure records of pressure transducer DMD 3 on April 16 were compared since the highest pressures occurred near this transducer. All tests were carried out with H_s =0.50 m and T_p =4.0 s and the results of the statistical analysis are displayed in Table 8-4 and Figure 8-3.

Table 8-4: Statistical analysis of the pressure data of tests with Hs=0.5m and Tp=4.0 s.

Test	*Pressure transducer [kPa]*	*No. of maxima [-]*	*Mean value [kPa]*	*Higher 50% [kPa]*	*Higher 66% [kPa]*	*Higher 90% [kPa]*	*Higher 98% [kPa]*	*Higher 99.6% [kPa]*	*Maximum value [kPa]*
16040801	DMD 3	1035	2.94	3.05	3.33	3.82	6.37	8.70	12.95
16040802	DMD 3	1123	2.96	2.06	2.57	5.07	13.12	22.24	33.79
16040803	DMD 3	1038	3.04	3.13	3.45	4.08	6.44	11.26	18.89

As can be observed from Table 8-4 and Figure 8-3 test 1 and test 3 on April 16 show a very good agreement; the statistical values are almost identical. Contrary to this test 2 has significantly higher

extreme values than the other tests and does not agree with the other tests at all. Because all tests have approximately the same number of samples this difference cannot be directly explained.

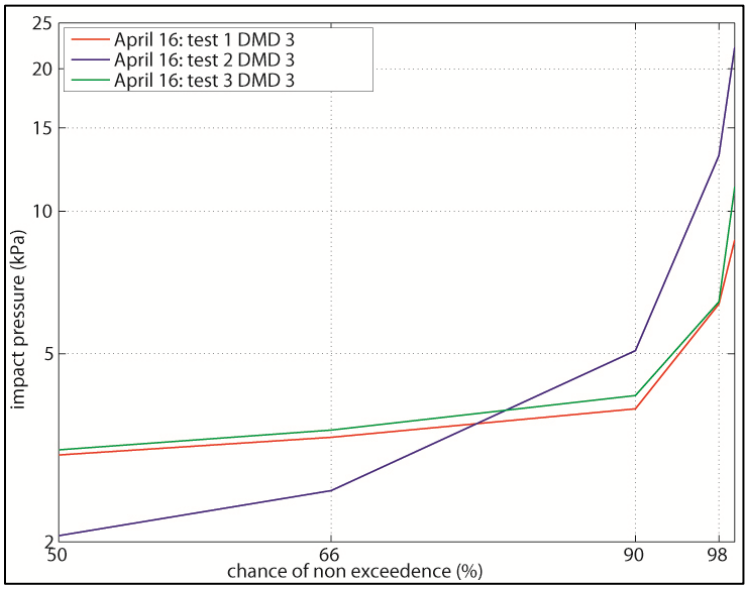

Figure 8-3: Comparison of pressure data of tests with Hs=0.5m and Tp=4.0 s.

To shed some light on this remarkable difference the pressure records of DMD of all three tests are once more compared in Figure 8-4. The difference between the pressure records is again striking; the number of high pressures peaks during test 2 (blue graph) is significantly greater and also the pressure magnitude of moderate impacts is in general considerably higher than the pressures in test 1 (red graph) and test 3 (green graph).

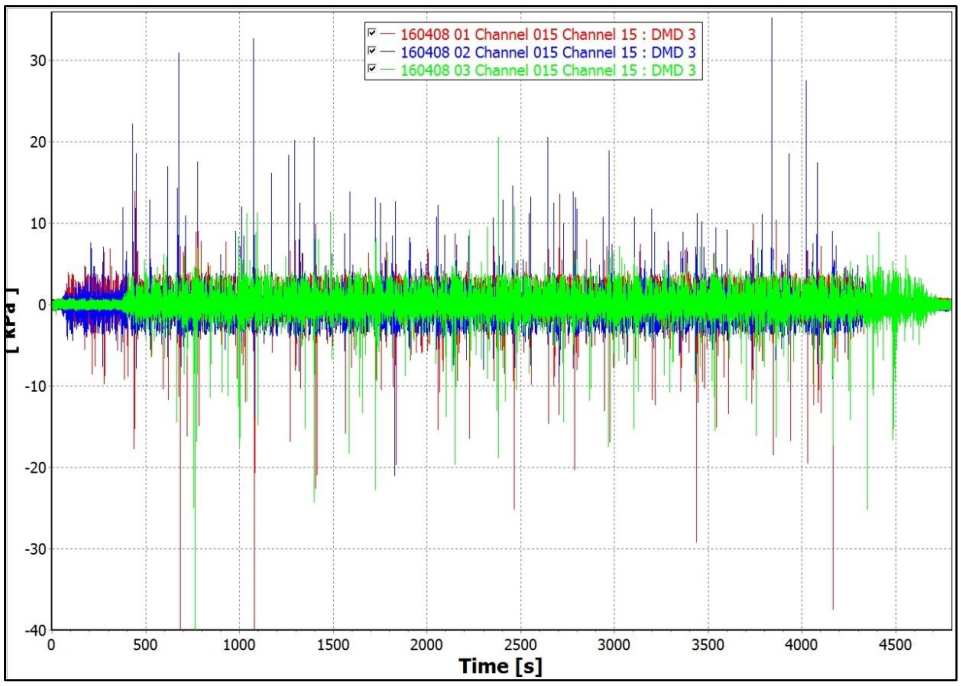

Figure 8-4: Comparison of the pressure records at DMD 3 of the tests on April 16.

This gives reason to question the correctness of the data obtained during test 2 on April 16. It is anticipated that the data needs calibration and is at this moment unreliable. This is also supported by the fact that the maximum pressure peaks during test 2 on April 16 are even higher than the maximum impact pressures during the tests with H_s =0.90 m and T_p = 5.0 s (Appendix B can be consulted for the pressure records of these tests).

8.2 Calibration

The WIPE model will be calibrated with the help of the data of the EroGRASS experiments. The visual observations of erosion of the grass cover in combination with the pressure records can be used to check the behavior of the model. In this analysis the maximum pressure during every wave period was selected as the maximum impact pressure. This approach was chosen to avoid selecting every wave impact peak separately, which is arbitrary and labor intensive.
However not every wave necessarily causes an impact pressure peak, consequently the input pressure data is can also be the result of a fluctuation of water pressure during run-up and run-down. Yet it is expected that these additional 'impact pressures' do not significantly influence the erosion process. The water pressure fluctuations are mostly lower in magnitude than the impact peaks and also the pressure gradients are more gradual.
Since the erosion process can be subdivided into aggregate erosion (AE) and block erosion (BE), the model will be separately calibrated for both processes. The calibration for aggregate erosion will be treated first, followed by block erosion. However before the model can be calibrated all input parameters need to be determined, which is discussed below.

8.2.1 Input parameters for calibration of both erosion types

Several coefficients were already derived in chapter 7, but the strength of the grass cover still needs to be defined. During the preparations of the experiments in the GWK the quality of the grass cover was determined by taking samples on several locations of the dike model.
For each sample the Root Volume Ratio was determined. The curve of the RVR which was obtained after sampling is displayed in Figure A-9 in the appendix. The value of the RVR near the surface was equal to 0.07, which is equivalent to a RAR value of approximately 0.0014.
For this RAR the critical uplift pressure p_c would be approximately 28 kPa, which is considered to betoo high. Furthermore this RAR is drastically higher than the RAR value for good grass given by other authors, which is approximately 0.0008. To exclude a possible overestimation of the grass strength, the grass cover is therefore considered as a good quality grass cover, with a RAR value of 0.0008 at the surface. The large deviation of the RVR from the usual values of good grass may be partly explained by the seasonal variation of the root diameters.
Besides the grass also the clay can provide strength. As category 2 clay was present in the grass cover the clay cohesion is assumed to be equal to 30.0 kPa (chapter 5). These and all other input parameters are summarized in Table 8-5.

Table 8-5: Input parameters for the calibration.

Parameter		*Value*
Root Area Ratio at the surface	RAR_0	0.0008
Grass tensile strength	t_r	$20 \cdot 10^6$ N/m^2
Root diameter	d_r	$0.13 \cdot 10^{-3}$ m
Root decay coefficient	β	22.32
Side wall coefficient	n_s	1-3
Clay cohesion	c_{clay}	$30 \cdot 10^3$ N/m^2
Critical clay strength according to Hoffmans et al. (2009)	$c_{clay,c}$	$c_{clay,c} = c_{clay} / 80$
Aggregate diameter at the surface	d_a	0.004 m
Saturated volumetric weight of soil	ρ_s	2000 kg/m^3
Volumetric weight of water	ρ_w	1000 kg/m^3
Porosity	n	0.4
Natural angle of repose	φ	35 degrees
Pressure reduction factor in cracks	μ	5 m^{-1}
Characteristic impact time	t_{impact}	0.350 s

8.2.2 Calibration aggregate erosion (AE)

For aggregate erosion the model is calibrated using only one factor: α_{soil} [-], which is included in the erosion parameter as follows:

$$p_c(z) = \left(1 - n + 0.5 n_s f\right)(\rho_s - \rho_w) g d_a(z) + \sigma_{grass,c}(z) \quad \text{with: } n_s = 2.0$$

$$E_p(z) = \alpha_{soil} \cdot \frac{\rho_s}{\rho_w} \cdot \frac{p_c(z)}{\sqrt{g d_a}(z)}$$

In appendix A the erosion events have been discussed, but during most tests aggregate erosion could not be clearly distinguished. From the middle of test 2 on April 22 aggregate erosion was observed regularly and smaller clumps of roots started to wash up more frequently. The total predicted erosion should be in the order of centimeters.
The aggregate erosion model will be calibrated on the pressure records of DMD 2 and DMD 3 of all tests, as the impact pressures at these locations were highest. Two calibration runs are performed and ideally these runs will need to consist of the tests displayed in Table 8-6.

Table 8-6: Test programs required for aggregate erosion calibration run 1 and 2 (AE1 and AE2).

Test	H_s *[m]*	T_p *[s]*	*Run 1 pressure transducer*	*Run 2 pressure transducer*	*Erosion events*
April 08 test 1	0.5	4.0	DMD 3	DMD 2	No data available
April 08 test 2	0.8	5.0	DMD 3	DMD 2	None
April 10 test 1	0.8	5.0	DMD 3	DMD 2	None
April 11 test 1	0.9	5.0	DMD 3	DMD 2	None
April 16 test 1	0.5	4.0	DMD 3	DMD 2	None
April 16 test 2	0.5	4.0	DMD 3	DMD 2	None
April 16 test 3	0.5	4.0	DMD 3	DMD 2	None
April 18 test 1	0.7	5.0	DMD 3	DMD 2	No data available
April 18 test 2	0.7	5.0	DMD 3	DMD 2	No data available
April 22 test 1	0.7	5.0	DMD 3	DMD 2	Visible Aggregate Erosion
April 22 test 2	0.9	5.0	DMD 3	DMD 2	Increasing Aggregate Erosion
April 22 test 3	0.9	5.0	DMD 3	DMD 2	Increasing Aggregate Erosion

Regrettably this test program is not entirely possible for the calibration run; data of test 1 on April 8 and of both tests on April 18 are not available. Furthermore the data of test 2 on April 16 are replaced by test 3 on April 16 because it is suspected that the data are incorrect (as was concluded in section 8.1). Although not all data is available for the simulation, it should not influence the result significantly as the wave conditions of these tests were reasonably mild. The test programs for both calibration runs are displayed in Figure 8-5, in the upper side of the graphs the date of the test is displayed which is accompanied by the test number if multiple tests were carried out on that date.
Clearly the loads of test program of AE run 2 (DMD2) are lower than the loads in AE run 1 (DMD3). In general the impact loads are lower at DMD 2, except for the tests with high wave heights of (0.80-0.90 m.). For both test programs high pressure peaks occur during tests on April 8, 10, 11 and 22-2 and 22-3. This indicates that the average wave impact point was presumably located in between these pressure transducers during these tests. Yet this is no surprise; it was already mentioned before that the impact pressures and the location of the impact point vary significantly per wave, even for regular waves. For the tests with milder conditions (tests on April 16 and 22-1) the impact pressures are clearly lower and the impact point is probably located closer to DMD 3.
The results of the simulations are displayed in Table 8-7, where N_{imp} is the number of wave impacts. $E_{p,0}$ and $p_{c,0}$ are respectively the erosion parameter and the critical impact pressure at the start of the simulation, while $E_{p,fail}$ and $p_{c,fail}$ represent respectively the erosion parameter and the critical impact pressure at the moment of failure of the grass cover or at the end of the simulation.

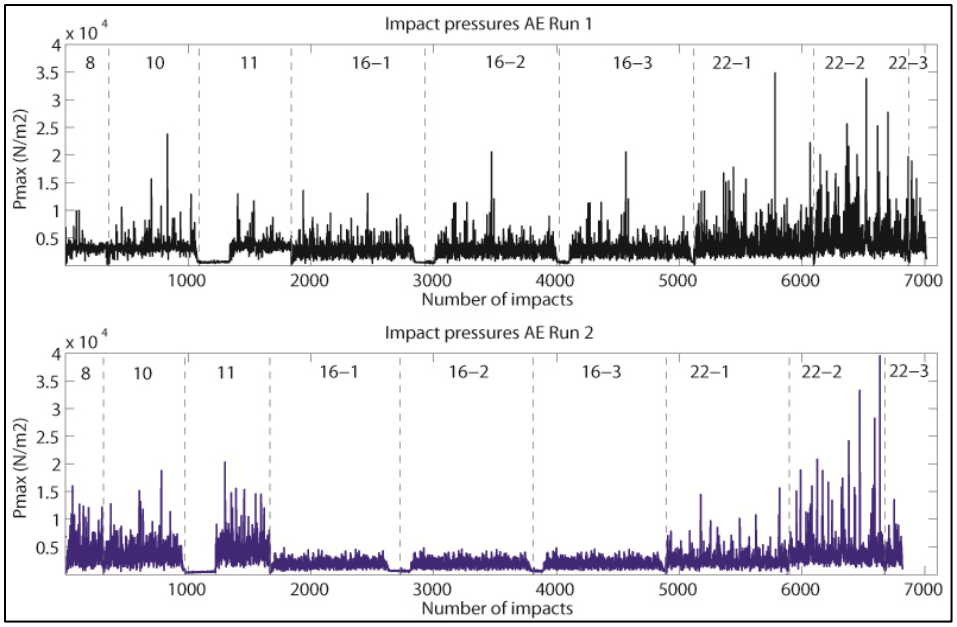

Figure 8-5: Test programs for Aggregate Erosion run 1 and run 2 (AE1 and AE2).

For the moment the characteristic length scale for the erosion depth y_m was assumed to be 0.05 m. Erosion will significantly speed up when the erosion depth has reached this value, because the strength of the grass cover is for the major part determined by the root reinforcement.
When failure occurred before the total test program had been completed, the last impact pressure before critical depth was reached was also included in the table. In chapter 7 the theoretical value of α_{soil} was determined at $5.5 \cdot 10^3$, but from Table 8-7 it can be observed that the model then predicts unrealistic low values for the erosion depth.

Table 8-7: Calibration results of calibration run 1 and run 2 (AE1 and AE2).

Run	*DMD*	α_{soil} *[-]*	$P_{c,0}$ *[N/m²]*	$P_{c,fail}$ *[N/m²]*	$E_{p,0}$ *[kg/m²s]*	$E_{p,fail}$ *[kg/m²s]*	N_{imp} *[-]*	P_{max} *[N]*	y_m *[m]*
AE1	3	$5.5 \cdot 10^3$	16051	16036	$8.913 \cdot 10^8$	$8.901 \cdot 10^8$	7012	-	$4.083 \cdot 10^{-5}$
AE1	3	55	16051	14361	$8.913 \cdot 10^6$	$8.901 \cdot 10^6$	7012	-	0.005
AE1	3	45	16051	13904	$7.293 \cdot 10^6$	$5.944 \cdot 10^6$	7012	-	0.0065
AE1	3	35	16051	13111	$5.672 \cdot 10^6$	$4.260 \cdot 10^6$	7012	-	0.0091
AE1	3	25	16051	13564	$4.051 \cdot 10^6$	$2.503 \cdot 10^6$	7012	-	0.0156
AE1	3	20	16051	8847	$3.241 \cdot 10^6$	$1.440 \cdot 10^6$	7012	-	0.0269
AE1	3	18	16051	6082	$2.917 \cdot 10^6$	$8.059 \cdot 10^5$	7012	-	0.0440
AE1	3	17	16051	5397	$2.755 \cdot 10^6$	$6.565 \cdot 10^5$	6919	7113	0.0505
AE2	2	$5.5 \cdot 10^3$	16051	16041	$8.913 \cdot 10^8$	$8.905 \cdot 10^8$	6819	-	$2.859 \cdot 10^{-5}$
AE2	2	55	16051	14990	$8.913 \cdot 10^6$	$8.078 \cdot 10^6$	6819	-	0.0031
AE2	2	45	16051	14740	$7.293 \cdot 10^6$	$6.453 \cdot 10^6$	6819	-	0.0038
AE2	2	35	16051	14336	$5.672 \cdot 10^6$	$4.826 \cdot 10^6$	6819	-	0.0051
AE2	2	25	16051	13563	$4.051 \cdot 10^6$	$3.190 \cdot 10^6$	6819	-	0.0076
AE2	2	20	16051	12818	$3.241 \cdot 10^6$	$2.356 \cdot 10^6$	6819	-	0.0101
AE2	2	15	16051	11372	$2.431 \cdot 10^6$	$1.504 \cdot 10^6$	6819	-	0.0156
AE2	2	10	16051	7348	$1.621 \cdot 10^6$	$5.674 \cdot 10^5$	6819	-	0.0354
AE2	2	9	16051	5485	$1.459 \cdot 10^6$	$3.556 \cdot 10^5$	6766	9073	0.052

Therefore also simulations with lower values of α_{soil} were carried out, which gave better results. Considering that the wave loads were less severe during calibration run 2 the erosion depth should be lower than was computed for calibration run 1, which is indeed the case. For the same calibration factor α_{soil} the erosion depth after run 2 is approximately a factor 2 smaller than the erosion depth after run 1.

It is suggested to apply a value of α_{soil} between 25 and 35 because for this range of α_{soil} the model predicts an erosion depth after calibration run 1 that ranges from almost 1 cm to slightly more than 2.5 cm. For the same range of α_{soil} the predicted erosion depth at pressure transducer DMD 2 is equal to 0.5-0.7 cm. In Figure 8-6 the erosion progression at DMD 3 for good quality grass and α_{soil} =30 is displayed. The dashed vertical lines indicate the test boundaries (similar to Figure 8-5).

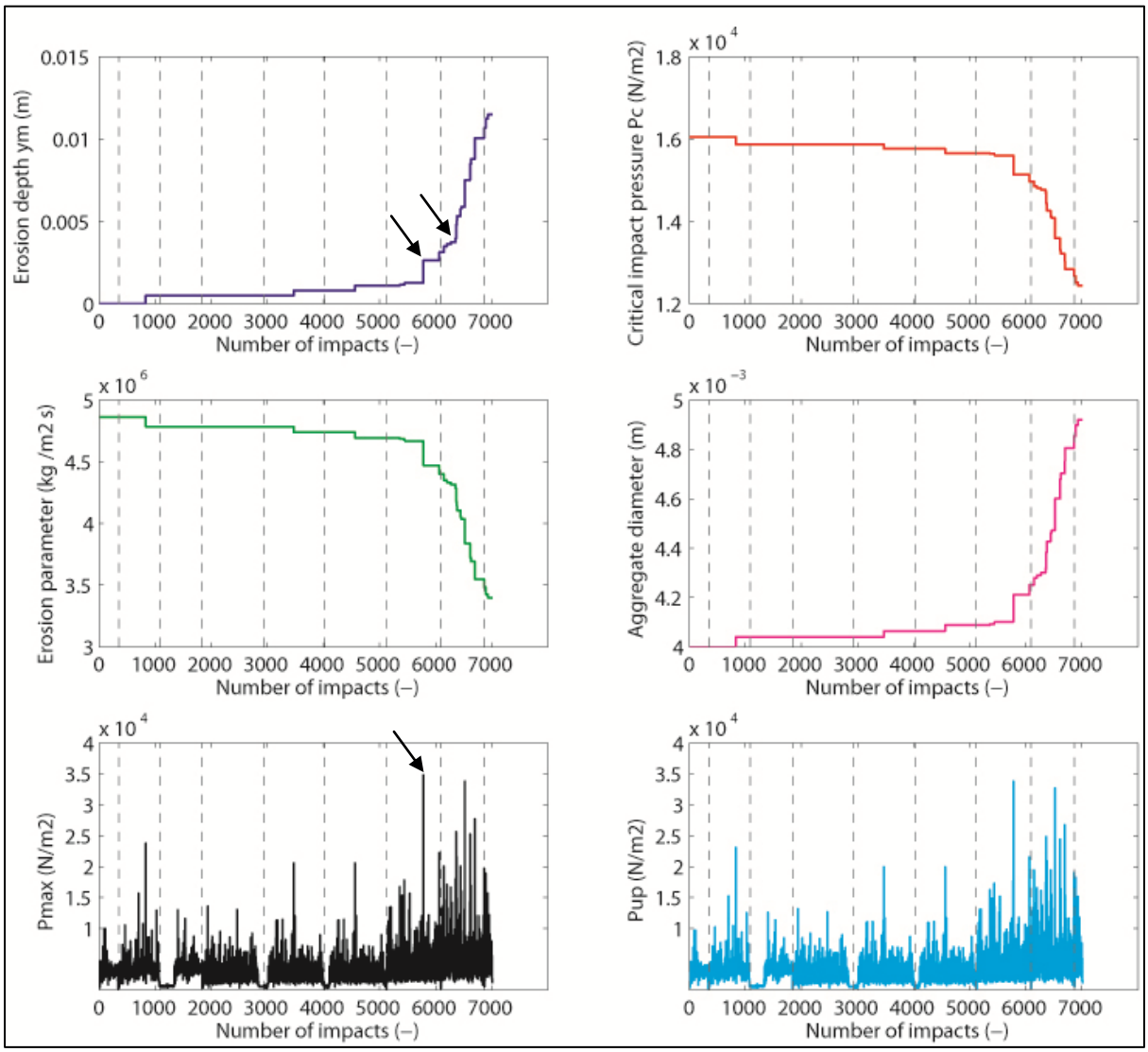

Figure 8-6: Predicted erosion at DMD 3 for RAR =0.0008 and α_{soil} =30 (calibration run AE1).

The figure clearly shows that the pressure damping is only marginal. During the first tests the erosion progression is slow; even during the first test with severe wave conditions and high pressure peaks (April 11, H_s =0.90 m) hardly any erosion is predicted. As expected the subsequent tests with mild wave conditions (April 16, H_s =0.50 m) do not induce significant aggregate erosion either. The erosion depth becomes gradually larger until the first test on April 22. Then an extreme impact pressure of approximately 35 kPa causes significant damage.
After this wave impact the erosion process is accelerated, which is visible during the subsequent tests on April 22 (indicated by the arrows in Figure 8-6). The behavior of the model is thus in accordance with the observed progression of aggregate erosion during the EroGRASS experiments.

8.2.3 General results aggregate erosion

For good quality grass sod the model gives satisfactory results, the model is therefore suitable for the

prediction of surface erosion of good quality grass covers. However for grass covers of lower quality (i.e. with low root densities) the model will predict more rapid erosion once a certain erosion depth has been exceeded. This is caused by the fact that the critical impact pressure is mainly determined by the grass strength. For high and average quality grass sod this is not a problem, as the grass strength is at least one order greater than the strength of the grass cover without roots. This is clearly visible in Figure 8-7 where the critical impact pressure is plotted for various root densities.

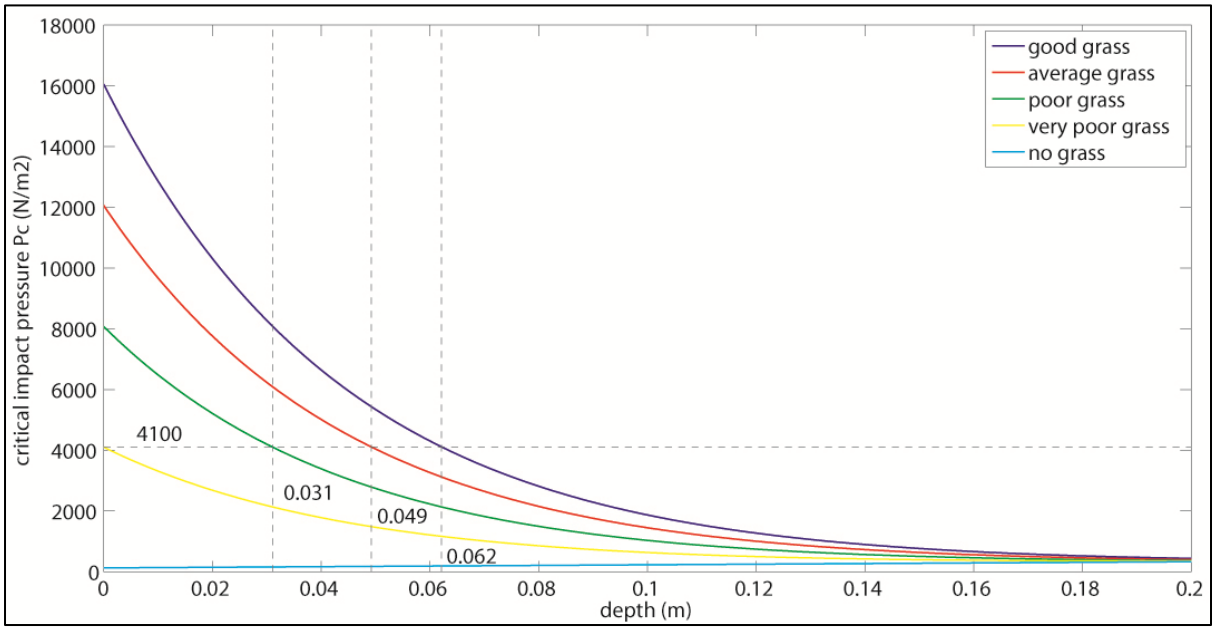

Figure 8-7: Predicted critical impact pressure for various grass qualities.

In the WIPE model the clay strength does not contribute to the aggregate erosion resistance, because the grass cover is assumed to be cracked at the surface. To prevent the model from predicting unrealistic high values of the erosion depth, when the root density has diminished significantly, a critical depth z_{crit} [m] is introduced.

The model is only applicable when the erosion depth is smaller than the critical depth. This critical depth is defined as the depth where the root density equals the root density that corresponds to the Root Area Ratio at the surface of very poor quality grass cover. This is equal to a RAR value of 0.0002 which is equivalent to a RVR of 0.01. This is merely a factor two greater than the limit value for the root density proposed by Stanczak for the transition between grass and clay (RVR =0.005).

In Table 8-8 the critical depths z_{crit} [m] for various grass qualities are given. These critical depths also correspond fairly well with the critical depth of 5 cm which was initially assumed in chapter 7.

Table 8-8: Critical depth and impact pressure for various grass qualities.

Grass quality	RAR_{crit} *[-]*	z_{crit} *[m]*	$p_c(z_{crit})$ *[N/m²]*
Good grass (RAR_0 =0.0008)	0.0002	0.0621	4115
Average grass (RAR_0 =0.0006)	0.0002	0.0492	4103
Poor grass (RAR_0 =0.0004)	0.0002	0.0311	4079

8.2.4 Calibration block erosion (BE)

For block erosion the model is calibrated using two factors; α_{soil} [-] for the erosion criterion and a crack growth parameter α_{crack} [-] to calibrate the extension of cracks. These factors are related to the relevant equations for block erosion as follows:

$$\frac{(p_{up}(d_{block}) - p_c(d_{block}) \cdot t_{impact}}{E_p(d_{block})} > z_{\min}$$

$$E_p(d_{block}) = \alpha_{soil} \cdot \frac{\rho_s}{\rho_w} \cdot \frac{p_c(d_{block})}{\sqrt{g d_{block}}}$$

$$\Delta A_{block} = \frac{\left(p_{up}(d_{block}) - \sigma_f(d_{block})\right) A_{block}}{\alpha_{crack}\left(\sigma_f(d_{block}) + c_{clay,c}\right)}$$

Two characteristic block erosion events were distinguished in Appendix A and both of these events will serve as a basis for a calibration run. Both of these events occurred near joints: a large block eroded after the test on April 11 and smaller blocks started to erode during test 1 on April 22. The WIPE model will thus be calibrated on these block erosion events in the next sections.

Calibration run 1: block erosion on April 11 at Row H

Erosion occurred at Row H during the test on April 11, which is close to pressure transducer DMD 2. The large block presumably failed due to a combination of reduced wall friction at the glass observation window and damage induced by impact pressures in the crack between the window and the grass mat. Also the eroded section was adjacent to a joint and worms were found at the surface of the erosion hole; consequently the sod was locally highly permeable. To take into account these weaknesses the value of n_s is taken as 1.0. The depth of the scour hole was roughly 0.10 m and the area of the eroded block A_{block} is estimated at approximately 0.23 m^2, which yields for the equivalent block diameter at the time of erosion d_{block} =0.48 m.

Ideally calibration run 1 will need to consist of the tests displayed in Table 8-9. Unfortunately test 1 on April 08 is not available and therefore its influence on the erosion process cannot be included. Because of the mild wave conditions during this test it is expected it did not play a major role in the erosion process anyway and that the exclusion of this test does not cause a large error. The total test program is displayed in Figure 8-8.

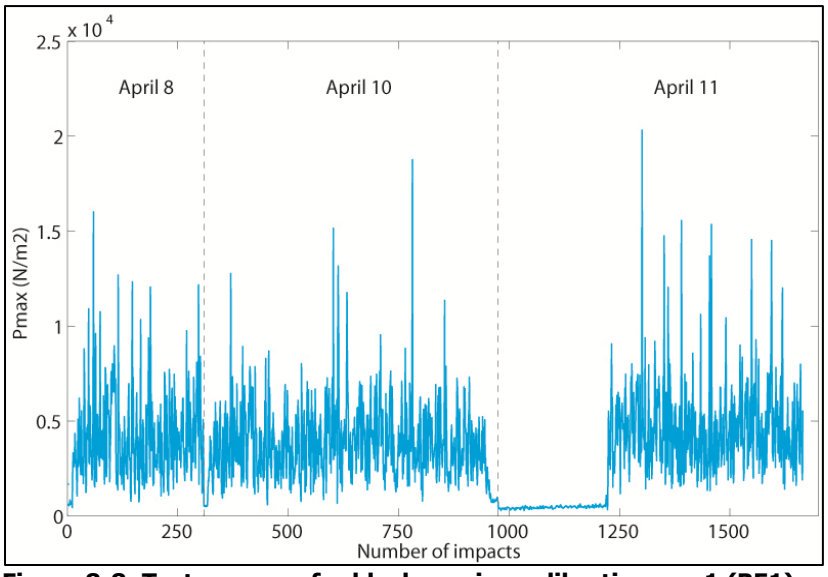

Figure 8-8: Test program for block erosion calibration run 1 (BE1).

Table 8-9: Test program required for block erosion run 1 (BE1).

Test	H_s *[m]*	T_p *[s]*	*Nearest pressure transducer*	*Erosion events*
April 08 test 1	0.5	4.0	DMD 2	No data available
April 08 test 2	0.8	5.0	DMD 2	None
April 10 test 1	0.8	5.0	DMD 2	None
April 11 test 1	0.9	5.0	DMD 2	Large block eroded at Row H

Results BE run 1

The predicted fracture strength with respect to depth $\sigma_f(z)$ is plotted in Figure 8-9. With n_s =1.0 the minimum fracture strength is predicted at a depth of 0.094 m. This agrees with the measured depth of the erosion hole after the test, which amounted approximately 0.10 m.

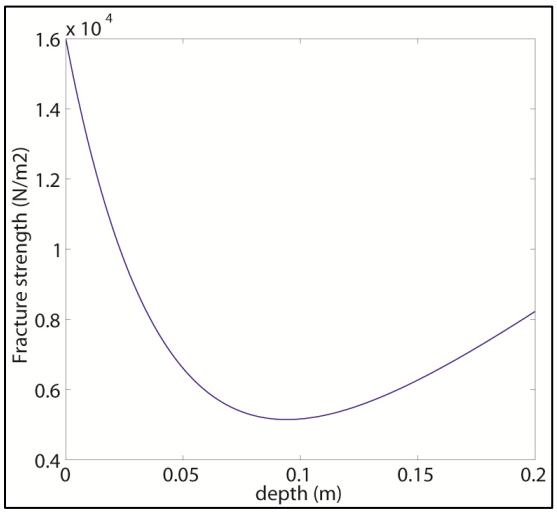

Figure 8-9: Fracture strength with respect to depth for n_s =1.0.

With $z_{\min}$ =0.094 m the first calibration run was performed, which yielded for the minimum fracture strength $\sigma_{f,\min}$ = 5151 N/m^2, for the initial block diameter $d_{block,0}$ =0.0115 m and for the initial critical uplift pressure $p_{c,0}$ =73720 N/m^2.The results of the calibration run are displayed in Table 8-10. Ideally the model should predict failure after a high impact pressure during the test on April 11 and the block diameter at this moment of failure should be approximately 0.48 m. For values of α_{soil} ranging from 2.13-3.24 these conditions are satisfied; failure occurs after an impact pressure of in the order of 20 kPa.

Table 8-10: Calibration results of block erosion calibration run 1 (BE1, DMD2).

α_{soil} *[-]*	α_{crack} *[-]*	$\sigma_{f,fail}$ *[N/m^2]*	$p_{c,fail}$ *N/m^2]*	$d_{block,0}$ *[m]*	$d_{block,fail}$ *[m]*	$E_{p,0}$ *[kg/m^{2}s]*	$E_{p,fail}$ *[kg/m^{2}s]*	N_{imp} *[-]*	$p_{\max}$ *[N/m^2]*	p_{up} *[N/m^2]*	y_m *[m]*
2.70	390	2952	4152	0.0115	0.502	$1.184\cdot10^6$	$1.011\cdot10^4$	1300	20319	7459	0.094
2.70	400	2953	4175	0.0115	0.494	$1.184\cdot10^6$	$1.024\cdot10^4$	1300	20319	7509	0.094
2.70	410	2954	4200	0.0115	0.487	$1.184\cdot10^6$	$1.037\cdot10^4$	1300	20319	7559	0.094
2.70	430	2954	4218	0.0115	0.476	$1.184\cdot10^6$	$1.060\cdot10^4$	1300	20319	7641	0.094
2.70	440	2955	4241	0.0115	0.468	$1.184\cdot10^6$	$1.076\cdot10^4$	1300	20319	7696	0.094
2.70	450	2957	3139	0.0115	0.461	$1.184\cdot10^6$	$1.530\cdot10^4$	1300	20319	7748	0.094
2.13	420	2983	4990	0.0115	0.332	$9.342\cdot10^5$	$1.178\cdot10^4$	780	18763	8161	0.094
2.14	420	2954	4218	0.0115	0.482	$9.386\cdot10^5$	$8.302\cdot10^3$	1300	20319	7596	0.094
2.70	420	2954	4218	0.0115	0.482	$1.184\cdot10^6$	$1.047\cdot10^4$	1300	20319	7596	0.094
3.24	420	2954	4218	0.0115	0.482	$1.421\cdot10^6$	$1.257\cdot10^4$	1300	20319	7596	0.094
3.25	420	2927	3483	0.0115	0.849	$1.425\cdot10^6$	$7.846\cdot10^3$	1655	-	-	0.0

For lower values the model predicts erosion earlier in the test program and for higher values no erosion is predicted. The appropriate diameter of the eroded block (0.48 m) is predicted for α_{crack} = 420. But the predicted block diameter does not differ greatly for values of α_{crack} between 390-450; the predicted block diameter is 0.46-0.50 m for these values of α_{crack} .In Figure 8-10 the block erosion process at DMD 2 for good quality grass and n_s =1.0 is displayed with α_{soil} =2.70 and α_{crack} =420. The dashed vertical lines indicate the test boundaries.

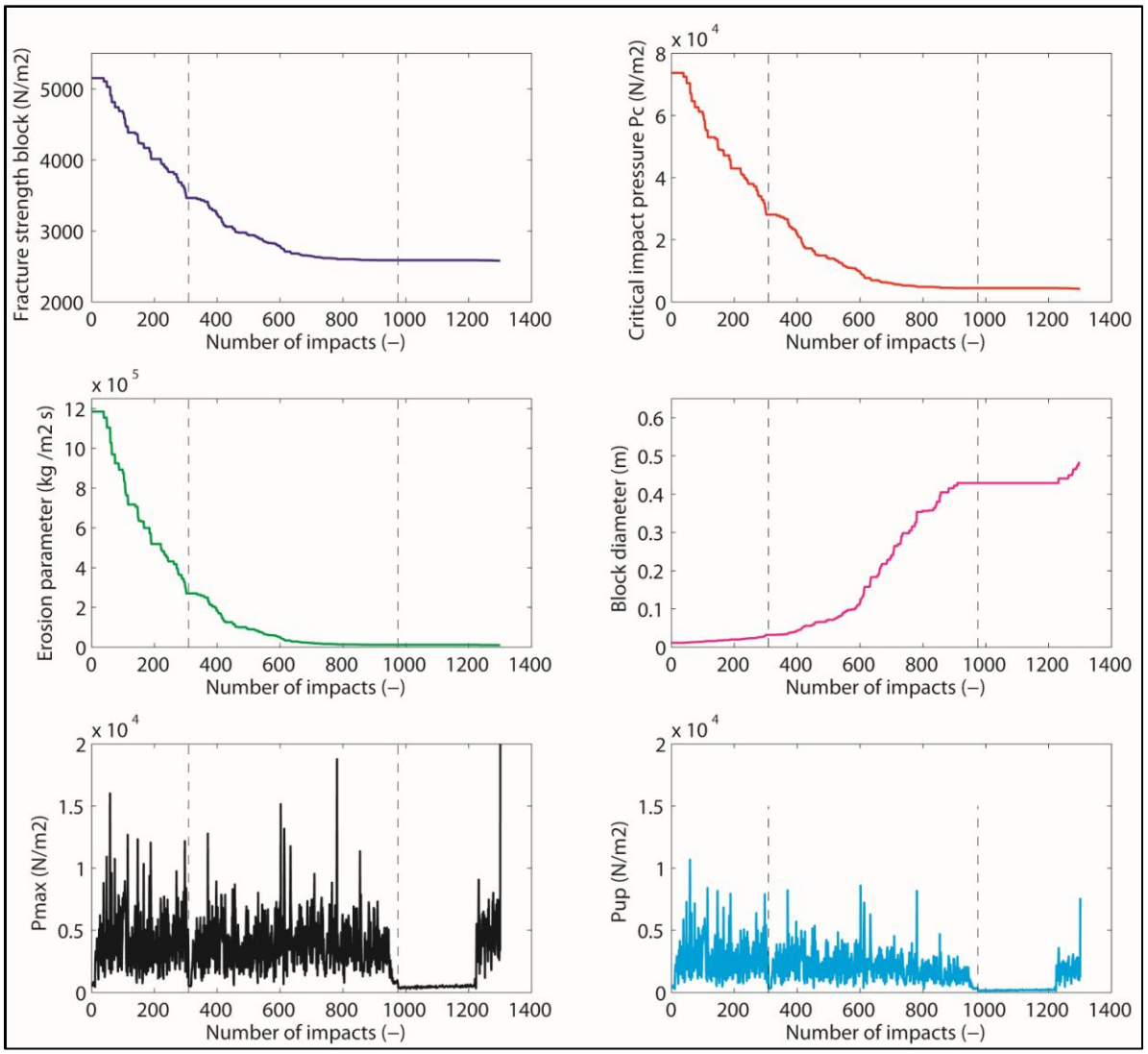

Figure 8-10: Predicted block erosion at DMD 2 for α_{soil} =2.70 and α_{crack} =420 (calibration run BE1).

On the basis of Figure 8-10 several remarks can be made. First of all block erosion is predicted after an impact of roughly 20 kPa during the test on April 11, which is in line with observations. The uplift pressure has then already dropped to approximately 7.6 kPa as a result of damping due to crack extension.
Furthermore the erosion parameter diminishes rapidly with increasing block diameter; after the first test (April 8) it has dropped to approximately 23% of its initial value whereas the block diameter has increased by approximately a factor 2.8 (0.032 m) compared to its initial value.
As the erosion parameter is dependent on the block diameter and the critical uplift pressure this rapid decrease is not a surprise. The critical uplift pressure declines dramatically as well during the first test because it is also dependent on the block diameter. Halfway the test on April 10 ($N_{imp} \approx 750$) the decline of the fracture strength, the critical impact pressure and the erosion parameter becomes

smaller and the slope of the graphs becomes milder: the erosion parameter at N_{imp} =750 is equal to approximately 17000 kg/m^{2}s, decreasing to a value of 10500 kg/m^{2}s at the end of the test program.

Calibration run 2: block erosion on April 22 Row I

Several clumps with roots start to wash up during the first test on April 22; these blocks probably came from grass mat I-L, which is near pressure transducer DMD 3. Also during the second test on April 22 multiple blocks (varying between 5 cm by 5 cm and 5 cm by 15 cm) erode from the grass cover. These observations were also done during test 3: grass mat I-L was severely damaged after the tests on April 22 and a large section next to the lower joint was eroded.
The depth of the erosion hole varied between 7 cm and 10 cm and also here worms were present at the surface of the erosion hole. This section of the grass cover is stronger than the one in run 1 because there is no glass wall next to the eroded section, n_s is therefore taken as 2.0 to take into account the joint and the burrowing animals. The size of the total eroded area was not determined, but it is known that the total erosion hole was the result of several cases of small block erosion. The calibration run will need to consist of the tests displayed in Table 8-11.

Table 8-11: Test program required for block erosion calibration run 2 (BE2).

Test	H_s *[m]*	T_p *[s]*	*Nearest pressure transducer*	*Erosion events*
April 08 test 1	0.5	4.0	DMD 3	No data available
April 08 test 2	0.8	5.0	DMD 3	None
April 10 test 1	0.8	5.0	DMD 3	None
April 11 test 1	0.9	5.0	DMD 3	None
April 16 test 1	0.5	4.0	DMD 3	None
April 16 test 2	0.5	4.0	DMD 3	Very high impact pressures
April 16 test 3	0.5	4.0	DMD 3	None
April 18 test 1	0.7	5.0	DMD 3	No data available
April 18 test 2	0.7	5.0	DMD 3	No data available
April 22 test 1	0.7	5.0	DMD 3	Block erosion starts at I-L
April 22 test 2	0.9	5.0	DMD 3	Erosion at I-L
April 22 test 3	0.9	5.0	DMD 3	Erosion at I-L

The test program for block erosion run 2 corresponds to the test program of aggregate erosion calibration run 1 (see section 8.2.2) therefore the same adaptations are proposed as before. The data of test 2 on April 16 are replaced by test 3 on April 16 and the tests on April 18 are left out of the simulation. For the sake of completeness the test program is once more displayed in Figure 8-11.

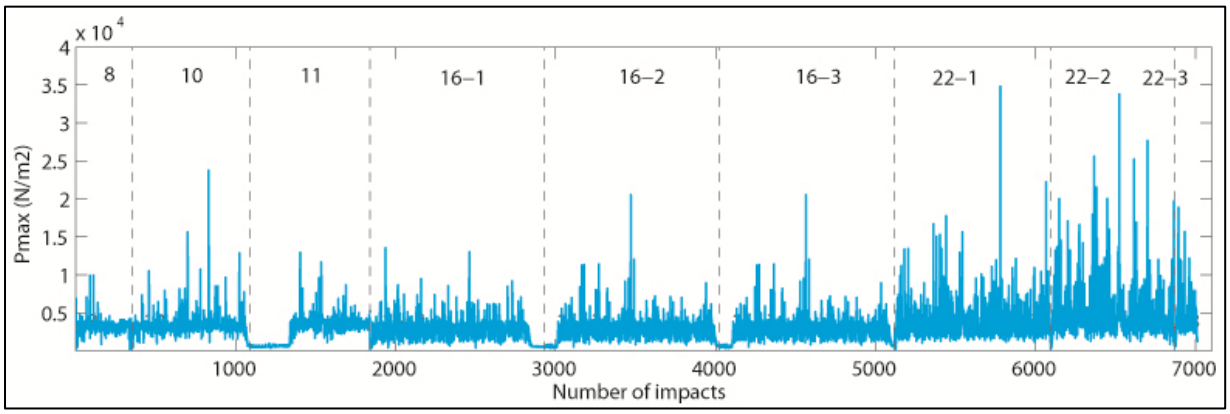

Figure 8-11: Test program for block erosion run 2 (calibration run BE2).

Results BE run 2

The fracture strength with respect to depth is plotted in Figure 8-12. With n_s =2.0 the depth of minimum fracture strength is 0.069 m. This agrees reasonably well with the observations after the tests; the depth of the scour hole was 0.07-0.10 m. With z_{min} =0.069 m the model was calibrated,

which yielded for the minimum fracture strength $\sigma_{f,\min}$ =7271 N/m^2, for the initial block diameter $d_{block,0}$ =0.0095 m and for the initial critical uplift pressure $p_{c,0}$ =154690 N/m^2.

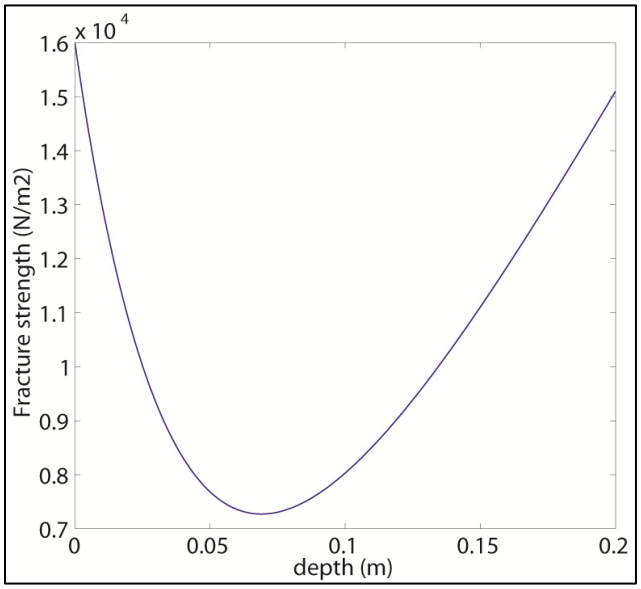

Figure 8-12: Fracture strength with respect to depth for n_s =2.0.

Ideally erosion during test 1 on April 22 should be predicted when the same factors as applied in run 1 are used. Therefore the erosion progression is firstly investigated with the calibration factors from calibration run 1. The erosion of a block with an area between 25 cm^2 and 75 cm^2 should be predicted, which means the block diameter should be in the range 0.050-0.087 m and erosion should be predicted during test 1 on April 22. The results of this calibration run are given in Table 8-12.
For the calibration factors obtained after calibration run 1 (α_{soil} =2.14-3.24, α_{crack} =390-450) the model does not have the desired behavior; failure occurs during test 2 on April 22 and the size of the eroded block is 0.51 m. Therefore more simulations were performed in order to find values of α_{soil} and α_{crack} for which the model showed better behavior. For α_{soil} =0.01-0.23 and α_{crack} =420-390 the model behavior was satisfactory, although not all values in these ranges give consistent results. This can be partly explained by the low value of the block diameter; the erosion resistance p_c is high and consequently failure can only be predicted for low values of α_{soil}. Nevertheless the model predicts failure for these values during test 1 on April 22 after an impact pressure of almost 35 kPa and the size of the eroded block is in the order of 0.080-0.087 m, which is in line with observations.

Table 8-12: Calibration results of block erosion calibration run 2 (BE2, DMD3).

α_{soil} [-]	α_{crack} [-]	$\sigma_{f,fail}$ [N/m^2]	$p_{c,fail}$ [N/m^2]	$d_{block,fail}$ [m]	$E_{p,0}$ [kg/m^{2}s]	$E_{p,fail}$ [kg/m^{2}s]	N_{imp} [-]	$p_{\max}$ [N/m^2]	p_{up} [N/m^2]	y_m [m]
3.24	420	4275	6644	0.5115	$3.280\cdot10^6$	$1.922\cdot10^4$	6522	33786	12877	0.069
2.7	420	4275	6644	0.5115	$2.733\cdot10^6$	$1.602\cdot10^4$	6522	33786	12877	0.069
2.14	420	4275	6644	0.5115	$2.166\cdot10^6$	$1.269\cdot10^4$	6522	33786	12877	0.069
1.0	420	4311	8245	0.3257	$1.012\cdot10^6$	$9.225\cdot10^4$	6365	25615	11862	0.069
0.01	420	4635	22473	0.0771	$1.012\cdot10^4$	$5.170\cdot10^2$	5779	34825	22648	0.069
0.01	390	4586	20281	0.0873	$1.012\cdot10^4$	$4.382\cdot10^2$	5779	34825	22276	0.069
0.23	390	4586	20281	0.0873	$2.328\cdot10^5$	$1.008\cdot10^4$	5779	34825	22276	0.069
0.15	400	4601	20982	0.0838	$1.519\cdot10^5$	$6.945\cdot10^3$	5779	34825	22404	0.069
0.08	410	4618	21714	0.0803	$8.099\cdot10^4$	$3.914\cdot10^3$	5779	34825	22529	0.069

In Figure 8-13 the block erosion progression during calibration run 2 is displayed for α_{soil} =0.23 and

α_{crack} =390. Especially the sudden change in the gradient of the block diameter is worth mentioning; the steepness of the block diameter graph (magenta) becomes significantly larger at the start of test 1 on April 22 ($N_{imp} \approx 5000$).

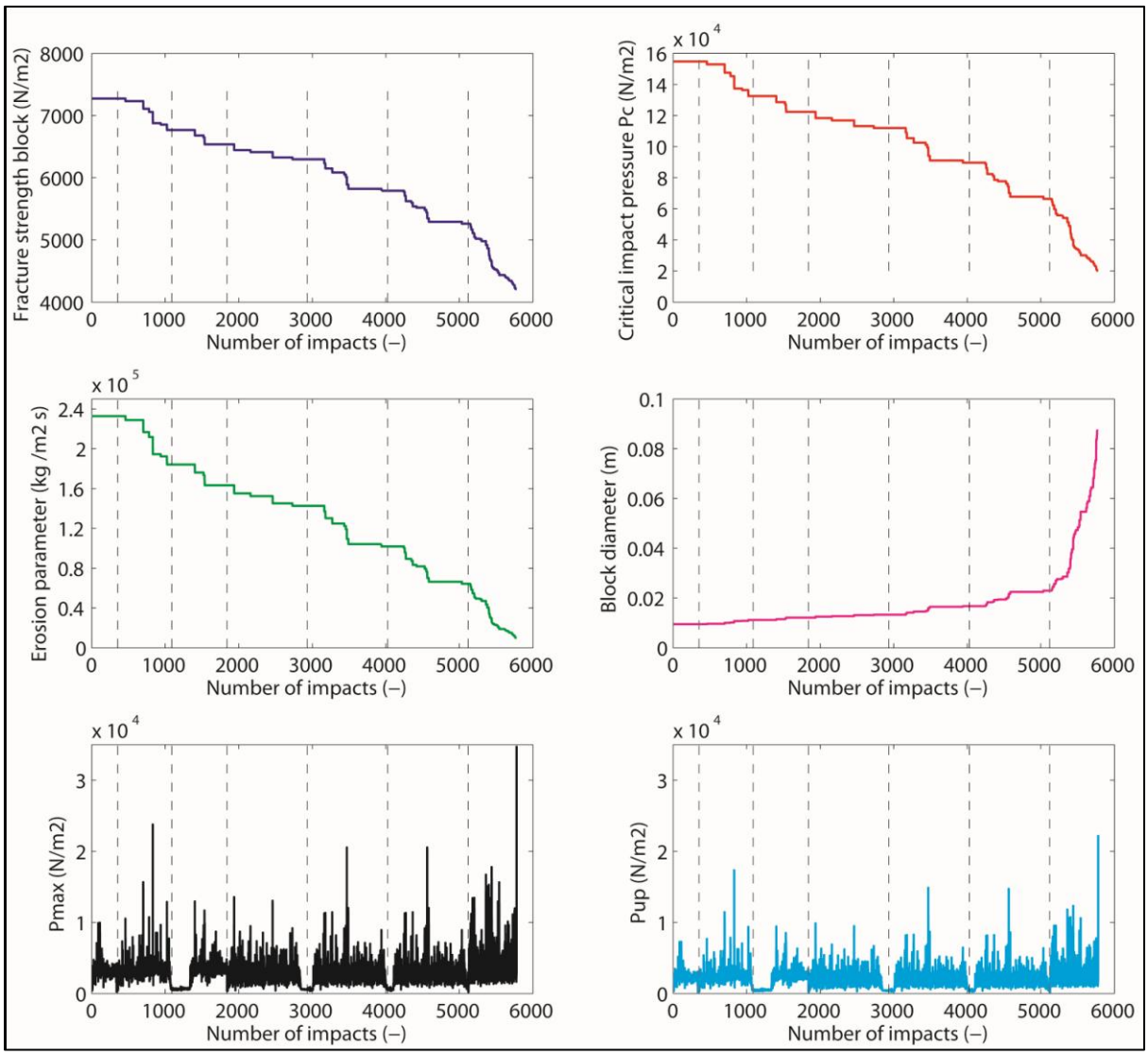

Figure 8-13: Predicted block erosion at DMD 3 for α_{soil} =0.23 and α_{crack} =390 (calibration run BE2).

Finally the values of α_{soil} and α_{crack} that were obtained after calibration run 2 are applied once more in calibration run 1. This yields Table 8-13 and Figure 8-14.

Table 8-13: Calibration results of block erosion run 1 with parameters of run 2 (BE1, DMD2).

α_{soil} [-]	α_{crack} [-]	$\sigma_{f,fail}$ [N/m^2]	$p_{c,fail}$ [N/m^2]	$d_{block,fail}$ [m]	$E_{p,0}$ [kg/m^{2}s]	$E_{p,fail}$ [kg/m^{2}s]	N_{imp} [-]	p_{max} [N/m^2]	p_{up} [N/m^2]	y_m [m]
0.23	390	2976	4785	0.3615	$1.009 \cdot 10^5$	$1.169 \cdot 10^3$	780	18763	7904	0.094
0.15	400	2978	4859	0.3501	$6.579 \cdot 10^4$	$7.866 \cdot 10^2$	780	18763	8001	0.094
0.08	410	2981	4925	0.3406	$3.509 \cdot 10^4$	$4.311 \cdot 10^2$	780	18763	8083	0.094
0.01	420	2983	4990	0.3316	$4.386 \cdot 10^3$	$5.533 \cdot 10^1$	780	18763	8161	0.094

It is clear that the results do not agree with the test observations; block erosion is now predicted during the test on April 10 after an impact pressure of almost 19 kPa and the size of the eroded block for this simulation varies between 0.33-0.36 m. Failure thus occurs too early and as a consequence

the eroded block is too small. Universal values of α_{soil} and α_{crack} can therefore not be given at this moment.

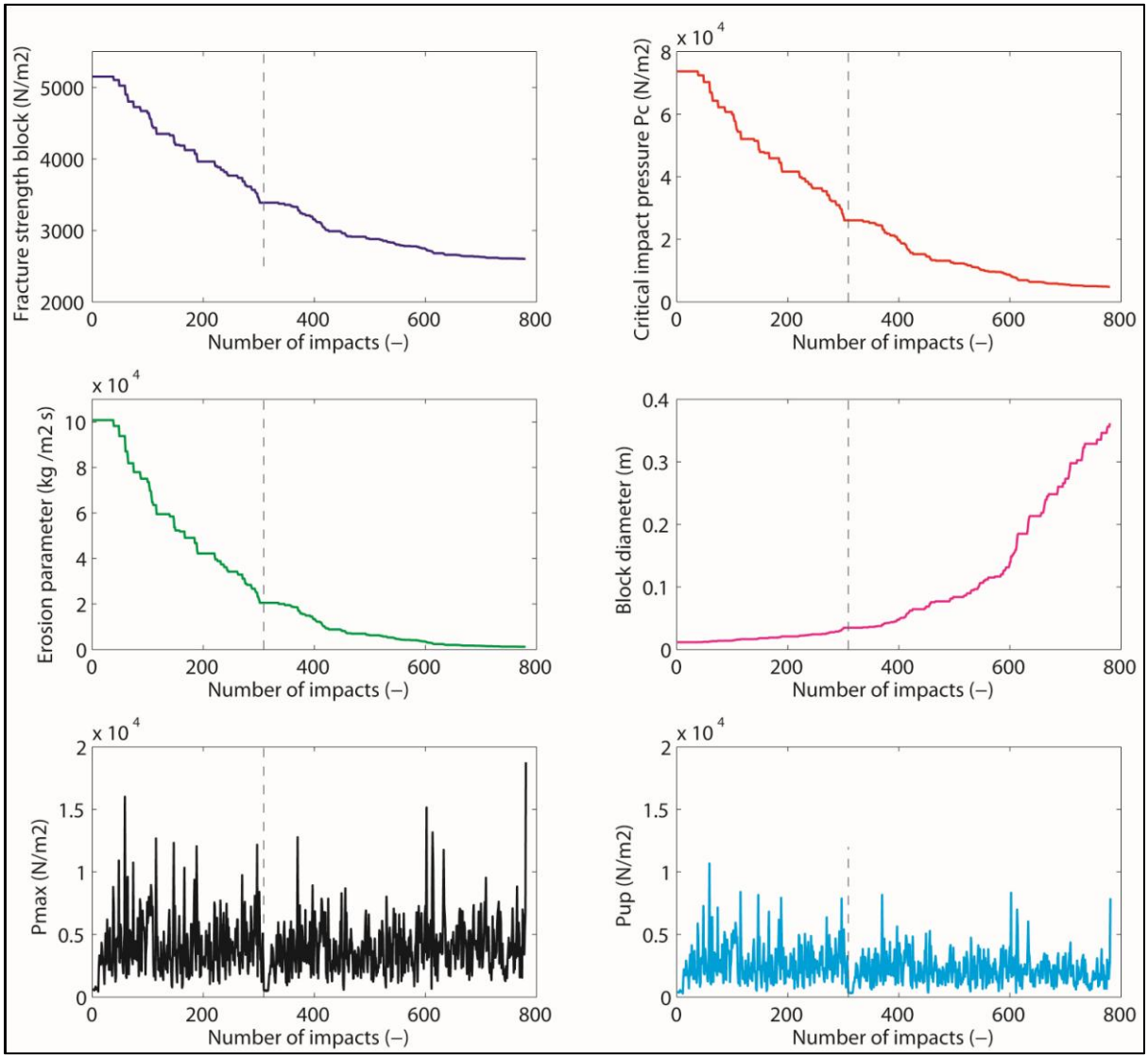

Figure 8-14: Predicted block erosion at DMD 2 for α_{soil} =0.23 and α_{crack} =390 (calibration run BE1).

8.2.5 General results block erosion

It appears that both test runs show the desired behavior for approximately the same value of the crack growth parameter (α_{crack} =390-420), indicating that this range of α_{crack} is appropriate for both block erosion cases. Contrary to this the value of α_{soil} varies significantly for both test runs (0.01-3.24), which is mainly caused by the difference in the critical impact pressure and the erosion parameter.

During calibration run 1 these strength terms are lower than during calibration run 2 and therefore the failure criterion is fulfilled sooner. Furthermore the fracture strength is lower for calibration run 1 as well and consequently mediocre impact pressures have an influence right from the start of the test. Hence the crack extends faster and the value of α_{soil} needs to be relatively high to prevent the prediction of premature failure. During calibration run 2 the crack extends more slowly, because mediocre impact pressures do not have significant influence early in the test program as a result of higher fracture strength. In addition the critical uplift pressure is particularly high for small block diameters, hence the value of α_{soil} ought to be lower in calibration run 2 to predict failure at the

correct moment.
As the model includes several parameters and effects which are variable with either depth or block diameter, these are discussed separately in more detail in the next sections. The results of both calibration runs will serve as a basis for this discussion and are summarized in Table 8-14.

Table 8-14: Overview results of block erosion calibration run 1 and 2.

Run	n_s	α_{soil} *[-]*	α_{crack} *[-]*	$d_{block,fail}$ *[m]*	$p_{c,0}$ *[N/m²]*	$p_{c,fail}$ *[N/m²]*	$p_{\max}$ *[N/m²]*	p_{up} *[N/m²]*	$E_{p,0}$ *[kg/m²s]*	$\sigma_{f,fail}$ *[N/m²]*	y_m *[m]*
BE 1	1.0	2.7	420	0.482	73720	4218	20319	7596	$1.184 \cdot 10^6$	2954	0.094
BE 2	2.0	0.23	390	0.0873	154690	20281	34825	22276	$2.328 \cdot 10^5$	4586	0.069

Pressure damping

For large crack lengths the uplift pressure declines dramatically. This effect is briefly discussed in this section. For this purpose the relative uplift pressure p_{up} / $p_{\max}$ is plotted in Figure 8-15 with respect to block diameter for $z_{\min}$ =0.10.

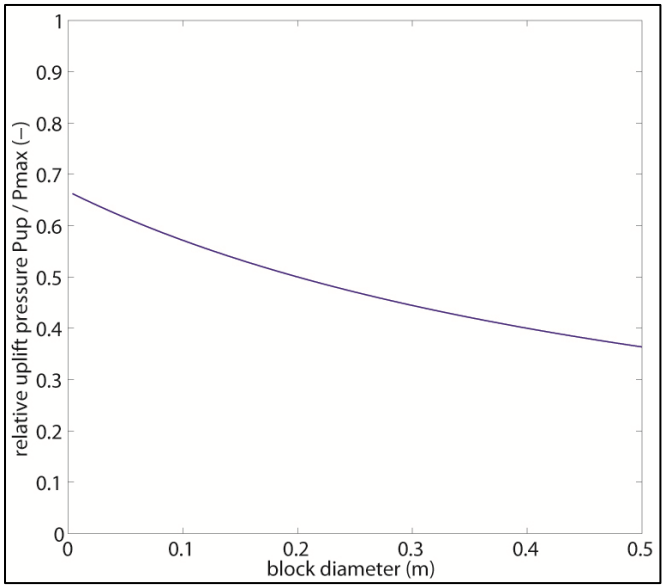

Figure 8-15: Predicted pressure damping versus block diameter for $z_{\min}$ =0.10 m.

Even when no horizontal crack has developed underneath the block yet, the pressure at the end of the vertical crack ($z_{\min}$ =0.10 m) diminishes to two third (67%) of the initial impact pressure. As the horizontal crack extends in the course of time, the uplift pressure is further reduced; in the case of d_{block} =0.50 m the uplift pressure has dropped to 36% of the initial impact pressure $p_{\max}$.
The influence of the block diameter on the magnitude of the uplift pressure in the model is thus strong, which was already apparent from Figure 8-10, Figure 8-13 and Figure 8-14 when comparing the progression of the block diameter with the impact pressure and the uplift pressure (magenta, black and cyan graphs).
Hence the damping effect of cracks is an important factor in the block erosion process, whereas this effect hardly plays a role for aggregate erosion.

Block erosion resistance

The block erosion resistance p_c [N/m²] is plotted against the block diameter in Figure 8-16 for the values listed in Table 8-14. The erosion resistance of both calibration runs is given for three intervals of the block diameter: 0.004-0.05 m, 0.05-0.10 m and 0.10-0.50 m.

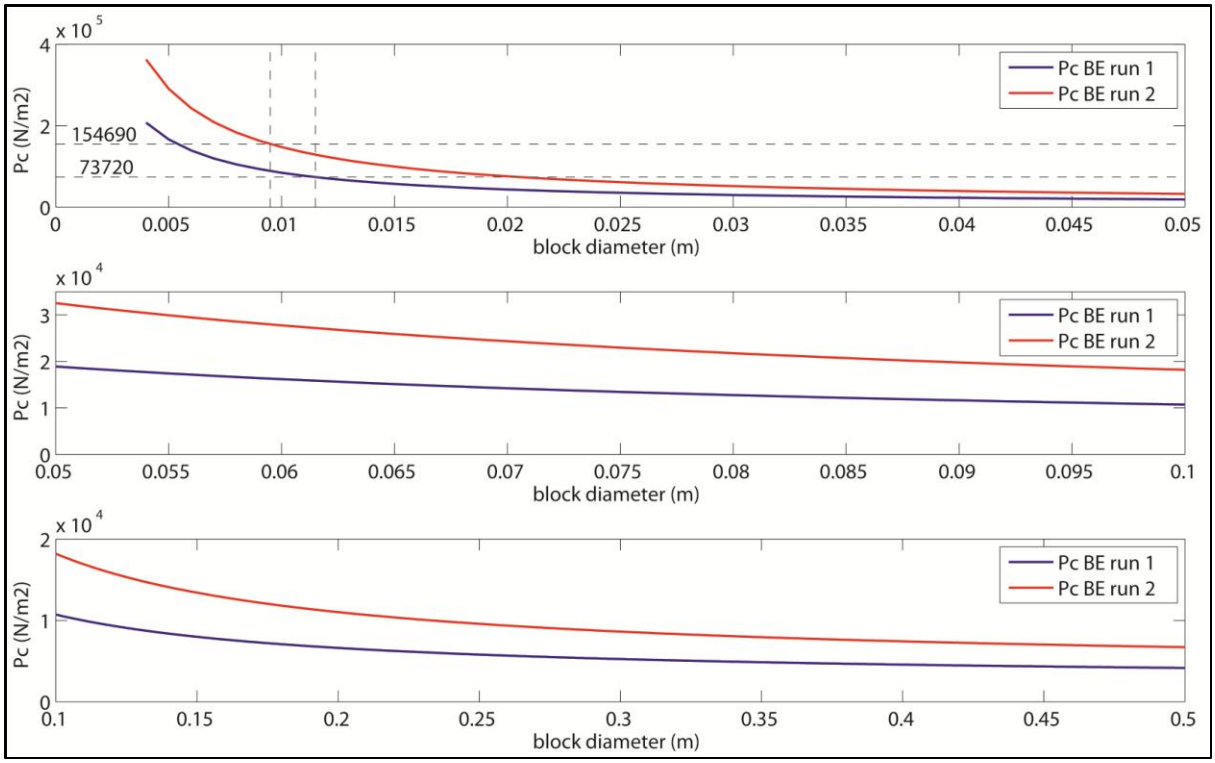

Figure 8-16: Predicted critical uplift pressures for BE1 and BE2 with respect to block diameter.

Between block diameters of 0.004 m and 0.05 m the erosion resistance diminishes dramatically to respectively 18.92 kPa and 32.56 kPa. For these small block diameters block erosion is unlikely to occur as extremely high impact pressures are required for this. The uplift pressures do not exceed the critical uplift pressure and thus the erosion criterion is not fulfilled regardless of the magnitude of the factor α_{soil} .

However for block diameters in the range of 0.05-0.10 m the critical uplift pressure declines further to values of respectively 10.72 kPa and 18.20 kPa. These uplift pressures can be induced by high impact pressures and block erosion might be triggered; within this range of block diameters the factor α_{soil} thus starts to be of importance. The same holds for larger block diameters; the erosion resistance gradually diminishes to values of respectively 4.16 kPa and 6.72 kPa for d_{block} =0.50 m.

Erosion parameter

The erosion parameter E_p [kg/m^{2}s] is plotted with respect to the block diameter in Figure 8-17 for both block erosion calibration runs (Table 8-14). The erosion parameters are given for three intervals of the block diameter: 0.004-0.05m, 0.05-0.10 m and 0.10-0.50 m.

It can be observed that the decline of the erosion parameter between especially block diameters of 0.004 m and 0.05 is substantial; the erosion parameters for both calibration runs decrease from respectively $5.66 \cdot 10^6$ kg/m^{2}s and $8.43 \cdot 10^5$ kg/m^{2}s to $1.46 \cdot 10^5$ kg/m^{2}s and $2.14 \cdot 10^4$ kg/m^{2}s on this interval. These high erosion parameters in combination with considerable critical uplift pressures make the occurrence of block erosion rather improbable. For this reason an appropriate value of α_{soil} is of less importance for small blocks.

Conversely the reduction of the erosion parameter on the interval d_{block} 0.05-0.50 m is less drastic (from respectively $1.46 \cdot 10^5$ kg/m^{2}s and $2.14 \cdot 10^4$ kg/m^{2}s to $1.01 \cdot 10^4$ kg/m^{2}s and $1.39 \cdot 10^3$ kg/m^{2}s) but now a correct value of α_{soil} is essential to predict the correct moment of failure.

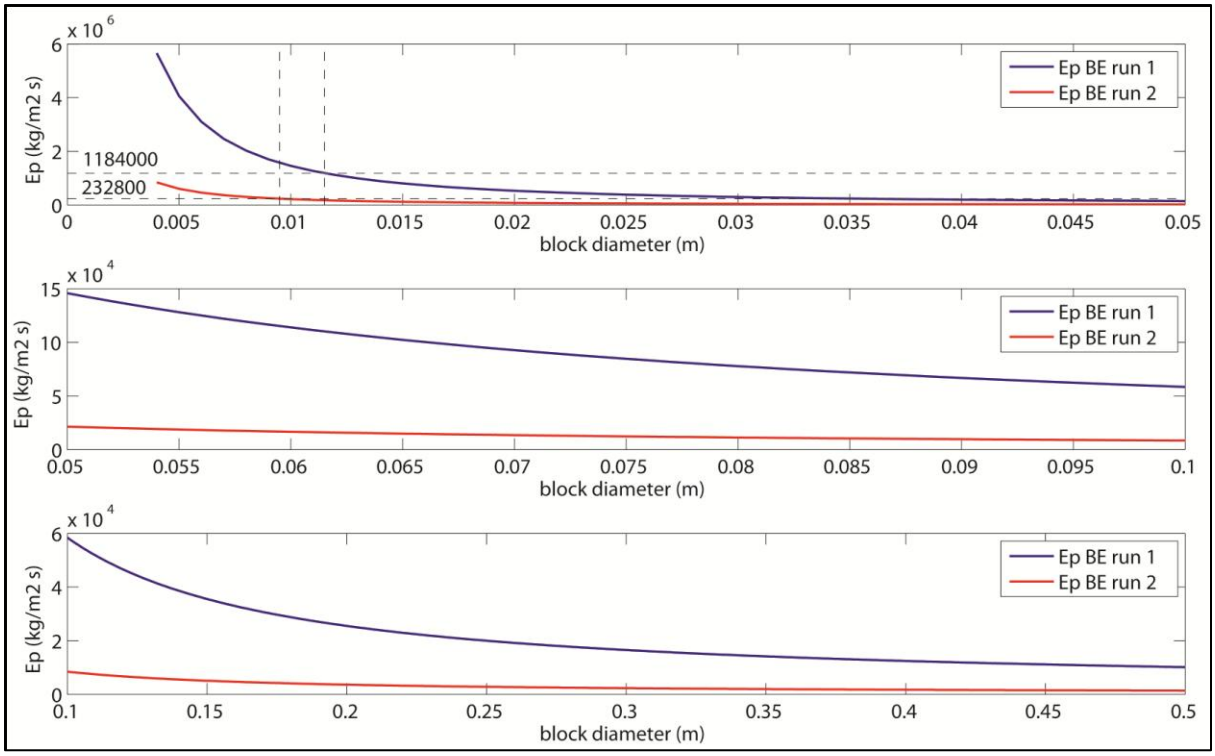

Figure 8-17: Predicted erosion parameters for BE1 and BE2 with respect to block diameter.

Side wall coefficient n_s

Besides the critical clay cohesion and the Root Area Ratio the choice for the side wall coefficient n_s determines the magnitude of the critical uplift pressure p_c and the fracture strength σ_f. As the values of n_s for both calibration runs were selected arbitrarily, the influence of small deviations of n_s on the strength terms is investigated in this section. The critical uplift pressure with respect to block diameter is displayed in Figure 8-18 for various values of n_s.

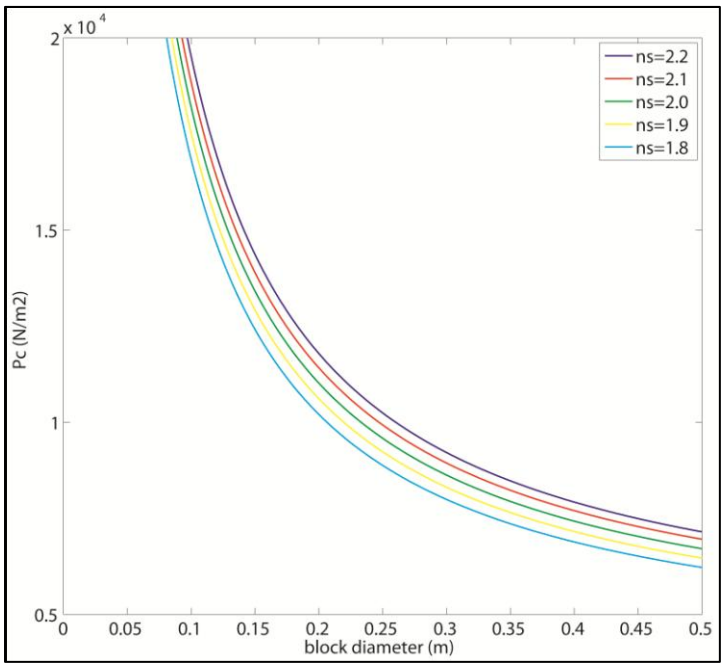

Figure 8-18: Critical uplift pressure with respect to block diameter for various values of n_s.

At first sight small deviations of the value of the side wall coefficient appear to have little influence on the critical uplift pressure. Nonetheless Table 8-15 was created with n_s ranging from 1.8-2.2 to quantify the differences between the erosion resistances for several block diameters. The value of calibration run 2 is used as the reference value (n_s =2.0).

Table 8-15: Critical uplift pressures for various values of n_s and block diameters.

p_c [N/m²]	d_{block} [m]					
n_s [-]	0.05	0.10	0.20	0.30	0.40	0.50
1.8	$3.011 \cdot 10^4$	$1.684 \cdot 10^4$	$1.020 \cdot 10^4$	$7.990 \cdot 10^3$	$6.884 \cdot 10^3$	$6.221 \cdot 10^3$
1.9	$3.136 \cdot 10^4$	$1.753 \cdot 10^4$	$1.061 \cdot 10^4$	$8.307 \cdot 10^3$	$7.155 \cdot 10^3$	$6.464 \cdot 10^3$
2.0	$\mathbf{3.256 \cdot 10^4}$	$\mathbf{1.820 \cdot 10^4}$	$\mathbf{1.102 \cdot 10^4}$	$\mathbf{8.623 \cdot 10^3}$	$\mathbf{7.426 \cdot 10^3}$	$\mathbf{6.708 \cdot 10^3}$
2.1	$3.371 \cdot 10^4$	$1.885 \cdot 10^4$	$1.141 \cdot 10^4$	$8.936 \cdot 10^3$	$7.697 \cdot 10^3$	$6.954 \cdot 10^3$
2.2	$3.498 \cdot 10^4$	$1.952 \cdot 10^4$	$1.179 \cdot 10^4$	$9.209 \cdot 10^3$	$7.921 \cdot 10^3$	$7.148 \cdot 10^3$
Average difference [N/m²]	1218	670	398	304	260	232
Average difference [%]	3.74	3.68	3.61	3.53	3.50	3.46

The difference between the respective values of the erosion resistance per block diameter was computed and averaged. Depending on the size of the block, an increase of 5% of the value of n_s (2.0 to 2.1) leads to an average increase of 3.46-3.74% of the critical uplift pressure. For large block diameters (0.30-0.50 m) the absolute difference of the erosion resistance is not very disturbing. Conversely the absolute differences for small block diameters are larger (600-1200 N/m²), which can be decisive for the occurrence of block erosion. An appropriate value of the side wall coefficient is therefore essential.

Moreover the side wall coefficient partially determines the fracture strength σ_f . The influence of n_s on the fracture strength is therefore also examined. In Figure 8-19 the fracture strength with respect to depth is depicted for various values of the side wall coefficient.

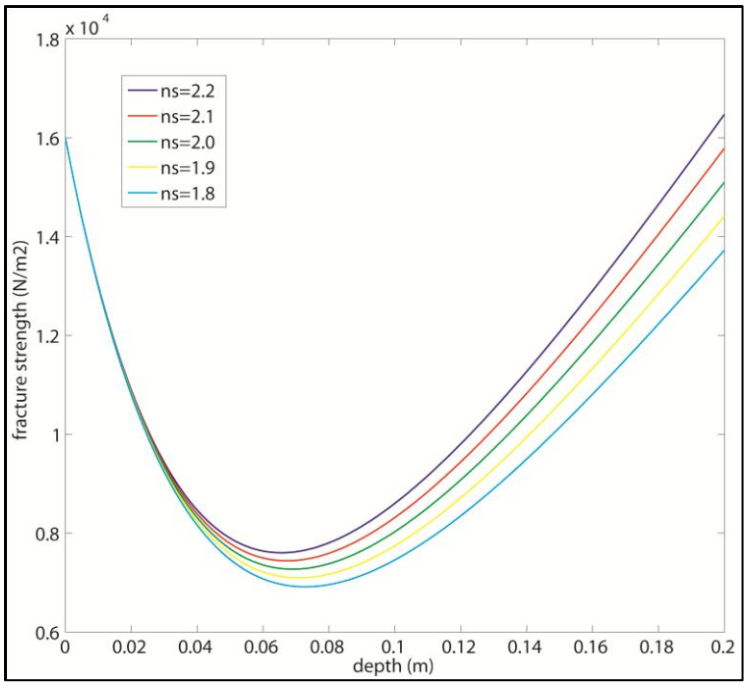

Figure 8-19: Fracture strength with respect to depth for various values of n_s .

It can be concluded from Figure 8-19 that the variation of the fracture strength for various values of n_s is only marginal at small depths but becomes larger at greater depths. Although the variation of the fracture strength at greater depth is apparent, this is not of relevance for the erosion process.

This insignificance can be attributed to the fact that the fracture strength at deeper parts of the grass cover is considerably higher than the minimum fracture strength, irrespective of the value of n_s. However the differences at the location of minimum fracture strength might be crucial and therefore deserve more attention. Hence the fracture strength and the depth of this minimum fracture strength were computed for several values of the side wall coefficient and summarized in Table 8-16. Once again the values of calibration run 2 are used as the reference values (n_s =2.0).

Table 8-16: Minimum fracture strength and $z_{\min}$ for various values of n_s.

n_s [-]	*Minimum fracture strength* $\sigma_{f,\min}$ [N/m²]	*Depth of minimum fracture strength* $z_{\min}$ [m]
1.8	6915	0.0730
1.9	7096	0.0710
2.0	**7212**	**0.0690**
2.1	7440	0.0670
2.2	7603	0.0660
Average difference [N/m²]	172	0.0175
Average difference [%]	2.38	2.54

In Table 8-16 the average relative difference between fracture strengths is approximately 2.4% when n_s increases by 5% and the average absolute difference amounts merely 172 N. Therefore it can be stated that small variations of the side wall coefficient are of less importance to the crack growth process at the depth of minimum fracture strength. On the other hand the side wall coefficient does determine for a certain part the location of minimum fracture strength and thus the block erosion depth.
Furthermore the location of minimum fracture strength and the magnitude of the minimum fracture strength are also strongly dependent on the initial block diameter. This can be clearly deduced from Figure 8-20 where the fracture strength is plotted against the block diameter. For small block diameters (d_{block} =0.004-0.05 m) the fracture strength declines rapidly, whereas it decreases only slightly for larger block diameters.

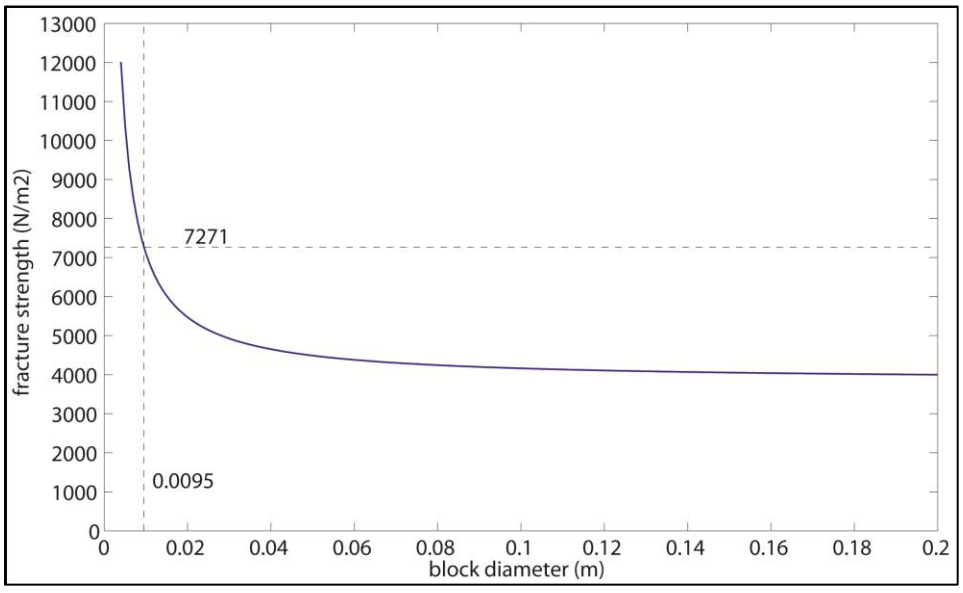

Figure 8-20: Fracture strength with respect to block diameter.

As the initial block diameter is chosen equal to the aggregate diameter in the WIPE model, the aggregate diameter distribution is of major importance. This is evident from Figure 8-20 while keeping in mind that that the aggregate diameter between depths 0.00-0.20 m has been assumed to vary between 0.004 m and 0.02 m.

8.3 Erosion by flow velocities

In this section the flow induced erosion of the stubble, which consists of loose particles, and the flow induced surface erosion of the grass cover underneath it will be investigated. The strength of the stubble is discussed first and this is followed by the surface erosion of the turf.

8.3.1 Surface erosion of loose aggregates

The top part of the grass cover layer consists of the stubble, a layer with loose particles and plant remains. This layer is said to erode very quickly, which will be verified in this section by application of the flow erosion model developed by Hoffmans et al. (2009).
A loose aggregate is not supported by roots and it has no friction or cohesion forces on its sides. Only the weight of the particle will provide resistance against the uplift pressure. For loose aggregates, incipient motion occurs when:

$$p_{up} \geq (1-n)(\rho_s - \rho_w) g d_a \tag{8-1}$$

When loaded by flow velocities a loose particle will move along the slope if the critical condition for movement is reached. This happens when the mean bed shear stress τ_0 equals the critical mean bed shear stress τ_c:

$$\tau_c = \alpha_\tau^{-1}(1-n)\left(\rho_s - \rho_w\right) g d_a \tag{8-2}$$

The critical velocity to reach this shear stress is proportional to the velocity squared.

$$\tau_0 = \frac{1}{c_0^2}\rho_w (r_0 U_0)^2 = 0.7\rho_w (r_0 U_0)^2$$ Identical to equation (6-13)

The critical depth averaged flow velocity U_c with $\Delta = \frac{\rho_s - \rho_w}{\rho_w}$ then is:

$$U_c = \frac{c_0}{r_0}\sqrt{\alpha_\tau^{-1}}\sqrt{\Delta g d} \tag{8-3}$$

Evaluating equation (8-3) for various aggregate diameters results in table Table 8-17.

Table 8-17: Critical velocity of loose particles for various aggregate diameters.

d_a [m]	U_c [m/s]
0.004	0.29
0.005	0.32
0.006	0.35
0.008	0.40

It is apparent that the critical velocity of loose particles is very low. Clearly the stubble is washed away by wave run-up and run-down very quickly. Erosion of the stubble can therefore not be defined as erosion, but should be regarded as the 'rinsing' of the grass cover.

8.3.2 Run-up and run-down velocities

Before the erosion by flow velocities can be predicted, the flow velocities have to be known first. The maximum flow velocities at the outer slope generally occur at MWL or slightly above it. With a given freeboard of 2.10 m the maximum up and down rush velocities for the EroGRASS wave characteristics can be predicted by applying equations (3-12) and (3-13). The predicted run-up velocities are depicted in Figure 8-21 and the predicted run-down velocities are displayed in Figure 8-22.

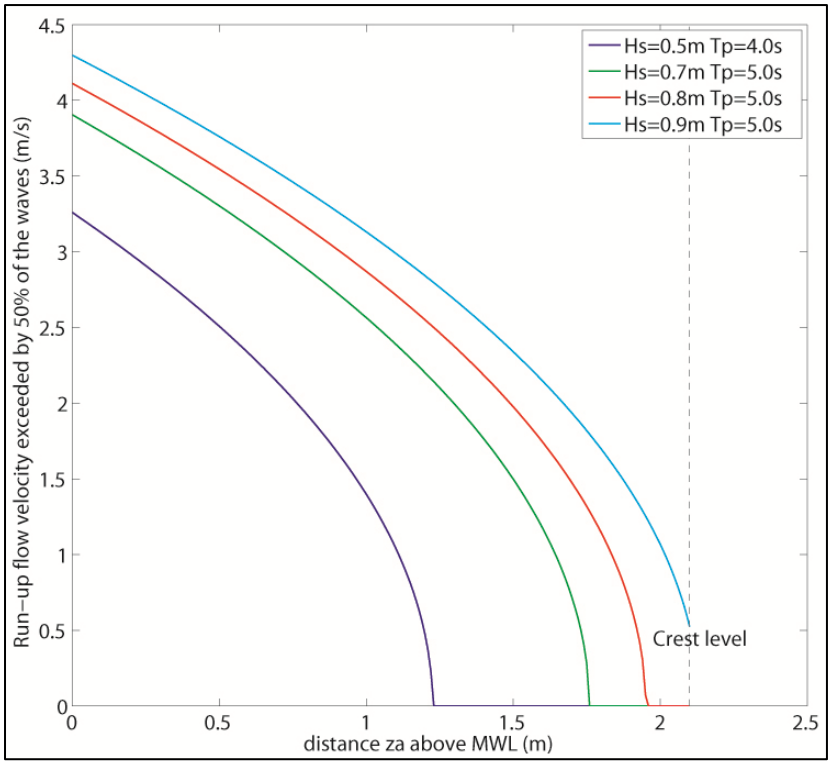

Figure 8-21: Predicted run-up velocities for wave characteristics of the EroGRASS experiments.

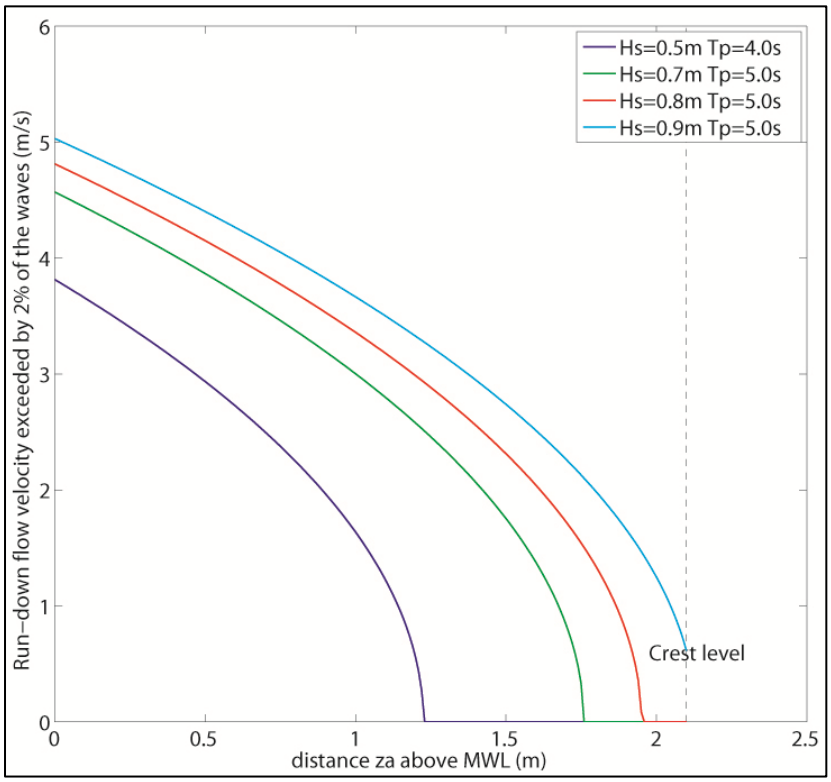

Figure 8-22: Predicted run-down velocities for wave characteristics of the EroGRASS experiments.

8.3.3 Erosion by flow

It can be concluded from Figure 8-21 and Figure 8-22 that flow velocities are highest for the test with H_s =0.9 m and T_p =5.0 s (cyan lines) and that the maximum flow velocities are of almost equal magnitude (approximately 5 m/s).
The erosion of the grass cover will be investigated at MWL for various grass qualities for all EroGRASS tests. Erosion predictions will be done with the EPM/Hoffmans model and for a good prediction it is essential to know the period of time that the load acts on the slope. From the EroGRASS data it appeared that the duration of high flow velocity peaks is roughly 1.0 s.
It is assumed that during each wave period the slope is loaded by both the run-up velocity and the down-rush velocity. For the moment it is thus supposed that the predicted flow velocities are reached by all waves and that these last for a period of time t_{flow} [s] of 1.0 s each. The total loading time is thus 2.0 s which is equal to 40% of the wave period. This approach is on the conservative side as waves may also overtop or may have lower flow velocities.
To determine the erosion speed per hour the simulation will consist of 720 waves and the flow velocities $u_{d,2}$ and $u_{u,50}$ are used as input. The total erosion depth is calculated as:

$$\sum_{N=1}^{N=820} y_{m,n} = \frac{(\omega U_0 - U_c)^2 \cdot t_{flow}}{E_{soil}} \tag{8-4}$$

Where:

t_{flow} = time for which the slope is exposed to flow velocity [s]

ω = turbulence coefficient= 2.25= (1.5+5·r_0) with r_0 =0.15 [-]

The simulation is done for grass of various qualities and constant clay quality; the results of this simulation are displayed in Table 8-18 and in Figure 8-23.
For good grass quality the flow velocities cause no problems, even for these extreme circumstances the erosion rate is just 1.5 mm to 2 mm per hour for significant wave heights of 0.8-0.9 m. For lower wave heights the erosion rate of good quality grass is even less than 1 mm per hour. The erosion caused by flow velocities during the experiments can thus indeed be neglected.

Table 8-18: Predicted erosion depths for the EroGRASS experiments due to flow velocities.

Grass quality	A_r / A *[-]*	c_{clay} *[kN/m²]*	*Erosion depth [m]* H_s *=0.5m* T_p *=4.0s*	*Erosion depth [m]* H_s *=0.7m* T_p *=5.0s*	*Erosion depth [m]* H_s *=0.8m* T_p *=5.0s*	*Erosion depth [m]* H_s *=0.9m* T_p *=5.0s*
Very poor	0.0002	30.0	$1.45 \cdot 10^{-2}$	$2.81 \cdot 10^{-2}$	$3.34 \cdot 10^{-2}$	$3.86 \cdot 10^{-2}$
Poor	0.0004	30.0	$3.00 \cdot 10^{-3}$	$7.87 \cdot 10^{-3}$	$9.93 \cdot 10^{-3}$	$1.20 \cdot 10^{-2}$
Average	0.0006	30.0	$6.30 \cdot 10^{-4}$	$2.74 \cdot 10^{-3}$	$3.76 \cdot 10^{-3}$	$4.81 \cdot 10^{-3}$
Good	0.0008	30.0	$1.10 \cdot 10^{-4}$	$9.44 \cdot 10^{-4}$	$1.47 \cdot 10^{-3}$	$2.04 \cdot 10^{-3}$

This is different for very poor and poor quality grass cover. Maximum flow velocities induced by low wave heights (H_s =0.50 m) will presumably already lead to serious damage even though the flow load and thus the erosion rates are probably overestimated in this analysis. For higher wave heights the erosion rates of very poor and poor quality sod increase drastically. Average quality grass sod is considered to be in the transition zone as the erosion rate is still limited for higher waves (H_s =0.8 -0.90 m).
It is therefore anticipated that for grass covers of very poor and poor quality the flow velocities on the slope start to play a role in the erosion process. Whereas it is expected that average quality grass will resist flow loads induced by lower wave heights and will only be damaged by the flow velocities induced by higher waves.

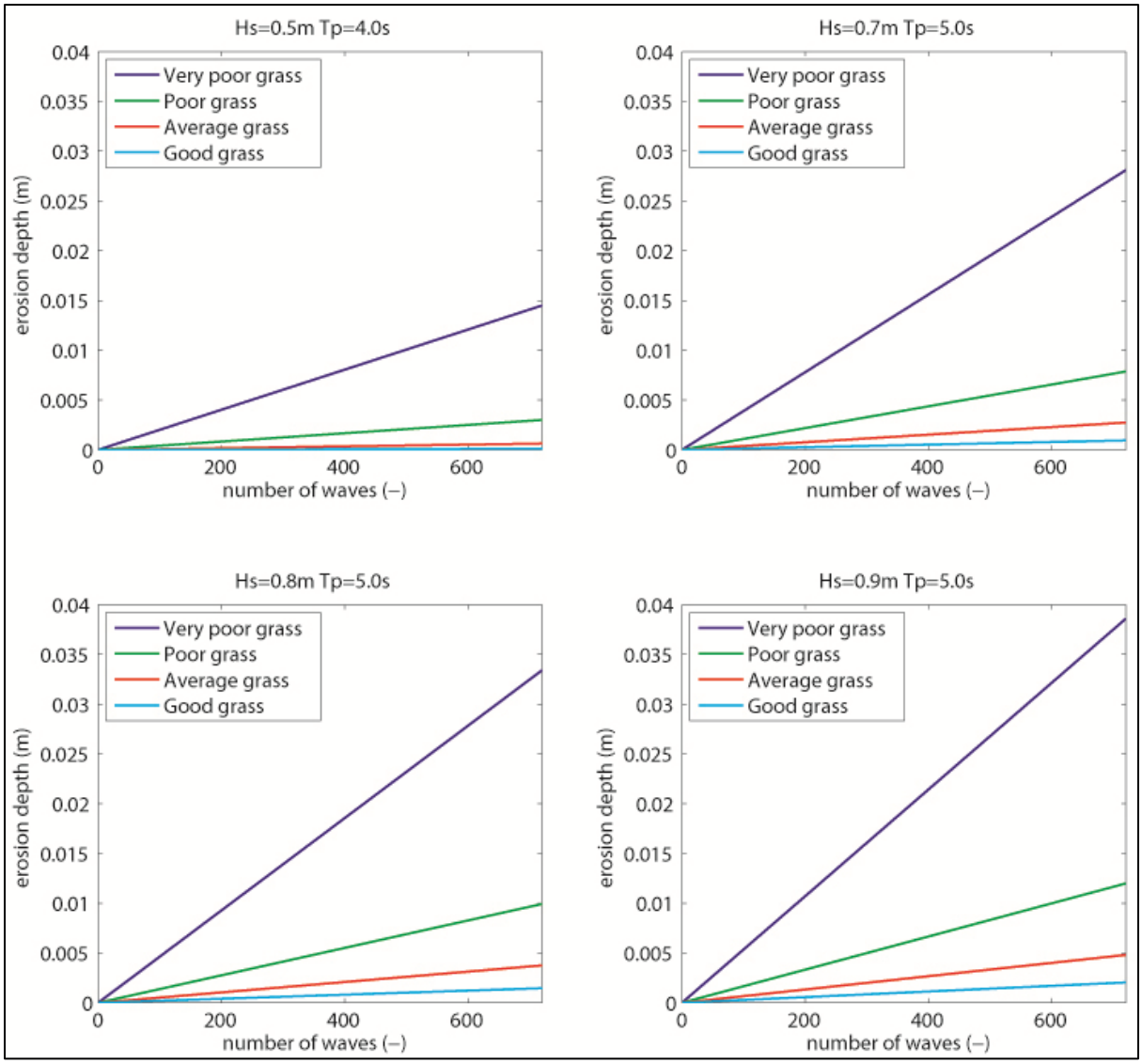

Figure 8-23: Erosion depths at MWL for various grass qualities and various wave conditions.

8.4 Discussion

8.4.1 Data analysis

Before the model was calibrated the input loads were analyzed and checked on reliability. For this purpose the pressure records of all available tests were subjected to a statistical analysis; unfortunately test 1 on April 8 and both tests on April 18 were not available.Furthermore the analysis was restricted to the pressure transducers that measured the highest pressures for each wave condition; DMD 2 and DMD 3.

Per wave period one maximum pressure was identified, consequently not all input pressures were by definition impact pressures. Yet it is expected that the quasi static pressures that were wrongfully included in the calibration programs had little influence on the outcome, as these pressures were relatively low.

After a comparison of the tests with equal wave conditions it appeared that the major part of the tests was reliable and thus suitable for calibration runs. However the pressures during test 2 on April 16 were unrealistically high, which is expected to be caused by a calibration error. This test was therefore excluded from the calibration runs. To a lesser extent it also remains uncertain if the data of the test on April 11 are correct, considering that the maximum pressures occurred at an unexpected location on the slope. Nonetheless this test was used for calibration.

Although these irregularities were presumably calibration errors this was not reflected in the observed wave heights as reflection analysis showed no anomalies worthwhile mentioning.

Finally the Root Volume Ratio which was obtained before the experiments by taking samples and subsequently interpolation was considered very high. To avoid an overestimation the value of the RAR was therefore adjusted to the value for good quality grass cover and consequently the outcome of the calibration might thus be on the conservative side.

8.4.2 Aggregate erosion

For aggregate erosion the model was calibrated using only the factor α_{soil} [-], which is included in the erosion parameter. The theoretical value of α_{soil}, which was determined in chapter 7, appeared to be too high. Therefore the model behavior was investigated for lower values of α_{soil} as well and eventually the behavior of the model was satisfactory for α_{soil} =25-35.

For these values the predicted erosion depth was in accordance with the observed progression of aggregate erosion during the EroGRASS experiments. The model predicted an erosion depth at DMD 3 (which was subjected to the highest impact pressures) that ranges from almost 1 cm to slightly more than 2.5 cm. For the same range the predicted erosion depth at pressure transducer DMD 2 was equal to 0.5-0.7 cm. Furthermore no significant erosion was predicted up until the first test on April 22; then an extreme impact pressure induces damage and the erosion process is accelerated.

Since the surface erosion depths were not determined during the EroGRASS experiments, more accurate results cannot be achieved. The exact erosion behavior was unknown and therefore the calibration was based on rough estimates. During most tests aggregate erosion could not be clearly distinguished and the erosion depth was estimated from photographs taken after each test. Moreover the moment of erosion was assumed from test logs and video data. Considering the above and bearing in mind that the results of the calibration are based on merely two calibration runs they should be treated with care.

Nonetheless the WIPE model is considered suitable for the prediction of erosion of a good quality grass cover. Adaptations will be required to make the model more compatible for the prediction of erosion of grass covers of various qualities. This is caused by the fact that the critical uplift pressure is mainly determined by the grass strength; as a result the predicted erosion depth for low quality grass cover is extremely high. To avoid this problem it was suggested to introduce a characteristic length scale for the erosion depth.

This critical depth is defined as the depth where the root density equals the Root Area Ratio at the surface of very poor quality grass cover (RAR =0.0002). The WIPE model is then applicable for good to poor quality grass. Depending on the grass quality the critical erosion depth then varies between 0.03 m and 0.06 m which corresponds fairly well with the critical depth of 5 cm which was initially assumed in chapter 7. An alternative solution could be to modify the strength modeling in such a way that the clay strength is incorporated. The critical length scale for the erosion depth will then perhaps become redundant.

8.4.3 Block erosion

For block erosion the model is calibrated using two factors; α_{soil} [-] for the erosion criterion and a crack growth parameter α_{crack} [-] to calibrate the extension of cracks. Two characteristic block erosion events were distinguished and each event served as a basis for a calibration run. Both of these events occurred near joints: a large block eroded after the test on April 11 and smaller blocks started to erode during test 1 on April 22.

The model was calibrated for both events but unfortunately this yielded no corresponding calibration factors. Especially α_{soil} showed a considerable spread for both calibration runs, whereas the variation of α_{crack} for both runs was limited.

Calibration factor α_{soil} can be regarded as a parameter that determines the moment when block erosion is triggered, whereas the crack growth factor α_{crack} determines the size of the eroded block. To a lesser extent the crack growth parameter influences the moment of failure too, since the block diameter affects the erosion parameter E_p the fracture strength σ_f and the erosion resistance p_c .

Calibration run 1 was based on the block erosion event at row H. The erosion hole had an area of approximately 0.23 m^2 a depth of 0.10 m and was the result of a single wave impact. Since the dimensions of this hole were determined afterwards the assumption that the predicted block diameter should be approximately 0.48 m will not contain much error. Only doubt might exist on the moment of failure, although failure was predicted after one of the highest impact pressures during the test on April 11 which is plausible.
Contrary to this the size of the erosion hole of calibration run 2 was not determined afterwards and the erosion hole was not the result of a single wave impact. Only the erosion depth was known and from the test log it was known that several clumps with roots started to wash up during the first test on April 22 and also during the second test on April 22 multiple blocks eroded from the grass cover. Unfortunately the exact erosion behavior during the tests for calibration run 2 was thus unknown and the assumed block size and the actual moment of failure for calibration run 2 will therefore be prone to some error.
The erosion resistance of different sections of the grass cover was estimated by selecting an appropriate value for the side wall coefficient n_s. As both erosion locations had different characteristics n_s was chosen differently for both grass cover sections. The values of the side wall coefficient at the respective locations were partly based on the predicted depths of minimum fracture strength; these should be equal to observed erosion depths after the tests.
Erosion events occurred near joints and worms were found in the erosion holes, which presumably affected the strength. Furthermore it is believed that the erosion process and the strength of the grass cover at row H (calibration run 1) were strongly influenced by the glass observation window next to this section.
Because of this it was concluded that the side wall coefficient for calibration run 1 should be significantly lower than for calibration run 2, which resulted in values of respectively 1.0 and 2.0 for the side wall coefficient at these locations. The above illustrates that determining the actual strength for grass covers with local weaknesses is troublesome and to some extent arbitrary. For both sections the erosion resistance could thus be chosen differently, although the equality of the predicted depths of minimum fracture strength and the observed erosion depths will limit the possibilities for variation. The consequences of a different value of the side wall coefficient were therefore briefly investigated.
Small deviations of the value of the side wall coefficient appeared to have relatively little influence on resistance were not very disturbing. Yet for small block diameters the absolute differences are larger, which might even be decisive for the initiation of block erosion.
Moreover the side wall coefficient partially determines the fracture strength σ_f. The variation of the fracture strength for various values of n_s is only marginal at small depths but becomes larger at greater depths. However the deviations in fracture strength at greater depth have no consequences for the erosion process because the fracture strength there is considerably higher than the minimum fracture strength, irrespective of the value of n_s. The variation of the fracture strength at the location of minimum fracture strength is thus of relevance, but the differences were found to be marginal.
Despite the small variations of $\sigma_{f,\min}$ for various values of n_s, the side wall coefficient is still important because it determines the location of minimum fracture strength $z_{\min}$ and thus the block erosion depth. Furthermore $z_{\min}$ and the magnitude of the minimum fracture strength are also strongly dependent on the initial block diameter. For small block diameters (d_{block} =0.004-0.05 m) the fracture strength declines rapidly, whereas it decreases only slightly for larger block diameters.
Because the initial block diameter is chosen equal to the aggregate diameter in the WIPE model, the aggregate diameter distribution is therefore of major importance.
In addition the block diameter is of importance as well for the erosion parameter E_p and the erosion resistance p_c; between block diameters of 0.004 m and 0.05 m both terms diminish dramatically. Nevertheless for small block diameters the erosion parameter is high and the critical uplift pressures are greater than the occurring uplift pressures, which is partly caused by the damping in the cracks.
For small block diameters only extremely high impact pressures will induce the uplift pressures that exceed the critical uplift pressure. The erosion criterion is therefore most probably not fulfilled

regardless of the magnitude of the factor α_{soil} .
Conversely the reduction of the erosion parameter and the critical uplift pressure for larger block diameters is less drastic, but now the magnitude of these terms comes in a range where failure can be triggered by high impact pressure peaks. For larger block diameters the correct value of the factor α_{soil} is therefore essential to predict the correct moment of failure. This is clearly observed during calibration run 2 where the critical uplift pressure is too high during the tests on April 16 for block erosion to occur even though the value of α_{soil} is rather low (0.23). After this the test program reaches test 1 on April 22, where the erosion resistance remains high but erosion nevertheless occurs for this low value of α_{soil} after a pressure peak of approximately 35 kPa. The above also illustrates that the chronological order of the wave impacts is important as well (sequential effect).

8.4.4 Erosion by flow velocities

Flow induced erosion was considered to be negligible during the development of the WIPE model. To verify this assumption the erosion of grass covers of various qualities due to flow velocities was predicted with the help of the EPM/Hoffmans model for the wave conditions used during the EroGRASS experiments.
The stubble, which consist of loose particles and plant remains, appeared to erode for flow velocities lower than 0.40 m/s. Undoubtedly the stubble is washed away by wave run-up and run-down very quickly, but this is not defined as erosion and should be regarded as the 'rinsing' of the grass cover.
Subsequently the surface erosion of the turf was investigated around MWL . Flow velocities induced by significant wave heights of up to 0.90 m caused no problems for good quality grass cover. The erosion caused by flow velocities during the EroGRASS experiments can thus indeed be neglected.
This is different for very poor and poor quality grass cover. Maximum flow velocities induced by low wave heights (H_s =0.50 m) will already lead to serious damage. Average quality grass sod is considered to be in the transition zone since the erosion rate was marginal for low waves and limited for higher waves.
It is anticipated that the erosion rates are overestimated in this analysis. First of all it was assumed that the slope is loaded during each wave by both the run-up velocity and the down-rush velocity; overtopping was considered not to occur. Secondly the predicted run-down velocity exceeded by 2% of the waves was considered to occur for each wave. In reality run-down velocities will be lower since the run-up height of a large portion of the incoming waves is lower. Conversely the strength of the grass cover was taken at the surface, where it is at a maximum. At a certain erosion depth flow velocities will therefore probably also affect the erosion process of good quality grass covers.

8.5 Conclusions

8.5.1 Data analysis

- The major part of the tests was reliable and thus suitable for calibration runs. However the pressures during test 2 on April 16 were unrealistically high; it was therefore replaced during calibration. Although it also remains uncertain if the data of the test on April 11 are correct, this test was used during calibration;
- The grass characteristics obtained before the EroGRASS experiments were very high. To avoid an overestimation of the grass cover strength the dike model was considered to be covered with good quality grass (RAR_0 =0.0008);
- Per wave period one maximum pressure was identified, consequently not all input pressures were by definition impact pressures. Yet it is expected that this had no significant influence on the outcome of the calibration.

8.5.2 Aggregate erosion

- For aggregate erosion the model was calibrated using only the factor α_{soil} [-], which is included in the erosion parameter. For α_{soil} =25-35 the model behavior was in accordance with the observed progression of aggregate erosion during the EroGRASS experiments;

- Since the surface erosion depths were not determined during the EroGRASS experiments, more accurate results cannot be achieved. Nonetheless the WIPE model is considered suitable for the prediction of aggregate erosion of a good quality grass cover;
- Because the critical uplift pressure is mainly determined by the grass strength, a critical erosion depth is introduced. This will prevent the prediction of unrealistically high erosion depths for inferior grass covers or for lower root densities at greater depth;
- The critical depth is defined as the depth where root density equals the root density of very poor quality grass cover (RAR=0.0002). Depending on the grass quality the critical erosion depth varies between 0.03 m and 0.06 m.

8.5.3 Block erosion

- For block erosion the model was calibrated using two factors. The calibration factor α_{soil} [-] can be regarded as a parameter that determines the moment when the erosion criterion is satisfied and block erosion occurs, whereas the crack growth factor α_{crack} determines the size of the eroded block. Furthermore α_{crack} also has some influence on the moment of failure as it affects the decay of the erosion parameter E_p the fracture strength σ_f and the erosion resistance p_c ;
- The model was calibrated on two characteristic block erosion events which both occurred near joints. This yielded a considerable spread in the values of α_{soil} (0.01-3.25), whereas the variation of α_{crack} (390-420) for both calibration runs was limited;
- It is expected that the scatter of α_{soil} is mainly caused by the small block diameter that was required during calibration run 2. For block diameters in the range d_{block} =0.0-0.10 m, a small increase of the block diameter has a relatively large influence on the decline of the strength parameters p_c , E_p and σ_f , but because the strength terms are especially high for very small block diameters ($d_{block} \leq 0.05$ m) extremely high impact pressures are required to cause block erosion. It is therefore highly unlikely that small blocks will erode, regardless of the magnitude of the factor α_{soil} ;
- The reduction of the strength terms is less drastic for larger block diameters, but the magnitude of these terms is in the range where failure can be triggered. For larger block diameters the correct value of the factor α_{soil} is therefore essential to predict the correct moment of failure;
- Damping in cracks is an important effect in the block erosion process, whereas this effect hardly plays a role for aggregate erosion;
- As the erosion resistance diminishes when the crack under the block grows, the chronological order of the wave impacts (sequential effect) has a great influence on the erosion process.
- The values of the side wall coefficient n_s could be chosen differently. This might cause important differences in the erosion resistance for small block diameters and can possibly affect the moment of erosion. Furthermore n_s partly determines the location of minimum fracture strength $z_{\min}$ and thus the block erosion depth;
- The initial block diameter has a strong influence on $z_{\min}$ and the magnitude of the minimum fracture strength $\sigma_{f,\min}$. Since the initial block diameter is chosen equal to the aggregate diameter in the WIPE model, the aggregate diameter distribution is of major importance.

8.5.4 Flow velocities

- The stubble is washed away by wave run-up and run-down very quickly, but this not defined as erosion;
- From the analysis it appeared that flow velocities induced by significant wave heights of up to

0.90 m caused no problems for good quality grass cover. Erosion by flow velocities during the EroGRASS experiments can therefore be neglected;

- For very poor and poor quality grass cover flow velocities caused by low waves (H_s =0.50 m) can already lead to serious damage. Average quality grass sod is considered to be in the transition zone;
- At a certain erosion depth flow velocities will start to affect the erosion process of good quality grass covers.

8.6 Calculation example

In the previous sections the model has been calibrated and verified as best as possible. In this section an example will be treated for the prediction of erosion of a grass cover on the basis of solely wave characteristics.

The grass cover in this example will be considered of good quality and the condition of the grass cover is assessed at average; several cracks and inconsistencies are present. Hence RAR_0 =0.0008, the critical erosion depth is 0.0621 m (Table 8-8) and the side wall coefficient n_s is assumed at 2.0.

The dike is loaded by waves for 6 hours (T_{storm} =21600 s) with a significant wave height H_s =0.60 m. The characteristic wave period during the storm T_m =5.0 s and the outer slope is assumed at 1:4. Furthermore it is supposed that for every 10 waves only 1 wave produces an impact pressure, consequently the wave impact coefficient α is equal to 0.10. The number of wave impacts during this storm can then be predicted as follows:

N_w =21600/5.0=4320 waves, $N_{imp} = \alpha N_w$ =0.10·4320 = 432 impacts.

All parameters required for the calculation are summarized in Table 8-19.

Table 8-19: Parameters for the calculation example.

Parameter		*Value*
Root Area Ratio at the surface	RAR_0	0.0008
Grass tensile strength	t_r	$20 \cdot 10^6$ N/m^2
Root diameter	d_r	$0.13 \cdot 10^{-3}$ m
Root decay coefficient	β	22.32
Side wall coefficient aggregate erosion	n_s	2
Side wall coefficient block erosion	n_s	2
Clay cohesion	c_{clay}	$30 \cdot 10^3$ N/m^2
Critical clay strength according to Hoffmans et al. (2009)	$c_{clay,c}$	$c_{clay,c} = c_{clay} / 80$
Aggregate diameter at the surface	d_a	0.004 m
Saturated volumetric weight of soil	ρ_s	2000 kg/m^3
Volumetric weight of water	ρ_w	1000 kg/m^3
Porosity	n	0.4
Natural angle of repose	φ	35 degrees
Pressure reduction factor in cracks	μ	5 m^{-1}
Characteristic impact time	t_{impact}	0.350 s
Calibration factor aggregate erosion	α_{soil}	35
Calibration factor block erosion	α_{soil}	1.35
Crack growth parameter	α_{crack}	420
Wave impact coefficient	α	0.10
Storm duration	T_{storm}	6 hours
Significant wave height	H_s	0.60 m
Characteristic wave period	T_m	5.0 s
Number of wave impacts	N_{imp}	432
Critical erosion depth for good grass cover	$y_{m,crit}$	0.0621 m

8.6.1 Prediction of wave impact pressures

As the impact pressures are not known they need to be estimated from the wave characteristics (see also section 7.2.1). Ultimately a sequence of wave impact pressures should be obtained which can be used as the load on the grass cover in the WIPE model.
Before a loading sequence can be generated the distribution of the impact pressures is required. The impact factor probability density function is therefore evaluated first. For smooth slopes of 1:4 the impact factor has the following probability density function:

$$p(q) = \frac{1}{\sigma_q \sqrt{2\pi}} e^{-\left[\frac{(q-q_{avg})^2}{2\sigma_q^2}\right]} \tag{8-5}$$

The impact factors have been divided into classes with a range of 0.2 and subsequently the probability of occurrence of each impact factor class has been computed using the probability density distribution. With mean q_{avg} =2.2 and standard deviation σ_q =0.70, this gives the green bar chart in Figure 8-24 left. The mean and standard deviation have been estimated by integrating the probability density distribution for several intervals until the obtained impact factors resembled the proposed values of the impact factor by Fuhrboter (1986) (Table 8-20).

Table 8-20: Predicted impact factors for slope of 1:4.

Impact factor q_i *[-]*	q_{50} *[-]*	q_{90} *[-]*	q_{99} *[-]*	$q_{99.9}$ *[-]*
Fuhrboter (1986)	2.2 ± 0.4	3.0 ± 0.5	3.9 ± 0.6	4.8 ± 0.7
Equation (8-5)	2.2	3.1	3.9	4.8

Multiplying each impact factor class with the number of wave impacts during the storm and using the relation $p_{\max} = q\rho g H_s$ yields the impact pressure distribution displayed in Figure 8-24 right.

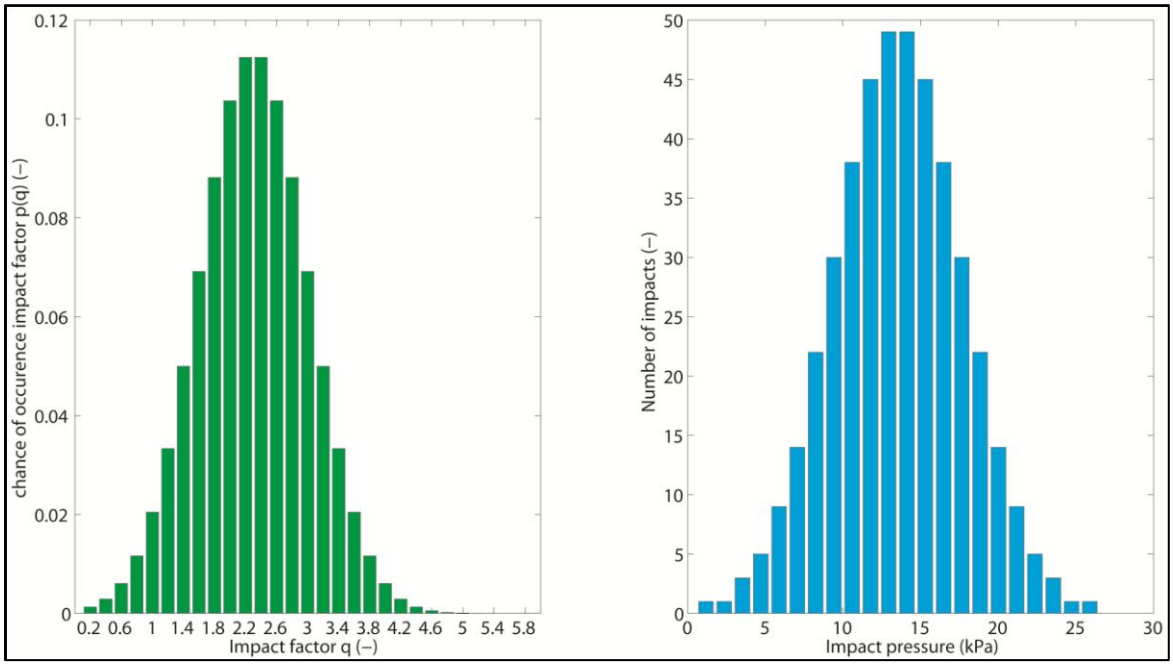

Figure 8-24: Probability of occurrence impact factor (left), impact pressure distribution (right).

Finally a loading sequence has been generated randomly from this impact pressure distribution. Obviously many permutations are possible for this impact pressure distribution and as has been pointed out earlier, it is recommended to generate numerous loading sequences and to run the WIPE model for all of these permutations. Yet in this example only one loading sequence is generated for the simulation of aggregate erosion and block erosion.

8.6.2 Aggregate erosion

The results of the simulation for aggregate erosion are displayed in Figure 8-25 and the loading sequence can be found in the bottom left (black graph).

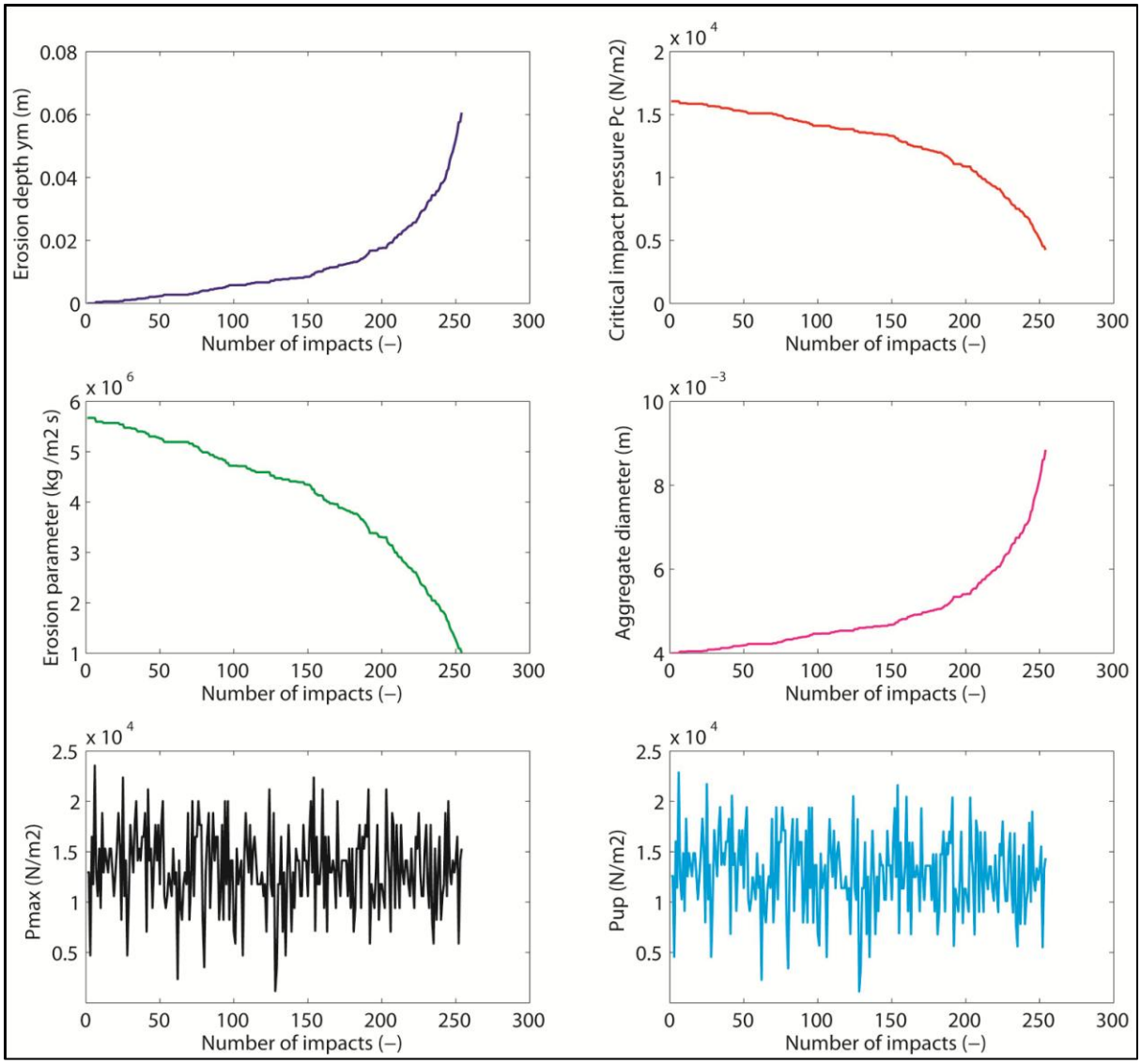

Figure 8-25: Simulation results for aggregate erosion.

It is clear that the grass cover is not able to withstand the wave loads for the entire storm duration; the highly erosion resistant layer of the grass cover has eroded entirely before the end of the wave loading period. The critical erosion depth of 0.0621 m is reached after 254 impacts. Under the assumption that the impact pressures are distributed equally over the storm duration the critical depth is reached after 254/432 of the storm duration. The critical erosion depth is then reached after approximately 3.5 hours.

For this relatively low significant wave height considerable erosion occurs already, which can only be attributed to the predicted high values of the impact pressures. These are comparable to the pressures measured by the pressure transducers during the test with significant wave heights of 0.90 m. The impact pressures for grass covers should thus presumably be lower. This discrepancy could be partly explained by the fact that the predicted impact pressures are valid for smooth slopes.

8.6.3 Block erosion

The results of the simulation for block erosion are given in Figure 8-26. Even though the impact pressures are relatively high for the given wave conditions block erosion does not occur. In the event that large cracks are present or are formed there are no extreme impact pressures in the loading

sequence which are high enough to induce block erosion.
Instead the horizontal crack gradually extends during the storm up to a length of more than 1.6 m. Consequently the uplift pressures are greatly reduced, which can also be observed from the cyan graph in the bottom right of Figure 8-26.

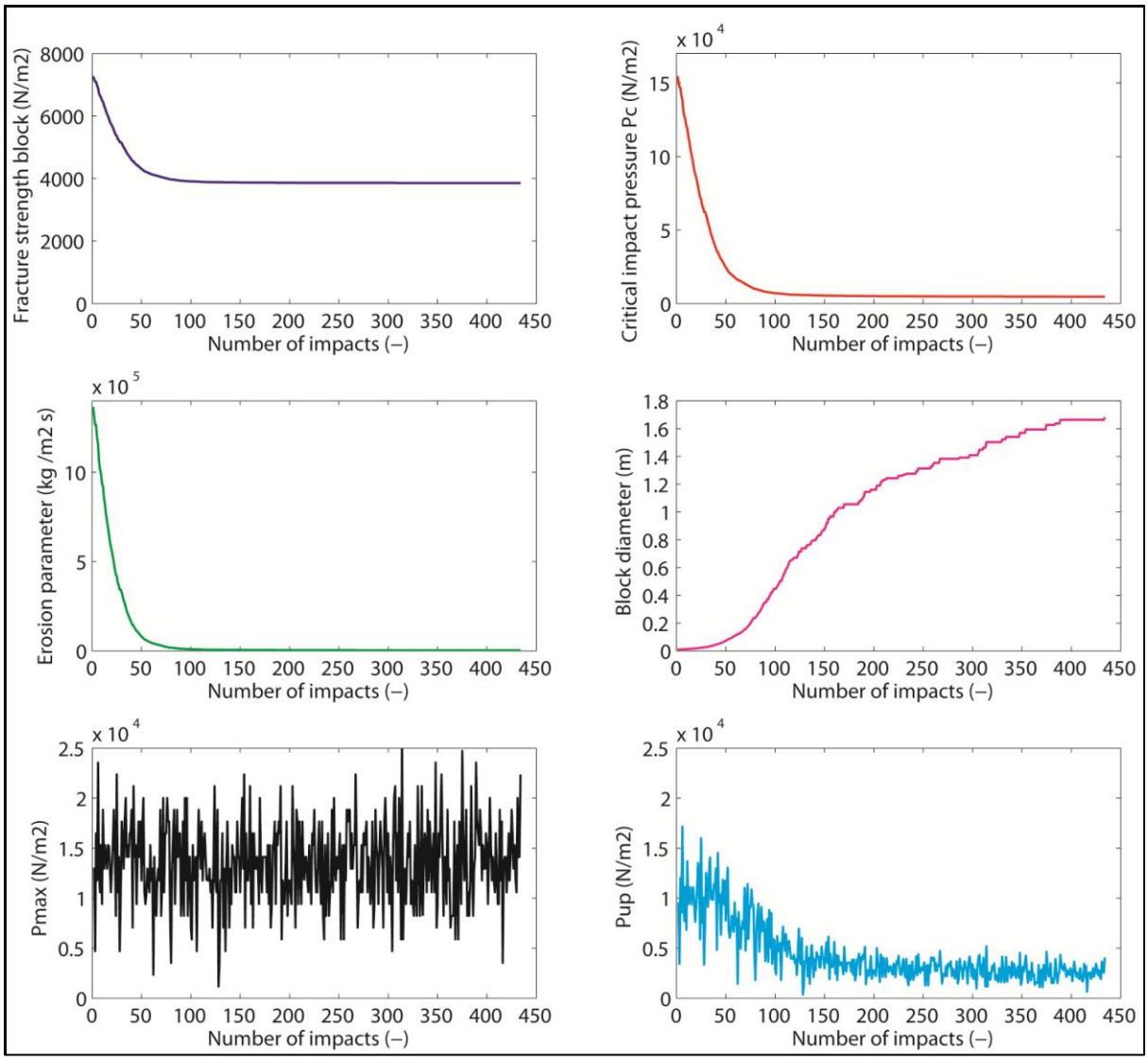

Figure 8-26: Simulation results for block erosion.

9 Conclusions and recommendations

9.1 Conclusions

9.1.1 Erosion process

9.1.2 Summary WIPE model

9.1.3 Calibration and verification results

9.1.4 Grass cover strength and management

9.2 Recommendations

9.2.1 Load

9.2.2 Grass cover strength

9.2.3 Failure mode

9.2.4 Experiments

9 Conclusions and recommendations

As explained in chapter 1 a hiatus in the knowledge on the erosion of grass on outer slopes currently exists. Against the background of enhanced hydraulic impact due to climate change the benefits of grass as a dike cover could be great, but a clear physical understanding of the failure of grass cover layers due to different wave loads is lacking. Therefore in this thesis a model has been developed that describes the initiation of erosion of grass covers on the outer slope by wave impact pressures: the WIPE model. The most important conclusions (section 9.1) and recommendations (section 9.1.4) for further research following from this study are presented in this chapter.

9.1 Conclusions

First the erosion process is described in theory. This is followed by a summary of the WIPE model and the results from the calibration and verification. Finally the general conclusions on grass cover strength and management are discussed.

9.1.1 Erosion process

Soon after installation a soil structure will develop in a grass cover layer and the soil will then consist of small aggregates. During wave loading the permeability of the covering layer is increased; direct wave impacts form or widen cracks at the surface and the pores and cavities in the turf are gradually saturated with water. Simultaneously the turf may be damaged at greater depth when an irregularity exists in the cover layer that allows impact pressures to penetrate into the soil.
For wave-induced erosion of grass cover layers on the outer slope two failure mechanisms can therefore be distinguished which can occur independently of each other:

1. Aggregate erosion: when the soil is cracked and saturated with water uplift pressures can develop underneath the aggregates shortly after a wave impact. At the surface small aggregates may then be lifted and washed away, which eventually results in an erosion hole.
2. Block erosion: impact pressures penetrate into the soil due to the presence of a large crack or irregularity. The balloon mechanism may then be triggered; at the location of minimum fracture strength a horizontal crack is formed. This crack gradually extends until it reaches a critical size. From this point a large block can instantly erode from the grass cover.

9.1.2 Summary WIPE model

The basic equation for the Wave Impact Pressure Erosion (WIPE) model reads:

$$y_m = \sum_{1}^{N_{imp}} \frac{\left(p_{up}(z) - p_c(z)\right) \cdot t_{imp}}{E_p(z)} \tag{9-1}$$

The load terms, the grass strength terms and the characteristic aggregate diameter with their recommended values are given in the boxes below. These terms are valid for both erosion mechanisms.

Load terms

$$N_{imp} = \alpha N_w, \; N_w = T_{storm} / T_m$$

$$p_{up}(z) = \frac{p_{\max}}{(1 + \mu d_c)}$$

Grass strength

$$\sigma_{grass,c}(z) = t_{r,c} \cdot RAR_0 \cdot e^{-\beta z}$$

$$c_{grass,c}(z) = 1.2 \cdot t_{r,c} \cdot RAR_0 \cdot e^{-\beta z}$$

Characteristic aggregate diameter

$$d_a = \sqrt{A / n_r} + 0.08 \cdot z$$

With:
N_{imp} = no. of impacts [-]; α = wave impact coefficient between 0.0-1.0 [-]; N_w = no. of waves in a storm [-]; t_{imp} = 0.35 [s]; μ = 5 [m^{-1}]; $t_{r,c}$ = $20 \cdot 10^6$ [N/m^2]; RAR_0 = Root Area Ratio at the surface [-]; β = 22.32 [m^{-1}]; z = depth [m]; A = soil area [m^2]; n_r = number of roots [-]

The basic equation (9-1) can be adapted to predict the erosion depth y_m [m] for either aggregate erosion (1) or block erosion (2).

1. **Aggregate erosion**

$$y_m = \sum_{1}^{N_{imp}} \frac{\left(p_{up}(z) - p_c(z)\right) \cdot t_{imp}}{E_p(z)}$$

$$y_m \le y_{m,crit}$$

Strength terms

$$p_c(z) = \left(1 - n + 0.5 n_s f\right) \cdot (\rho_s - \rho_w) \cdot g d_a(z) + \sigma_{grass,c}(z)$$

$$E_p(z) = \alpha_{soil} \cdot \left(\frac{\rho_s}{\rho_w}\right) \cdot \frac{p_c(z)}{\sqrt{g d_a}(z)}$$

With:
$y_{m,crit}$ = critical erosion depth between 0.03-0.06 [m]; n =0.4 [-]; n_s =2.0 [-]; $f = \tan\varphi$ [-]; φ =35 [-]; ρ_s =2000 [kg/m^3]; ρ_w =1000 [kg/m^3]; g =9.81 [m/s^2]; and α_{soil} =35 [-].

2. **Block erosion**

$$y_m = z_{\min} \text{ [m]}$$

$$\text{When } \frac{(p_{up}(d_{block}) - p_c(d_{block}) \cdot t_{imp}}{E_p(d_{block})} > z_{\min} \qquad (9\text{-}2)$$

Where $z_{\min}$ [m] is the depth of the minimum fracture strength $\sigma_{f,\min}$ [N/m^2].

Strength terms

$$p_c = (1-n)(\rho_s - \rho_w) g z_{\min} + \frac{0.5 \cdot n_s f (\rho_s - \rho_w) g \cdot z_{\min}^2}{d_{block}} + \frac{n_s \left(\int_0^{z_{\min}} c_{grass,c}(z) + c_{clay,c} \cdot z_{\min}\right)}{d_{block}} + \sigma_{grass,c}(z_{\min})$$

$$E_p(d_{block}) = \alpha_{soil} \cdot \frac{\rho_s}{\rho_w} \cdot \frac{p_c(d_{block})}{\sqrt{g d_{block}}}$$

Crack formation

$$\sigma_f = (1-n)(\rho_s - \rho_w) g z + \frac{0.5 n_s f (\rho_s - \rho_w) g \cdot z^2}{d_{block}} + \sigma_{grass,c}(z)$$

$$\Delta A_{block} = \frac{\left(p_{up}(d_{block}) - \sigma_{f,\min}(d_{block})\right) A_{block}}{\alpha_{crack}\left(\sigma_{f,\min}(d_{block}) + c_{clay,c}\right)} \qquad \text{Where: } A_{block} = {d_{block}}^2 \text{ [m}^2\text{]}$$

With recommended values:
$d_{block,0} = d_a$ [m]; n_s =2.0 [m]; $c_{clay,c}$ = c_{clay} /80 [N/m^2]; c_{clay} =30 [kN/m^2]; α_{soil} =1.35 [-] and α_{crack} = 420 [-].

9.1.3 Calibration and verification results

Calibration was performed on the data of the EroGRASS experiments. Unfortunately not all test data could be considered reliable but the major part of the tests was suitable for calibration runs. Furthermore the moment of failure and the erosion depths were for the major part estimated as mostly only indicative erosion data was available. As the calibration was performed with limited data it is clear that the interpretation of the results should be done with caution. Nonetheless conclusions were drawn from the results of the calibration and verifications. These are subdivided below into conclusions regarding the load, aggregate erosion and block erosion.

Load

- Due to the diminishing strength of the grass cover with depth the chronological order of wave impacts is an important factor in the erosion process and complicates the prediction of erosion of grass covers;
- Damping in cracks is a relevant effect in the block erosion process, whereas this effect hardly plays a role during aggregate erosion. However if cracks widen considerably due to the balloon mechanism, the pressure attenuation in cracks could be negatively affected;
- Erosion induced by flow velocities was considered to be negligible for the good quality grass cover during the EroGRASS experiments. From a preliminary analysis it appeared that the wave conditions during the experiments indeed cause no problems for good quality grass cover. At a certain erosion depth flow velocities will however start to affect the erosion process.

Aggregate erosion

- Calibration of aggregate erosion was done with solely the parameter α_{soil} [-], which is included in the erosion parameter. For α_{soil} =25-35 the model behavior resembled the observed progression of aggregate erosion during the experiments;
- For low root densities the WIPE model predicts excessive erosion rates since the critical uplift pressure is dominated by the grass strength. Therefore a critical erosion depth is introduced, which is defined as the depth where root density equals the root density of very poor quality grass cover (RAR =0.0002). Depending on the grass quality the critical erosion depth then varies between 0.03 m and 0.06 m;
- The WIPE model is considered suitable for the prediction of aggregate erosion for good quality grass covers. However it is expected that the performance of the WIPE model will be unsatisfactory for poor quality grass covers, despite the introduction of the critical depth. Yet for lower quality grass covers the model will require adaptations to be applicable anyway as in addition to the impact pressures flow velocities will start to play role in the erosion process.

Block erosion

- The model was calibrated on two characteristic block erosion events with the help of two parameters: unfortunately the value of α_{soil} has a considerable scatter (0.01-3.25), whereas the variation of α_{crack} (390-420) for both calibration runs is limited;
- Extremely high impact pressures are required to cause block erosion for very small block diameters ($d_{block} \leq 0.05$ m). It is therefore highly unlikely that small blocks will erode, regardless of the magnitude of the factor α_{soil} . It is expected that this partly caused the scatter in the value of α_{soil} ;
- Different values for the side wall coefficient n_s and thus different erosion resistances during both calibration runs might improve the calibration results. However the possibilities for variation are limited because n_s partly determines the predicted erosion depth;
- To obtain more reliable and uniform results for block erosion more data is required.

9.1.4 Grass cover strength and management

Block erosion and aggregate erosion have been identified as the governing failure mechanisms for erosion by wave impact pressures. For aggregate erosion to occur a poor condition of the soil is required and the same holds for block erosion; large cracks or inconsistencies are a prerequisite for failure to occur.
The condition of the grass cover will gradually deteriorate during wave loading, but the initial condition of the grass cover layer is determined by the degree of soil structure. The initial condition of the soil thus partly determines when the grass cover becomes susceptible to erosion. Hence limiting soil structure and cracks is crucial and will make the grass cover less susceptible to erosion.
In addition to its large influence on the failure mode, soil structure also affects the erosion resistance in the top decimeters of the grass cover as it limits the effect of cohesion and friction forces. Because of this management and maintenance of grass covers should preferably also consider the compaction of the soil.
The erosion resistance of grass covers is dominated by the reinforcing effect of the roots. Roots stimulate the biological processes that produce the cementing substances that enable the clustering of small particles in the form of aggregates. Small aggregates can be interconnected by penetrating roots and the hair roots that are anchored within them, whereas larger aggregates are kept in place by the filter effect of the total network of roots as well as root penetration.
From an engineering point of view a dense root network of many thin roots is therefore to be preferred over a less dense network of thicker roots. Many small roots will presumable lead to a more structured grass cover with smaller aggregates, but at the same time these aggregates will be highly interconnected due to the abundance of roots. Contrary to this a network of thick roots will cause less soil structure with relatively large aggregates, but the total grass cover will probably have not as much coherence because the aggregates are interconnected by fewer roots.
Furthermore grass species with thick roots and large leafs are likely to create unfavorable circumstances for the growth of other species; which can result in locally lower root densities and thus weak locations. In addition their roots will penetrate deeper into the covering layer which will probably cause larger cracks and inconsistencies in the covering layer, which enables the possibility of block erosion. Conversely a large amount of long roots, and thus a relatively high root density at greater depth, will also provide more resistance against block erosion.
As the root density decays with depth, the root length is also of importance for the erosion resistance at the surface. Yet mainly the amount of roots in the top 5-8 cm is of relevance; root densities at greater depth and thus longer root lengths have less influence on the erosion resistance at the surface. Nonetheless roots need to be sufficiently long to prevent pull-out from occurring.
Both thin roots and thick roots are thus required to prevent aggregate and block erosion and grass cover management should therefore primarily be aimed at obtaining a dense root system with many thin roots and some thick roots in the top part of the cover layer. General consensus exists that this is accomplished with management category A: haying and mowing twice a year or grazing with sheep without fertilizing.
Both haying and mowing and grazing with sheep are good management methods. Mowing a few times a year is relatively simple and does not require much effort but has the drawback that the grass cover might be damaged in the process when the mowing equipment is very heavy. Contrary to this grazing with sheep requires more effort but is not expected to cause severe damage to the grass cover. Grazing with sheep has a positive effect on the root development in the upper region of the grass cover and can be done continuously during the entire growing season from April to October with few sheep, but the sections that have not been grazed will still require mowing.
The alternative is to graze intensively two to four times during the growing season, which requires more sheep for a short period of time. The latter method is preferred as it is less likely that sheep trails and bare spots will develop. Furthermore it is expected that a herd of sheep will also compact the upper parts of the grass cover during grazing which will reduce soil structure. Since a soil structure will redevelop sooner or later in the grass cover due to climatic effects the beneficial effect is merely temporarily, but the soil is once again compacted by the herd of sheep during the next grazing period.
Finally the grass must be sufficiently short before the start of the winter to prevent the formation of tussocks and thus the formation of weak spots due to less incident sunlight.

9.2 Recommendations

The calculation example in section 8.6 showed how the model could be applied in engineering practice. However it also demonstrated that some hurdles still need to be taken before it can be adequately utilized in this way. Therefore some recommendations are given below; these are subdivided into categories and briefly treated in the next sections.

9.2.1 Load

The uplift pressures within grass covers induced by wave impacts should be examined in more detail.
For the model to be applicable in practice it is first of all essential to improve the relation given by Führböter between wave characteristics, the geometry of the dike and impact pressures, because generally only the hydraulic conditions are known at dike sections. This could also include developing a relation between the number of waves and the number of wave impacts.
Research on the pressure reduction within cracks in grass cover could also be performed as it is an important effect in the block erosion process. Furthermore it should be checked if the impact pressures are fully converted by the pore water into uplift pressure or that pressure losses occur during this process.
Moreover a method should be developed to account for the sequential effect of the wave impacts and the influence of the flow velocities on outer slope erosion should be more thoroughly enquired into.
Finally it is recommended to check if significant differences arise when dynamic effects such as the time shift between impact and uplift pressure, the impact duration and the inertia of the block are taken into account. Furthermore the impact duration used in the WIPE model is a maximum boundary value. It should be checked whether the method to estimate the impact duration is also valid for permeable grass covers.

9.2.2 Grass cover strength

In the WIPE model the strength of a grass cover is mainly attributed to the reinforcing effect of the roots and thus the quality of the grass, while the influence of the clay quality is considered of less importance. Yet it might be that clay quality has a greater influence on the strength of the turf and that the strength is in fact more dependent on the synergy of grass and clay, this should be investigated.
It should also be checked whether assumptions made during the strength modeling in the WIPE model are disputable. Furthermore the model describes the erosion of good grass and is in fact not applicable for poor grass and bare clay at this moment. Additional studies could look into the possibilities and the required modifications to make the model applicable for grass covers of every grass quality.
Besides this it goes without saying that more research must be carried out on the properties of grass and clay to improve grass erosion models in general. This is discussed for both materials individually below.

Grass

Because the grass cover strength is dominated by the grass strength, the grass tensile strength $t_{r,c}$ and the root diameter d_r are essential parameters. At present the grass cover strength is obtained by assuming an average root diameter and an average tensile strength for all roots, whereas many roots with different diameters are present in the turf. Furthermore it is assumed that all roots break simultaneously and that pull-out does not occur.
It is therefore suggested to investigate the root diameter distribution of grass species present on dikes, because the root diameter distribution could have a significant influence on the failure modes of roots as well as on the tensile strength of the roots. The grass strength could be underestimated if a negative exponential relation between the grass tensile strength and the root diameter exists. Conversely the grass strength could also be overestimated because root pull-out it is not considered. In addition the root length distribution should be quantified if pull-out is to be taken into account. Besides this the cementation process due to the roots and the anchorage of the hair roots in the soil could be enquired in more detailed.
Moreover it is important to check if there are significant differences between the characteristics described above for dead and living plants and between different grass species on several types of

dikes. Grass species on a sea dike may greatly differ from grass species at a river dike (salt versus fresh water) but also the characteristics of grass on sea dikes at different locations could vary.
This was also demonstrated by the difference between the root densities obtained during the EroGRASS experiments (Danish grass) and the average root densities of grass on Dutch dikes according to Sprangers and Hoffmans. Reasons for this discrepancy could be the difference in species and age of the grass mats, the seasonal variation and possibly a different climate. Ideally grass dikes should be categorized and guideline values should be formulated for grass on each of these types of dikes.

Clay

Additional research on the erosion process of cohesive soil and the appropriate values for the critical clay strength and the clay rupture strength is desirable.
The proposed value for the critical clay strength as applied in the WIPE model is a minimum boundary value and should perhaps be increased. Furthermore the erosion resistance of clay is controlled by a great number of interacting and related factors. Ideally governing factors for the cohesion of the clay should be identified and if possible their influence on the strength of the clay should be quantified. For instance the influence of moisture content could be valuable to predict the fluctuation of the clay strength due to infiltrating water during wave loading.
Besides this, soil structure development deserves more investigation as it determines the erosion resistance of clay for a large part. Of particular interest are the condition of the grass cover and the presence of cracks after a soil structure has already developed. Also a more accurate aggregate diameter distribution should be obtained because it has a strong influence on the erosion resistance, the fracture strength and the erosion depth in the WIPE model.
All of the suggestions above do not necessarily require new experiments; much research has been carried out in the past on the erosion and strength properties of clay and reinterpretation of the data of this research could be valuable.

9.2.3 Failure mode

In theory erosion is initiated at weaker locations such as dead plants or bare spots. Although these are reinforced by the surrounding grass they can still erode if the size of the weak location is sufficiently large. The critical size of a weak spot should thus be studied more thoroughly and preferably also the influence of the grass quality surrounding it. With the help of the grass influence area and the critical size for several grass qualities an estimate can be given for the erosion resistance of bare spots.
In this research not much attention has been paid to weak spots at the surface though. Yet failure due to the presence of cracks and other inconsistencies has been treated extensively; block erosion will only occur if these are present in the grass cover. Research on the growth of these cracks by wave loading will therefore be useful and in addition the occurrence of the balloon mechanism could be verified. Finally the crack formation process by wave impacts at the surface also deserves more attention to improve the strength modeling for aggregate erosion.

9.2.4 Experiments

Several considerations and recommendations can be given for experiments on the erosion of grass in the future. Unfortunately there is no technique to scale grass covers at this moment, therefore experiments on the erosion of grass must be carried out at full scale which is costly and time consuming.
For constructional reasons the grass cover of the EroGRASS experiments needed to consist of many smaller sections of grass sod. Inevitably this led to irregularities at the surface and cracks between the sections. Although these were repaired best as possible these irregularities had a significant influence on the erosion process. If possible the installation method of the grass cover should therefore be improved. A potential improvement of the installation could be to close off part of the flume and to assign this space to a dike model with a grass cover, in such a way that the grass cover is given sufficient time to recover from the installation. This area should preferably be outside to allow the grass to grow as it would on a real dike.
Furthermore the erosion must be monitored in more detail. It is suggested to continue gathering visual data during and after the tests, but also to collect especially numerical data of the moment of

erosion and the erosion depths or the size of eroded blocks. A clock could be installed for this purpose, while surface erosion depths could be measured with plaster casts or lasers.
In addition it could be useful to install more pressure transducers to investigate the pressure variation with respect to depth, although this will probably weaken the sod locally. Moreover it should be considered to carry out tests with wave conditions that increase in magnitude, starting with the mildest wave conditions. An indication of the maximum allowable significant wave height can then be obtained.
Alternatively a device similar to the wave overtopping simulator could be developed to carry out experiments in the field. Simulating wave impacts with a sufficiently small interval between the impacts will be a great challenge though. Besides this developing such a device might be expensive, but as there will be no need to excavate, transport and install the grass sods it could be feasible. Furthermore with this wave impact simulator erosion data at many different test locations could be gathered, which results in a large amount of valuable erosion data of different grass qualities.

References

G. J. Akkerman, V. K. A. J. Gerven, H. A. Schaap and J. W. v. d. Meer (2007). Workpackage 3: Development of alternative overtopping-resistant sea defences, Phase 3: Wave Overtopping Erosion Tests at Groningen Sea Dyke, ComCoast, Delft.

J. J. Bakker, R. J. C. Mom and G. J. Steendam (2008). Factual report: Wave overtopping tests on a Frisian Wadden Sea dike (in Dutch), 07i107B, Deltares, Van der Meer Consulting, Royal Haskoning, Alterra, Infram, Marknesse.

J. A. Battjes (1974). Surf similarity, 14th International Conference Coastal Engineering, Copenhagen, Denmark.

W. v. d. Bos (2006). Erosion resistance of a grass revetment during wave overtopping (in Dutch), MSc thesis, Faculty of Civil Engineering and Geosciences, Delft University of Technology, Delft.

G. N. Bullock, A. R. Crawford, P. J. Henson, M. J. A. Walkden and P. A. D. Bird (2001). The influence of air and scale on wave impact pressures, Coastal Engineering. 42

M. P. Davidse (2009). Experimental analysis; the relation between wave loading and resulting strain in an asphaltic concrete revetment., MSc thesis, Faculty of Civil Engineering and Geosciences, Delft University of Technology, Delft.

N. Doorn (2007). Task 4 - Understanding and predicting failure modes. Activity 4.1 - failure modes for revetments, V2-1-P2, FLOODsite, Delft.

A. Führböter (1986). Model and prototype tests for wave impact and run-up on a uniform 1:4 slope, Coastal Engineering. 10

A. Führböter and U. Sparboom (1988). Full-scale wave attack of uniformly sloping sea dykes, 21st International Conference Coastal Engineering, Malaga, Spain.

P. Geisenhainer and H. Oumeraci (2008). Seadike breach initiation and development, large scale experiments in GWK, T06-08-12, FLOODsite.

M. Genet, A. Stokes, F. Salin, S. B. Mickovski, T. Fourcaud, J. F. Dumail and R. v. Beek (2005). The influence of cellulose content on tensile strength in tree roots, Plant and soil 278,1-9

G. J. Hanson and K. R. Cook (2004). Apparatus, test procedures and analytical methods to measure soil erodibility in situ, Trans. ASAE. 20(4)

G. J. C. M. Hoffmans, H. J. Verheij, A. v. Hoven and G. J. Akkerman (2009). Surface instability of grass and clay caused by wave overtopping, ASCE Journal of Hydraulic Engineering (submitted, to be published in 2010), Deltares, Delft University of Technology, Royal Haskoning.

S. Husrin (2007). Laboratory experiments on the erosion of clay, T04-07-12, FLOODsite.

M. Klein-Breteler and G. M. Smith (1996). Grass dikes: supplementary analysis of water movements on the inner slope (in Dutch), H1565 / H1991, WL Delft Hydraulics, Delft.

G. A. M. Kruse (1998). Analyse van deltagootproeven op een grastalud., CO-356460/05, Grondmechanica Delft.

G. A. M. Kruse and J. D. Nieuwenhuis (2000). Impact of weathering on erosion resistance of cohesive soil, 8th IAEG Congress, Vancouver, Canada.

M. B. Lesser and J. E. Field (1983). The impact of compressible liquids, Annual reviews Fluid Mechanics. 15

J. W. v. d. Meer and M. Klein-Breteler (1990). Measurement and computation of wave induced velocities on a smooth slope, 22nd International Conference Coastal Engineering Delft, the Netherlands.

T. E. Mirtskhoulava (1991). Scouring by flowing water of cohesive and noncohesive beds, Journal of Hydraulic Research. 29

J. A. Muijs and J. T. C. M. Sprangers (1991). Green seadikes in North Germany and Denmark, report of a study tour 3-7 June 1991. (in Dutch), Rijkswaterstaat, Dienst Weg- en Waterbouw 1997.

G. Müller, G. Wolters and M. J. Cooker (2003). Characteristics of pressure pulses propagating through water-filled cracks, Coastal Engineering. 49

H. Oumeraci, T. Staal, S. Pfoertner, G. Ludwigs and M. Kudella (2010). Hydraulic performance, wave loading and response of elastocoast revetments and their foundation. -A large scale model study-, LWI report no. 988, Leichtwei-Institut für Waßerbau Technische Universität Braunschweig, Braunschweig.

M. Paulissen (2009). Memo: Root diameters and tensile strength dike grassland (in Dutch), Wageningen, Alterra Wageningen.

T. Piontkowitz, R. Hassan, M. Dyer, S. Utili, T. Ploompuu and A. Kont (2007). Failure of grass cover layers at seaward and shoreward dike slopes, proposal, Hydralab III.

T. Piontkowitz, H. J. Verhagen, H. J. Verheij, T Mai Cao, D. Dassanayake, D. Roelvink, S Utili, M. Zielinski, A. Kont and T. Ploompuu (2009). EroGRASS - Failure of grass cover layers at seaward and shoreward dike slopes. design, construction and performance., EroGRASS user group, Lemvig (Denmark).

C. Pohl and W. Richwien (2006). Die Bemessung der Außenböschung von Seedeichen unter Ansatz des festigkeitssteigernden Einflusses der Grasnarbe. Dokumentation zum 2. Symposium Sicherung von Dämmen, Deichen und Stauanlagen, Siegen, Institut für Grundbau, Bodenmechanik, Tunnelbau und Felsmechanik, Universität Duisburg-Essen.

N. Pollen (2006). Temporal and spatial variability in root reinforcement of streambanks: Accounting for soil shear strenght and moisture, Catena Vol. 69 2007

N. Pollen and A. Simon (2005). Estimating the mechanical effects of riparian vegetation on the stream bank stability using a fiber bundle model, Water resources research. Vol. 41

Rijkswaterstaat (2008). Addendum I for the guide to rivers, in aid of the design of river dikes (in Dutch), Ministry of Transport, Public Works and Water Management.

H. Schüttrumpf (2001). Wellenüberlaufströmung bei Seedeichen - Experimentelle und theoretische Untersuchungen. Mitteilungen aus dem Leichtweiß-Institut für Wasserbau der Technischen Universität Braunschweig, PhD thesis, Technischen Universität Braunschweig, Braunschweig.

H. Schüttrumpf (2005). Layer thicknesses and velocities of wave overtopping flow at seadikes, Coastal Engineering. 52

G. M. Smith, J. W. W. Seijffert and J. W. v. d. Meer (1994). Erosion and overtopping of a grass dike. Large scale model tests, 24th International Conference Coastal Engineering, Kobe, Japan.

J. T. C. M. Sprangers (1996). Extensive grassland management on sea dikes (in Dutch), Wageningen, Landbouwuniversiteit Wageningen.

J. T. C. M. Sprangers (1999). Vegetation dynamics and erosion resistance of sea dyke grassland, Wageningen, Department of Environmental Sciences Wageningen, section Nature conservation and Plant ecology, Wageningen Agricultural University

G. Stanczak (2007). Laboratory tests on the erosion of clay revetment of sea dike with and without a grass cover induced by breaking wave impact, FLOODsite.

G. Stanczak (2008a). Breaching of sea dikes initiated by breaking wave impacts, T06-09-03, FLOODsite.

G. Stanczak (2008b). Breaching of sea dikes initiated from the seaside by breaking wave impacts, PhD thesis, Faculty of Architecture, Civil Engineering and Environmental Sciences, University of Braunschweig, Braunschweig.

TAW (1996). Technical report clay on dikes (in Dutch), Ministry of Transport, Public Works and Water Management.

TAW (1997). Technical report erosion resistance of grassland as dike covering, Ministry of Transport, Public Works and Water Management.

TAW (1998). Fundamentals water defences (in Dutch), Ministry of Transport, Public Works and Water Management.

TAW (1999). Technical report grass sod as a dike cover (in Dutch), Ministry of Transport, Public Works and Water Management.

TAW (2003). Technical report asphalt for water defences (in Dutch), Ministry of Transport, Public Works and Water Management.

R. Thoman and S. Niezgoda (2008). Determining erodibility, critical shear stress, and allowable discharge estimates for cohesive channels: case study in the powder river basin of Wyoming, Hydraulic Engineering ASCE. (December 2008).

A. Valk (2009). Wave overtopping, impact of water jets on grassed inner slope transitions, MSc thesis, Faculty of Civil Engineering and Geosciences, Delft University of Technology, Delft.

M. M. d. Visser (2007). A clay layer as a revetment for sea dikes, the behaviour of clay under wave loading, MSc thesis, Faculty of Civil Engineering and Geosciences, Delft University of Technology, Delft.

G. v. Vledder (1990). Literature survey to wave impacts on dike slopes, Delft, Delft Hydraulics.

VTV (2006). VTV 2006, Guidelines safety assessment for primary sea defences (in Dutch), Ministry of Transport, Public Works and Water Management.

WetterskipFryslan (2009). Green dike profiles of the province Friesland, Requested at the Wetterskip Fryslan, Leeuwarden.

H. Witte (1988). Druckschlagbelastung durch Wellen in deterministischer und stochastischer Betrachtung, PhD thesis, Technische Universität Carolo Wilhelmina Braunschweig, Braunschweig.

G. Wolters and G. Müller (2004). Field and large scale model tests of wave impact pressure propagation into cracks, 29th International Conference Coastal Engineering, Lisbon, Portugal.

M. J. Young (2005). Wave overtopping and grass cover layer failure on the inner slope of dikes, MSc thesis, UNESCO-IHE, Delft.

List of parameters

a	Crack depth	[m]
A	Surface area of the soil	[m^2]
A_{block}	Block area	[m^{-2}]
A_r	Cross sectional area of the roots	[m^2]
A_{sg}	Area of the surrounding grass	[m^2]
A_{ws}	Area of the weak spot	[m^2]
b	Parameter describing the influence of the roots on the erodibility	[-]
B	Hydraulic load	[ft^3/s]
B_c	Critical hydraulic load	ft^3/s]
c	Cohesion	[N/m^2]
c_0	Coefficient	[-]
$c_{1,i}$	Coefficient for wave run-up exceeded by i% of the waves	[-]
$c^*_{1,i}$	Coefficient for wave run-up exceeded by i% of the waves	[-]
c_2	Layer thickness coefficient	[-]
c_3	Run-up coefficient (1.5 for wave spectra and 1.0 for regular waves)	[-]
c_{clay}	Effective clay cohesion	[N/m^2]
$c_{clay,c}$	Critical clay strength	[N/m^2]
c_{grass}	Grass cohesion	[N/m^2]
$c_{grass,c}$	Critical root cohesion	[N/m^2]
c_u	Undrained shear strength	[N/m^2]
C	Chézy coefficient	[$m^{1/2}/s$]
C_E	Overall strength parameter	[$m^{-1}s^{-1}$]
C_f	Clay fatigue rupture strength	[N/m^2]
$C_{headcut}$	Material headcut coefficient	[s^2]
C_{ws}	Circumference weak spot	[m]
d_a	Aggregate diameter	[m]
d_{block}	Block diameter	[m]
d_c	Distance in crack	[m]
d_r	Root diameter	[m]
dx/dt	Headcut velocity	[ft/hr]
E	Erosion rate per unit area of the bed	[kg/m^2s]
E_p	Erosion parameter depending on the qualities of both clay and grass	[kg/m^2s]
E_{soil}	Erosion parameter depending on the qualities of both clay and grass	[m/s]
f	Friction factor tan φ	[-]
F_i	Force	[N]
F_{po}	Pull-out force	[N]
g	Acceleration of gravity	[m/s^2]
h	Water layer thickness during wave run-up and run-down	[m]
H	incident wave height	[m]

H_h	Headcut height	[ft]
H_s	Significant wave height	[m]
I_c	Consistency index	[-]
k_0	Depth-averaged turbulent kinetic energy	[m^2/s^2]
$k_{d,i}$	Empirical detachability coefficient	various
k_h	Headcut erodibility index	[-]
k_p	Erosion parameter for wave impacts	various
l_i	Length scale	[m]
L	Root length	[m]
L_0	Wave length at deep water	[m]
L_c	Crack length	[m]
m	Front slope 1: m of the structure	[-]
M	Sediment coefficient	[kg/sm^2]
MWL	Mean Water Level	[m]
n	Porosity	[-]
n_a	Average air content in water layer	[-]
n_r	Number of roots	[-]
n_s	Side wall coefficient	[-]
N_{imp}	Number of waves causing an impact	[-]
N_w	Number of waves in a storm	[-]
p_c	Critical uplift pressure	[N/m^2]
p_i	Pressure at point i	[N/m^2]
$p_{\max,i}$	Maximum impact pressure exceeded by i% of the waves	[N/m^2]
p_{up}	Uplift pressure underneath an aggregate after wave impact	[N/m^2]
p_w	Pore water pressure	[N/m^2]
q	Specific discharge	[ft^3/s ft]
q_{avg}	Average impact factor	[-]
q_i	Impact factor exceeded by i% of the waves	[-]
r_0	Depth-averaged relative turbulence intensity	[-]
R_d	Volume of the eroded soil by impact	[m^3]
R_h	Hydraulic radius that equals the flow depth	[m]
R_{imp}	Relative impact time	[-]
$R_{u,i\%}$	Maximum run-up height exceeded by i% of the waves	[m]
RVR	Root Volume Ratio	[-]
RAR	Root Area Ratio	[-]
RAR_0	Root Area Ratio at the surface	[-]
RAR_{crit}	Critical Root Area Ratio	[-]
s	Root spacing	[m]
S_b	Energy slope	[-]
t	Time	[s/h]
t_e	Fall time	[s]

t_d	Impact duration	[s]
t_{imp}	Characteristic impact time	[s]
$t_{imp,w}$	Impact time of an individual wave	[s]
t_k	Rise time	[s]
t_r	Grass tensile strength	[N/m^2]
$t_{r,c}$	Critical grass tensile strength	[N/m^2]
t_w	Characteristic time for which the maximum flow velocity occurs	[m/s]
T	Regular wave period	[s]
T_{imp}	Total impact time during a storm	[s]
T_m	Average wave period	[s]
T_{storm}	Storm duration	[s]
$u_{d,i}$	Wave run-down flow velocity exceeded by i% of the waves	[m/s]
$u_{u,i}$	Wave run-up flow velocity exceeded by i% of the waves	[m/s]
u_*	Bed shear velocity	[m/s]
U	Air water mixture velocity	[m/s]
U_0	Depth averaged flow velocity	[m/s]
U_c	Depth averaged critical flow velocity	[m/s]
U_{char}	Characteristic flow velocity	[m/s]
U_m	Representative flow velocity during overtopping	[m/s]
$U_{\max}$	Maximum flow velocity per overtopping event	[m/s]
w	Water layer damping coefficient	[-]
w_c	Water content	[-]
x_a	Horizontal coordinate with the zero point at Mean Water Level	[m]
x_i	x-coordinate of point i	[m]
x_{imp}	Horizontal coordinate impact point with x=0 at MWL	[m]
x_z	Horizontal run-up length	[m]
x_*	Residual run-up length	[m]
y_m	Erosion depth	[m]
z	Depth	[m]
z_a	Vertical position above Mean Water Level	[m]
z_{crit}	Critical depth	[m]
z_d	Reference level of wave run-down	[m]
z_{imp}	z-coordinate impact point with z=0 at MWL	[m]
$z_{\min}$	Depth of minimum fracture strength	[m]
z_{ref}	Reference level	[m]
Z_d	Wave run-down height	[m]
Z_{imp}	Vertical distance below Mean Water Level (MWL) of the impact point	[m]
α	Outer slope angle of the structure	[-]
α	Coefficient determining the number of waves causing an impact between 0.0-1.0	[-]
α_{imp}	Angle of incidence breaking wave	[-]

α_{int}	Erosion intensity coefficient	[-]
α_{crack}	Crack extension coefficient	[-]
α_{cs}	Coefficient of clay cohesion increase over depth	[m^{-1}]
α_{E}	coefficient	[-]
$\alpha_{fatigue}$	Clay fatigue factor = 0.035	[-]
α_{imp}	Angle of incidence of a breaking wave on the outer slope	[-]
α_{soil}	Calibration coefficient	[-]
α_{τ}	Pressure fluctuation coefficient	[-]
β	Coefficient of root decrease over depth	[m^{-1}]
γ_{eff}	Effective soil unit weight	[N/m^3]
γ_{s}	Saturated soil unit weight	[N/m^3]
γ_{w}	Unit weight water	[N/m^3]
Δ	Relative density	[-]
ε_{i}	Erosion rate	various
θ	Root angle of rotation	[-]
λ	Characteristic length scale	[m]
λ_{grass}	Influence length of the roots	[m]
μ	Pressure reduction coefficient	[m^{-1}]
ν	Kinematic viscosity of water	[m^2/s]
ξ_{d}	Irribaren number at the toe of the dike	[-]
ρ_{d}	Dry density of the soil	[kg/m^3]
ρ_{s}	Density of the soil	[kg/m^3]
ρ_{w}	Density of water	[kg/m^3]
σ	Normal stress	[N/m^2]
σ_{f}	Fracture stength	[N/m^2]
$\sigma_{0,grass,c}$	Critical grass normal strength at the surface	[N/m^2]
σ_{grass}	Grass normal strength	[N/m^2]
$\sigma_{grass,c}$	Critical grass normal strength	[N/m^2]
σ_{s}	Soil strength	[N/m^2]
τ	Soil shear stress	[N/m^2]
τ_{0}	Mean bed shear stress	[N/m^2]
τ_{c}	Critical shear stress	[N/m^2]
τ_{clay}	Shear strength of clay	[N/m^2]
τ_{total}	Total shear stress obtained by cohesion	[N/m^2]
φ	Internal angle of friction	[-]
φ_{eff}	Effective angle of internal friction	[-]
χ	Air-water ratio	[-]
ψ	Erosion coefficient	[m^2/s]
ω	Turbulence coefficient	[-]

Appendices

Wave impact on grass covered outer slopes

B.C. Mous
C1143360
Faculty of Civil Engineering & Geosciences

Appendices
April 2010

TU Delft Delft University of Technology

ROYAL HASKONING

Table of contents

Appendix A EroGRASS experiments 2008

To gain more insight in the erosion process of grass by wave impact and wave overtopping, model tests have been performed in the Große WellenKanal (Large Wave Flume) of the Coastal Research Centre - a joint centre of the University of Hannover and the Technical University of Braunschweig, Germany. This appendix describes the setup of the experiments and the erosion observations. Section A.1 discusses the general flume layout and the dike model including the measuring and observation techniques is treated in section A.2. Subsequently the test program is treated in section A.3 followed by a description of the properties of the grass cover in section A.4. After this the general erosion observations are briefly discussed in section A.5. The chapter is concluded with a thorough analysis of the erosion events that occurred during each test in section A.6.

A.1 Flume layout

The Large Wave Flume (GWK) of the Coastal Research Centre in Hannover (Germany) is 5 m wide, 7 m deep and 324 m long (Figure A-1). The maximum water depth in the flume is 5.0 m.
Regular waves can be generated with heights up to $H \approx 2.50$ m and irregular waves with significant heights up to $H_s \approx 1.5$m. The prototype of the dike model was therefore adjusted in its dimensions and geometry to allow for large scale testing in the wave flume. [Piontkowitz et al. 2009]
The model was positioned near the middle of the flume (168 m from the wave generator) to allow sufficient room for the storage of the overtopped water and to enable the observation of the influence of breaking waves on the seaward slope of the dike model through an observation window.

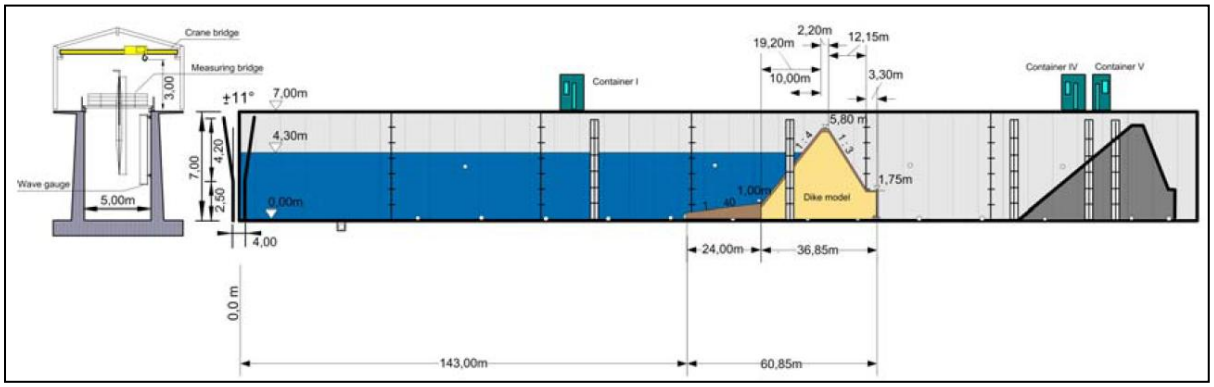

Figure A-1: Overview of GWK and the position of the model in the flume. [Piontkowitz et al. 2009]

A.2 Dike model

The slope of the landward side of the dike model is 1:3 and the slope of the seaward side of the dike model is 1:4. This relatively steep slope was preferred over 1:6 to improve the generation of wave impacts on the seaward slope and to minimize the damping effect of the backwash layer. The height of the dike model was 5.8 m and the crest was 2.2 m wide. (Figure A-2)

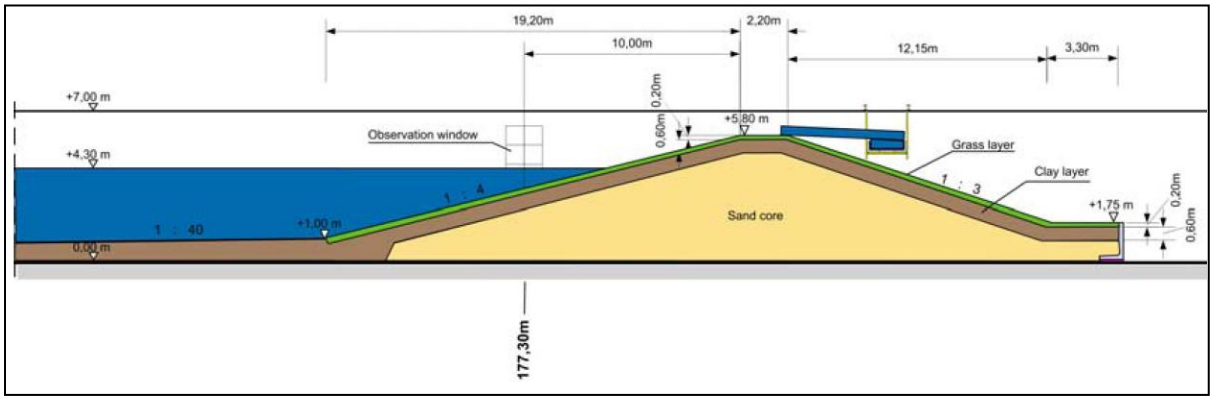

Figure A-2: Cross section of the dike model. [Piontkowitz et al. 2009]

The dike model consisted of a sand dike core, a clay layer and a grass cover. On both slopes and on the dike crest a clay layer with a thickness of 0.6 m was installed. On top of the clay layer 0.2 m thick grass sods were placed to complete the dike model with a grass cover layer, adding up to a total cover layer thickness of 0.8 m. The grass and clay slices were excavated from a green sea dike in Ribe, Denmark and transported to Germany. [Piontkowitz, Hassan et al. 2007]
In front of the dike model a sloping foreshore was installed to ensure proper conditions for the development of waves (shoaling) in front of the dike model. The slope of the foreshore was 1:40 with a length of 24 m and the height of the foreshore at the dike toe was 1.0 m above the flume bottom.

A.2.1 Measuring and observation techniques

The test program was divided into two phases. In the first phase the initiation of grass erosion on the seaward slope due to wave impact and wave run-up and run-down flow was studied. In the second phase the initiation of grass erosion on the landward slope due to wave overtopping was investigated; phase 2 is beyond the scope of this research and is not further discussed. During the test program several measuring and observation devices were used:

- Wave gauges
- Pressure transducers
- Velocimeters (mini-propellers)
- Overtopping container
- Video and photo cameras

These devices are described in the following paragraphs.

A.2.2 Wave gauges

For wave analysis three arrays of four wave gauges are present in the wave flume and the positions of these wave gauges are listed in Table A-1.

Table A-1: Location of wave gauges.[Piontkowitz et al. 2009]

Array	*Wave gauge*	*Distance from wave paddle [m]*
Array 1	1	50.1
	2	52.2
	3	55.9
	4	61.3
Array 2	5	79.05
	6	81.15
	7	84.85
	8	90.25
Array 3	9	116.0
	10	118.0
	11	120.0
	12	122.0

A.2.3 Pressure transducers

To measure the wave impact pressures five pressure transducers (PT) with a capacity of 5 bar were installed on the outer slope near the observation window. The distance between two transducers was 1.25 m corresponding to the width of a sod, while the horizontal distance between two pressure transducers is 1.2 m (Figure A-3).
This distance was applied to prevent the digging of a hole through the sod and thus damage during the installation of the device. It was expected this would have a negative influence on the stability of the grass sod. [Geisenhainer and Oumeraci 2008] The distance relative to the flume bottom and the wave generator are listed in Table A-2.

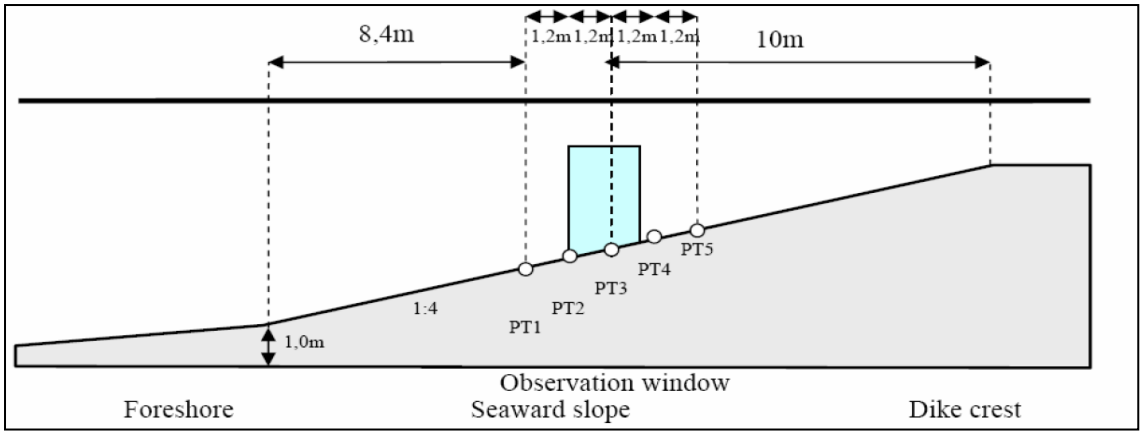

Figure A-3: Position of pressure transducers and observation window. [Piontkowitz et al. 2009]

Table A-2: Position of the pressure transducers (PT).

PT	*Distance from wave paddle [m]*	*Distance above flume bottom [m]*
1	176.5	3.1
2	177.7	3.4
3	178.9	3.7
4	180.1	4.0
5	181.3	4.3

A.2.4 Velocimeters (mini-propellers)

The flow velocities on the slope were measured on five locations with mini propellers with a diameter of 2.2 cm (Schiltknecht). These propellers have a measuring range of 0.02 to 5.0 m/s. The location of these velocimeters on the slope is depicted in Figure A-4.

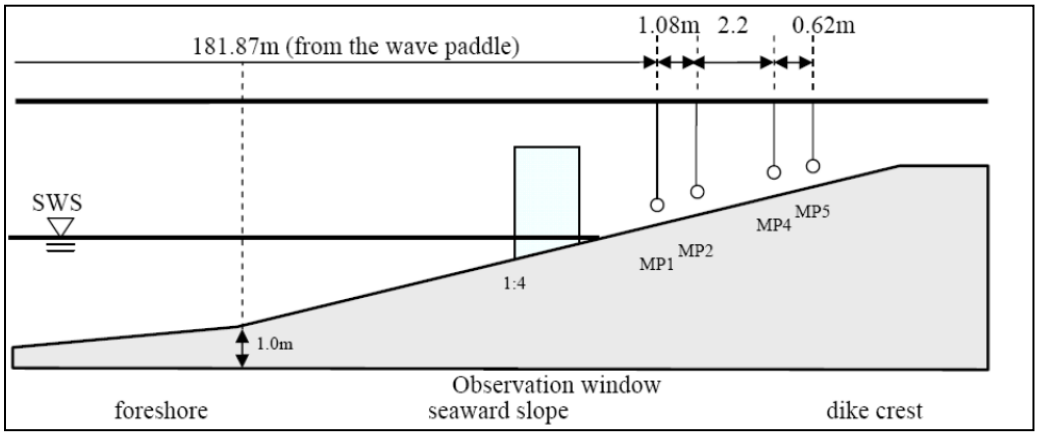

Figure A-4: Position of the mini propellers on the slope. [Piontkowitz et al. 2009]

To avoid disturbances to the propeller due to the grass layer or grass swards the distance between the grass layer and the propeller has to be sufficiently large. Furthermore, in the area around the propeller the length of the grass swards had to be limited, the swards in the vicinity of the propellers were cut for this purpose. Nevertheless the propellers were frequently disturbed by floating grass and the analysis of the flow velocity should be done with caution. [Geisenhainer and Oumeraci 2008]

A.2.5 Overtopping container

The amount of overtopped water was measured with an overtopping container. Although the overtopping quantities are not relevant for this research, the measuring device is nevertheless briefly described. The container was seated on three bearings; two bearings were rigid and the third bearing consisted of a load cell. This transducer recorded the weight of the container while it was filled with overtopping water (Figure A-5). The entrance of the inlet was located at the landward edge of the dike crest. [Piontkowitz et al. 2009]

Figure A-5: Overtopping container with inlet and hose system. [Piontkowitz et al. 2009]

A.2.6 Video and photo cameras

To monitor the erosion process all tests were recorded with video cameras and many photos were taken of the slope after each test. During tests including wave impact (phase 1), the digital cameras were installed on the southern gangway of the flume (Figure A-6), one camera pointing towards the seaward slope and the other one pointing in the opposite direction. [Piontkowitz et al. 2009]

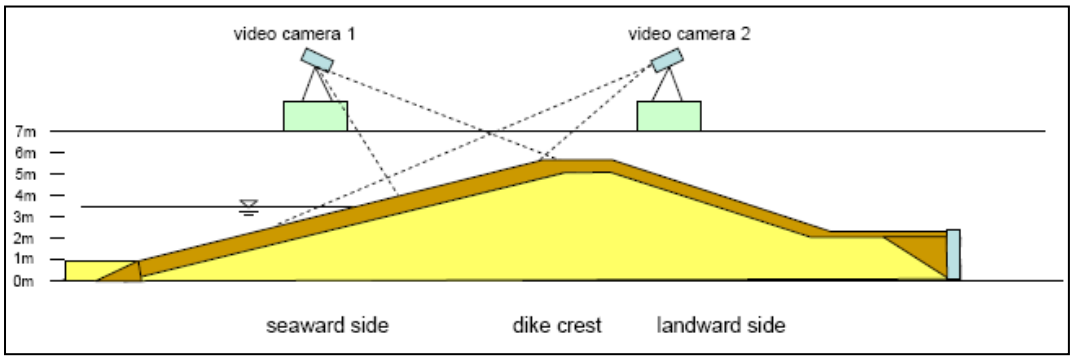

Figure A-6: Location of the video cameras. [Piontkowitz et al. 2009]

Grass sods, which were damaged during the wave impact tests, were photographed after each test run. The signboard in Figure A-7 shows the hydrodynamic parameters of the test performed before the photo was taken.

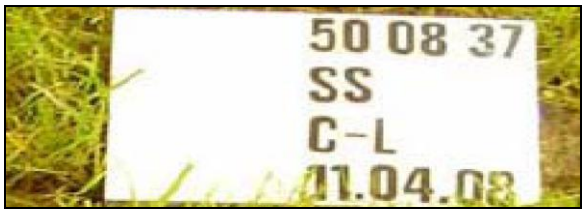

Figure A-7: Sign board. [Piontkowitz et al. 2009]

The first number in the first row defines the peak period H_s ('50' = 5.0 s). The second number represents the significant wave height H_s ('08' = 0.8 m) and the last number indicates the water depth ('37' = 3.7 m). The abbreviations in the second and third row stand for 'SS' = seaward slope and 'C-L' is the identification code of the grass sod ('C' = row C; 'L' = left grass sod of the row from the middle). Identification of the rows starts with 'A' at the seaward toe in upward direction. The positions of the grass sods in one row are coded with 'L' = left grass sod, 'M' = middle grass sod, and 'R' = right grass sod. The positions of the grass sods are defined by standing in front of the dike model and looking at the seaward slope. In some cases, the middle grass sod was coded with 'ML', 'MM' and 'MR'. 'ML' means left side of middle grass sod, 'MM' stands for the middle part of the middle grass sod, and 'MR' represents the right side of the middle grass sod. The last row on the signboard indicates the date of the photo. [Piontkowitz et al. 2009]

A.2.7 Grid

After installation of the grass cover a grid was painted on the northern flume wall. The distance between the vertical lines was 1.0 m, whereas the distance between the horizontal lines was 0.5 m. The grid was painted following the entire dike surface (seaward slope, crest, landward slope).

Figure A-8: Grid on the flume wall.

A.3 Test program

The applied wave spectra are based on a TMA spectrum, which is a modified JONSWAP spectrum accounting for limited water depth. The water level in the flume was kept constant during test phase 1 and test phase 2. The effect of a tide could not be simulated in the flume. Table A-3 gives an overview of the hydraulic parameters of each test run, i.e. peak period T_p, the significant wave height H_s and the water depth d.

Table A-3: Hydraulic parameters wave impact tests.

Hydraulic Parameter	*April 8 / 16*	*April 18 / 22*	*April 8 / 10*	*April 11 / 22*
T_p [s]	4.0	5.0	5.0	5.0
H_s [m]	0.5	0.7	0.8	0.9
d [m]	3.7	3.7	3.7	3.7
No. of tests	4	3	2	4
Performed tests	April 8 test 1 April 16 test 1 April 16 test 2 April 16 test 3	April 18 test 1 April 18 test 2 April 22 test 1	April 8 test 2 April 10 test 1	April 11 test 1 April 22 test 2 April 22 test 3

After each test the GWK was emptied, which lasted 4 hours. Filling the flume took 5 hours; consequently testing was normally interrupted by one day without testing. After each test run the damage of the grass cover was surveyed and documented by photos. When the grass cover was damaged, the grass sod concerned was replaced by a new grass sod. [Piontkowitz et al. 2009]

A.3.1 Channel distribution

For the data analysis special software was used. L~Davis (LWI Data Analysis and Visualisation Software) is especially developed by the LeichtWeiß Institute for this purpose.
Each measuring device had its own channel to record the measurements. For most tests 28 channels were in use; an overview of the channels and the measuring devices is given in Table A-4. For the purpose of this research the DMD devices are most relevant.

Table A-4: Channel distribution

Channel	*Measuring device*	*Measured parameter*
1-12	Wave gauge	Surface elevation, H ,T
13-17	DMD	Pressure [kPa]
18-22	Schiltknecht	Flow velocity [m/s]
23-27	WP Delft	Flow depth
28	Overtopping container	Overtopping quantity [kPa]

A.4 Grass and clay properties

Before the tests were carried out the properties of the soil and the grass cover layer were determined. The quality of the grass was determined by taking 6 samples, subsequently the Root Volume Ratio was determined; the results are depicted in Figure A-9. The RVR shows a logarithmic decline with increasing depth, which corresponds with samples analyzed by Stanczak (2008). [Piontkowitz et al. 2009]

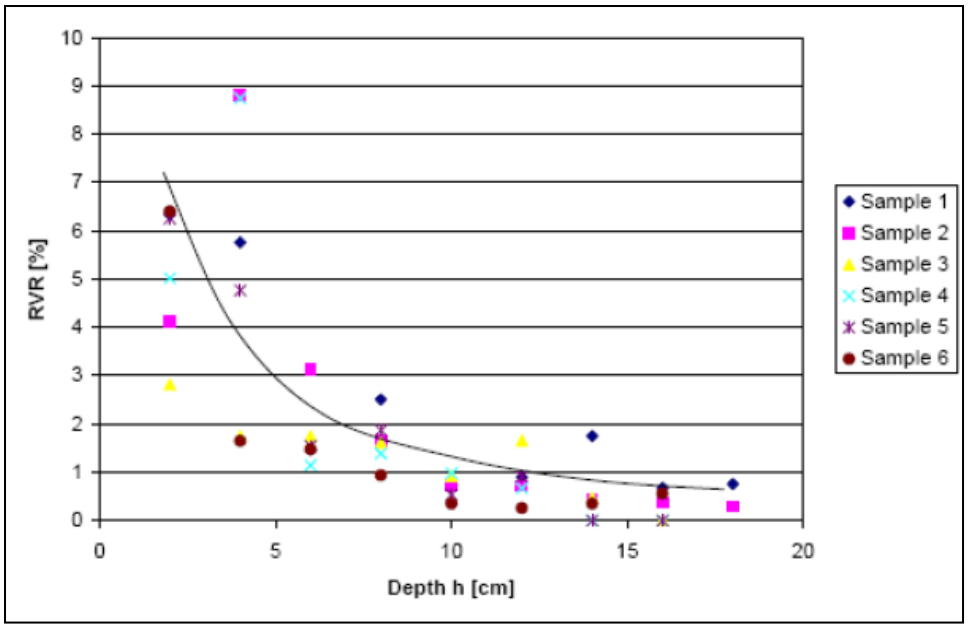

Figure A-9: Root Volume Ratio of the grass cover used for the model. [Piontkowitz et al. 2009]

The properties of the clay were also investigated; the soil properties of the clay of the foreland and the clay applied as a revetment differ. Both parts were constructed with other types of clay. From a previous experiment the properties of the foreshore (clay type A) were already known. The soil properties of the revetment (clay type B) were investigated by members of Strathclyde University at the LeightWeiß Institute. [Piontkowitz et al. 2009] Properties of both types of clay are given in Table A-5.

Table A-5: Soil properties of the clay. [Piontkowitz et al. 2009]

Soil property	*Clay type A Foreshore*	*Clay type B Clay Revetment*
Sand content	12%	20%
Clay content	35%	25%
Liquidity Limit w_L	77%	61%
Plasticity Limit I_P	45%	28%
Dry density	1.612 t/m^3	1.575 t/m^3
Water content	40 - 50%	26 - 35%

Using the requirements in Table 2-1, clay type A can be qualified as erosion resistant clay (category 1). Clay type B fails the plasticity limit criterion of erosion resistant clay, but the difference is marginal.

Type A

$w_l : 77 > 45\%$

$I_p : 45 > 0.73(77 - 20)$

$Sand : 12 < 40$

Type B

$w_l : 61 > 45\%$

$I_p : 28 < 29.63$

$Sand : 20 < 40$

According to the guidelines clay type B should be considered as moderately erosion resistant clay (category 2). It can be argued that clay type B has more resemblance with clay of category 1 than

with clay of category 2 because the liquid limit criterion for category 2 is not satisfied. Nevertheless clay type B will be considered as moderately erosion resistant clay.

A.5 General erosion and damage observations

A.5.1 Damage by single wave impacts

The first damage of the grass cover occurred at the observation window in the flume wall during the tests on April 11 2008. The wave parameters were T_p = 5.0 s, H_s = 0.9 m and the water depth was 3.7 m (See also Table A-3). The damage was induced by a single wave impact and is shown in Figure A-10; the initial state of the grass cover is displayed left. The damaged grass cover is located at row H right next to the observation window, but only a part of the 90 cm wide grass cover element was eroded. The erosion hole next to the observation window can be clearly distinguished. Besides this it can also be observed that the grass cover is severely weakened at the left part of the grass cover element (Figure A-10 right).

Figure A-10: Grass before wave impact damage (left), first damage after wave impact (right).

The dimensions of the eroded area are depicted in Figure A-11. The marked area A in this figure shows that there was also an area directly located next to the observation window but that was not eroded. It appeared that the eroded clay was part of the uppermost region of the grass cover layer as the hole was merely 10 cm deep.[Piontkowitz et al. 2009]

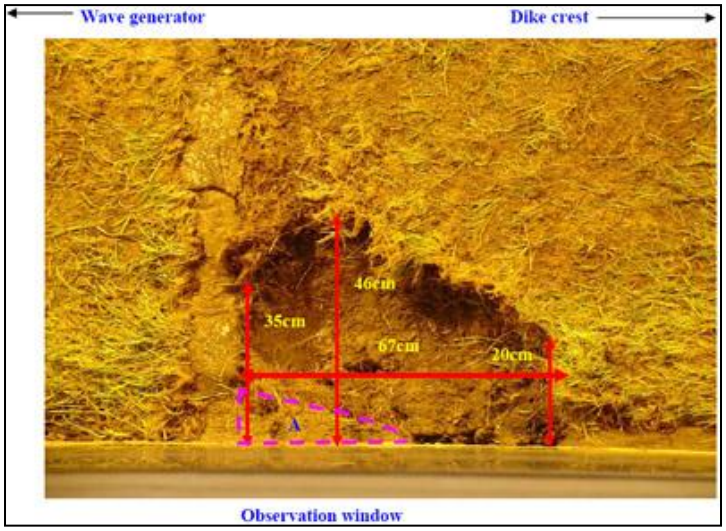

Figure A-11: Dimensions of the eroded block. [Piontkowitz et al. 2009]

A.5.2 Damage over entire test duration

During the entire test duration, different kinds of damage or stages of damage were observed. Round aggregates of different sizes were observed on the dike surface and within the topsoil.(Figure A-12)

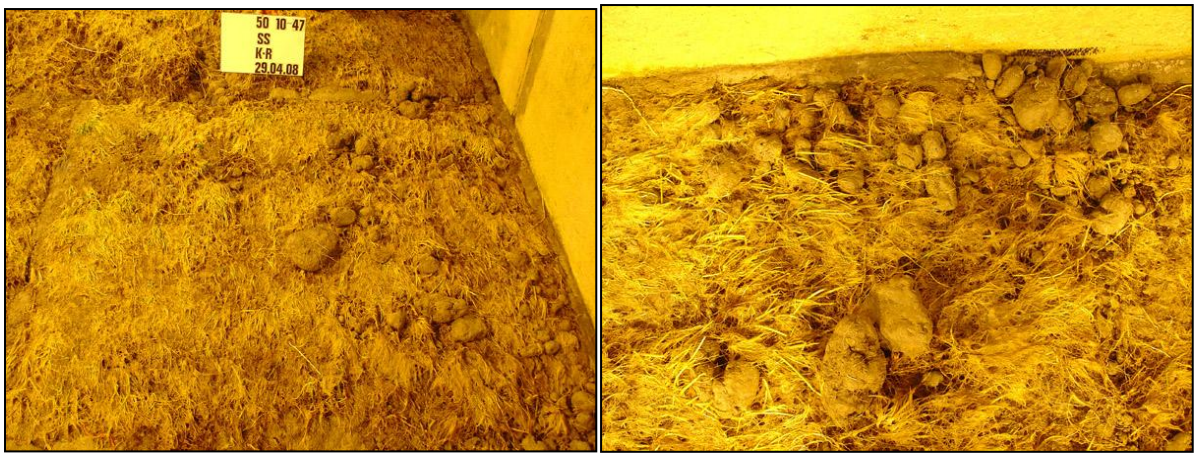

Figure A-12: Round balls were formed on the surface (left) and within the top soil (right). [Piontkowitz et al. 2009]

The development of these balls was not the result of loose clay lumps being moved up and down the slope as the balls were also observed in the soil with a dense root network. Damage between the joints of the grass pieces sometimes occurred, which sometimes redeveloped after repairs. Moreover, small holes were registered after the tests. The degradation of the grass layer in the breaker zone caused during both the impact tests (phase 1) and the overtopping tests (phase 2) is shown in Figure A-13. The grass cover (swards and leafs) in the lower part of the seaward slope remained longer green and alive than the grass within the breaker zone.

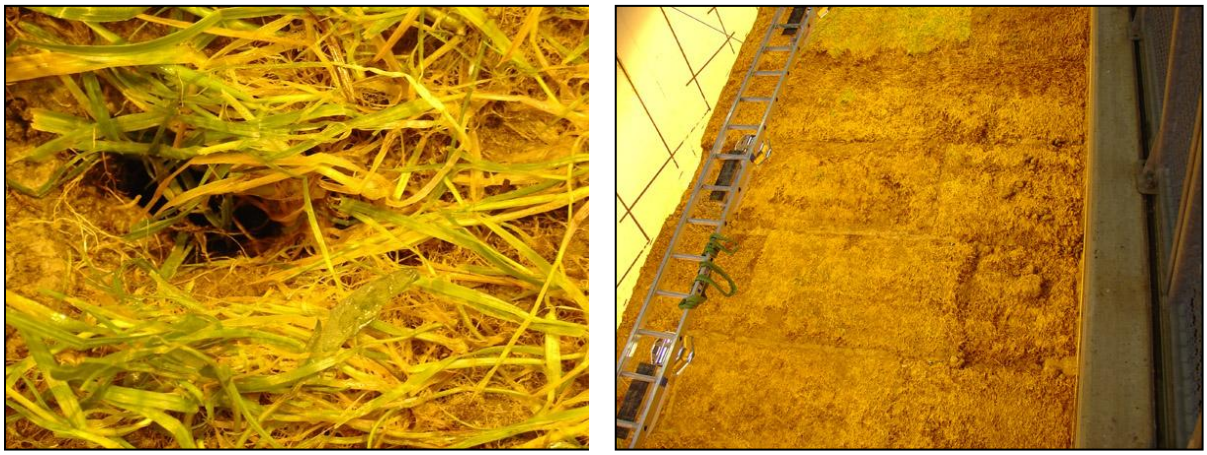

Figure A-13: Small holes were formed during the tests (left). Grass cover in breaker zone was less green than lower parts of the outer slope (right). [Piontkowitz et al. 2009]

A.6 Erosion events per test

During the experiments the progression of erosion was registered by photographing the grass cover after every test day. Also video files are available; these are accompanied by an observation log. The available material has been studied and combined to obtain an estimate of the erosion.
Remarkable events during the tests and significant changes in geometry after the test have been gathered and analyzed in this section which resulted in Table A-6.

Table A-6: Erosion events during the EroGRASS experiments.

Date	*Test number*	H_s *[m] /* T_p *[s] Load duration [s]*	*Comments*	*Erosion type*	*Location*
April 8	1	0.5 m / 4.0 s	No visible erosion	No significant erosion	
April 8	2	0.8 m / 5.0 s 1800 s	No visible erosion	No significant erosion	
April 10	1	0.8 m / 5.0 s 3800 s	No visible erosion	No significant erosion	
April 11	1	0.9 m / 5.0 s 2550 s	Large block erosion occurs near observation window	Block erosion	Row H –Far right side
April 16	1	0.5 m / 4.0 s 4400 s	Clay that was placed on joint breaks off	Block erosion	Row J – Left side
April 16	2	0.5 m / 4.0 s 4400 s	No visible erosion	No significant erosion	
April 16	3	0.5 m / 4.0 s 4400 s	No visible erosion	No significant erosion	
April 18	1	0.7 m / 5.0 s 5000 s	No visible erosion	No significant erosion	
April 18	2	0.7 m / 5.0 s 5000 s	No visible erosion	No significant erosion	
April 22	1	0.7 m /5.0 s 5000	Some blocks of 10 x 5 cm break off	Block erosion	Presumably I-L
April 22	2	0.9 m / 5.0s 4100 s	Next to the joint a block of $5 \cdot 15$ cm breaks off, also small lumps with roots start to erode: sometimes visible aggregate erosion	Block erosion, aggregate erosion	M-ML
April 22	3	0.9 m / 5.0s 750 s	Next to the joint	Block erosion	I-L, M-ML

From Table A-6 it can be observed that erosion was not visible after the tests with mild wave conditions. After these tests there were no erosion holes, but it is expected that minor aggregate erosion occurred nevertheless. This aggregate erosion was however difficult to distinguish as it caused only minor and gradual damage. The total surface erosion is therefore estimated to be in the order of centimeters.
As explained before the location of erosion is indicated by the grass sod number. The location of the rows of the grass cover and the positions of the pressure transducers are depicted in Figure A-14. It was however not always possible to identify the location of erosion during the observations of the tests and pointing out the location afterwards was not always successful either. In the next sections the most important erosion events per test (see Table A-6) are discussed and assessed.

A.6.1 April 11 Row H (test number 11040801)

A large block eroded during this test as a result of a single impact (see also Figure A-10). The erosion occurred next to the observation window. At first it was suggested that the eroded section could have been a weak spot in the cover layer, however this was rather improbable for such a large section. Therefore the explanation that the large block had failed due to reduced wall friction at the glass observation window and by impact pressures in the crack between the window and the grass mat is more plausible. Also the eroded section was adjacent to a joint and worms were found at the surface of the erosion hole, which may have weakened the grass cover locally as well.

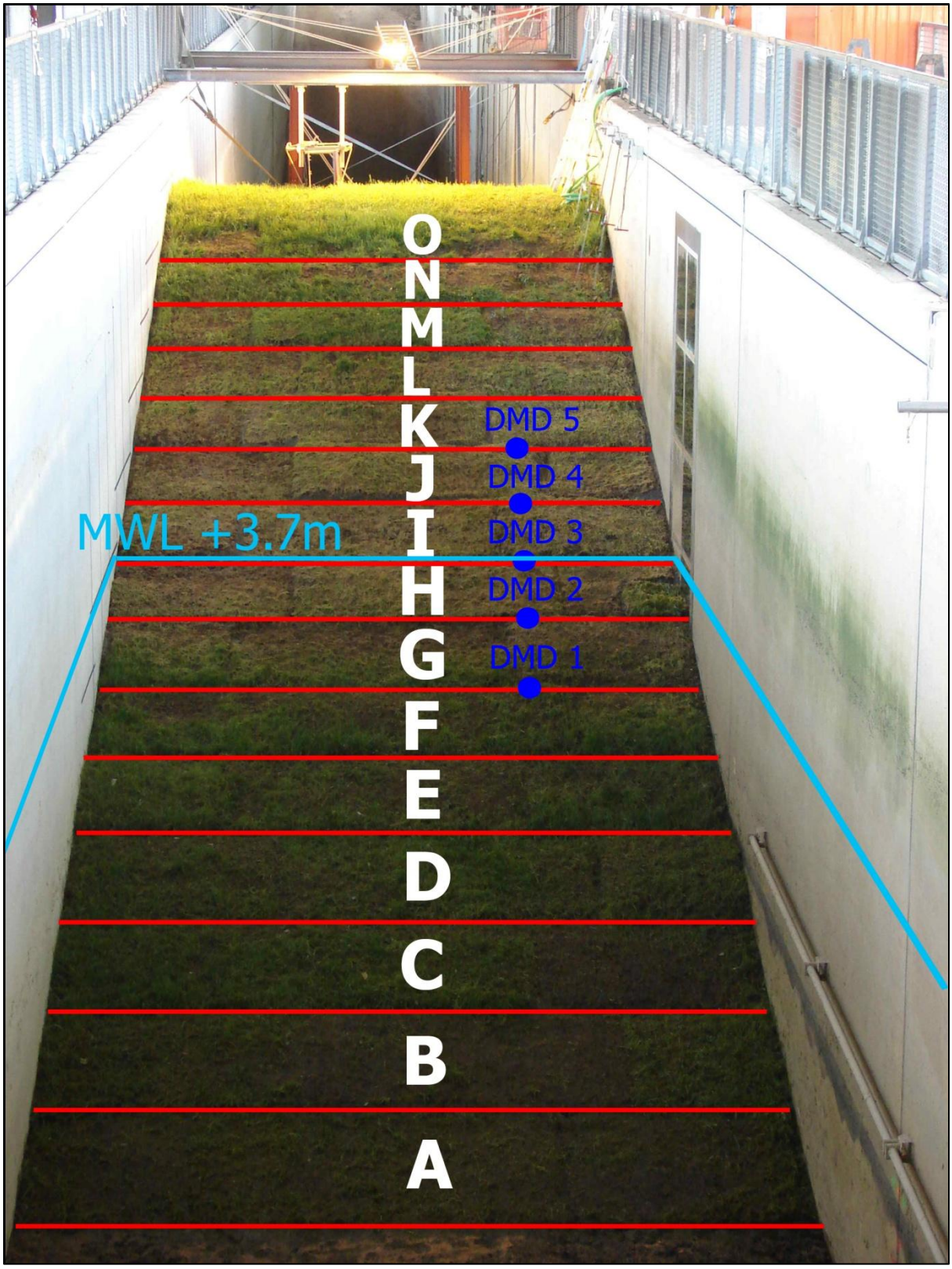

Figure A-14: Overview of the rows and the location of the pressure transducers in the grass cover.

A.6.2 April 16: erosion at Row J (test number 16040801)

No significant other erosion occurs during this test except for a piece of clay that breaks of during test 1 at the right top side of grass mat J-L. As this was a portion of clay that was placed on top of a joint for repairs it is not representative for the grass cover itself; the piece of clay is a weak section without root penetration that has only small adhesion to the rest of the cover (Figure A-15). Furthermore

during the subsequent tests 2 and 3, which had the same conditions, no block erosion occurred. Because of this, the erosion of J-L: will be neglected.

Figure A-15: Erosion at J-L after test 16040801, clay placed on the joints was eroded.

A.6.3 April 22: Increasing block erosion (22040801/22040802/22040803)

Several clumps of roots wash up during the first test, but it was not possible to determine where these eroded blocks came from. Considering the size of the erosion hole at grass mat I-L after all tests it is expected that these block came from grass mat I-L.
Also during the second test multiple blocks (varying between 15 cm by 5 cm and 5 cm by 5 cm) erode from the grass cover. The erosion locations could not be determined during the test except for one: small clumps of roots break off at the bottom left corner of grass mat M-ML. (Figure A-16) It is also noted that many smaller clumps of roots started to wash up more frequently during test 2. Aggregate erosion thus started to play a part as well in the erosion process during these tests.

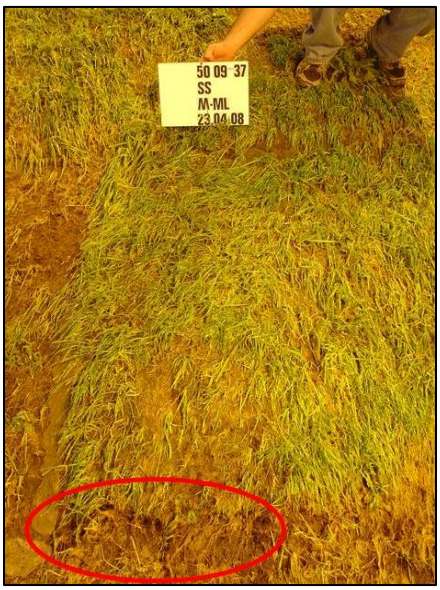

Figure A-16: Aggregate erosion at M-ML after tests of April 22.

These observations were also done during test 3: block erosion as well as aggregate erosion occurred. In particular grass mat I-L was severely damaged; a large section next to the lower joint was eroded. (Figure A-17 left) The depth of the erosion hole in the grass cover varied between 7 cm and 10 cm (Figure A-17 right) and also here worms were present at the surface of the erosion hole.

Figure A-17: Erosion of grass mat I-L near the lower joint (left). Depth of the erosion hole (right).

Another important observation during these tests was the crack that could be observed through the observation window Figure A-18. This crack appears to be undermining a large piece of the grass cover and looks very similar to the balloon mechanism. This observation confirms the possibility of the presence and the growth of horizontal cracks underneath grass sods.

Figure A-18: Horizontal crack formation under a large section of the grass cover.

A.6.4 Discussion and conclusions

All large erosion holes were located adjacent to joints, which makes the assumption that erosion is initiated at weaker locations highly plausible. This trend also squares with the proposed failure mechanism for block erosion. Inevitably the joints between the grass cover sections have cracks, which remained after installation of the sections. And even if no cracks were present initially, it is supposed that these were formed in a slightly later stage when the clay on the joints, which has little or no roots, was subjected to wave loads. This allows the wave impact pressure to penetrate deeper into the grass cover, enabling the possibility of crack formation in the turf and subsequent block erosion. Another factor that could have played a part was the burrowing of animals; worms were found in the erosion holes in grass mat I-L and H-R, which probably weakened the turf as well. Block erosion occurred in the form of clumps with a width varying between 5 and 70 cm. In general the

diameter of an eroded block generally varied between 5 cm and 15 cm, which was ripped from the subsoil at a depth of the 7 cm to 10 cm.
Regarding aggregate erosion it can be concluded that the tests with a significant wave height of 0.5 m generally posed no problem for the grass cover. Erosion rates were accelerated during test with a significant wave height of 0.7 m but only minor damage was caused. Only during the tests with a significant wave height of 0.9 m significant damage was inflicted.

Appendix B Pressure records

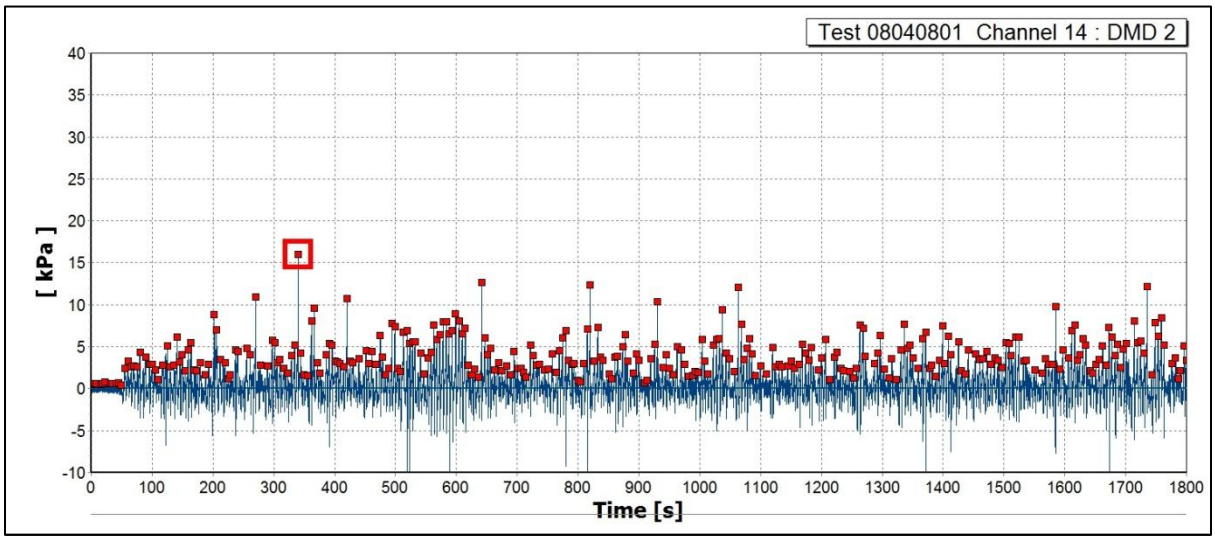

Figure B-1: April 08 test 1: pressure transducer 2.

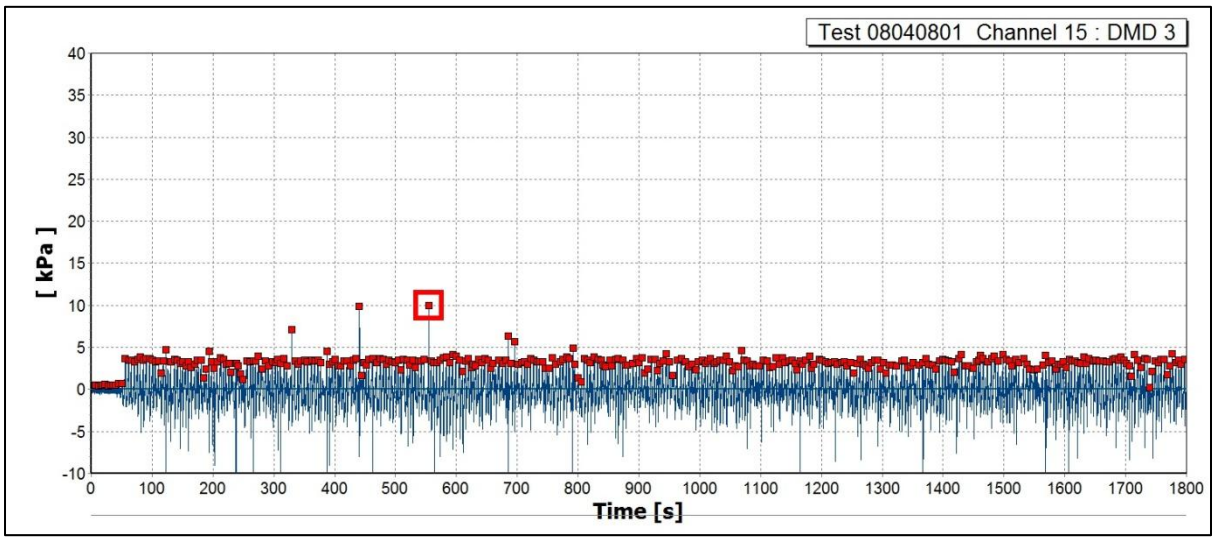

Figure B-2:April 08 test 1: pressure transducer 3.

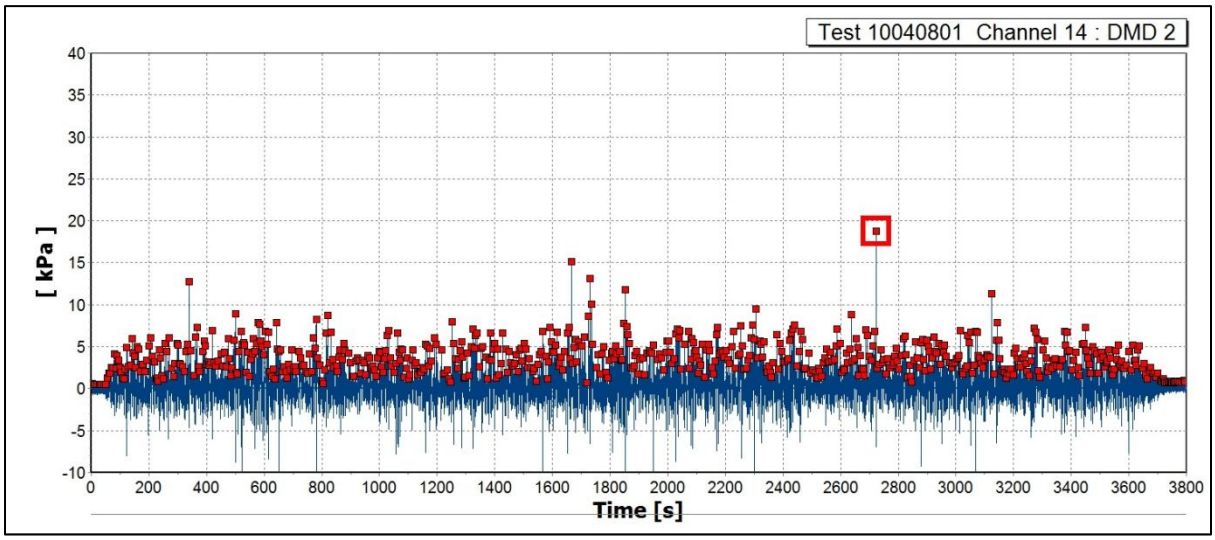

Figure B-3: April 10 test 1: pressure transducer 2.

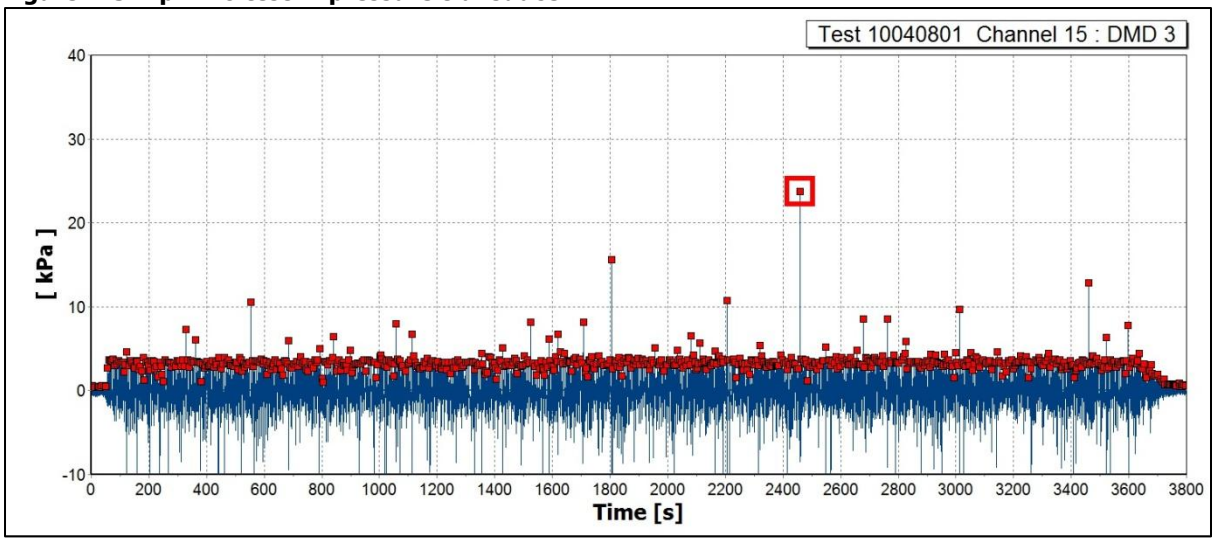

Figure B-4: April 10 test 1: pressure transducer 3.

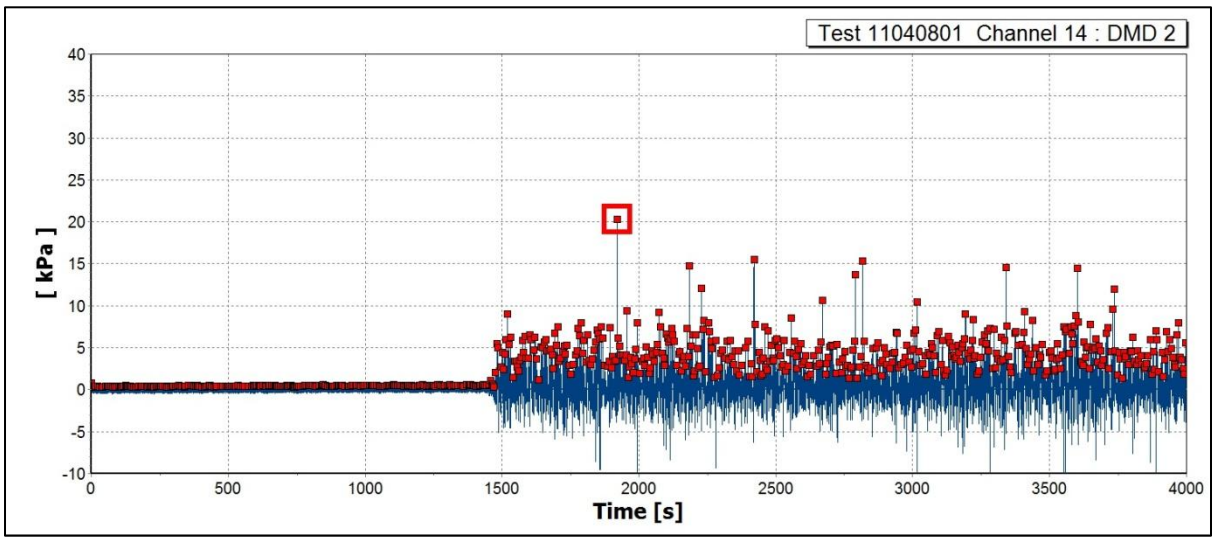

Figure B-5: April 11 test 1: pressure transducer 2.

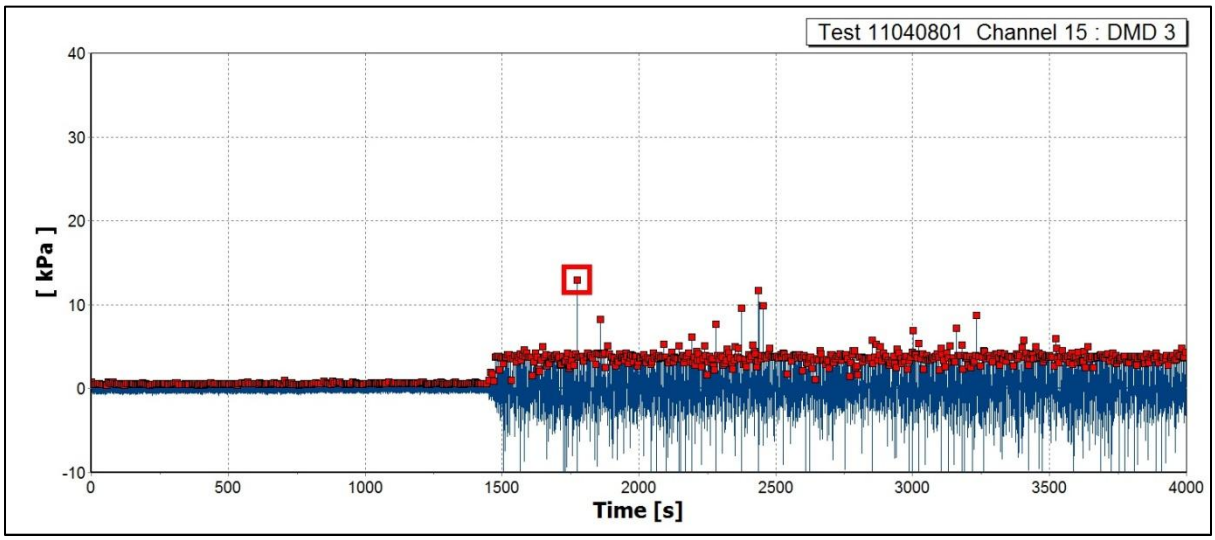

Figure B-6: April 11 test 1: pressure transducer 3.

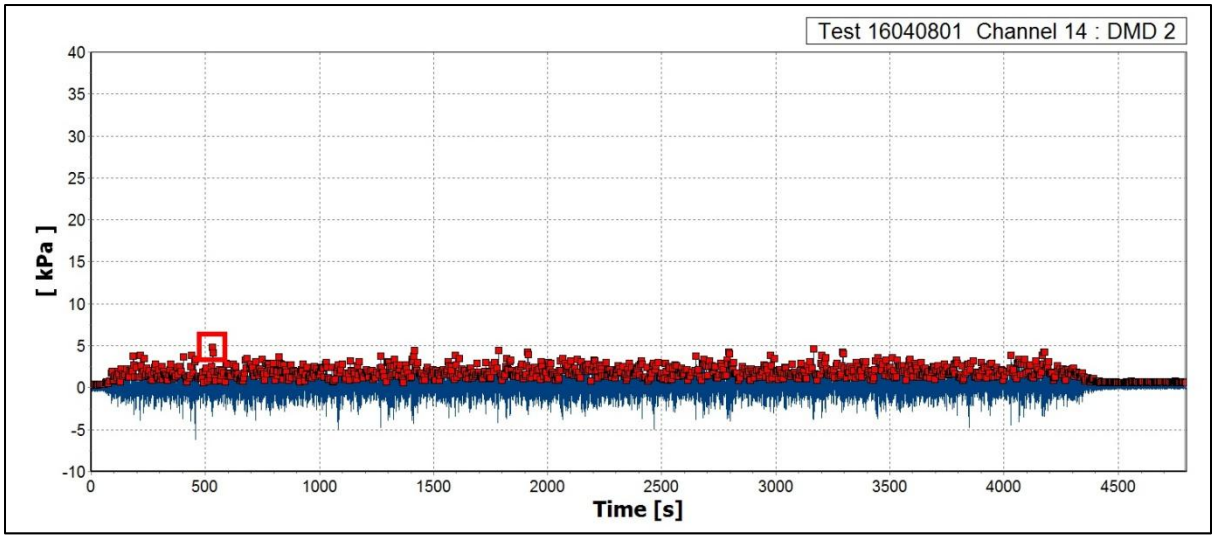

Figure B-7: April 16 test 1: pressure transducer 2.

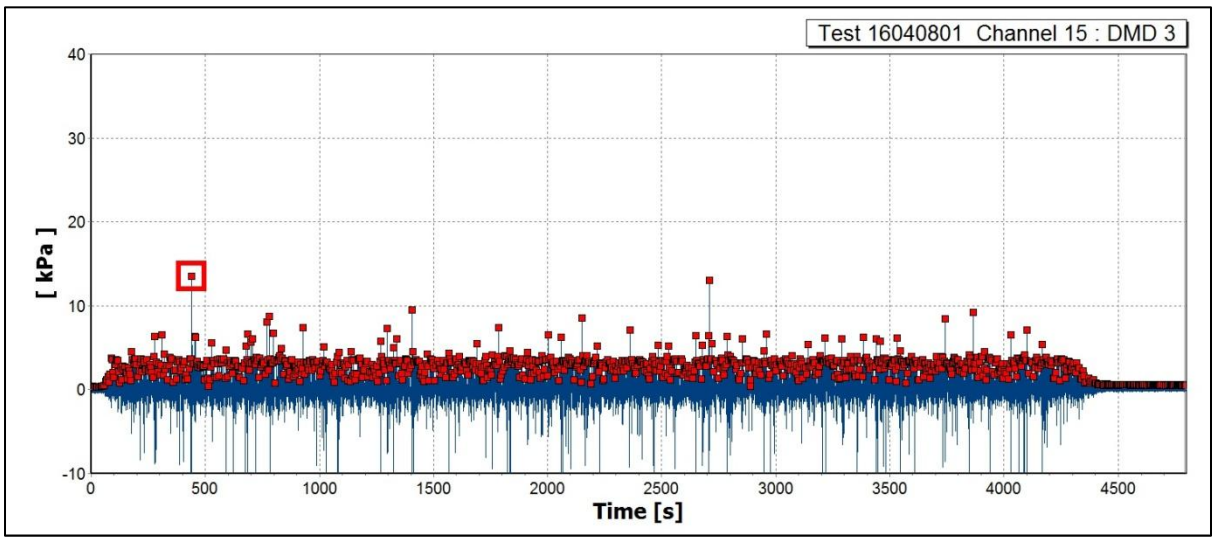

Figure B-8: April 16 test 1: pressure transducer 3.

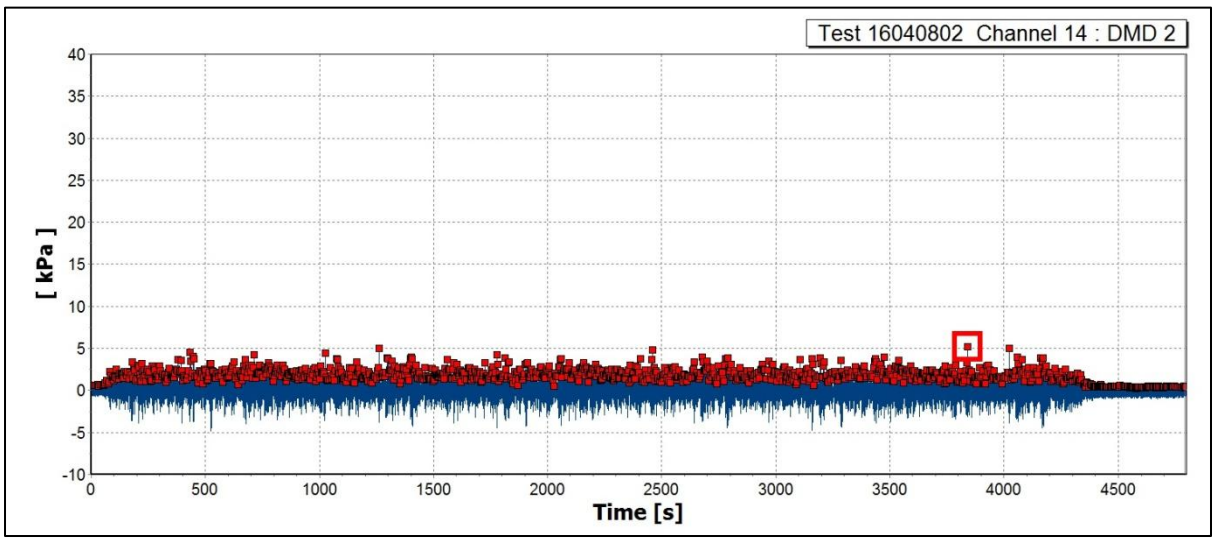

Figure B-9: April 16 test 2: pressure transducer 2.

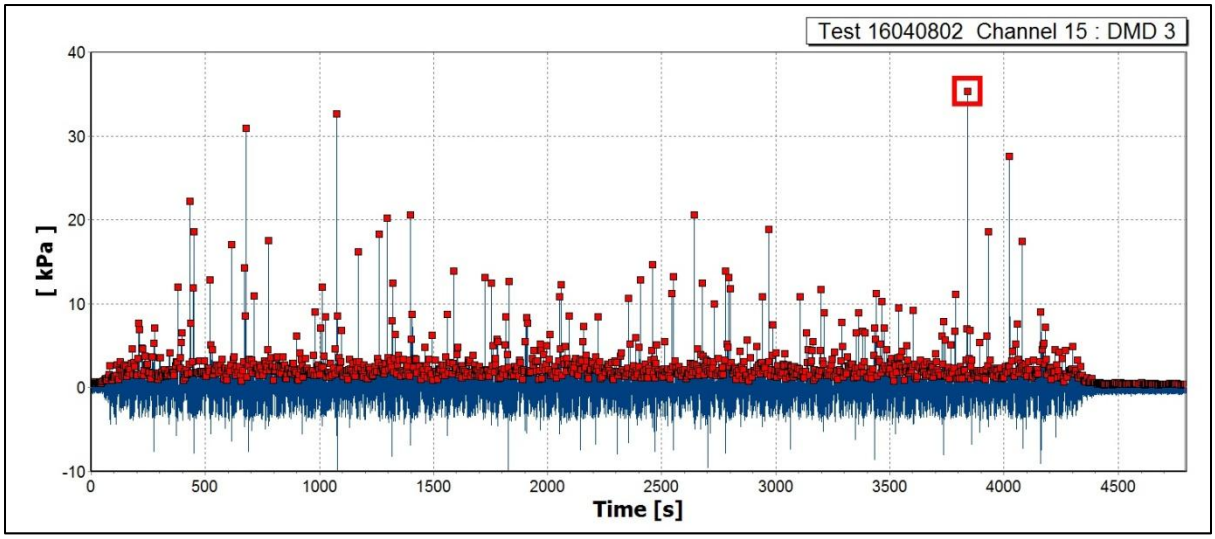

Figure B-10: April 16 test 2: pressure transducer 3.

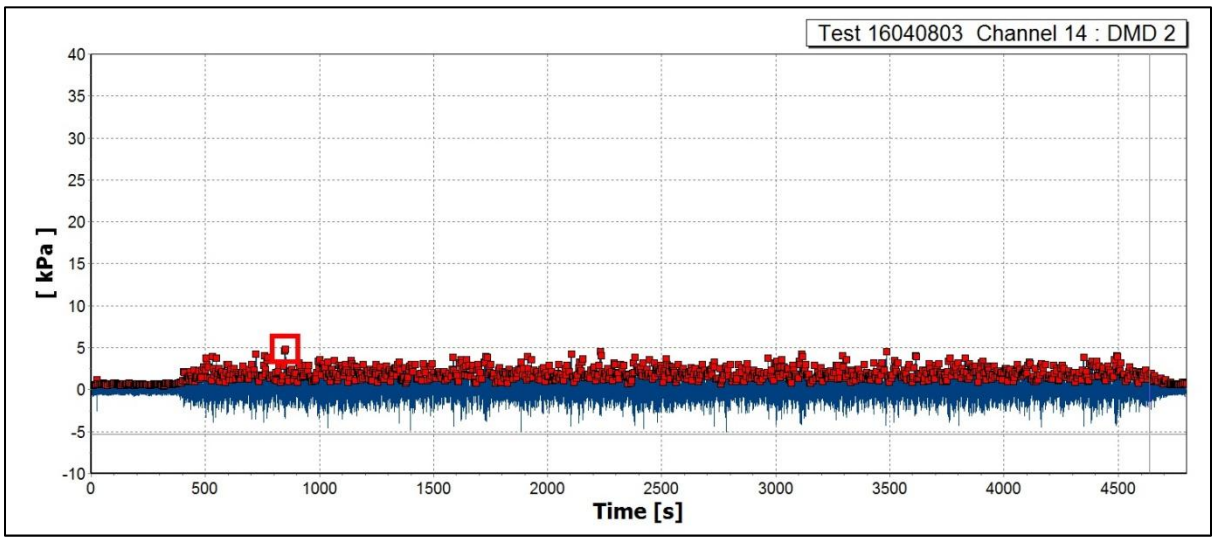

Figure B-11: April 16 test 3: pressure transducer 2.

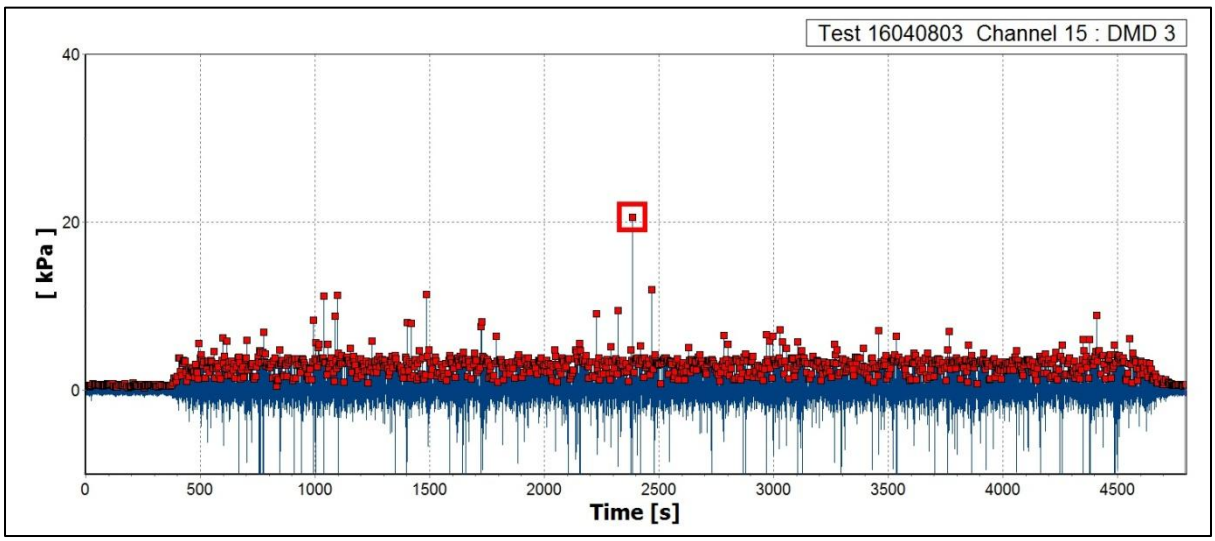

Figure B-12: April 16 test 3: pressure transducer 3.

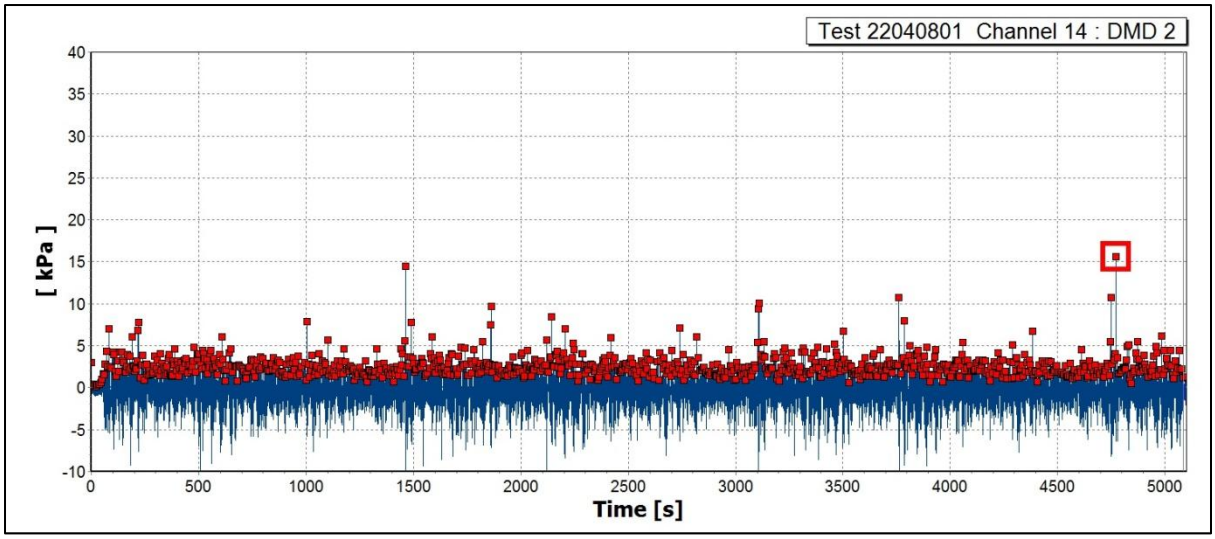

Figure B-13: April 22 test 1: pressure transducer 2.

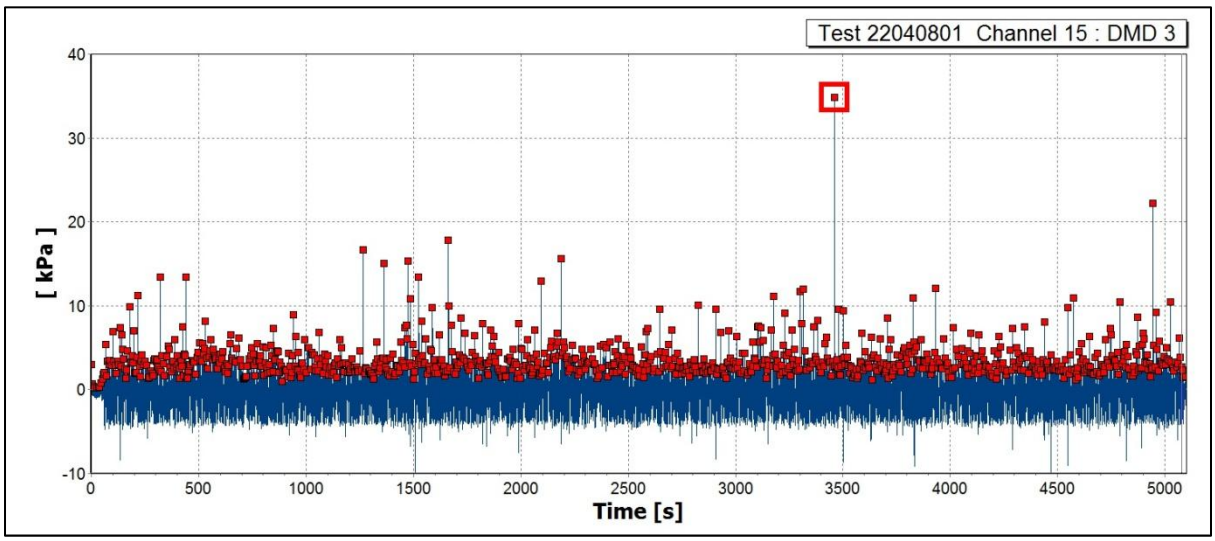

Figure B-14: April 22 test 1: pressure transducer 3.

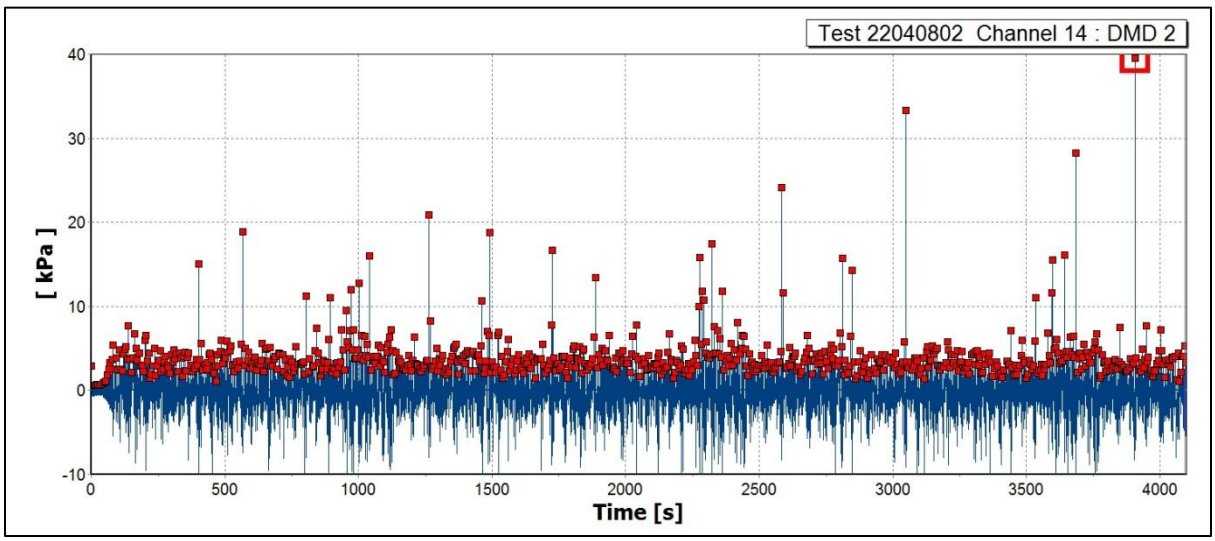

Figure B-15: April 22 test 2: pressure transducer 2.

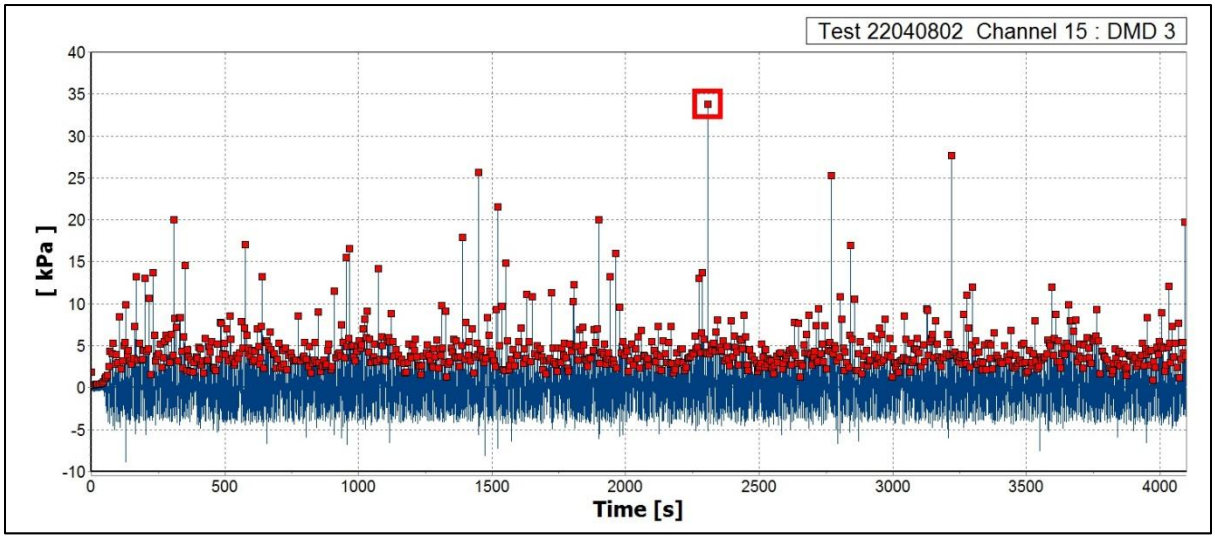

Figure B-16: April 22 test 2: pressure transducer 3.

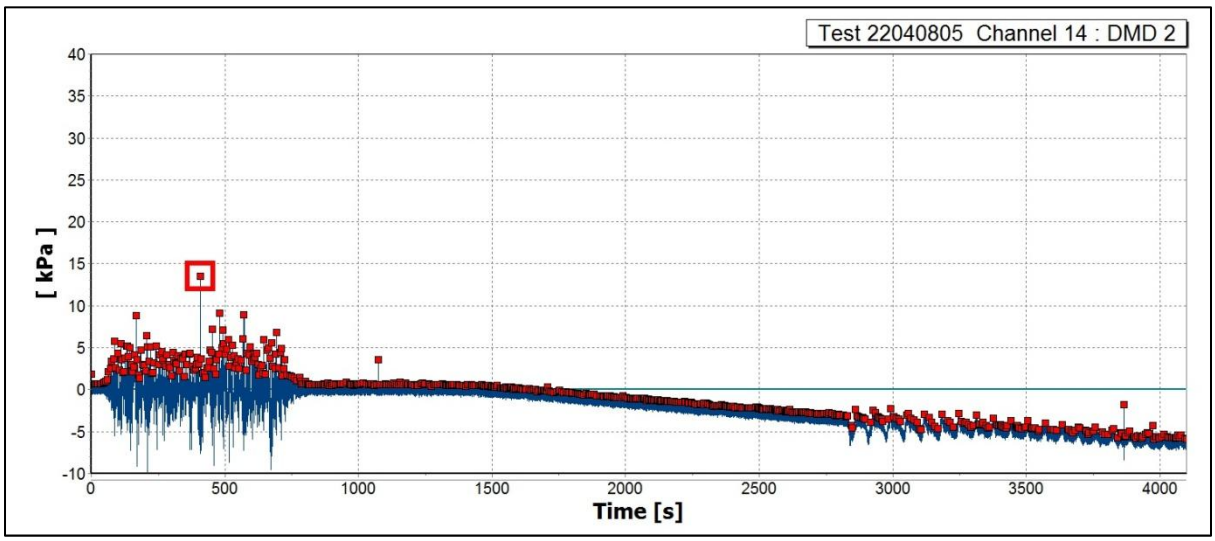

Figure B-17: April 22 test 3: pressure transducer 2.

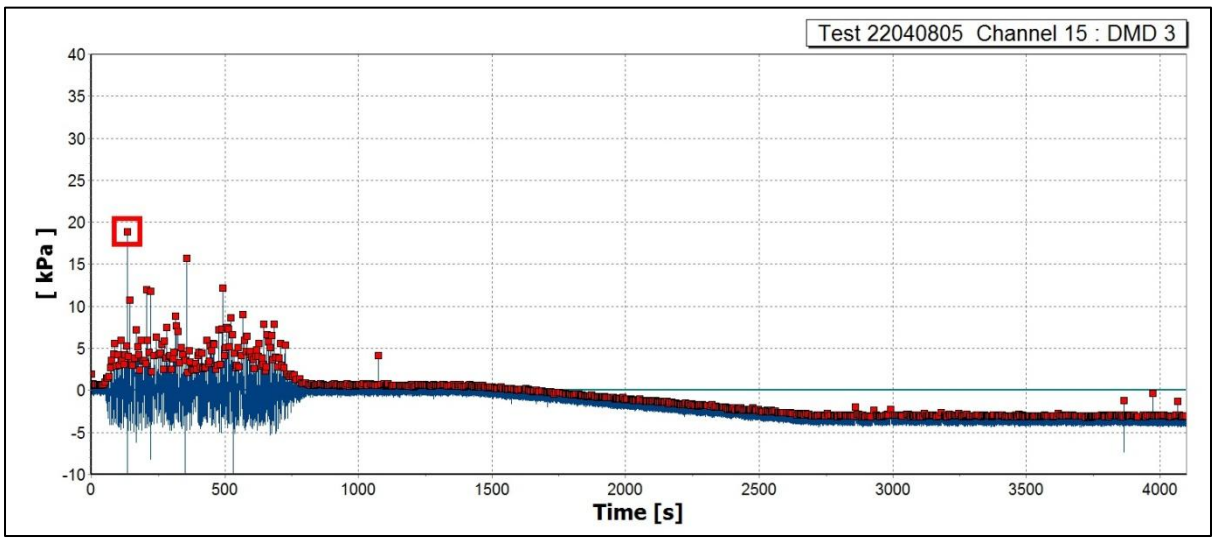

Figure B-18: April 22 test 3: pressure transducer 3.

Appendix C Erosion zones of clay covers

When a grass cover has completely been eroded the strength of the cover is determined by the clay layer. As the failure of cohesive soil is not only a process of removal of individual grains, aggregates of different sizes can be removed from the cover layer and even sliding of large parts can occur. The failure mechanisms of a clay cover are:

- Erosion of small pieces. (pieces of 10^{-3}-10^{-2} m)
- Block erosion (pieces of 10^{-2}-10^{-1} m)
- Sliding (pieces of 10^{-1} m-several meters)

These failure mechanisms can be divided over the different locations on the slope as defined by Smith on the basis of the experiments in the Delta Flume in 1992 (See also Figure C-1)[Smith, Seijffert et al. 1994]:

1. Downwards of the wave impact zone: abrasion and sliding;
2. In the wave impact zone: abrasion, block erosion and sliding;
3. Above the wave impact zone: sliding.

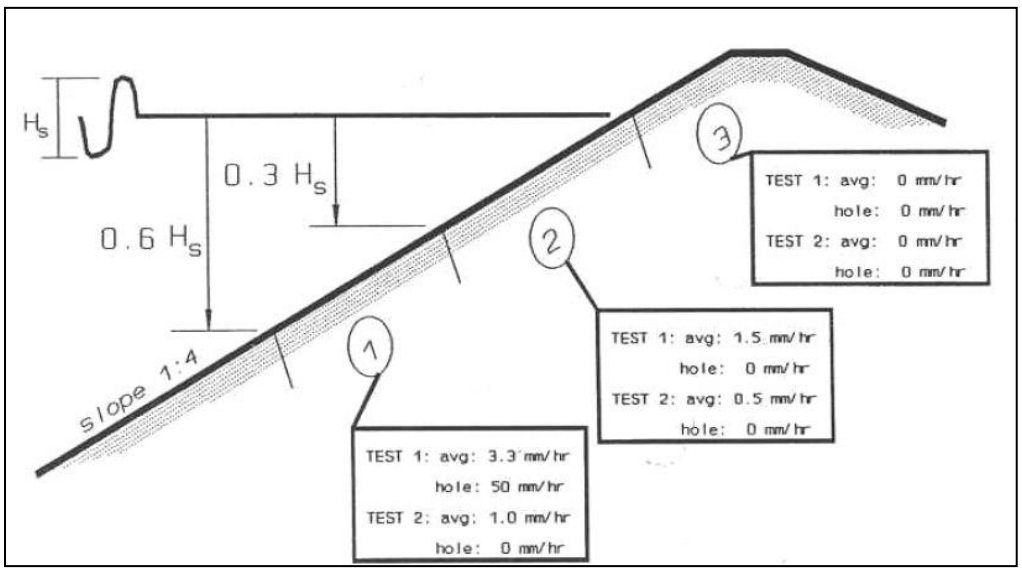

Figure C-1: Erosion zones along the slope. [Smith et al. 1994]

However Smith's theory is based on a few experiments and a study of all available wave loading tests on clay conducted by de Visser showed that the theory of these erosion zones does not completely correspond to all experiments. A complicating factor is that there are many interaction possibilities between the failure mechanisms and the different zones:

- Wearing erosion (abrasion) downwards of the wave impact zone can lead to sliding downwards, in and above the wave impact zone;
- Sliding leads to differences in the shape of the profile and thus different erosion behaviour (valid for every zone);
- Also wearing erosion and block erosion can lead to a different profile and thus different erosion behaviour.

[Kruse 1998; Kruse and Nieuwenhuis 2000; source: de Visser 2007]

After an initial erosion hole has developed, the erosion profile of the clay has a steep slope with the shape of a cliff. The differences between the angles of the steep slopes of different experiments are large; they differ from 20°-70°. If a hole had developed and it was given sufficient time to develop further into the clay a steep erosion profile with a cliff shape was the result.[de Visser 2007]

Appendix D Water pressures in clay during wave loading

During the Delta flume experiments on the residual strength of clay under stone revetments in 1992 the water pressures in the clay layer during wave attack were monitored. The water pressure gradients in the clay layer were expected to be an important factor for the erosion of clay under waves and soil structure development. [de Visser 2007] In the section below a summary is given of the observations during these experiments extracted and rephrased from de Visser (2007).

Water pressures were recorded during the experiments and the water pressure meters gave an increase in pressure readings during wave impact. This increase propagates into the subsoil by a pressure wave, or the wave flows into the dike body through cracks in the clay. By a combination of these two factors the water pressure in the subsoil is expected to give a pressure increase which is correlated with the water pressure changes in the slope.
Analysis showed that these water pressure gradients most probably occur due to damage to the covering layer. This squares with more recent research by Pohl and Richwien (2006) who state that instationary pore water pressures can build up during wave attack in clay covers that are damag by cracks and biological processes.
During the experiments the water pressures in the clay were often high and had a pattern that is similar to the water pressure pattern of the wave load. However, there were no systematic trends observed in: the average water pressure over time, the pressure differences in the water pressure meters, which were lying above each other, or in phase and damping differences.
The pressure distribution in the soil did not correspond with the distribution of the pressure on the surface during wave impact. Sometimes the pressure deeper in the clay was higher than just below the surface. It is suggested that the movement of the clay blocks is a reason for the bad correlation between the measurements in and on the slope.
On the other hand it appeared that regular pressure gradients greater than the submerged weight of clay in upward direction also occurred. Changes in the position of aggregates during the period of loading can lead to a better hydraulic connection with the surface. The erosion of clay however does not progress rapidly; cohesion and interlocking of the aggregates delay the erosion process and therefore it was concluded that fatigue plays a role. [Hofmann 1993; Hofmann 1995; source: de Visser 2007]
Therefore the upwards water pressures during a wave were further investigated with the help of numerical models such as STEENZET/2 and PLUTO. It was established that the water pressure gradients during wave impact are large enough to plastically deform the slope over a large area of the surface. This can make the clay locally unstable and therefore there is the possibility of collapse.
During the wave impact the acting gradients are the largest just after a wave impact, on a position just beneath the point of impact along the slope, and are directed out of the slope. These gradients are of a short duration and the outwards directed peaks are working on small areas just next to the impact pressure peak. However one or several wave impacts do not always cause immediate failure over a large area of the slope; instead removal of blocks takes place. Therefore it is expected that the material properties of the clay (cohesion and interlocking) are degraded under the influence of wave impacts, which is a process of fatigue.[de Visser 2007]
At a certain time the coherence is insufficient and individual blocks can be washed way. The above illustrates that high uplift pressures of a short duration can be induced within a cracked clay layer, possibly causing Block Erosion. These conclusions show many similarities with more recent research by Pohl and Richwien (2006), which is discussed in appendix E.

Appendix E Pore number and consistency index

Cracks are always present in the dike due to shrinkage and expansion or biological activity. According to Pohl and Richwien (2006) the maximum crack depth in the German climate is a threefold of the shrinkage size. Because of the occurrence of biotic macro pores a minimum crack depth equal to the root depth (0.2m) has to be assumed. Pohl and Richwien suggested in 2006 that the strength of clay depends on the rate of compression and the consistency. Therefore a demand for the pore number to absorb the loads from the wave impact was proposed. [Pohl and Richwien 2006]
The wave impact pressure to be expected once every 1000 waves on a slope 1:m according to Führböter is equal to: $(24/m)\cdot\rho_w\cdot g\cdot H_s$.
The wave impacts hit the cover layer which is already damaged by cracks, burrowing animals and infiltration. It is suggested that due to the compressive stresses on the surface caused by these wave impacts an instationary pore water pressure builds up, which decreases quickly with depth as a result of the small soaking width. Depending on the permeability and the deformation properties of the soil a pore water overpressure exists shortly after the impact lasting for approximately a third of the wave period, which reduces in time. The magnitude of the uplift pressure is of the same order as the impact pressure only smaller and acts along an arbitrary plane. [Pohl and Richwien 2006]
On the assumption of a sliding surface of 45° for saturated soil and when neglecting the dead load of the soil, a required strength of the cover layer of 50% of the wave impact pressure is found.
For the undrained case, the angle of repose is assumed to be 0°, and the sum of the root cohesion c_{grass} and the undrained shear strength of the soil c_u represents the strength of the cover layer.

The required strength c_u then follows from equation (E-1):

$$c_u \geq \frac{12}{m}\cdot\rho_w\cdot g\cdot H_s - c_{grass}\cdot\frac{d_{rp}}{d_c},\ \text{with}\ \frac{d_r}{d_c}\leq 1 \qquad \text{(E-1)}$$

Where:

d_{rp}	= root penetration depth	[m]
d_c	= crack depth	[m]

Richwien (1993) proved a logarithmic course for the reduction of strength with the consistency index for a soil consisting of aggregates:

$$c_u(w_{sat}) = c_u(w_p)^{I_{C,sat}} \qquad \text{(E-2)}$$

Where:

$c_u(w_{sat})$	= undrained shear strength at saturation	[kN/m^2]
$c_u(w_p)$	= undrained shear strength at plasticity limit	[kN/m^2]
w_{sat}	= water content at saturation, $= n\cdot\frac{\rho_w}{\rho_d}$	[-]
I_c	= consistency index, $= \frac{w_L - w}{w_L - w_p}$	[-]

This finally results in the demand for the pore number to be able to absorb the impact pressure:

$$n \leq \frac{\rho_d}{\rho_w}\cdot\left[w_l - \frac{\ln(12/m\cdot\rho_w\cdot g\cdot H_s - c_r\cdot d_{rp}/d_c)}{\ln c_u(w_p)}\cdot(w_l - w_p)\right] \qquad \text{(E-3)}$$

Where:

n	= pore number	[-]

ρ_d = dry density of the soil $\rho_d = \rho_s \cdot (1-n)$ [kg/m^3]

w_L = liquid limit [-]

w_p = plasticity limit [-]

[Pohl and Richwien 2006]

The rewritten form of equation (E-1) with $p_{\max}$ becomes:

$$n \leq \frac{\rho_d}{\rho_w} \cdot \left[w_l - \frac{\ln(0.5\, p_{\max} - c_w \cdot d_{rp} / d_c)}{\ln c_u(w_p)} \cdot (w_l - w_p) \right] \qquad \text{(E-4)}$$

Appendix F Pressure reduction in cracks

According to Müller and Wolters at al. (2003) the pressure reduction in closed end cracks is given by Figure F-1. The pressure reduction for small cracks of 0.5-3.0 mm at a crack distance of d_c = 500 mm is equal to approximately 75%.

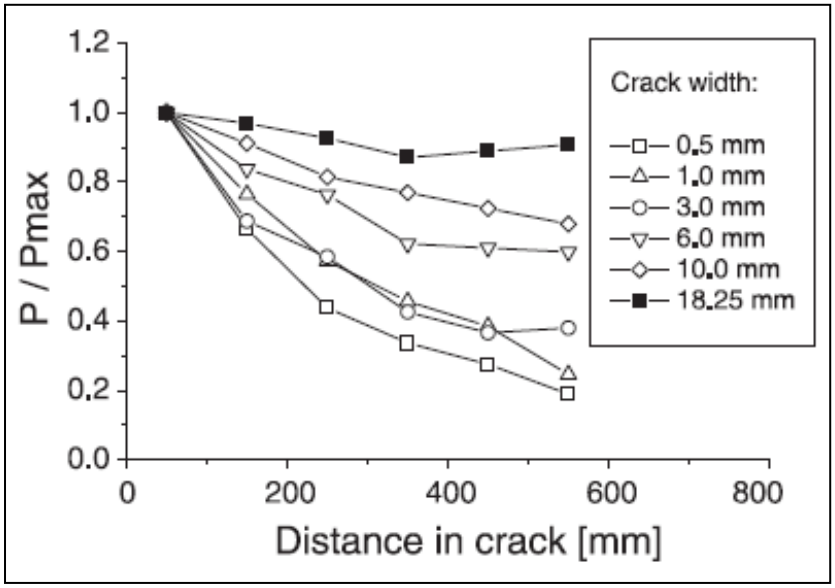

Figure F-1: Pressure reduction in closed end cracks. [Müller et al. 2003]

Appendix G Air-water ratio

Giving an accurate estimate of the aeration in breaking waves and the backwash layer proves to be difficult; at the moment only indications can be given for a number of cases. For instance the average air content n_a in an overtopping water layer in the equilibrium state is given by Hager (1990) [source: Klein Klein-Breteler and Smith 1996] as:

$$n_a = 0.75(\sin\alpha)^{0.75} \tag{G-1}$$

As there is no possibility yet to quantify the temporal and spatial variability of the changing bubble field in breaking waves, the fluid is generally assumed to be a homogenous mixture of air and water. The proportion of air is then defined as the voids ratio β :

$$\beta = \frac{V_a}{V_{aw}} = \frac{V_a}{V_a + V_w} \tag{G-2}$$

Where V_a is the volume of air, V_w represents the volume of water and V_{aw} is the volume of the air water mixture. [Bullock et al. 2001]

Air behaves differently in fresh water than in sea water, this was investigated by Bullock et al. (2001) by performing both laboratory tests and field tests at a breakwater. Bubbles formed in fresh water are generally larger and have the tendency to coalesce more. Because larger bubbles are more buoyant than small bubbles they rise faster and air can thus escape more quickly in fresh water than in salt water. For a given level of aeration the number of bubbles in salt water is greater. Furthermore the air content in salt water can increase as the small bubbles more frequently remain in the water for several waves. [Bullock et al. 2001]

The test results indicated that there is very little difference between the fresh and seawater values for a given voids ratio; the values of the maximum pressure for the fresh water tended to be 2% to 3% higher. However the compressibility of air is of far less significance in small-scale models than it is in prototype scale; the increases in pressure above atmospheric pressure are much lower for prototype scale. For full scale waves the difference between fresh water waves and salt water waves could thus be much larger.

Furthermore the air content of sea water breakers in the field was significantly higher than the air content of the salt water laboratory drop tests even though the waves were, to scale, lower. This shows that aeration is subject to a scale effect even when seawater is used in the model. [Bullock et al. 2001]

Regardless if the water is salt or fresh there is a clear tendency for the pressure to reduce as either the aeration or the violence of the impact increases. Based on the laboratory test data Bullock et al. (2001) developed a simple equation for the pressure reduction factor (PRF):

$$PRF = 1.0 - 0.2\sqrt{M_{imp}}(1.0 - e^{-k\delta}) \tag{G-3}$$

Where:

M_{imp}	= violence of the impact	[kg m/s]
k	= empirical coefficient	[-]
δ	= percentage voids ratio	[-]

Appendix H Erosion parameters

In this chapter several methods to quantify erosion parameters for cohesive soils, with and without grass, are discussed.

H.1 Comparison with Stanczak and Hoffmans et al.

In chapter 7 the erosion parameter was determined theoretically and in chapter 8 it was calibrated for aggregate erosion and block erosion. In this section the erosion parameter for aggregate erosion in the WIPE model is compared with the erosion parameters of the impact erosion model by Stanczak and the erosion by overflow model by Hoffmans et al.

H.1.1 Erosion parameter according to Stanczak

Stanczak (2008b) derived the following erosion relation for erosion due to pressure impacts after laboratory experiments:

$$d_i = k_{d,p} \cdot p \cdot e^{-wh}$$

Where:

d_i	= erosion depth	[m]
k_d	= detachability coefficient	[m^3/N]

The value of the erosion coefficient depends on the strength of the clay; for strong clay (TAW clay category 1) this detachability factor is given by:

$$k_{d,p,i} = 0.35 \cdot \arctan[110 - (w_c - 0.43)] \cdot 10^{-12}$$

The value of the detachability parameter varies with soil quality; which is related to the water content. The detachability parameter can thus be considered to be a function of water content.
The detachability coefficient for grass $k_{d,g,p}$ [m^3/N] is obtained by modifying the detachability coefficient of clay with the RVR:

$$k_{d,g,p} = \frac{k_{d,p}}{b \cdot RVR^2}$$

Where:

RVR	= Root Volume Ratio in percent	[-]
b	= parameter describing the influence of roots on the erodibility = 5	[-]

H.1.2 Erosion parameter comparison

To compare the Aggregate Erosion parameter of the new model [kg/m^{2}s] with the erosion parameters of Stanczak ($k_{d,g,p}$ [m^2 s^2/kg]) and Hoffmans et al. (E_{soil} [m/s]) the following assumptions were made:

RAR_0 =0.0000-0.0008
RVR = 50 $\cdot RAR$
$c_{clay,c} = c_{clay}$ /80
c_{clay} =15-45 kN/m^2
w_c =0.30
d_a = 0.004 m

The values of the erosion parameters are compared in Table H-1, using the following relations:

$$\frac{t_{imp}}{E_p} \equiv k_{d,g,p}$$

$$\frac{E_p}{\rho_s} \equiv E_{soil}$$

Table H-1: Comparison of erosion parameter for Aggregate Erosion with Stanczak and Hoffmans.

Grass quality	*Clay strength*	$\frac{t_{imp}}{E_p}$ *[m²s²/kg]* α_{soil} *=5.5· 10³*	$\frac{t_{imp}}{E_p}$ *[m²s²/kg]* α_{soil} *=30.0*	*Stanczak* $k_{d,g,p}$ *[m² s²/kg]*	E_p / ρ_s *[m/s]* α_{soil} *=5.5· 10³*	E_p / ρ_s *[m/s]* α_{soil} *=30.0*	*Hoffmans* E_{soil} *[m/s]*
no grass	weak		$9.00 \cdot 10^{-4}$			3.57	$4.33 \cdot 10^{4}$
no grass	moderate		$9.00 \cdot 10^{-4}$			3.57	$8.18 \cdot 10^{4}$
no grass	strong		$9.00 \cdot 10^{-4}$	$3.13 \cdot 10^{-11}$		3.57	$1.20 \cdot 10^{5}$
very poor	weak		$5.27 \cdot 10^{-6}$			$6.09 \cdot 10^{2}$	$8.65 \cdot 10^{5}$
very poor	moderate		$5.27 \cdot 10^{-6}$			$6.09 \cdot 10^{2}$	$9.03 \cdot 10^{5}$
very poor	strong		$5.27 \cdot 10^{-6}$	$6.26 \cdot 10^{-12}$		$6.09 \cdot 10^{2}$	$9.42 \cdot 10^{5}$
poor	weak		$2.64 \cdot 10^{-6}$			$1.21 \cdot 10^{3}$	$1.69 \cdot 10^{6}$
poor	moderate		$2.64 \cdot 10^{-6}$			$1.21 \cdot 10^{3}$	$1.72 \cdot 10^{6}$
poor	strong		$2.64 \cdot 10^{-6}$	$1.57 \cdot 10^{-12}$		$1.21 \cdot 10^{3}$	$1.76 \cdot 10^{6}$
average	weak		$1.77 \cdot 10^{-6}$			$1.82 \cdot 10^{3}$	$2.51 \cdot 10^{6}$
average	moderate		$1.77 \cdot 10^{-6}$			$1.82 \cdot 10^{3}$	$2.55 \cdot 10^{6}$
average	strong		$1.77 \cdot 10^{-6}$	$6.96 \cdot 10^{-13}$		$1.82 \cdot 10^{3}$	$2.58 \cdot 10^{6}$
good	weak	$3.95 \cdot 10^{-10}$	$1.32 \cdot 10^{-6}$		$4.45 \cdot 10^{5}$	$2.43 \cdot 10^{3}$	$3.33 \cdot 10^{6}$
good	moderate	$3.95 \cdot 10^{-10}$	$1.32 \cdot 10^{-6}$		$4.45 \cdot 10^{5}$	$2.43 \cdot 10^{3}$	$3.36 \cdot 10^{6}$
good	strong	$3.95 \cdot 10^{-10}$	$1.32 \cdot 10^{-6}$	$3.91 \cdot 10^{-13}$	$4.45 \cdot 10^{5}$	$2.43 \cdot 10^{3}$	$3.41 \cdot 10^{6}$

For very poor to good grass quality the erosion parameter of the WIPE model is approximately an order 10^6 greater than the one proposed by Stanczak. This is not surprising because Stanczak did not apply a critical impact pressure; consequently a low value of the erosion parameter is required. Equivalently for very poor to good grass the WIPE erosion parameter is an order 10^3 smaller than the parameter proposed by Hoffmans. This difference can be directly attributed to the adapted value of α_{soil}.

In the case of no grass, the difference between the WIPE model erosion parameter and the parameters of Stanczak and Hoffmans is significantly greater. This difference is caused by the fact that the strength of clay has no influence on the erosion resistance for aggregate erosion in the WIPE model. This problem is avoided by the definition of a critical erosion depth. The WIPE model describes the erosion of grass and is in fact not applicable for bare clay at this moment.

H.2 Erosion parameter according to Hanson and Cook

Hanson and cook (2004) developed a method to determine the erodibility of cohesive soils in situ with a jet test apparatus and an analysis tool was presented based on the data of 25 test locations in Wyoming. The complete data list of all 25 locations is given in Figure H-1.

Table 1. Summary of Field Data Collected from 25 Test Sites Located in the Powder River Basin of Northeastern Wyoming

Site identification	USC	τ_c (Pa)	k_d ($cm^3/N \cdot s$)	LL	PI	w	DR	Act	Sand[a]	Silt[a]	Clay[a]	SG	γ_d	pH	EC	Or	CEC	SAR
38-1[b]	ML	10.34	0.45	44.4	16.8	38.1	12.8	0.59	30.3	41.2	28.6	2.39	1,554	7.22	2.69	2.63	19.80	1.23
38-2[b]	CL	0.53	0.57	37.1	14.3	45.4	12.1	0.52	26.0	46.7	27.3	2.71	1,606	7.75	3.59	1.46	17.10	1.19
IS 4	CH	6.57	0.28	58.0	34.0	25.3	27.7	0.85	12.5	47.3	40.2	2.51	1,137	7.41	0.71	2.88	24.40	0.55
41-1	CL	9.95	0.61	46.1	24.5	20.2	44.0	0.80	23.6	43.7	30.6	2.59	1,292	7.46	3.61	1.77	18.70	7.79
S 6-1	CH	0.11	1.64	57.5	37.5	21.0	5.2	2.02	36.7	41.0	18.6	2.65	1,376	7.56	7.90	2.12	21.90	3.77
S 6-2	CH	0.30	2.33	51.0	29.0	27.3	30.3	1.15	28.2	43.6	25.2	2.63	1,426	7.92	6.21	1.45	9.90	11.10
S 8-1	CL	0.50	2.38	39.3	17.9	9.3	17.0	0.94	46.1	34.9	19.0	2.77	1,267	7.50	3.76	1.45	17.80	2.24
S 8-2	CL	3.40	0.69	39.9	21.0	9.3	28.9	0.75	28.3	43.7	28.0	2.75	—[c]	7.58	3.86	1.10	16.10	4.93
48-1	GM	12.98	0.35	55.3	35.8	25.1	31.8	3.15	11.9	39.4	11.3	2.59	1,431	7.50	7.60	1.60	18.30	12.60
59-1[b]	CL	3.16	0.68	43.6	18.8	36.3	8.7	0.64	25.7	44.9	29.4	2.42	1,686	7.56	1.99	1.58	20.00	4.68
59-2[b]	CL	1.31	2.01	34.6	13.4	15.4	18.5	0.86	42.5	42.0	15.5	2.59	1,653	7.86	0.50	1.36	17.80	8.31
17-1	CL	6.37	0.39	47.0	22.3	28.5	19.0	1.42	16.3	68.1	15.7	2.35	1,626	7.30	1.51	3.90	19.60	0.71
17-2	CL	9.78	1.59	48.5	23.6	31.0	15.0	1.29	18.4	63.3	18.3	2.37	1,586	7.80	3.29	3.84	22.90	5.55
19-1	CH	0.59	1.35	55.5	27.6	16.0	11.7	1.22	11.6	55.7	22.7	2.55	1,529	7.40	3.43	3.94	20.80	0.94
19-2	CH	2.87	0.84	63.0	33.7	27.8	9.8	0.90	4.5	49.9	37.6	2.65	1,309	7.20	3.21	4.27	23.40	0.99
21-1	CL	14.84	0.37	47.7	24.4	12.0	34.0	3.78	27.9	65.6	6.5	2.63	1,314	7.26	1.34	5.59	25.00	1.14
21-2	CL	2.02	1.14	46.0	22.0	11.4	14.1	1.45	24.6	60.2	15.2	2.63	1,341	7.47	1.25	2.91	18.90	0.62
16-1	CH	1.15	1.63	66.0	35.2	30.0	8.4	1.08	2.4	61.6	32.7	2.35	—[c]	7.80	3.40	3.11	23.40	5.11
16-2	CH	1.64	0.87	72.0	42.8	15.0	7.7	1.27	2.1	61.1	33.8	2.38	1,307	7.80	2.26	3.12	22.20	4.93
5-1	CH	1.18	1.10	56.5	26.8	42.0	11.6	1.19	20.8	56.7	22.5	2.68	1,309	7.90	4.48	3.12	18.50	8.39
5-2	MH	1.88	0.68	55.3	21.3	38.9	11.3	0.85	12.7	62.2	25.1	2.45	1,495	7.90	5.32	3.18	15.40	7.86
4-1	CH	15.35	0.27	64.0	32.5	43.5	23.5	1.07	0.0	69.5	30.5	2.26	1,349	7.30	8.47	5.24	26.50	13.73
SH17-1	CH	8.36	0.41	61.5	36.6	25.3	15.2	1.28	17.9	53.7	28.5	2.54	1,328	7.90	10.3	2.66	16.40	12.09
3-2	CL	3.23	0.65	37.5	18.7	27.9	32.0	1.64	46.2	38.4	11.4	2.72	1,613	8.10	2.70	1.56	12.40	9.19
SH14-1	MH	6.54	0.39	56.0	23.0	18.0	28.0	2.83	55.4	36.5	8.1	2.51	—[c]	8.00	10.8	2.64	20.80	16.41

Note: USC=unified soil classification; LL=liquid limit (%); PI=plasticity index (%); w=water content (%); DR=dispersion ratio; Act=activity; Sand =percent sand (%), Silt=percent silt (%); Clay=percent clay (%); SG=specific gravity; γ_d=in situ dry density (kg/m^3); EC=electrical conductivity (DS/M); Or=organic matter (%); CEC=cation exchange capacity (cmol); and SAR=soil adsorption ratio.

[a]Remainder from 100% =percent gravel.

[b]CBNG-produced water was being discharged in the channel at these sites during testing.

[c]No in-situ soil sample collected at this site.

Figure H-1: soil erodibility test data. [Hanson and Cook 2004]

To give an estimate of the critical soil shear strength and a detachability factor according to the method proposed by Hanson and Cook, the soil characteristics of the GWK tests and the test locations are compared. No grass strength is incorporated. The soil characteristics of the tests in the GWK that closely match the soil data obtained in these field tests are displayed in Table H-2.

Table H-2: Test location data that match the GWK soil data.

Location	τ_c [N/m^2]	Kd [cm^3/N s]	Sand [%]	Clay [%]	Liquid limit [%]	Plasticity index [%]	Water content [%]	Dry density [t/m^3]
GWK test	**6.05**	**0.98**	20	25	61	28	26-35	1.575
38-1	10.34	0.45	30.3	28.6	44.4	16.8	38.1	1.554
17-2	9.78	1.59	18.4	18.3	48.5	23.6	31.0	1.586
19-1	0.59	1.35	11.6	22.7	55.5	27.6	16.0	1.529
5-1	1.18	1.10	20.8	22.5	56.5	26.8	42.0	1.309
SH17-1	8.36	0.41	17.9	28.5	61.5	36.6	25.3	1.328
average	6.05	0.98	19.8	30.15	53.28	26.28	30.48	1.461

After extrapolation of all data Hanson and Cook gave the following relationship between critical shear stress and the erosion parameter (correlation 0.56):

$$k_d = 1.11\tau_c^{-0.37} \quad \text{(H-1)}$$

H.3 Erosion parameter according to Thomann and Niezgoda

Thomann and Niezgoda analyzed the data from Wyoming as well and developed the following formula, which is based on the five most significant parameters [Thoman and Niezgoda 2008].

$$\tau_c = 77.28 + 2.2(Act) + 0.26(DR) - 13.49(SG) - 6.4(pH) + 0.12(w) \quad \text{(H-2)}$$

Where:

Act	= activity	[-]
DR	= dispersion ratio	[-]
SG	= specific gravity	[-]
pH	= pH value	[-]
w	= water content	[-]

To determine the erosion resistance of grass the approach by Temple et al. (1987) is used. On the assumption that vegetation acts as a boundary interface some of the shear stress can be absorbed by the vegetation in channels. The maximal allowable vegetal stress $\tau_{c,v}$ is equal to:

$$\tau_{c,v} = 0.75 C_I$$

Where:

$$C_I = 2.5\left(L\sqrt{M}\right)^{1/3}$$

Where:

C_I	= retardance index	[-]
L	= stem length	[m]
M	= stem density	[No/m2]

Appendix I Matlab code

I.1 Aggregate Erosion code

```
clc;
clear;
format long e;

%material properties
rhow=1000;                      % density of water                  [kg/m3]
rhos=2000;                      % density of the soil               [kg/m3]
g=9.81;                         % acceleration of gravity           [m/s2]
z=0;
da=0.004+0.08*z;                % aggregate diameter                [m]
n=0.4;                          % porosity                          [-]
phi=35;                         % natural angle of repose           [-]
cclay=30000;                    % clay cohesion                     [N/m2]
cclayc=cclay/80;                % critical clay cohesion            [N/m2]
dr=0.13*10^-3;                  % root diameter                     [m]
tr=20e6;                        % root tensile strength             [N/m2]
f=tand(phi);                    % friction factor side walls        [-]
ns=2;                           % number of side walls              [-]
B=22.32;                        % Beta root decay coefficient       [m-1]

% load properties
mur=5;                          % pressure reduction coefficient for cracks [m-1]
timpact=0.350;                  % averaged impact duration          [s]
ndata=xlsread('excellijsten\stuurlijst\AE\Run1\SLAE08-10-11-16-22-
DMD3_without_April16test2_April18_DMD3.xlsx',1);

%%
%strength
ym=0;
run=0;
RAR0=0.0008

for j=[1:7012]
z=z+ym;                         % depth                             [m]
if z>0.05
        break
end

da=0.004+0.08*z;                % aggregate diameter at depth z     [m]
RARz=RAR0.*exp(-B.*z);          % RAR profile                       [-]
sigmagrassc=1.0.*RARz.*tr;      % grass normal critical strength at depth [N/m2]
Pc=(1-n+0.5*ns*f)*(rhos-rhow)*g*da + sigmagrassc;
                                % critical impact pressure          [N/m2]

%load
Pmax=ndata(j,1);                %impact pressure                   [N/m2]
Pup=Pmax./(1+mur.*(1.5*da));    %uplift pressure                   [N/m2]
Pmaxstored(j,:)=Pmax;
Pupstored(j,:)=Pup;

%detachability parameter
alfasoil=30;                    % calibration parameter             [-]
```

```
Ep=alfasoil*(rhos/rhow)*Pc/sqrt(g*da);   % detachability parameter impact erosion
                                         [kg/m2 s]
%erosion of aggregates
if Pup>Pc;
ym=((Pup-Pc)*timpact)/Ep;                %erosion depth              [m]
else
ym=0;
end

ymstored(j,:)=ym;
zstored(j,:)=z;
Pcstored(j,:)=Pc;
Epstored(j,:)=Ep;
totalerosion(j,:)=sum(ymstored);
dastored(j,:)=da;
k(j,:)=j;
run=run+1
end
```

I.2 Block Erosion code

```
clc;
clear;

%Soil properties
rhow=1000;                  % density of water              [kg/m3]
rhos=2000;                  % density of the soil           [kg/m3]
n=0.4;                      % porosity                      [-]
phi=35;                     % natural angle of repose       [-]
f=tand(phi);                % friction factor side walls    [-]
cclay=30000;                % clay cohesion                 [N/m2]
cclayc=cclay/80             % critical clay cohesion        [N/m2]
g=9.81;                     % acceleration of gravity       [m/s2]

%Grass properties
dr=0.13e-3;                 % root diameter                 [m]
tr=20e6;                    % root tensile strength         [N/m2]
B=22.32;                    % Beta root decay coefficient                 [m-1]
ns=2;                       % number of side walls providing strength     [-]

% load properties
mur=5;                      % pressure reduction coefficient for cracks   [m-1]
timpact=0.350;              % averaged impact duration                    [s]

%Initial block size
z=0.0:0.001:0.20;
dblock=0.004+0.08*z;        % aggregate diameter                          [m]

 %%
%initial values
ym=0;
RAR0=0.0008;                % RAR at the surface depending on grass quality [-]
RARz=RAR0.*exp(-B.*z);      % Valk RAR profile                              [-]
nr=RARz./(0.25.*pi.*dr.^2);
sigmagrass0=1.0.*RAR0.*tr;  % grass normal strength at the surface       [N/m2]
sigmagrassc=1.0.*RARz.*tr;  % grass normal critical strength at depth z  [N/m2]
cgrassc=1.2*tr.*RARz;       % critical grass cohesion                    [N/m2]

Sigmaf=((1-n).*(rhos-rhow).*g.*z+sigmagrassc+(0.5.*ns.*f.*(rhos-
rhow).*g.*(z).^2)./dblock)   % fracture strength                  [N/m2]
[Sigmafmin,I]=min(Sigmaf);  % lowest value of Sigmas at index I of z  [N/m2]
zmin=0.001*(I-1)
RARzmin=RAR0*exp(-B*zmin);  % Root Area Ratio at zmin
sigmagrasscmin=1.0.*RARzmin*tr;% grass normal critical strength at zmin   [N/m2]
cgrasscmin=1.2*tr*RARzmin;

%integrate grass cohesion contribution
syms d
cgrasscd=1.2*tr.*RAR0.*exp(-B.*d);
cgrasscint=int(cgrasscd,d,0,zmin);
cgrasscint=double(cgrasscint)
dblock=0.004+0.08*zmin;

ndata=xlsread('excellijsten\stuurlijst\BE\Run2\SLBE08-10-11-16-22-
DMD3_without_April16test2_April18.xlsx',1)
```

```
%%
run=0;
% Large cracks / block erosion
for j=[1:7012]
Sigmafblock=(1-n).*(rhos-rhow).*g.*zmin +sigmagrasscmin + (0.5.*ns.*f.*(rhos-
rhow).*g.*(zmin).^2)./dblock;                    %fracture resistance block   [N/m2]
Sigmasblock=(1-n).*(rhos-rhow).*g.*zmin +sigmagrasscmin+(0.5.*ns.*f.*(rhos-
rhow).*g.*(zmin).^2)./dblock +ns.*(cgrasscint+(cclayc.*zmin))./dblock;
                                                 % critical uplift pressure block [N/m2]
%load
Pmax=ndata(j,1);                                 %impact pressure     [N/m2]
Pup=Pmax./(1+mur.*(zmin+0.5*dblock));            %uplift pressure [N/m2]
Pmaxstored(j,:)=Pmax;
Pupstored(j,:)=Pup;

%detachability parameter
alfasoil=0.23;                                   % calibration parameter [-]
alfacrack=390;                                   % calibration parameter cracks
Ep=alfasoil*(rhos/rhow)*Sigmasblock/sqrt(g*dblock);    % detachability parameter
impact erosion [kg/m2 s]

%crack growth
if Pup>Sigmafblock
DeltaAblock=((Pup-Sigmafblock)*dblock^2)/(alfacrack*(cclayc+Sigmafblock));
else
DeltaAblock=0;
end
dblock=dblock+sqrt(DeltaAblock);
Ablock=dblock.^2;

%Blockerosion
if ((Pup-Sigmasblock)*timpact)/Ep;>zmin                  %erosion criterion
ym=zmin
break
        else
        ym=0;
        end

Epstored(j,:)=Ep;
ymstored(j,:)=ym;
Ablockstored(j,:)=Ablock;
dblockstored(j,:)=dblock;
Epstored(j,:)=Ep;
Sigmafblockstored(j,:)=Sigmafblock;
Sigmasblockstored(j,:)=Sigmasblock;
totalerosion(j,:)=sum(ymstored);
k(j,:)=j;
run=run+1
end
```

Appendix J Executive summary

1 Introduction and objective

Against the background of enhanced hydraulic loads due to climate change there will be a need for improvement of the flood defence system in the Netherlands in the future to prevent events such as the storm surge disaster in 1953 and the river flooding in the 90's from happening again.
Improving the existing dikes could be done by raising them and applying traditional heavy revetment types such as placed concrete block revetments (pitched revetments) or asphalt, but alternative solutions are being investigated. These days there is a growing interest in grass as a dike cover because it is a cheap and a sustainable dike protection.
Many river dikes have a grass cover and on traditional dikes with a stone revetment grass is usually applied in the higher part of the wave run-up zone already. If it can be confirmed that even during these new conditions grass is a reliable dike cover material and thus has sufficient strength to withstand the enhanced loads on both inner and outer slope an upgrade of the dike could be less drastic or will even be redundant.
A clear physical understanding of the failure of grass cover layers due to different wave loads is indispensable to achieve this. Yet at the moment there is a hiatus in the knowledge on the erosion resistance of grass covers on especially the outer slope. For this reason large scale tests have been performed in the Große WellenKanal (Large Wave Flume) in Hannover in 2008 for both EroGRASS and FLOODsite.
The main objectives of the EroGRASS project were to investigate in detail the failure of grass cover layers due to wave impact, wave run-up and run-down flow and wave overtopping anywhere along the dike profile (seaward slope, dike crest and shoreward slope) [Piontkowitz, Verhagen et al. 2009]. The obtained data during the EroGRASS experiments could provide valuable information to come to a more accurate description of the erosion process of grass covers on the outer slope. With the help of the EroGRASS data the study presented here aimed to develop a model that describes the initiation of erosion of a grass cover layer on the outer slope by wave attack. The objectives were to:

- Determine the erosion process of a grass cover layer on an outer slope;
- Determine the strength and the spatial variability of the strength of a grass cover layer;
- Determine the load on and the distribution of the load along the outer lope;
- Develop an erosion model for grass covers on the outer slopes;
- Calibrate and verify the erosion model.

To reach these objectives a theoretical approach was followed: a desk study was performed resulting in an overview of existing knowledge and relevant research carried out in the past. Furthermore an analysis of the experiments carried out for the EroGRASS project in the GWK in Hannover in 2008 was done.
The results of this research could contribute to the development of new design guidelines and the improvement of the assessment guidelines in the future.

2 Theoretical background

2.1 Wave impact

The type of loading on the outer slope by waves on is strongly bound to the breaker type, which is determined by the Iribarren number ξ_d at the toe of the structure. Plunging breakers produce highest impact pressures and are most relevant for this research.
It is expected that most damage to the grass cover is inflicted by wave impacts and their accompanying impact pressure peaks. Hence it is assumed that the flowing water in the run-up and run-down tongues merely transports loose particles; the influence of flow velocities in the wave impact zone is thus neglected.
Impact pressures are very dynamic and of short duration but can be significant in size. In various studies it is found that the maximum wave impact pressure varies per wave even if the incident waves are regular. A theoretical distribution for maximum impact pressures has therefore been proposed by Führböter in 1966. He suggested a log-normal distribution for the maximum wave

impact pressures. This has been confirmed by subsequent studies; for all types of experiments the impact pressures are generally log-normally distributed [Führböter 1986; Witte 1988].
As mentioned above the air content of the falling water mass greatly affects the magnitude of the impact pressures and Führböter attempted to quantify the air content in an equation for the impact pressure but in the end preferred to use a simpler equation. The most recent and commonly used formula for maximum wave impact pressure was proposed by Führböter and Sparboom (1988) and is given by equation (1):

$$p_{\max,i} = q_i / m \cdot \rho_w g H \tag{1}$$

Where $p_{\max,i}$ is the maximum impact pressure not exceeded by i% of the cases, q_i is the corresponding impact factor, m is the front slope, ρ_w is the density of water, g is the acceleration of gravity and H is the incident wave height.
The decrease of the impact pressure on gentler slopes is the result of the cushioning effect of the water layer that remains after the preceding wave. For waves on asphaltic revetments the wave impact pressure can be represented by a triangular shape with base equal to the significant wave height H_s. Van Vledder (1990) concluded in a desk study that the maximum wave impact pressures occur at about half the wave height below the still water level and that the size of the impact area is approximately half the wave height. Later Schüttrumpf (2001) was able to approximate the location of the wave impact on the slope, for regular as well as irregular waves, as a function of the surf similarity parameter at the toe of the structure.

$$\frac{Z_{imp}}{H_s} = 0.8 + 0.6 \tanh\left(\xi_d - 2.1\right) \tag{2}$$

Where Z_{imp} is the vertical distance below Mean Water Level (MWL) of impact point. For regular waves the location of impact is more or less at a fixed position. For random waves, however, this position varies significantly.
The wave impact can be separated into three time sections. The time needed to reach the maximum pressure peak is often referred as the compression time or the rise time t_k, whereas the time needed for the pressure to reduce from the maximum pressure to the quasi-static pressure is referred to as the expansion time or the fall time t_e. The sum of the compression time and the expansion time is the wave impact duration t_d.
Führböter and Sparboom (1988) found impact durations of 10-200 ms and rising times of 10-60 ms. After data analysis of wave impact tests on Elastocoast revetments, performed in the GWK in Hannover, a conservative relation was obtained for the rise time t_k [Oumeraci, Staal et al. 2010]. The expression for the normalized rise time for a slope of 1:3 reads:

$$\frac{t_k}{T} = 0.047 \cdot \left(\frac{p_{\max}}{\rho g H_s} \right)^{-0.71} \quad \text{for } 1.6 < \frac{p_{\max}}{\rho g H_s} < 7.5 \tag{3}$$

Equation (3) gives an upper limit for the rise time for impact on and underneath Elastocoast revetment. Contrary to the rise time, the impact duration t_d has the tendency to increase with increasing impact factor; the following relation was proposed [Oumeraci et al. 2010]:

$$\frac{t_d}{t_k} = 6.2 + 2.7 \tanh\left(\frac{p_{\max}}{\rho g H_s} - 4.5 \right) \quad \text{for } 1.6 < \frac{p_{\max}}{\rho g H_s} < 7.5 \tag{4}$$

Where it is suggested that the ratio t_d / t_k must exceed 2.0 (rise time and fall time are identical) and

should be not much larger than 12.0.

2.2 Composition of a grass cover layer

A well developed grass cover is highly erosion resistant; this erosion resistance is partly obtained by the grass sward but mainly caused by the root system. The roots penetrate the soil causing a soil structure, but at the same time the roots bond the soil together resulting in a tough and flexible layer which has a much higher erosion resistance than bare soil.
Apart from the armouring effect of the roots, the roots stimulate chemical processes which develop the cementing substances that are responsible for the bonding forces in the clay. The reinforcing effect of the roots diminishes with depth. Near the surface the cohesion of the roots is dominating the strength. As depth increases the root cohesion decreases and at a certain depth the cohesion and friction of the clay become dominating for the strength. A typical grass cover layer consists of several layers, each with its own characteristics; the various layers are indicated in Figure 2-4.

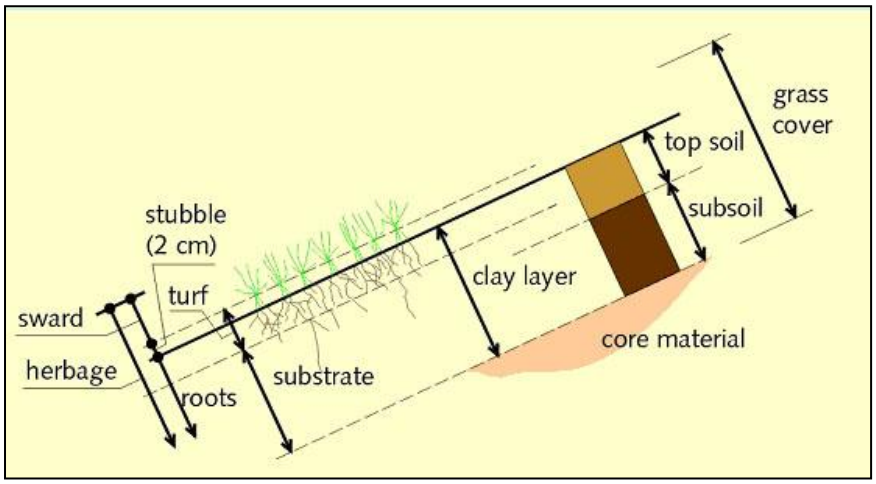

Figure 2: Definition sketch of a grass cover layer. [TAW 1997]

The grass cover can be subdivided into a number of zones [TAW 1997; Stanczak 2008]; each zone has different erosion behaviour. The uppermost layer of the turf, the stubble, generally consists of loose soil and plant remains; this layer is washed away very quickly by the waves and it is 1 to 3.5 cm thick. Immediately below the stubble is the turf which is loosely packed and usually closely rooted; this part is highly erosion resistant and only slowly eroded away and it is 1 to 5 cm thick.
In the bottom part of the turf the sod is more closely packed but the number of roots is considerably smaller. The number of roots diminishes with depth up to the substrate where the influence of the roots becomes negligibly small. This soil is more susceptible to erosion.
Because of oscillating water levels and climatic effects clay has a fluctuating water content which causes shrinkage and swelling. Consequently extensive pores and cracks usually occur in the top part of grass covers. As the boundaries of these cracks are subject to extreme wetting and drying conditions as well more cracks can be formed and eventually the soil is broken into small lumps. The aggregates can range from less than 2 mm to as much as 20 cm; the smaller particles are found directly underneath the grass sward. Soil structure limits the resistance of clay against wave loading significantly and decreases with depth. The formation of cracks and holes in the soil is also induced by root penetration and other biological activities such as the burrowing of animals (worms, insects, moles, mice, etc).

3 Erosion process

Soon after installation a soil structure will develop in a grass cover layer and the soil will then consist of small aggregates. During wave loading the permeability of the covering layer is increased; direct wave impacts form or enlarge cracks at the surface and the pores and cavities in the turf are gradually saturated with water. This enables uplift pressures to develop underneath the aggregates shortly after the wave impact.
Simultaneously the turf may be damaged at greater depth when an irregularity exists in the cover

layer that allows impact pressures to penetrate into the soil. For wave-induced erosion of grass cover layers on the outer slope two failure mechanisms can therefore be distinguished which can occur independently of each other: aggregate erosion and block erosion.

3.1 Aggregate erosion

When the top layer of the sod is very permeable due to soil structure and small cracks, the breaking wave impacts can even be in direct contact with the pore water (Figure 4-6 left). The impact pressure can then be transmitted to the pore water pressures in upwards direction can be generated temporarily underneath a soil aggregate (Figure 4-6 right). The erosion of small particles increases permeability even more and the sod can become spongy, which amplifies all of the processes described above.

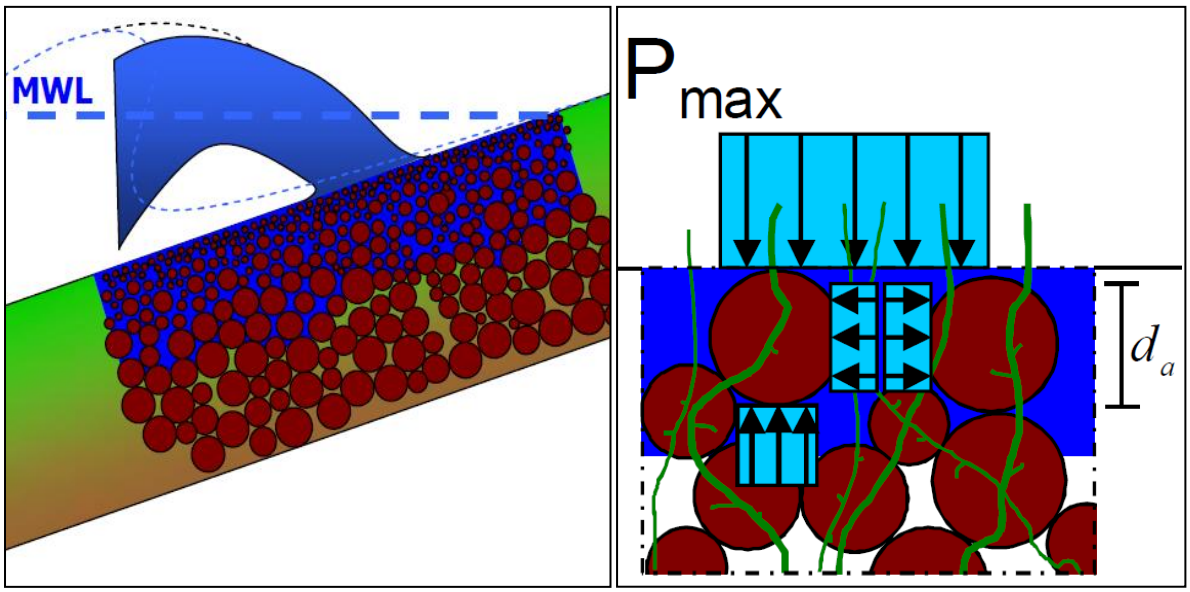

Figure 3: Wave impact in direct contact with pore water (left) results in upward pressure (right).

3.2 Block erosion

Cracks and cavities in the grass cover are deformed and enlarged due to the persistent wave impacts and the erosion of small pieces. The turf becomes spongier and at a certain moment shrinkage cracks that were already present in the deeper part of the cover layer are opened up or larger cracks are formed by the deformation of the side walls of small cracks by subsequent impacts. This allows the water and the impact load to reach deeper parts of the grass cover.

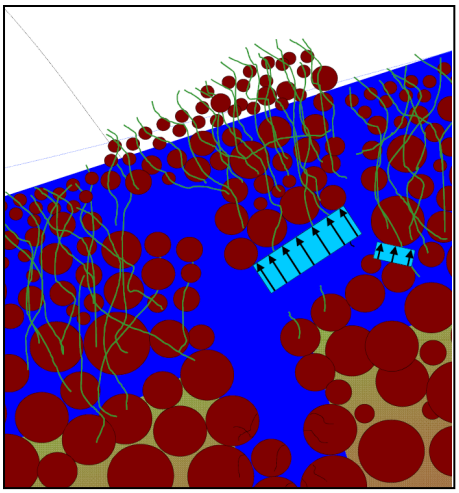

Figure 4: Balloon formation in the turf can lead to instant erosion of a large block of the turf.

In this stage the explosive effect of impact in water filled cracks can play a major part in the erosion process. Shortly after the wave impact pressure at the surface has diminished, a high pressure is still present deep within the crack.
The balloon mechanism may then be triggered: at the weak location underneath the turf a crack is formed and the created space underneath the turf is filled with water which will remain there. The result is a bulge, or blister, on the surface of the covering layer. This crack gradually extends until it reaches a critical size. From this point a large block can instantly erode from the grass cover (Figure 4-8).

3.3 Initiation of erosion

Predicting the erosion of particularly the highly erosion resistant zone of the turf is essential as it is the toughest part of the grass cover. When this tough layer has been eroded away the erosion rate will dramatically increase; the damage is ongoing. The initiation of erosion is therefore defined as the moment when the point of no return is reached and ongoing damage is triggered. A critical erosion depth is therefore introduced; at this depth the strength of the covering layer has diminished to such an extent that for limited wave action erosion already occurs. This critical depth is estimated to be at the underside of the highly erosion resistant layer at a depth of approximately 5-7 cm. It can be reached by aggregate erosion, but it could also be reached instantly by block erosion.

4 WIPE model

The uplift pressures caused by breaking wave impacts on the outer slope can lead to erosion of the outer slope and two failure mechanism have been distinguished which can separately initiate failure of the grass cover layer. To describe the initiation of erosion of grass covers on the outer slope by wave impact pressures the Wave Impact Pressure Erosion model has been developed. The assumptions during the development of this model and its various terms are discussed below.

4.1 Basic erosion relation

The erosion relation for the WIPE model is based on the well known shear stress based equation for the erosion of cohesive material [Hanson and Cook 2004] given by equation (5), which has been applied in many flow and jet erosion models. It is assumed thus that impact pressures and shear stresses have similar erosion relations even though their failure mechanisms are completely different.

$$\varepsilon_{flow} = k_d \left(\tau_e - \tau_c \right) \tag{5}$$

Where ε_{flow} is the erosion rate due to flow and k_d is a detachability coefficient. A similar approach was followed by Stanczak (2008) for the development of an impact erosion model. The basic equation for the WIPE model reads:

$$y_m = \sum_{1}^{N_{imp}} \frac{\left(p_{up}(z) - p_c(z) \right) \cdot t_{imp}}{E_p(z)} \tag{6}$$

This basic equation can be applied to obtain limit states for the two types of erosion, which were already distinguished above: aggregate erosion (AE) and block erosion (BE). Erosion is expressed as a depth y_m [m] and occurs only when the uplift pressure p_{up} [N/m^2] generated by a wave impact, exceeds the strength, which is given as a critical uplift pressure p_c [N/m^2]. Both the strength term and the load term are dependent on the depth z. The uplift pressure due to a wave impact on the slope is assumed to last for a characteristic time t_{imp} [s]. The load during one characteristic impact time is assumed to be constant; waves are modelled as block impacts over time. The rate of erosion is determined by the erosion parameter E_p [kg/m^{2}s], which is inversely proportional to the strength of the grass cover.

4.2 Load term p_{up}

To predict erosion depths with the erosion relation given in equation (6) impact pressures are required. The model was verified with the help of the pressure data obtained during the EroGRASS experiments in the GWK. Consequently the loads on the slope are already known and the erosion model can be calibrated by determining the maximum impact pressure for each wave.
However for the model to be applicable in the absence of pressure data, the impact pressures need to be predicted. A conversion from wave characteristics to loads is thus required before the model can be utilized. For the prediction of impact pressures, provided that the wave characteristics are known, it is suggested to use the approach of Führböter (1986; 1988) as given in equation (1). As pressure damping by the backwash layer has already been accounted for in the impact factor [Führböter and Sparboom 1988] there is no need to model this effect separately.

4.2.1 Influence of cracks

Generally cracks are filled with water only, but during a wave impact they actually are filled with an air-water mixture. This mixture can have a significantly larger compressibility than pure water due to the presence of air bubbles, which results in a higher rate of energy dissipation and a lower velocity of pressure propagation [Bullock, Crawford et al. 2001].
The crack width is usually left out of consideration but according to Müller (2003) the crack width has influence on the pressure magnitude as well. The air content, and thus the damping effect of the water-air mixture, depends on the crack width; smaller cracks have a greater damping effect on the pressure in the crack [Müller, Wolters et al. 2003]. Furthermore the pressure magnitude is not affected by sudden changes in geometry and it is expected that this also applies for pressure propagation into fissured soil. For especially cracks with small widths (0.5-3.0 mm), there is thus a tendency for the pressure to reduce in magnitude as the distance from the crack entrance increases. [Müller et al. 2003; Wolters and Müller 2004] Hence the pressure within a small crack in the grass cover is reduced with increasing distance from the crack entrance. To quantify this effect the experiments on pressure propagation in closed end cracks by Muller et al. (2003) were approximated (Figure 7-4).

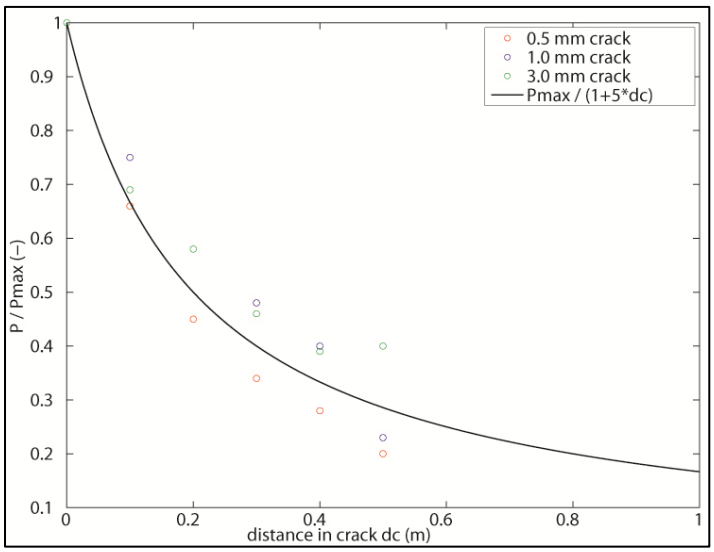

Figure 5: Approximation of impact pressure reduction in small cracks.

This eventually yielded equation (7) for the uplift pressures at a distance d_c in small cracks.

$$p_{up} = \frac{p_{\max}}{(1+\mu d_c)} \tag{7}$$

Where p_{up} is the uplift pressure underneath an aggregate after wave impact, d_c is the distance in the crack from the surface and μ is a pressure reduction coefficient (5.0).

4.3 Strength terms

4.3.1 Grass strength

Estimating the root reinforcement of soil is generally done with a modified version of the Mohr Coulomb equation where the reinforcing effect of the roots is represented by an additional cohesion c_{grass}. Mostly this root cohesion is estimated with the help of the simple perpendicular root model developed by Wu et al. (1979). This root equation requires the root tensile strength t_r and the root diameter d_r. Where a root crosses the shear zone the strength can be resolved into components perpendicular ($\sigma_r = t_r \cdot \cos\theta$) and parallel ($T_r = t_r \cdot \sin\theta$) to the shear zone. The formulae for the artificial grass cohesion c_{grass} and the normal grass stress σ_{grass} read:

$$c_{grass} = t_r \frac{A_r}{A}\left(\cos\theta \tan\varphi + \sin\theta\right) \tag{8}$$

$$\sigma_{grass} = t_r \frac{A_r}{A}\cos\theta \tag{9}$$

Where A_r / A is the Root Area Ratio (RAR), θ the root angle of rotation and φ is the angle of internal friction. As the term $\left(\cos\theta \tan\varphi + \sin\theta\right)$ is fairly insensitive to changes in θ and φ, it is close to 1.2 for a large range of θ and φ and the root cohesion may be rewritten as:

$$c_{grass} = 1.2 t_r \frac{A_r}{A} \tag{10}$$

Because the root density diminishes with depth the grass strength should decrease as well with depth. Sprangers carried out field measurements in 1999 and derived an exponentially decreasing function for Root Volume Ratio (RVR) depth profiles of 24 Dutch grass dikes. Later Stanczak (2007) carried out laboratory tests as well and derived a similar function for the RVR; both functions showed good agreement.

However for the calculation of the grass strength the RAR is required. Fortunately Valk (2009) was able to relate the RVR and RAR by comparing the function of Stanczak with the data of Sprangers, and derived the following expression: $RVR = 50 \cdot RAR$. Subsequently exponential functions were proposed by Valk (2009) and Hoffmans et al. (2009) for the decay of the root density with respect to depth. Combining both functions yields the following function for the RAR with respect to depth

$$RAR(z) = RAR_0 \cdot e^{-\beta z} \tag{11}$$

Where RAR_0 is the root density at the surface and β is a root decay coefficient equal to 22.32 m^{-1}. Equation (11) is used to introduce depth dependency for the grass strength which results in the equations for the grass strength with respect to depth:

$$\sigma_{grass,c}(z) = t_{r,c} \cdot RAR_0 \cdot e^{-22.32 z} \tag{12}$$

$$c_{grass,c}(z) = 1.2 t_{r,c} \cdot RAR_0 \cdot e^{-22.32 z} \tag{13}$$

4.3.2 Characteristic aggregate diameter

When it is assumed there are no loose aggregates at the surface of the cover layer ach root supports a small block of soil with a certain dimension, depending on the number of roots in the area. The turf area per root A_t can be calculated by dividing the cover layer area by the number of roots n_r. The root spacing s, the average distance between two roots, is then equal to the square root of the turf

area per root: $s = \sqrt{A/n_r}$.

As the soil structure is generally less in lower quality grass sod than in good quality sod, the characteristic aggregate diameter d_a is related to the root spacing to account for the grass quality. Yet the aggregate diameters due to soil structure increase with depth. Based on observations by Sprangers (1999) the characteristic aggregate diameter at a depth of 0.20 m is taken as 20 mm. For good quality grass the aggregate diameter with respect depth can be approximated as:

$$d_a = \sqrt{A/n_r} + 0.08 \cdot z \tag{14}$$

4.3.3 Basic strength equation

The turf element model [Hoffmans, Verheij et al. 2009] is used as a basis to model the strength of the grass cover as it provides a clear physical description of the strength of the grass cover. Because the grass strength is depth dependent an index 0 is introduced for the strength at the surface. The strength of an aggregate depends on the number of sides of the block n_s that have physical contact with the surrounding soil. In this way the amount of small cracks and pores in the soil partly determines the erosion resistance of an aggregate. The condition of the soil can then be divided into 4 classes as n_s ranges from 0 to 3. At the surface a particle will break loose if the critical condition for movement is reached. The forces on a cube $l_x l_y l_z$ are:

F_p	= maximum lift force	$F_p = p_{up} \cdot l_x l_y$
F_w	= weight due to gravity	$F_w = (1-n)(\rho_s - \rho_w) g \cdot l_x l_y l_z$
F_s	= shear force	$\Sigma F_s = f(\rho_s - \rho_w) g (l_x + l_y)(l_z)^2$
F_c	= cohesion force	$\Sigma F_c = (c_{grass,c} + c_{clay,c}) \cdot \{2(l_x + l_y) l_z + l_x l_y\}$
F_g	= grass reinforcement	$F_g = \sigma_{grass,c} \cdot l_x l_y$

Where n is the porosity, ρ_s is the density of the soil , ρ_w is the density of water, p_{up} is the maximum uplift pressure under the aggregate and f is a friction factor ($\tan\varphi$). Furthermore n_s is the side wall coefficient, $c_{clay,c} = c_{clay}$ /80 and c_{clay} is the mean clay cohesion. Incipient motion occurs when:

$$F_p \geq F_w + \Sigma F_s + \Sigma F_c + F_g$$

$$p_{up} \geq \left(1 - n + 0.5 f \cdot n_s\right)(\rho_s - \rho_w) g z + n_{s\cdot}(c_{clay,c} + c_{grass,c}(z)) + \sigma_{grass,c}(z) \tag{15}$$

Equation (15) will be adapted for the two specific erosion mechanisms. This yields a limit state equation for surface erosion of fixed aggregates and a limit state equation for the erosion of blocks. In both limit states the strength of the grass cover is for a major part determined by the reinforcement due to roots.

4.3.4 Aggregate erosion

At a certain moment cracks are present everywhere at the surface of the cover layer due to soil structure and impact pressures. An aggregate is exposed to uplift pressures, when the grass-clay aggregate is fixed at three sides at most and not at the underside.

Incipient motion at the surface occurs when the uplift pressure p_{up} induced by the wave impact exceeds the critical uplift pressure p_c . With $z = d_a$, $c_{grass,c}(d_a) = c_{0,grass,c}$ and $\sigma_{0,grass,c}(d_a) = \sigma_{0,grass,c}$ equation (15) becomes:

$$p_c = (1-n+0.5n_s f)\left((\rho_s - \rho_w) g d_a + \frac{n_s \cdot (c_{clay,c} + c_{0,grass,c}) + \sigma_{0,grass,c}}{1-n+0.5n_s f} \right) \quad (16)$$

Yet if at the surface the cover layer is severely cracked cohesion forces will not act on the sidewalls of the block. Soil aggregates can still be in contact with the surrounding soil though and wall friction can still play a role. In that case the soil aggregate is fixed at the underside of the block by only a root and equation (16) can be simplified. The equation for the soil strength $\sigma_s(z)$ for aggregates at the surface then reads:

$$\sigma_s(z) = (1-n+0.5n_s f) \cdot (\rho_s - \rho_w) g d_a + \sigma_{grass,c}(z) \quad (17)$$

4.3.5 Block erosion

Block erosion occurs on the condition that a large crack is present or that another hole or local irregularity reaches deeper parts of the turf, allowing impact pressures to penetrate into the soil.
The crack walls are deformed horizontally due to the impact pressures in the cracks and consequently soil aggregates may move and are compressed against the surrounding soil. Macro pores can become clogged and eventually this will allow uplift pressures to develop at larger surfaces than only the aggregate areas.
However before uplift pressures can develop a horizontal crack has to be formed. For cracks to develop the soil has to be fractured which is most likely to occur at the location of minimum fracture resistance σ_f [N/m^2], which is defined as follows:

$$\sigma_f \geq (1-n)(\rho_s - \rho_w) g z + \frac{0.5 n_s f (\rho_s - \rho_w) g \cdot z^2}{d_{block}} + \sigma_{grass,c}(z) \quad (18)$$

Where d_{block} is the block diameter. The block area A_{block} at the moment of initial crack formation is assumed to be proportional to the characteristic aggregate size ($A_{block,0} = d_a^2$). As a result of the packing of aggregates and possible overlapping of aggregates the friction of the whole column of soil contributes to the fracture resistance, whereas clay and grass cohesion are still assumed to be negligible due to soil structure and the fact that these forces are not immediately mobilized during crack formation process.
However the walls of the crack are compressed during wave impacts in the crack. Consequently the blocks of soil in the crack wall are pushed against the surrounding soil, which enables friction to develop at one or more sides of the blocks. The factor n_s determines the influence of friction due to surrounding soil and can be considered as a parameter that represents to what extent the soil is structured or has inconsistencies. Differentiation of equation (18) to z gives the depth $z_{\min}$ where the fracture resistance σ_f is at a minimum.
When a crack has been formed it will grow according to the balloon mechanism and once the crack reaches a critical length part of the turf may be ripped out of the subsoil, leading to block erosion. To model the block erosion process, the eroded blocks are assumed to be box-shaped with base A_{block} [m^2] and height $z_{\min}$ [m]. The initial block area $A_{block,0}$ will be equal to the base of an aggregate (d_a^2) but as the horizontal crack extends, the block area and thus the uplift force increase as well. Once a critical value of the block area has been reached the block can be washed away. Failure can thus occur by a single extreme impact pressure but also by milder, more frequently occurring impact pressures. By applying $l_x = l_y = d_{block}$ and $l_z = z_{\min}$ the limit state equation for block erosion can be determined:

F_p = maximum lift force $F_p = p_{up} \cdot A_{block}$

F_w = weight due to gravity $F_w = (1-n)(\rho_s - \rho_w) g \cdot A_{block} z_{\min}$

F_s = shear force $\Sigma F_s = 0.5 n_s \cdot f(\rho_s - \rho_w) g \cdot d_{block}) \cdot z_{\min}^2$

F_c = cohesion force $\Sigma F_c = (n_s \cdot d_{block}) \left(\int_0^{z_{\min}} c_{grass,c}(z) + c_{clay,c} \cdot z_{\min} \right)$

F_g = grass reinforcement $F_g = \sigma_{grass,c}(z_{\min}) \cdot A_{block}$

Using the condition for incipient motion and dividing by A_{block} yields the critical uplift pressure for block erosion:

$$p_{up} \geq (1-n)(\rho_s - \rho_w) g z_{\min} + \frac{0.5 \cdot n_s f(\rho_s - \rho_w) g \cdot z_{\min}^2}{d_{block}} + \frac{n_s \left(\int_0^{z_{\min}} c_{grass,c}(z) + c_{clay,c} \cdot z_{\min} \right)}{d_{block}} + \sigma_{grass,c}(z_{\min}) \qquad (19)$$

Unlike the erosion resistance of small aggregates, which is not influenced by cohesion due to cracks, the erosion resistance of large blocks is probably increased by cohesion forces. Horizontal roots can provide support between the block and the soil in its vicinity. Furthermore it is not unlikely that the side walls of the block are partly packed together again due to the compression caused by the impacts. In combination with the diminishing soil structure some sections of the block sides may thus have cohesion.
In contrast to the critical clay cohesion, which is constant, the grass cohesion in equation (19) is variable with respect to depth and needs to be integrated.

4.3.6 Crack growth and failure criterion

Once an initial crack has been formed the crack can grow or block erosion can occur, this is dependent on the magnitude of the impact pressure. When only the fracture strength is exceeded the block of soil is slightly lifted which causes crack extension at the fixed ends of the block. As the increase of the crack length should also depend on the clay quality the increase of the block area ΔA_{block} is assumed to be equal to the residual uplift pressure divided by the fracture strength and the clay critical strength:

$$\Delta A_{block} = \frac{\left(p_{up} - \sigma_f \right) A_{block}}{\alpha_{crack} (\sigma_f + c_{clay,c})} \qquad (20)$$

Where α_{crack} is a crack growth parameter. Block erosion can be triggered when the critical strength p_c is exceeded by the uplift pressure p_{up}. Yet in this case the total block has to be lifted during an impact, hence inertia plays a role. Since the WIPE model is static it is suggested that erosion occurs only when the following criterion, as a compensation for inertia and other dynamic effects, is satisfied:

$$\frac{(p_{up} - p_c) \cdot t_{imp}}{E_p} > z_{\min} \qquad (21)$$

4.4 Erosion parameter

The erosion parameter is a function of the combined strength of grass and clay in the grass cover, similar to in the turf element model by Hoffmans et al. (2009). The parameter is inversely proportional to the strength. Analogous to the erosion parameter E_{soil} for flow velocities the erosion parameter for impact erosion E_p [m/s] can be defined as follows:

$$E_p = \alpha_{soil} \frac{p_c}{\rho_w \sqrt{g d_a}} \text{ and } \alpha_{soil} = 5.5 \cdot 10^3 \quad (22)$$

It is however preferred to express the erosion rate in [m/s] rather than in [kg/m^{2}s]. To accomplish this, the erosion rate is divided by the density of the soil ρ_s, which leads to the following basic impact erosion relation: $\frac{dy_m}{dt} = \frac{p_{up} - p_c}{E_p}$. Where E_p [kg/m^{2}s] is the impact erosion parameter defined as:

$$E_p = \alpha_{soil} \cdot \frac{\rho_s}{\rho_w} \cdot \frac{p_c}{\sqrt{g d_a}} \quad (23)$$

4.4.1 Characteristic impact time and sequential effect

Since the wave loading is discontinuous it is preferred to use a more practical form of the WIPE model for the prediction of erosion during a storm. The erosion depth for the number of waves causing an impact N_{imp} can then be predicted according to the following relation:

$$y_m = \sum_{1}^{N_{imp}} \frac{\left(p_{up}(z) - p_c(z) \right) \cdot t_{imp}}{E_p(z)} \quad (24)$$

The uplift pressures generated by wave impacts are peak pressures and discontinuous, the uplift pressures are thus active for only a small portion of the storm duration. Ideally the impact time for each individual wave should be determined but this is labor intensive and this data is mostly not available. The averaged impact time for the EroGRASS wave conditions was therefore estimated. With the help of equations (3) and (4) and $p_{\max,50}$, the rise times and impact durations were computed. The obtained characteristic impact time t_{imp} amounts 0.350 s and represent the upper bound of the impact duration, this value is thus on the conservative side. The number of waves causing an impact can be related to the number of waves in a storm, this relation could have the following form:

$$N_{imp} = \alpha N_w \quad (25)$$

Where α is a wave impact coefficient between 0.0 and 1.0. The value of α can be obtained by determining the number of wave impacts from either pressure data using a threshold pressure or from visual observations. The number of waves can be obtained from reflection analysis.
Due to the diminishing strength of the grass cover with depth the chronological order of the wave impact pressures is an important factor as well. This is contrary to cases where it is supposed that damage occurs due to a single extreme value of the impact pressure.

5 Calibration and verification

The WIPE model was calibrated and verified with the data of the EroGRASS experiments. The erosion events during these tests as well as the model input are discussed shortly in section 5.1 and the calibration results are treated in section 5.2, followed by erosion by flow velocities in section 5.3.

5.1 Erosion events and model input

To gain more insight in the erosion process of grass by wave impact and wave overtopping, model tests have been performed in the Große WellenKanal (Large Wave Flume) of the Coastal Research Centre - a joint centre of the University of Hannover and the Technical University of Braunschweig, Germany [Piontkowitz et al. 2009].
The erosion observations during and after the test were used as a basis for calibration. Aggregate

erosion started to play a role in the erosion process during the tests with a significant wave height of 0.90 m. Yet after the tests there were no erosion holes due to aggregate erosion, indicating that only minor and gradual damage was inflicted. The total surface erosion depth was therefore estimated to be in the order of centimeters.
During the tests also several cases of block erosion were observed; two of these were suitable for a calibration run. The depth of the scour holes varied between 0.07-0.10m, whereas the equivalent block diameter $d_{block} = \sqrt{A_{block}}$ varied between 0.08-0.48 m. Both eroded sections were adjacent to a joint and also worms were found at the surface of the erosion holes, which may have weakened the grass cover locally.
The pressure records of the EroGRASS experiments were used for the calibration. Per wave period one maximum pressure was identified, consequently not all input pressures were by definition impact pressures. Yet it is expected that the quasi static pressures that were wrongfully included in the calibration programs had little influence on the outcome, as these pressures were relatively low.
Furthermore the grass characteristics were modified. During the preparations of the experiments in the GWK the quality of the grass cover was determined by taking samples on several locations of the dike model. The value of the RVR near the surface was equal to 0.07, which is equivalent to a RAR value of approximately 0.0014.
To exclude a possible overestimation of the grass strength, the grass cover was therefore considered as a good quality grass cover, with a RAR value of 0.0008 at the surface.

5.2 Calibration results

5.2.1 Aggregate erosion

The aggregate erosion model was calibrated with two runs using only one factor: α_{soil} [-], which is included in the erosion parameter as follows:

$$p_c(z) = \left(1 - n + 0.5 n_s f\right)(\rho_s - \rho_w) g d_a(z) + \sigma_{grass,c}(z) \quad \text{with: } n_s = 2.0$$

$$E_p(z) = \alpha_{soil} \cdot \frac{\rho_s}{\rho_w} \cdot \frac{p_c(z)}{\sqrt{g d_a}(z)}$$

The theoretical value of α_{soil}, which was determined in section 4.4, appeared to be too high. Therefore the model behavior was investigated for lower values of α_{soil} and eventually the behavior of the model was satisfactory for α_{soil} =25-35.
The WIPE model is considered suitable for the prediction of erosion of a good quality grass cover. Yet adaptations will be required to make the model more compatible for the prediction of erosion of grass covers of various qualities. This is caused by the fact that the critical uplift pressure is mainly determined by the grass strength; as a result the predicted erosion depth for low quality grass cover is extremely high. To solve this problem it was suggested to introduce a characteristic length scale for the erosion depth. This critical depth z_{crit} [m] is defined as the depth where the root density equals the Root Area Ratio at the surface of very poor quality grass cover (RAR =0.0002). The WIPE model is then applicable for good to poor quality grass covers and depending on the grass quality the critical erosion depth varies between 0.03 m and 0.06 m.

5.2.2 Block erosion

For block erosion the model was calibrated using the factors α_{soil} and α_{crack} .These factors are related to the relevant equations for block erosion as follows:

$$\frac{(p_{up}(d_{block}) - p_c(d_{block}) \cdot t_{impact}}{E_p(d_{block})} > z_{\min}$$

$$E_p(d_{block}) = \alpha_{soil} \cdot \frac{\rho_s}{\rho_w} \cdot \frac{p_c(d_{block})}{\sqrt{g d_{block}}}$$

$$\Delta A_{block} = \frac{\left(p_{up}(d_{block}) - \sigma_f(d_{block})\right) A_{block}}{\alpha_{crack}\left(\sigma_f(d_{block}) + c_{clay,c}\right)}$$

The calibration factor α_{soil} [-] can be regarded as a parameter that determines the moment when the erosion criterion is satisfied and block erosion occurs, whereas the crack growth factor α_{crack} determines the size of the eroded block. Furthermore α_{crack} also has some influence on the moment of failure as it affects the decay of the erosion parameter E_p, the fracture strength σ_f and the erosion resistance p_c.

As the model was calibrated on merely two characteristic block erosion events the value of α_{soil} unfortunately has a considerable scatter (0.01-3.25). Contrary to this the variation of α_{crack} (390-420) for both calibration runs is limited. The scatter in the value of α_{soil} can be partly explained by the small block diameter (0.08 m) for one of the calibration runs; for small block diameters the erosion resistance p_c is high and consequently failure can only be predicted for low values of α_{soil}.

5.3 Erosion by flow velocities

The erosion of the grass cover was investigated at MWL for various grass qualities for all EroGRASS tests. Erosion predictions were done with the flow erosion model by Hoffmans (equation (26)) while it was assumed that during each wave period the slope is loaded by both the run-up velocity and the down-rush velocity, and that the flow duration amounts 1.0 s for both velocities.

$$\sum_{N=1}^{N_w} y_{m,n} = \frac{(\omega U_0 - U_c)^2 \cdot t_{flow}}{E_{soil}} \tag{26}$$

Where t_{flow} is the flow velocity and ω is the turbulence coefficient ($1.5+5 \cdot r_0 = 2.25$ with r_0 =0.15).

On the basis of this conservative approach it was concluded that for good grass quality the flow velocities cause no problems and that the erosion caused by flow velocities during the experiments could indeed be neglected.

6 Conclusions and recommendations

In the next sections the WIPE model is summarized, followed by conclusions and recommendations.

6.1 Summary WIPE model

The basic equation for the Wave Impact Pressure Erosion (WIPE) model reads:

$$y_m = \sum_{1}^{N_{imp}} \frac{\left(p_{up}(z) - p_c(z)\right) \cdot t_{imp}}{E_p(z)} \tag{27}$$

The load terms, the grass strength terms and the characteristic aggregate diameter with their recommended values are given in the boxes below. These terms are valid for both erosion mechanisms.

Load terms

$$N_{imp} = \alpha N_w,\ N_w = T_{storm} / T_m$$

$$p_{up}(z) = \frac{p_{\max}}{(1+\mu d_c)}$$

Grass strength

$$\sigma_{grass,c}(z) = t_{r,c} \cdot RAR_0 \cdot e^{-\beta z}$$

$$c_{grass,c}(z) = 1.2 \cdot t_{r,c} \cdot RAR_0 \cdot e^{-\beta z}$$

Characteristic aggregate diameter

$$d_a = \sqrt{A / n_r} + 0.08 \cdot z$$

With:

N_{imp} = no. of impacts [-]; α = wave impact coefficient between 0.0-1.0 [-]; N_w = no. of waves in a storm [-]; t_{imp} = 0.35 [s]; μ = 5 [m^{-1}]; $t_{r,c}$ = $20 \cdot 10^6$ [N/m^2]; RAR_0 = Root Area Ratio at the surface [-]; β = 22.32 [m^{-1}]; z = depth [m]; A = soil area [m^2]; n_r = number of roots [-]

The basic equation (27) can be adapted to predict the erosion depth y_m [m] for either aggregate erosion (1) or block erosion (2).

3. Aggregate erosion

$$y_m = \sum_{1}^{N_{imp}} \frac{\left(p_{up}(z) - p_c(z)\right) \cdot t_{imp}}{E_p(z)}$$

$$y_m \le y_{m,crit}$$

Strength terms

$$p_c(z) = \left(1 - n + 0.5 n_s f\right) \cdot (\rho_s - \rho_w) \cdot g d_a(z) + \sigma_{grass,c}(z)$$

$$E_p(z) = \alpha_{soil} \cdot \left(\frac{\rho_s}{\rho_w}\right) \cdot \frac{p_c(z)}{\sqrt{g d_a}(z)}$$

With:

$y_{m,crit}$ = critical erosion depth between 0.03-0.06 [m]; n =0.4 [-]; n_s =2.0 [-]; $f = \tan\varphi$ [-]; φ =35 [-]; ρ_s =2000 [kg/m^3]; ρ_w =1000 [kg/m^3]; g =9.81 [m/s^2]; and α_{soil} =35 [-].

4. Block erosion

$$y_m = z_{\min} \text{ [m]}$$

$$\text{When } \frac{(p_{up}(d_{block}) - p_c(d_{block}) \cdot t_{imp}}{E_p(d_{block})} > z_{\min} \qquad (28)$$

Where $z_{\min}$ [m] is the depth of the minimum fracture strength $\sigma_{f,\min}$ [N/m^2].

Strength terms

$$p_c = (1-n)(\rho_s - \rho_w) g z_{\min} + \frac{0.5 \cdot n_s f (\rho_s - \rho_w) g \cdot z_{\min}^2}{d_{block}} + \frac{n_s \left(\int_0^{z_{\min}} c_{grass,c}(z) + c_{clay,c} \cdot z_{\min}\right)}{d_{block}} + \sigma_{grass,c}(z_{\min})$$

$$E_p(d_{block}) = \alpha_{soil} \cdot \frac{\rho_s}{\rho_w} \cdot \frac{p_c(d_{block})}{\sqrt{g d_{block}}}$$

Crack formation

$$\sigma_f = (1-n)(\rho_s - \rho_w)gz + \frac{0.5 n_s f (\rho_s - \rho_w) g \cdot z^2}{d_{block}} + \sigma_{grass,c}(z)$$

$$\Delta A_{block} = \frac{\left(p_{up}(d_{block}) - \sigma_{f,\min}(d_{block})\right) A_{block}}{\alpha_{crack}\left(\sigma_{f,\min}(d_{block}) + c_{clay,c}\right)} \qquad \text{Where: } A_{block} = d_{block}^{\ 2} \text{ [m}^2\text{]}$$

With recommended values:
$d_{block,0} = d_a$ [m]; n_s =2.0 [m]; $c_{clay,c}$ = c_{clay} /80 [N/m^2]; c_{clay} =30 [kN/m^2]; α_{soil} =1.35 [-] and α_{crack} = 420 [-].

6.2 Results calibration and verification

6.2.1 Load

- Due to the diminishing strength of the grass cover with depth the chronological order of wave impacts is an important factor in the erosion process and complicates the prediction of erosion of grass covers;
- Damping in cracks is a relevant effect in the block erosion process, whereas this effect hardly plays a role during aggregate erosion. However if cracks widen considerably due to the balloon mechanism, the pressure attenuation in cracks could be negatively affected;
- Erosion induced by flow velocities was considered to be negligible for the good quality grass cover during the EroGRASS experiments. At a certain erosion depth flow velocities will however start to affect the erosion process.

6.2.2 Aggregate erosion

- Calibration of aggregate erosion was done with solely the parameter α_{soil} [-], which is included in the erosion parameter. For α_{soil} =25-35 the model behavior resembled the observed progression of aggregate erosion during the experiments;
- For low root densities the WIPE model predicts excessive erosion rates since the critical uplift pressure is dominated by the grass strength. Therefore a critical erosion depth is introduced, which is defined as the depth where root density equals the root density of very poor quality grass cover (RAR =0.0002);
- It is expected that the performance of the WIPE model will be unsatisfactory for poor quality grass covers, despite the introduction of the critical depth. Yet for lower quality grass covers the model will require adaptations to be applicable anyway as in addition to the impact pressures flow velocities will start to play role in the erosion process;

6.2.3 Block erosion

- A small increase of the block diameter for block diameters below 0.10 m has a relatively large influence on the decline of the strength parameters p_c , E_p and σ_f , but because the strength terms are especially high for very small block diameters ($d_{block} \leq 0.05$ m) extremely high impact pressures are required to cause block erosion. It is therefore highly unlikely that small blocks will erode, regardless of the magnitude of the factor α_{soil} . Conversely the reduction of the strength terms is less drastic for larger block diameters, but the magnitude of these terms is in the range where failure can be triggered. For larger block diameters the value of the factor α_{soil} is therefore essential to predict the correct moment of failure;
- An appropriate value of the side wall coefficient n_s is important for especially the erosion resistance of small block diameters and partly determines the location of minimum fracture strength $z_{\min}$ and thus the block erosion depth;

- The initial block diameter has a strong influence on $z_{\min}$ and the magnitude of the minimum fracture strength $\sigma_{f,\min}$. Since the initial block diameter is chosen equal to the aggregate diameter, the aggregate diameter distribution is of major importance;
- To obtain more reliable and uniform results for block erosion more data is required.

6.3 Recommendations

6.3.1 Load

For the model to be applicable in practice it is first of all essential to improve the relation given by Führböter between wave characteristics, the geometry of the dike and impact pressures. This could also include developing a relation between the number of waves and the number of wave impacts. Research on the pressure reduction within cracks in grass cover should also be performed as it is an important effect in the block erosion process. Furthermore it should be checked if the impact pressures are fully converted by the pore water into uplift pressure or that pressure losses occur during this process.

6.3.2 Grass cover strength

The grass tensile strength and the root diameter are essential parameters, which are at the moment average values applied to all roots. If indeed a negative exponential relation between the grass tensile strength and the root diameter exists the root diameter distribution could have a significant influence on the tensile strength of the roots as well as on the failure modes of roots. It is therefore suggested to investigate the root diameter distribution of grass species present on dikes,
Moreover it is important to check if there are significant differences between the grass characteristics of different species on several types of dikes. Grass species on a sea dike may greatly differ from grass species at a river dike (salt versus fresh water) but also the characteristics of grass on sea dikes at different locations could vary. Ideally grass dikes should be categorized and guideline values should be formulated for grass on each of these types of dikes.
Soil structure development also deserves more investigation. Of particular interest are the condition of the grass cover and the presence of cracks after a soil structure has already developed. Also a more accurate aggregate diameter distribution should be obtained.

6.3.3 Failure mode and management

In this research not much attention has been paid to weak spots at the surface, yet failure due to the presence of cracks and other inconsistencies has been treated extensively; block erosion will only occur if these are present in the grass cover. Research on the growth of these cracks by wave loading will therefore be useful and in addition the occurrence of the balloon mechanism could be verified. Moreover the crack formation process by wave impacts at the surface also deserves more attention to improve the strength modeling for aggregate erosion.
The condition of the grass cover will gradually deteriorate during wave loading, but the initial condition of the grass cover layer is determined by the degree of soil structure. The initial condition of the soil thus partly determines when the grass cover becomes susceptible to erosion. Hence limiting soil structure and cracks is crucial and will make the grass cover less susceptible to erosion.
Both thin roots and thick roots are required to prevent aggregate and block erosion and grass cover management should be aimed at obtaining a dense root system with many thin roots and some thick roots in the top part of the cover layer. General consensus exists that this is accomplished by management category A: haying and mowing twice a year or grazing with sheep, without fertilizing. The latter is preferred as grazing with sheep has a positive effect on the root development in the upper region of the grass cover. Furthermore it is expected that intensive grazing with many sheep several times a year in addition to this will compact the soil and thus reduce soil structure.

6.3.4 Experiments

For constructional reasons the grass cover of the EroGRASS experiments consisted of many smaller sections of grass sod. Inevitably this led to irregularities at the surface and cracks between the sections, which had a significant influence on the erosion process. If possible the installation method of the grass cover should therefore be improved. A potential improvement for the installation could

be to close off part of the wave flume and to assign this space to a dike model with a grass cover, in such a way that the grass cover is given sufficient time to recover from the installation. This area should preferably be outside to allow the grass to grow as it would on a real dike.
Alternatively a device similar to the wave overtopping simulator could be developed to carry out experiments in the field, which has the great benefit that there will be no need to excavate, transport and install the grass sods.

References

G. N. Bullock, A. R. Crawford, P. J. Henson, M. J. A. Walkden and P. A. D. Bird (2001). The influence of air and scale on wave impact pressures, Coastal Engineering. 42

A. Führböter (1986). Model and prototype tests for wave impact and run-up on a uniform 1:4 slope, Coastal Engineering. 10

A. Führböter and U. Sparboom (1988). Full-scale wave attack of uniformly sloping sea dykes, 21st International Conference Coastal Engineering, Malaga, Spain.

G. J. Hanson and K. R. Cook (2004). Apparatus, test procedures and analytical methods to measure soil erodibility in situ, Trans. ASAE. 20(4)

G. J. C. M. Hoffmans, H. J. Verheij, A. v. Hoven and G. J. Akkerman (2009). Surface instability of grass and clay caused by wave overtopping, ASCE Journal of Hydraulic Engineering (submitted, to be published in 2010), Deltares, Delft University of Technology, Royal Haskoning.

G. Müller, G. Wolters and M. J. Cooker (2003). Characteristics of pressure pulses propagating through water-filled cracks, Coastal Engineering. 49

H. Oumeraci, T. Staal, S. Pfoertner, G. Ludwigs and M. Kudella (2010). Hydraulic performance, wave loading and response of elastocoast revetments and their foundation. -A large scale model study-, LWI report no. 988, Leichtwei-Institut für Waßerbau Technische Universität Braunschweig, Braunschweig.

T. Piontkowitz, H. J. Verhagen, H. J. Verheij, T Mai Cao, D. Dassanayake, D. Roelvink, S Utili, M. Zielinski, A. Kont and T. Ploompuu (2009). EroGRASS - Failure of grass cover layers at seaward and shoreward dike slopes. design, construction and performance., EroGRASS user group, Lemvig (Denmark).

J. T. C. M. Sprangers (1996). Extensive grassland management on sea dikes (in Dutch), Wageningen, Landbouwuniversiteit Wageningen.

J. T. C. M. Sprangers (1999). Vegetation dynamics and erosion resistance of sea dyke grassland, Wageningen, Department of Environmental Sciences Wageningen, section Nature conservation and Plant ecology, Wageningen Agricultural University

G. Stanczak (2007). Laboratory tests on the erosion of clay revetment of sea dike with and without a grass cover induced by breaking wave impact, FLOODsite.

G. Stanczak (2008). Breaching of sea dikes initiated from the seaside by breaking wave impacts, PhD thesis, Faculty of Architecture, Civil Engineering and Environmental Sciences, University of Braunschweig, Braunschweig.

TAW (1997). Technical report erosion resistance of grassland as dike covering, Ministry of Transport, Public Works and Water Management.

A. Valk (2009). Wave overtopping, impact of water jets on grassed inner slope transitions, MSc thesis, Faculty of Civil Engineering and Geosciences, Delft University of Technology, Delft.

G. v. Vledder (1990). Literature survey to wave impacts on dike slopes, Delft, Delft Hydraulics.

H. Witte (1988). Druckschlagbelastung durch Wellen in deterministischer und stochastischer Betrachtung, PhD thesis, Technische Universität Carolo Wilhelmina Braunschweig, Braunschweig.

G. Wolters and G. Müller (2004). Field and large scale model tests of wave impact pressure propagation into cracks, 29th International Conference Coastal Engineering, Lisbon, Portugal.